universität wien

DISSERTATION

Characterization of novel tumor stroma markers identified by gene expression profiling of human cancer tissues and 3D co-culture models

angestrebter akademischer Grad

Doktor der Naturwissenschaften (Dr. rer.nat.)

Verfasserin / Verfasser:	Mag. Christian RUPP
Dissertationsgebiet (lt. Studienblatt):	Molekulare Biologie
Betreuerin / Betreuer:	Univ. Doz. Dr. Wolfgang SOMMERGRUBER

Wien, im August 2010

Danksagungen

An dieser Stelle möchte ich mich ganz herzlich bei all jenen Menschen bedanken, die für das Zustandekommen dieser Arbeit einen wichtigen Beitrag geleistet haben:

Bei meiner Familie und all meinen Freunden, für ihre moralische Unterstützung und die Geduld mit der sie mein gelegentliches „Gesudere“ ertragen haben.

Bei Prof. Dr. Pilar Garin-Chesa, für die spannende Themenstellung, die kompetente fachliche Betreuung und die hervorragende Zusammenarbeit der letzten Jahre.

Bei meinen Kollegen und Kolleginnen Helmut, Christina, Oliver und Daniela für deren Unterstützung bei vielen Dingen des Laboralltags und den ganzen Spaß, den wir miteinander hatten.

Bei Univ. Doz. Dr. Wolfgang Sommergruber für die offizielle Betreuung meiner Arbeit und das Interesse, das er dieser entgegenbrachte.

Weiters möchte ich mich herzlich bei Prof. Dontscho Kerjaschki und dem Team des Institutes für Pathologie am AKH sowie bei Dr. Nobert Schweifer und Dr. Christian Haslinger (Boehringer-Ingelheim Austria) für die Unterstützung bei der bioinformatischen Auswertung meiner Daten bedanken. Außerdem gilt mein Dank Matthias Artaker (MFPL) und Harini Nivarthi (LBI) für deren Unterstützung bei den bei den „Knock-down“ bzw. Xenograft Experimenten.

Table of contents:

1. Abstract / Kurzbeschreibung

The tumor stroma plays an important role in tumorigenesis. During cancer progression it undergoes changes in architecture, gene expression and secretion of proteolytic enzymes that are essential for the invasive and metastatic phenotype of malignant tumors. Cancer associated fibroblasts (CAFs) represent the major cellular component of the stroma and recent studies demonstrated the prognostic and therapeutic significance of CAF-related molecular signatures.

The identification and characterization of genes and signaling pathways involved in the molecular interactions between tumor and stromal cells has been the focus of this study. For that purpose we have used two complementary approaches: the identification of novel tumor stroma targets in human colon cancer samples using whole genome Affymetrix GeneChip® analysis and the validation of theses targets in a newly established of 3D co-culture model that mimics the cellular and molecular heterogeneity of human cancers. We have demonstrated increased expression of gene sets related to hypoxia, epithelial-to-mesenchymal transition (EMT) and TGFβ pathway activation in CAFs *vs* their normal counterparts in both systems. The putative TGFβ target IGFBP7 (insulin-like growth factor binding protein 7) was identified as a tumor stroma marker of epithelial cancers and as a tumor antigen in mesenchyme-derived sarcomas. IGFPB7 was shown to promote anchorage-independent growth in malignant mesenchymal cells and malignant epithelial cells with an EMT-phenotype, whereas a tumor suppressor function was observed in tumor epithelial cells.

In summary, we have demonstrated that a number of important signaling pathways involved in cancer progression and metastasis are specifically dysregulated in the tumor stroma both in our *in vivo* screen and in the *in vitro* 3D model, illustrating the value of these approaches for the identification and characterization of novel stromal markers.

Das Tumor-Stroma ist für das Tumorwachstum entscheidend. Im Zuge der Tumor-Progression verändert sich das Stroma hinsichtlich seiner Zusammensetzung sowie seines Genexpressionsmusters und begünstigt durch die Freisetzung von proteolytischen Enzymen und Wachtumsfaktoren das lokale Tumorwachstum und die metastatische Ausbreitung. Tumor-assoziierte Fibroblasten (TAFs) bilden die zelluläre Hauptkomponente des Stromas und sind vorrangig für die Produktion dieser Faktoren verantwortlich. TAFs gewinnen daher als mögliche Angriffspunkte für gezielte Tumortherapien zunehmend an Bedeutung. Neuere Studien unterstreichen zudem die prognostische Relevanz TAF-bezogener Genexpressionsmuster.

Der Fokus dieser Studie liegt auf der Identifizierung und Charakterisierung von Genen und Signaltransduktionswegen, welche in die molekularen Interaktionen zwischen Tumor- und Stromazellen involviert sind. Zu diesem Zweck bedienten wir uns zweier unterschiedlicher Ansätze: der Identifizierung von neuen Tumor-Stroma Markern in Gewebeproben humaner Kolonkarzinome durch genomweite Genexpressionsanalyse mittels Affymetrix GeneChip® und der Validierung der so identifizierten Marker in einem neu etablierten dreidimensionalen *in vitro* Co-Kultur Modell, welches die zellluläre und molekulare Heterogenität humaner Tumore widerspiegelt.

Im Vergleich von „normalen“ Fibroblasten und TAFs, zeigen TAFs in beiden Systemen ein deutlich erhöhtes Expressionslevel von Genen, die mit Hypoxie, epithelialer-mesenchymaler Transition (EMT) und TGFβ-Aktivierung in engem Zusammenhang stehen. Das potentielle TGFβ-Zielgen IGFBP7 wurde im Zuge dieser Analyse als Tumor-Stroma Marker in epithelialen Tumoren identifiziert, während IGFBP7 in Tumoren mesenchymalen Ursprungs (Sarkomen) als Tumor-Antigen fungiert. Weiters konnten wir zeigen, dass IGFBP7 in mesenchymalen Tumorzellen oder epithelialen Tumorzellen mit EMT-Phänotyp das substratunabhängige Wachstum beschleunigt, in epithelialen Tumorzellen dieses aber verlangsamt.

Zusammenfassend erweisen sich sowohl der *in vivo* Ansatz, als auch das *in vitro* Co-Kultur Modell als geeignete Systeme zur Identifizierung und Charakterisierung von neuen Tumor-Stroma Markern.

2. Summary

2.1 Tumor stroma and its role in tumorigenesis

Solid tumors consist of a complex mixture of neoplastic epithelial cells and non-neoplastic cells, collectively referred to as "tumor stroma". These include specialized fibroblasts, activated blood and lymphatic endothelial cells and infiltrating immune cells embedded in an insoluble protein network, the extracellular matrix (ECM) [1] (**Fig. 1**). During the past years it has become increasingly evident that the tumor stroma plays an important role in cancer initiation and progression and clinicopathologic studies have shown that the molecular composition of the tumor stroma correlates with prognostic factors, patient survival and response to treatment in several cancer types [2-5].

Tumor growth beyond a critical size of 1-2 mm^3 is dependent upon the formation of new capillaries and the process of tumor-induced angiogenesis (neoangiogenesis) has become

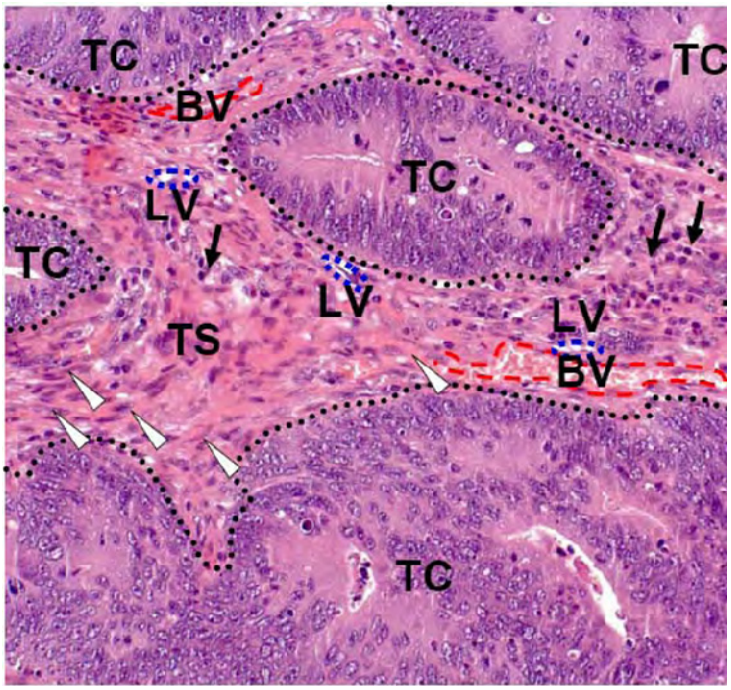

Figure 1. ***Histological heterogeneity of human cancers.*** A section of a human colon adenocarcinoma stained with hematoxylin-eosin showing a heterogeneous mixture of tumor cells (TC) and stromal cells including fibroblasts (white arrowheads), endothelial cells forming blood and lymphatic vessels (BV, LV; area of presence marked with dashed red or blue lines, respectively) and immune cells (black arrows), characteristic of most epithelial cancers.

one of the best studied host mediated responses to cancer [6, 7]. It involves the secretion of pro-angiogenic factors, such as endothelial growth factor (VEGF) by the tumor cells, which promotes the proliferation and migration of vascular endothelial cells and vessel sprouting

[8, 9]. Tumor blood vessels are morphological and functional different from their normal counterparts, they are irregularly shaped, dilated, tortuous and often have dead ends. Furthermore, tumor blood vessels carry distinct molecular markers in their endothelium, in the covering pericytes and in their ECM composition, which distinguishes them from the normal vasculature [10].

Cancer associated fibroblasts (CAFs) represent the major cellular component of the stroma in epithelial cancers and are the main source for connective tissue components in the ECM, including collagens and structural proteoglycans, as well as various classes of proteolytic enzymes, such as cysteine-, serine-, and matrix metalloproteases (MMPs) and a broad variety of growth factors [11]. Examples of growth factors that are highly expressed by CAFs include hepatocyte growth factor (HGF), members of the epidermal growth factors (EGFs), fibroblast growth factors (FGFs) and cytokines such as stromal-derived factor (SDF)-1 or IL-6 [12], contributing to the role of CAFs in enhancing the malignant epithelial transformation in several cancer models, whereas normal fibroblasts were reported to prevent progression of transformed epithelial cells [13-15].

Different subpopulations of stromal fibroblasts exist within tumors and are characterized by a partly overlapping expression of markers such as fibroblast activation protein alpha (FAPα) [16], α-smooth muscle actin (α-SMA)[17], platelet-derived growth factor (PDGF) receptors [18] and fibroblast specific protein (FSP)-1 [19]. This heterogeneity in marker expression may in part be explained by the diverse origin of CAFs, which are reported to be derived from resident local fibroblasts, bone-marrow derived progenitor cells or from transformed epithelial cells which have undergone epithelial-to-mesenchymal transition (EMT) during tumorigenesis [5, 20].

Several of these markers are being investigated as therapeutic targets in clinical studies and the identification and characterization of novel molecular stromal targets has been the focus of my undergraduate studies and of my PhD thesis. A summary of these investigations is presented here.

2.2 Endosialin/TEM1

Endosialin is a highly sialylated, C-type lectin-like surface receptor structurally related to thrombomodulin and complement receptor C1qRp [21]. First identified with a monoclonal antibody, mAb FB5 [22], endosialin was discovered independently through large scale expression profiling of human cancer endothelial cells with the SAGE (serial analysis of gene expression) method

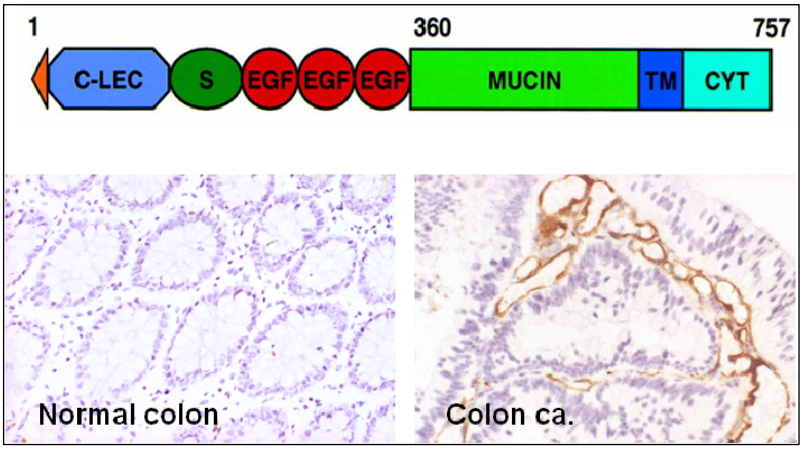

Figure 2. ***Endosialin domain architecture and expression patterns.*** The schematic molecular structure of endosialin is shown which consists of an N-terminal signal leader peptide (triangle), a C-type lectin domain (C-LEC), a Sushi/SCR/CCP domain (S), three EGF-like repeats (EGF), the mucin domain (MUCIN), the transmembrane domain (TM) and a short, cytoplasmic tail (CYT). In human tumors endosialin is specifically expressed by tumor endothelial cells, pericytes and activated tumor fibroblasts, as demonstrated by IHC on this colon adenocarcinoma. The protein is undetectable in normal tissues, as in the example of the normal colonic mucosa shown here [21].

leading to the alternative designation of tumor endothelial marker 1 (TEM1)[23]. Endosialin/TEM1 is expressed to varying degrees by tumor endothelial cells, pericytes and stromal fibroblasts in cancer samples [22, 24, 25], whereas the protein is undetectable in most normal tissues [26] (**Fig.2**). During my undergraduate studies, I analyzed the expression of endosialin/TEM1 during mouse embryonic development and its induction in cancers using xenograft models of human cancer. As the mAb FB5 did not show cross-reactivity with the mouse protein, we generated a mouse specific peptide antibody and characterized its specificity to bind to mouse endosialin by immunoblotting and by immunocytochemistry on mouse endosialin transfected 293T cells. Analysis of endosialin expression during mouse embryonic development by immunohistochemistry (IHC) revealed that the protein was selectively expressed by the endothelial cells of the dorsal aorta in 9.5-day embryos (**Fig.3**). At later stages (10.5 to 14.5 days p.c.) endosialin expression was found in the small capillaries of the perineural vascular plexus, in small capillaries, which invade the developing

brain as well as in the intersomitic vessels and in the vessels sprouting from the dorsal aorta. The endothelial nature of the stainings was confirmed using additional endothelial cell markers such as VEGFR2. In addition, endosialin expression was observed at certain epithelial/mesenchymal interfaces, most prominently at sites of tissue folding or

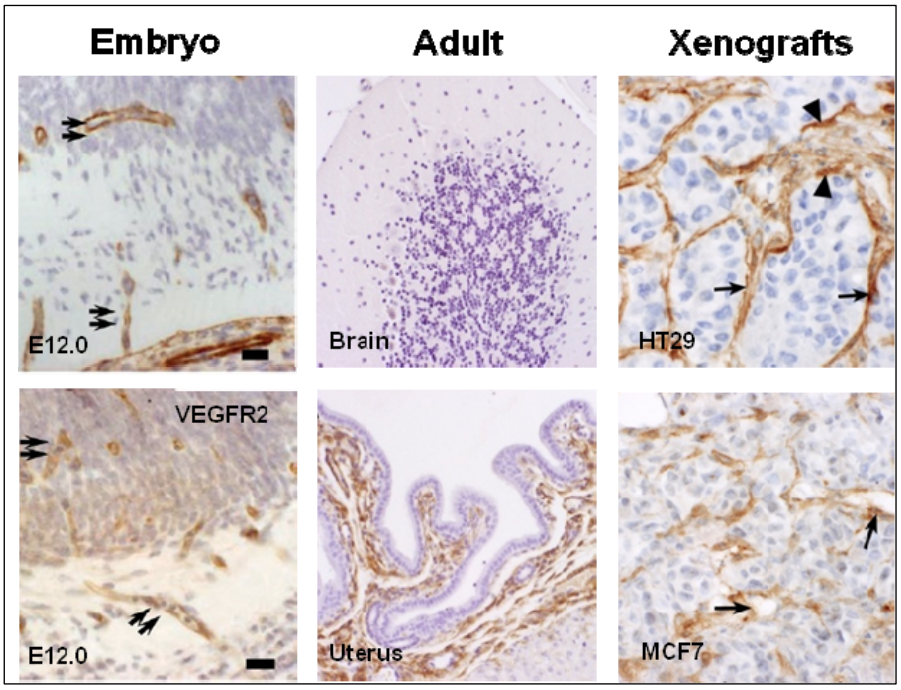

Figure 3. ***Endosialin expression during mouse embryonic development and in xenograft models.*** During embryonic mouse development endosialin is transiently expressed in small and medium-sized blood vessels, including those (double arrows) inside the brain. The number and pattern of endosialin-positive vessels is similar to those expressing VEGFR-2 (double arrows). Endosialin is undetectable in all vascular structures in the adult mouse as shown here on a section from the brain. The only adult tissue with endosialin expression was the uterus, with endosialin expression seen in fibroblastic stromal cells of the cycling endometrium. In subcutaneous cancer xenograft models, endosialin is induced in the host-derived tumor stroma, both in vascular endothelium (arrows) and in activated stromal fibroblasts (arrowheads) as shown for HT29 and MCF7 representing a colorectal carcinoma and a breast cancer model respectively [27].

invagination (e.g. optic cup, oropharynx, lung buds and hair follicles). In the adult mouse, endosialin/TEM1 was undetectable in blood vessels or mesenchymal cells in all organs examined, with the exception of the uterus, in which endosialin was present in the endometrial fibroblasts. Comparable to the expression patterns observed in human tumors, endosialin/TEM1, was found to be expressed by endothelial cells and fibroblasts in the tumor stroma of mouse xenograft models such as HT-29, COLO205, MCF7 and MDA-MB-231, representing examples of colorectal and breast cancer [27] (**Fig.3**).

An endosialin/TEM1 knock-out mouse model was generated [28], the mice were fertile and developed normally. However, when human HCT116 colon carcinoma cells were implanted orthotopically onto the serosal surface of the large intestine of nude endosialin -/- mice, both the tumor take and the growth rate were considerably reduced, indicating that

endosialin might play an important role in tumor progression [28]. Recent studies have shown that endosialin/TEM1 might interact with extracellular matrix components, including collagen type I, IV and fibronectin, suggesting that endosialin may be involved in promoting cell adhesion and migration processes during tumor invasion and metastasis [29]. A humanized Endosialin/TEM1 blocking antibody (MORAb-004) is currently in clinical studies and based on its ability to target the endothelial cells and the peri-vascular stromal component of the tumors it might provide a therapeutic benefit in a broad range of tumors.

2.3 Fibroblast activation protein alpha (FAPα)

Fibroblast activation protein alpha (FAPα) is an integral cell surface protein selectively expressed by activated stromal fibroblasts in several types of human epithelial cancers. In normal tissues, FAPα expression is highly restricted to developing organs, healing wounds, and tissue remodeling. Epithelial tumor cells and most normal adult human tissues lack FAPα expression [16, 22, 26, 30-32]. FAPα is a serine protease capable of degrading type I collagen which places FAPα into the group of enzymes involved in tumor tissue remodeling [30, 33, 34] (**Fig.4**).

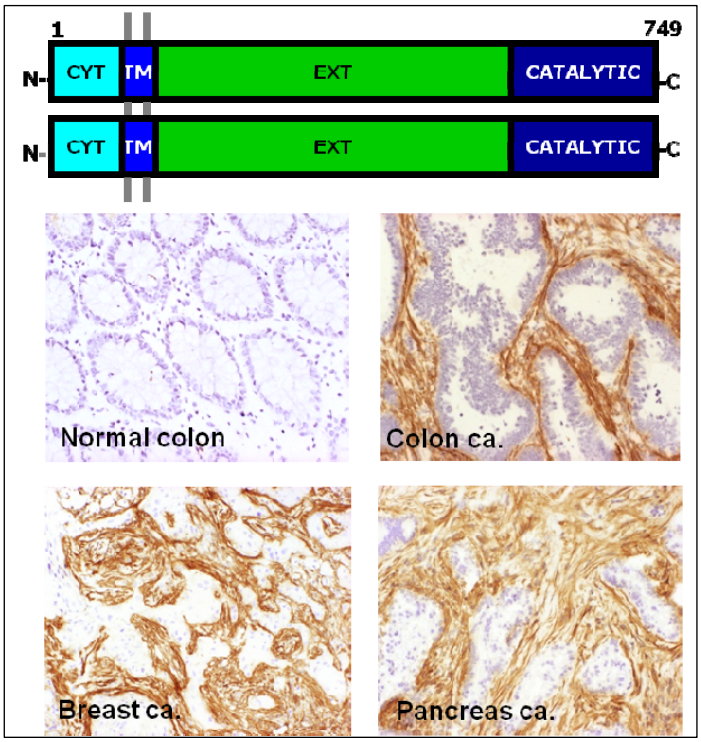

Figure 4. ***FAPα structure and function***. FAPα is a 95-kDa type II transmembrane glycoprotein and belongs to the post-proline dipeptidyl aminopeptidase family. The catalytic domain of FAPα contains a serine protease consensus sequence in which the catalytic triad has been identified. FAPα has been shown to function as a homodimer and is expressed in >90% of common human epithelial cancers by cancer associated fibroblasts as demonstrated here in colon, breast and pancreas carcinomas. FAPα is not detected in normal adult tissues, see example of normal colon [26, 35].

FAPα activity can be detected in tumor samples and shows a good correlation with FAPα expression detected by IHC [32, 34]. Based on its selective expression in the reactive stroma of many epithelial cancers, its lack of expression in normal adult tissues, and its protease activity, FAPα has proven an ideally suited stroma target to be exploited in the clinic. Two different approaches have been used to exploit FAPα as a therapeutic target in tumors. The first was to employ FAPα -specific monoclonal antibodies. Following this concept, we have recently developed a novel antibody-maytansinoid conjugate (FAP5-DM1), targeting a shared epitope of human, mouse and cynomolgus monkey FAPα. Using this conjugate in stroma-rich histotypic cancer xenograft models we were able to induce long-lasting inhibition of tumor growth and complete regressions in models of lung, pancreas and head and neck cancers, with no evidence of toxicity [36] (**Fig.5**).

The second approach was to target the enzymatic activity of FAPα with small molecule inhibitors such as PT-630, which was recently shown to result in a marked inhibition of tumor growth in xenograft and syngeneic mouse models [37].

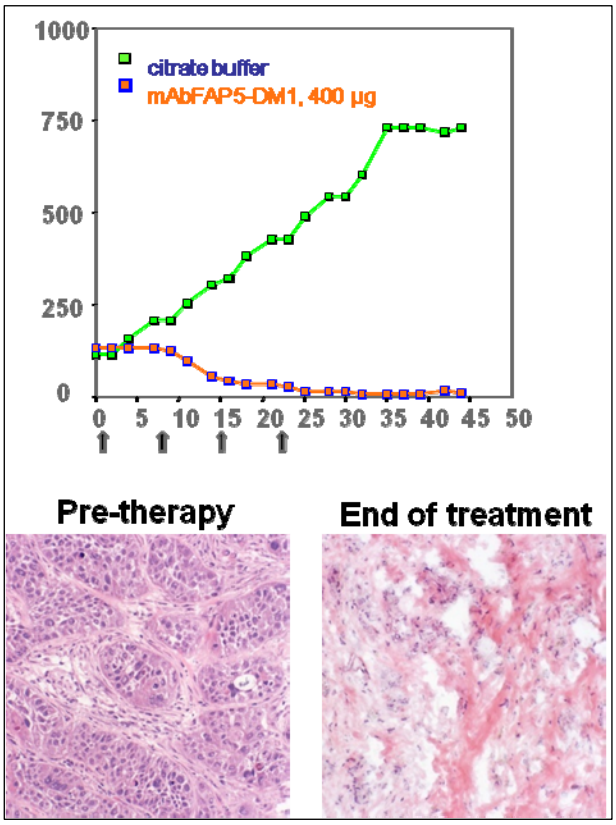

Figure 5. ***Efficacy of mAb FAP5-DM1 in human cancer xenograft models.*** Nude mice bearing established LXFA629 lung tumors were treated i.v. with either vehicle control (PBS; green, filled square) or mAb FAP5-DM1 at 400 µg/kg DM1 (purple, filled square) for four cycles.Tumor sizes are represented as median of six or eight mice. Arrows indicate days of treatment. Morphologic changes upon treatment are shown with H&E stained tissue sections. A connective tissue scar was observed to replace the tumors at the end of treatment [36].

2.4 iLCM screen: Identification of new tumor stroma targets by gene expression profiling

Transcriptional profiling of cancer specimens has provided novel insights into the molecular characterization of tumors. Expression signatures are being used to generate diagnostic tools and prognosis predictors and to provide new genetic markers that may serve as novel therapeutic targets [38-41]. Most of these studies have used bulk tumor samples, therefore the specific contribution of malignant epithelial cells and stromal cells to the signatures is unclear in most cases. The method of laser capture microdissection (LCM) to obtain selected populations of cells from tumors has provided considerable advantages to the bulk methods [2, 42]. However, as the challenge was to distinguish normal, resting stromal cells from reactive stromal changes in cancer tissues, LCM guided exclusively by general tissue stains, for instance haematoxylin/eosin (H&E) may not have been sufficient. For this purpose, we have implemented existing antibody labeling protocols [43, 44] and developed a novel protocol that reduced the critical staining time and enabled us to extract high quality RNA after the immuno-LCM (iLCM) procedure. Moreover, we used the highly sensitive Agilent RNA6000 Pico LabChip system to assess the RNA quality in our material before and after iLCM. Using these procedures, RNA from distinct tumor compartments was isolated, analyzed, amplified and used for transcription profiling [45] (**Fig.6**).

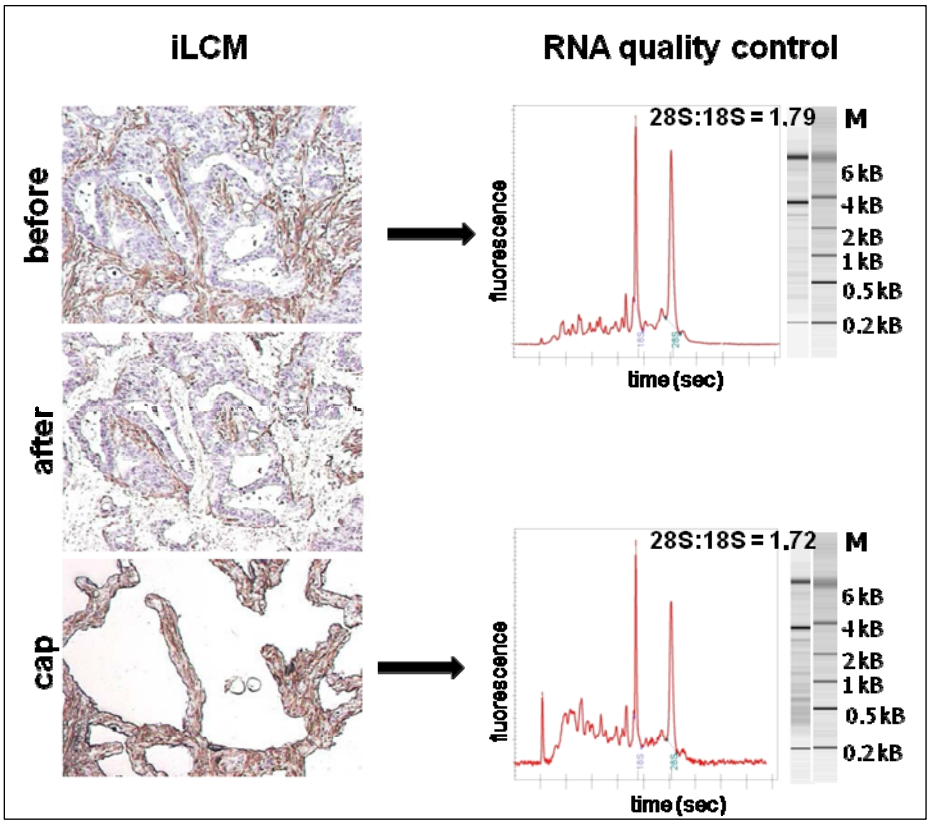

Figure 6. ***Immuno-LCM (iLCM).*** Laser capture microdissection (LCM) is a technology for rapid and easy procurement of pure cellular subpopulations from its complex tissue milieu, under direct microscopic visualization. To capture the selected cells, a thin polymer film is placed in direct contact with the section. A laser beam then activates the polymer and transfers the cells onto the polymer film. Using our protocol FAPα positive activated tumor fibroblasts were captured from colorectal cancer samples. The quality of the RNA was assessed with the Agilent Bioanalyzer. RNA quality was ranked as sufficient when the ratio between 28S and 18S rRNA peaks was above 1.70 [45].

In order to identify novel tumor stroma targets and to analyze the molecular pathways activated in CAFs, we examined a set of colon cancer samples including their normal tissue counterparts with our iLCM screen and performed whole genome Affymetrix GeneChip® analysis to obtain transcriptional signatures from the tumor cells and the activated tumor stroma that were compared with the expression profiles from normal colonic epithelium and normal fibroblasts, derived from the same patients (Rupp C et al., submitted) (**Fig.7**).

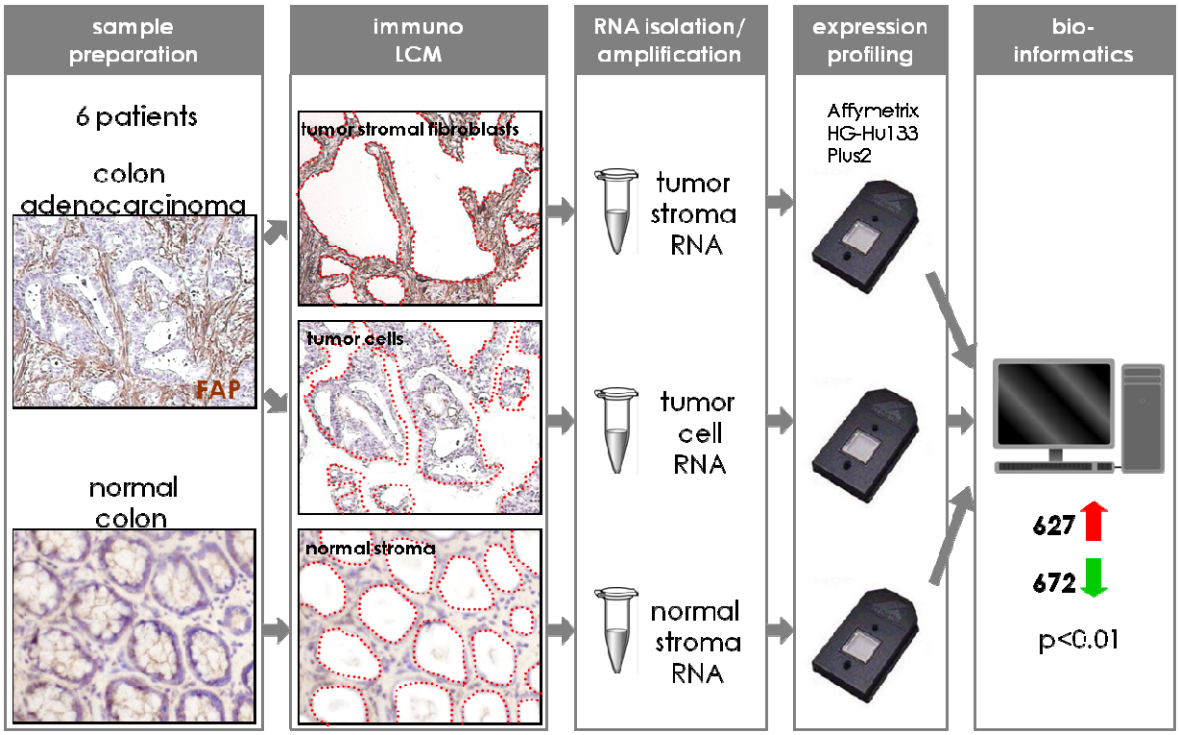

Figure 7. ***Work flow for identification of novel tumour stroma markers by expression profiling analysis.*** The antibody-guided laser capture microdissection allowed the separation of epithelial cells from the activated stromal compartment in colon cancer samples. Activated tumor stromal fibroblasts were visualized by immunohistochemical staining with an antibody to FAPα . In the figure, the borders between epithelial and stromal structures are indicated by red dotted lines. Normal fibroblasts were isolated from normal colonic tissue after hematoxylin staining and morphological examination. After RNA isolation and amplification whole genome Affymetrix GeneChip® analysis was performed followed by bioinformatic evaluation to identify novel tumor stroma targets. Numbers and arrows indicate the numbers of genes and their change in transcript levels; red: up, green: down.

After normalization and bioinformatic analysis, the three compartments (tumor cells, tumor stroma and normal stroma) could be clearly separated by unsupervised hierarchical cluster analysis. Among genes overexpressed in the tumor stroma *vs.* normal stroma we found well established tumor stroma markers such as PDGFRβ, FGFR1, MMP2 or FAPα, which was used as a marker for capturing activated fibroblasts. Interestingly, induced genes included several members of the Wnt-signaling pathway such as secreted frizzled-related protein 2 (SFRP2), WNT2, WNT5a or Wnt-1 induced protein 1 (WISP-1) (**Fig.8**). WISP-1 (Wnt-1 induced secreted protein 1) has recently been demonstrated to be induced in the tumor stroma in a paracrine fashion by Wnt-1 released by the tumor cells [46, 47] and to bind to biglycan on the fibroblast surface [48]. WNT5a, a gene involved in the non-canonical Wnt signaling, was recently shown to be induced in fibroblasts during cocultivation with a pancreatic carcinoma

cell line, suggesting that it could contribute to the strong desmoplastic reaction commonly found in this type of cancer [49].

For the further identification of tumor-stroma specific genes we used the gene-set enrichment analysis (GSEA) with two gene-set collections derived from the Molecular Signature Database (Broad Institute): the curated-gene sets, c2 and the c5 gene ontology (GO)-gene sets [50]. Among the GO datasets most significantly enriched were gene sets involved in wound healing, extracellular matrix deposition, inflammatory response, cell migration, cytokine activity, cell-matrix adhesion, vascular development, collagens, transmembrane receptor tyrosine kinase activity, cell-cell adhesion, angiogenesis, MMP activity, insulin receptor signaling and response to hypoxia (**Fig.8**). In addition, we identified 192 significantly enriched curated gene sets including gene sets related to hypoxia, epithelial-to-mesenchymal transition (EMT), IL-6 and TGFβ pathway activation.

Enriched hypoxia related gene sets contained several genes encoding angiogenic growth factors such as VEGFC or angiopoetin-like 4 (ANGPTL4). Other genes in that category encoded collagens (COL1A2, COL4A1, COL5A1, COL9A1 and COL18A1) and their modifying enzymes lysyl oxidases (LOXs) and lysyl oxidase-like 2 (LOXL2). Recently, collagen cross-linking has been identified as a critical regulator of desmoplasia implying that the nature and level of ECM cross-links could impact cancer risk and alter tumor behavior [51]. Lysyl oxidases are copper-dependent amine oxidases that initiate the process of covalent intra- and intermolecular cross-linking of collagens [52]. They are up-regulated in many types of cancer [53] and are induced by hypoxia inducible factor (HIF-1) and TGFβ, two key regulators of tumor growth [54]. Interesting examples for enriched genes related to IL-6 treatment comprised several pro-inflammatory cytokines such as CXCL3 or IL-6 itself. IL-6 is induced during wound healing, is up-regulated in fibroblasts during fibrosis and is associated with chronic inflammatory disease such as rheumatoid arthritis [55]. Gene-sets involved in EMT included the mesenchymal marker N-cadherin (CDH2), several tumor promoting matrix metalloproteinases such as MMP2 or MMP12 and extracellular matrix proteins implicated in invasion and metastasis including tenascin C (TNC), laminin B1 (LAMB1) or secreted protein acidic and rich in cysteine (SPARC). Many of these EMT related genes were also found among TGFβ induced gene sets, together with genes encoding fibrillar collagens (COL1A1, COL1A2, COL3A1 and COL5A2) and members of the insulin-like growth factor binding proteins family,

such as IGFBP3, and IGFBP5. Both proteins are implicated in the initiation and/or perpetuation of fibrosis by inducing the production of extracellular matrix components [56].

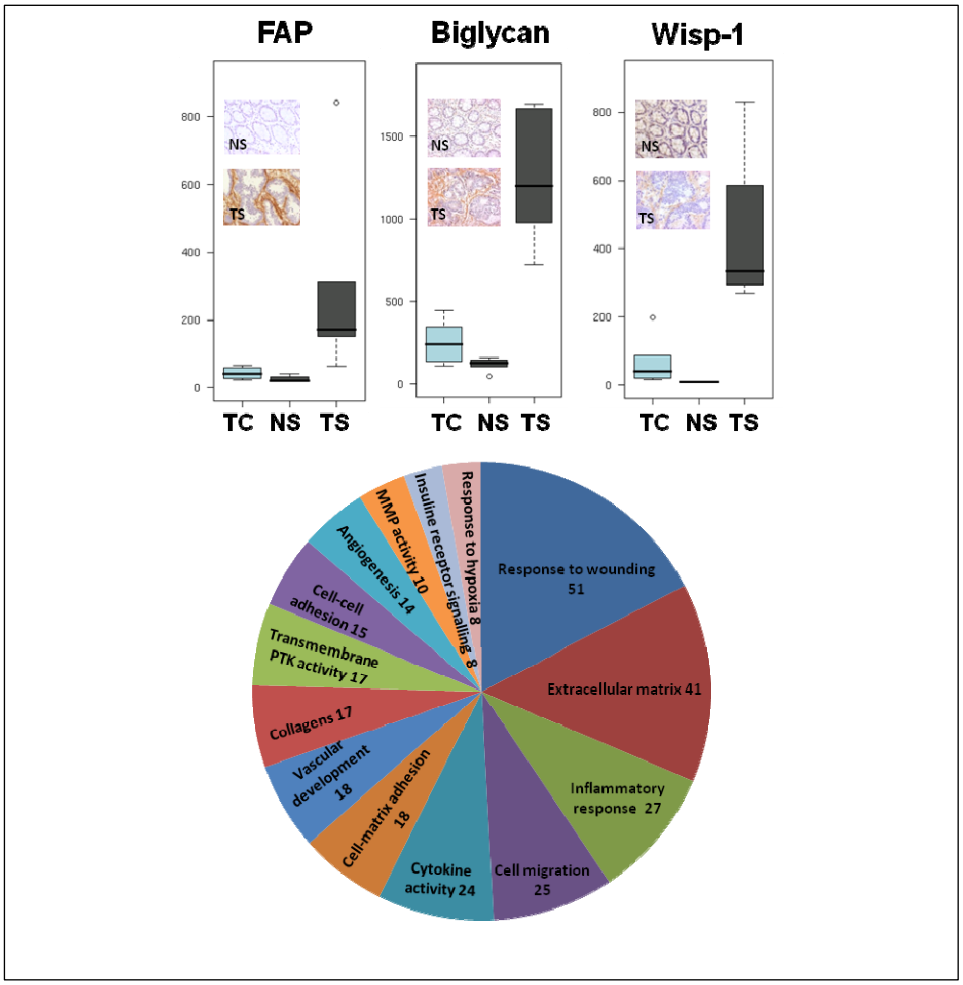

Figure 8. ***Genes and gene-sets induced in the tumor stroma*.** Well characterized tumor stroma markers such as FAPα , biglycan or Wisp-1 were found to be significantly elevated in the tumor stroma compartment *vs.* the normal stroma. The expression levels are indicated by whisker box plots, the bold centre-line indicates the median; the box represents the interquartile range (IQR). Whiskers extend to 1.5 times the IQR. TC, tumor cells; NS, normal stroma; TS, tumor stroma. Immunohistochemical stainings demonstrate the induction of these genes at the protein level (inserts). Gene-Set Enrichment Analysis (GSEA) revealed gene sets involved in response to wounding, extracellular matrix deposition, inflammatory response and cell migration significantly upregulated in the tumor stroma. The number of enchriched genes in each category are represented in a pie chart.

CAF induced fibrosis has been demonstrated to contribute to the early stages of malignant transformation and to the contraction of the interstitial space, which is believed to be a key contributor to the higher interstitial fluid pressure frequently found in solid tumors [57].

Another TGFβ target, IGFBP7 [58], has appeared as one of the most significantly induced tumor stroma markers in our screen and the following section of this summary will deal with the characterization of this molecule (**Fig.9**).

2.5 Characterization of insulin-like growth factor binding protein 7 (IGFBP7)

Insulin-like growth factor binding protein 7 (IGFBP7) or IGFBP-related protein 1 (IGFBP-rp1) is a secreted protein and belongs to a group of low-affinity IGF binders, which have been implicated in diverse biological roles independent of their ability to bind IGF. Numerous studies demonstrated their direct association with a variety of extracellular and

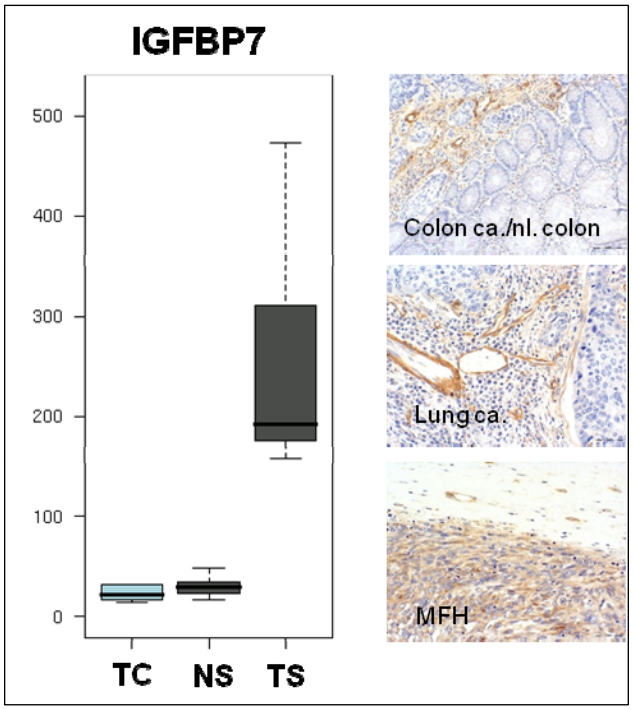

Figure 9. ***Induction of IGFBP7 in the tumor stroma.*** The whisker box plot shows the induction of IGFBP7 in the tumor stroma (TC, tumor cells; NS, normal stroma; TS, tumor stroma). As demonstrated by immunohistochemical staining on representative examples of colon and lung carcinomas, IGFBP7 is expressed in cancer associated fibroblasts and tumor vessels in those epithelial cancer samples. In soft tissue sarcomas, such as MFH (malignant fibrous histiocytoma), IGFBP7 is expressed by the malignant mesenchyme-derived cells.

cell surface molecules with effects on cell proliferation and adhesion [59, 60]. The cDNA of IGFBP7 was originally designated mac25 and shown to be expressed in normal human leptomeningial cells but scarcely in meningiomas [61]. A mouse homolog, sharing 94,4 % overall sequence homology to human IGFBP7 has been identified [62]. IGFBP7 knock-out mice showed significant changes in ovaries, muscle tissues and liver even though the mice were viable [63].

The IGFBP7 protein contains 256 amino acids, with molecular mass of 33 kDa. IGFBP7 is a cell adhesion glycoprotein, which is regulated by proteolytic cleavage into a two-chain form by

the membrane-bound serine protease matriptase (MT1-SP1) [64]. IGFBP7 is expressed in blood vessels in various human cancer tissues including and it is therefore also referred to as "angiomodulin" [61, 65]. Previous studies have shown that IGFBP7 is a selective biomarker for tumor-associated vessels in glioblastoma, that it is pro-angiogenic and induced by Smad-2 dependent TGFβ signaling [58]. Variable IGFBP7 expression in tumor cells has also been reported in different tumor types and the expression to be modulated by DNA methylation, retinoic acid and TGFβ [59, 66, 67]. In this context, some studies suggested that IGFBP7 might function as a secreted tumor suppressor [66, 68, 69].

IGFBP7 was found as one of the most significantly induced tumor stroma target in our iLCM screen. Immunohistochemical analysis showed IGFBP7 to be expressed in tumor associated vessels and activated tumor fibroblasts in colorectal cancer samples. Further stainings of different tumor types revealed that IGFBP7 is frequently induced in the stromal compartment of epithelial cancers and that in soft tissue sarcomas, IGFBP7, is expressed by the malignant mesenchymal cells. (**Fig.9**). The expression in malignant mesenchymal cells was also confirmed by Western blotting on a panel of cell lines, including the fibrosarcoma line HT1080. Moreover, high expression of IGFBP7 was observed in cancer cell lines which have undergone EMT , such as Caki-1 and SW480, whereas colon cancer cell lines which maintained an epithelial phenotype such as LS174T, HT-29, DLD-1 lacked IGFBP7 expression. To establish the potential role of IGFBP7, shRNA mediated knock-down experiments were carried out in HT1080 and Caki-1 cells. The knock-down resulted in >90% reduction of IGFBP7 on the protein level and in a significant reduction in the number of colonies growing anchorage independently in soft-agar culture, indicating that in those cells IGFBP7 acts as a promoter of anchorage-independent growth (**Fig.10**). On the other hand, we could show that IGFBP7 reduces anchorage-independent growth when overexpressed in tumor cells with an epithelial phenotype such as in the colon cancer cell line DLD-1 and that in those cells, IGFBP7 is present as a two-chain form, which previously has been reported to result from proteolytic cleavage by the type II transmembrane serine protease matriptase [64]. Matriptase is a strictly epithelial serine protease and processing of IGFBP7 by this enzyme was shown to greatly reduce its insulin / IGF-dependent growth promoting activity and to enhance its adhesion activity [64].

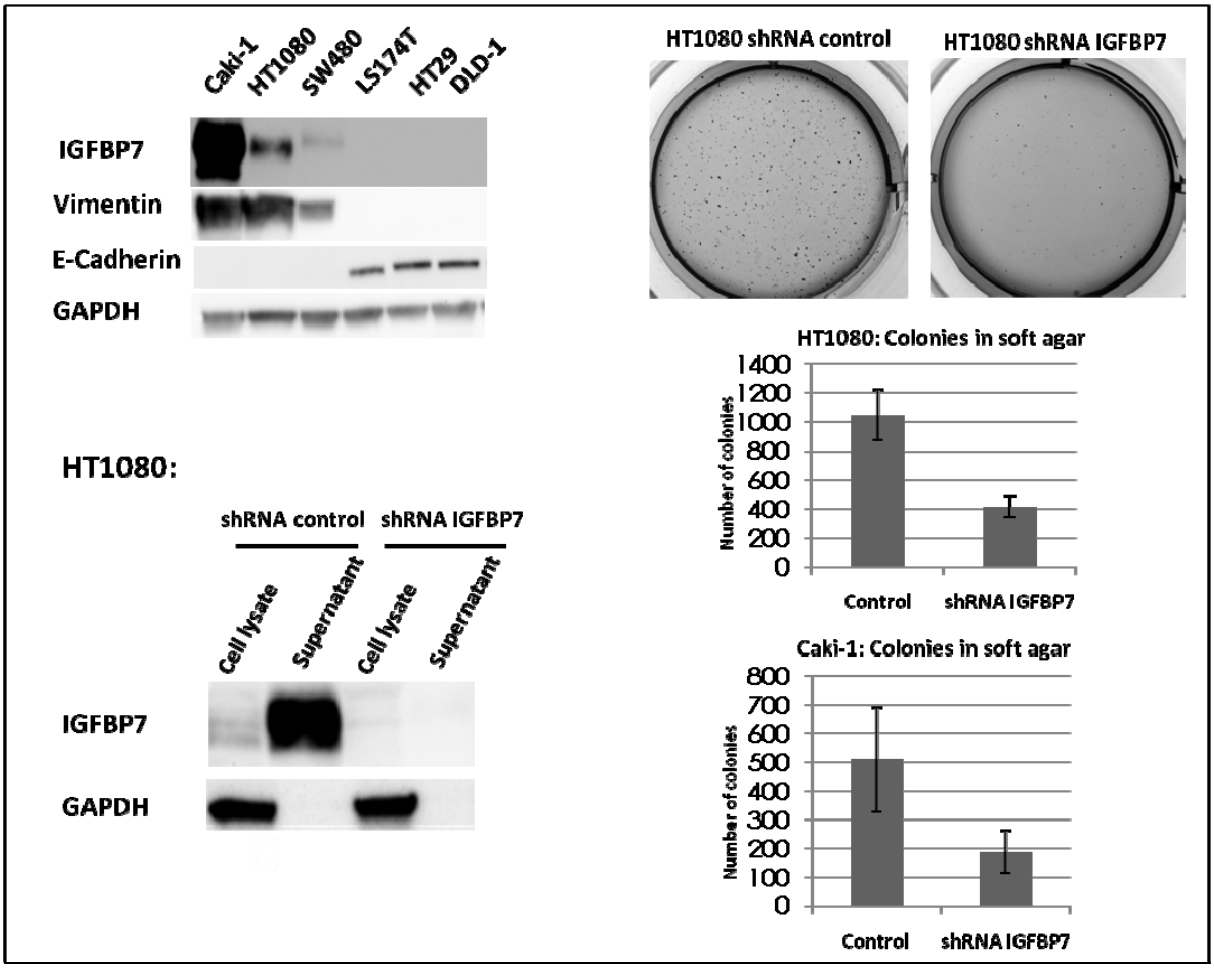

Figure 10. ***IGFBP7 is expressed by malignant mesenchyme-derived cells and tumor cells with a mesenchymal phenotype and promotes anchorage-independent growth in these cells.*** As demonstrated by Western blotting, IGFBP7 is expressed by fibrosarcoma cells HT1080 and epithelial cells with a mesenchymal phenotype (Caki-1, SW480). Tumor cells with an epithelial phenotype (LS174T, HT29,DLD-1, Colo205) are IGFBP7 negative. E-cadherin and vimentin were used as markers to determine the phenotype of the cell lines. GAPDH was used as a loading control. Soluble IGFBP7 was detected in the supernatant, vimentin, E-Cadherin and GAPDH in the corresponding cell lysates. In HT1080 cells, shRNA mediated IGFBP7 knock-down resulted in >90% protein reduction in the supernatant and a significant reduction of anchorage independent growth in soft agar. The graphs show the average results of three independent experiments.

Thus, IGFBP7 might act as a tumor suppressor secreted by fibroblasts and endothelial cells during early-stage tumorigenesis and as a promoter of tumorigenesis, when tumor cells have acquired a mesenchymal phenotype after undergoing EMT. To further substantiate this model, we have knocked-down E-cadherin in DLD-1 cells. These knock-down cells displayed a mesenchymal phenotype, activation of β-catenin and a significant induction of IGFBP7 expression in comparison to the control cells. These results are comparable to the data

demonstrating the induction of IGFBP7 following E-cadherin knock-down in a breast cancer model sytem [70].

In summary, we have shown that cancer-associated fibroblasts express increased levels of genes related to EMT and TGFβ-induction and that IGFBP7, a tumor stroma marker and potential TGFβ target might have a dual function as a tumor suppressor of tumor growth during early tumorigenesis or as a promoter of tumor growth in later stages .

2.6 3D in vitro model system to study tumor - tumor stroma interactions

In order to study the molecular mechanism that control the heterotypic tumor - tumor stroma interactions *in vitro*, we have developed a novel 3D *in vitro* co-culture system, which recapitulates the tumor heterogeneity observed *in vivo* (Dolznig H et al., submitted) (**Fig.11**). Cells grown in three-dimensional (3D) scaffolds or as 3D multicellular spheroids more closely resemble the architecture of tissues and tumors *in vivo* than conventional 2D cultures. Moreover, they offer the opportunity to analyze the activation of differentiation programs and the pathways involved in cell migration and invasion as the tumor cells in this model are grown in a heterotypic and physiologically relevant context [11, 71, 72]. Organotypic 3D co-culture models have been used to study the functional interplay between genetically altered epithelial cells and fibroblasts [73, 74] and to study fibroblast-led invasion in models of skin, breast, pancreatic and brain cancers [75, 76].

Our novel experimental set-up combined multi-cellular spheroids, 3D collagen gel cultures and co-cultures of human epithelial cancer cells with normal human fibroblasts or CAFs in one assay (**Fig.11**). We have used this novel 3D system for molecular analysis and have established transcriptional profiles from the different cellular components grown in collagen gels in mono-cultures and compared the gene expression responses induced upon co-cultivation. Intriguingly, we observed a remarkable concordance between the gene sets obtained in our *ex vivo* study and this *in vitro* co-culture system. Gene-Set Enrichment Analysis (GSEA) and Pathway analysis (Ingenuity®) revealed datasets and gene-networks that were significantly enriched in both screens. Gene-sets involved in extracellular matrix deposition, angiogenesis, wound healing and EMT were significantly up-regulated in both studies. Many of the genes identified in our study have been reported in studies performed *in vitro* including the “wound response signature” of fibroblasts in response to serum

stimulation [77] a hypoxia-associated response [78] as well as the signatures obtained from co-cultures of cancer cells and fibroblasts cell lines of different origins [79, 80]. Using independent datasets from human cancers, it was shown that the "wound-response signature" was strongly predictive of metastasis and progression in breast, lung and gastric cancers and was an independent predictor of outcome in a follow-up study in breast cancer [77].

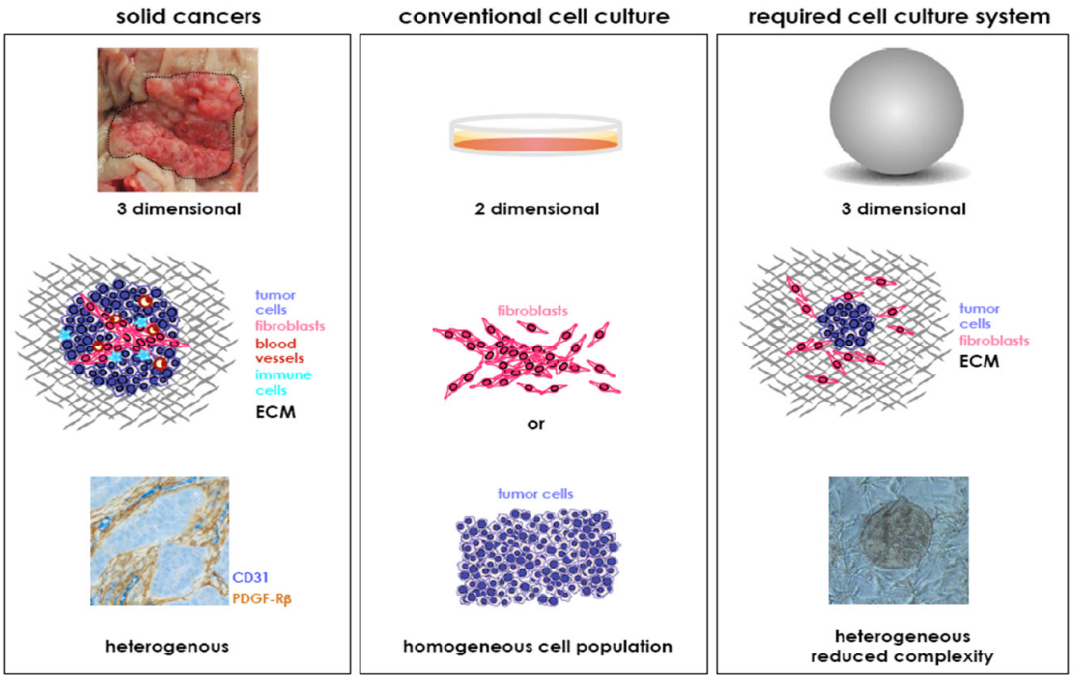

Fig ure 11. ***Modelling adenocarciomas in vitro.*** Carcinomas are heterogeneous mixtures of malignant cells and stromal cells and grow as three dimensional structures. An example for this heterogeneity is shown in a histologic picture from a human non-small cell lung cancer (left panel). Tumor cell clusters (blue) are separated by strands of activated fibroblasts which are PDGFR-β positive (brown) and blood vessels with CD31 positive endothelial cells (dark blue). In conventional cell culture models, cells are grown as homogeneous cultures on plastic surfaces. Using 3D cultures in the presence of ECM components, the heterotypic interactions of tumor cells and stromal cells can be studied in detail. A phase contrast picture of this model shows a culture of tumor cells grown as a multicellular spheroid, co-cultured with fibroblast embedded in a collagen I gel, recapitulating the in vivo heterogeneity**.**

In summary, our results demonstrate that our 3D co-culture system is a powerful tool to identify molecules involved in the paracrine tumor – stroma interactions. Furthemore, the model can be used to study the function of new molecular targets and to test the outcome of new drugs.

2.7 Summary & conclusions

The rapid progress of research in molecular cancer biology has contributed to a better understanding of the role of the tumor stroma during tumor growth and metastasis formation and has led to the identification of selected tumor stroma markers that serve as targets for novel therapies.

The core objectives of my studies were based on two complementary approaches, the identification of novel tumor stroma targets in human tumor samples using whole genome Affymetrix Gene-Chip® analysis and the validation of these targets in a newly established 3D co-culture model which mimics the cellular and molecular heterogeneity of human cancers. A number of monoclonal antibodies, small-molecule inhibitors and anti-sense approaches have been developed and investigated in pre-clinical models, some of these molecules have recently entered clinical development. Refining our understanding of the molecular mechanisms that control the tumor-stroma interaction will contribute to the development of more personalized medicines.

2.8 References

1. Tlsty, T.D., and Coussens, L.M. (2006). Tumor stroma and regulation of cancer development. Annu Rev Pathol *1*, 119-150.

2. Finak, G., Bertos, N., Pepin, F., Sadekova, S., Souleimanova, M., Zhao, H., Chen, H., Omeroglu, G., Meterissian, S., Omeroglu, A., et al. (2008). Stromal gene expression predicts clinical outcome in breast cancer. Nat Med *14*, 518-527.

3. Farmer, P., Bonnefoi, H., Anderle, P., Cameron, D., Wirapati, P., Becette, V., Andre, S., Piccart, M., Campone, M., Brain, E., et al. (2009). A stroma-related gene signature predicts resistance to neoadjuvant chemotherapy in breast cancer. Nat Med *15*, 68-74.

4. Scaife, C.L., Shea, J., Emerson, L., Boucher, K., Firpo, M.A., Beckerle, M.C., and Mulvihill, S.J. Prognostic significance of PINCH signaling in human pancreatic ductal adenocarcinoma. HPB (Oxford) *12*, 352-358.

5. Ostman, A., and Augsten, M. (2009). Cancer-associated fibroblasts and tumor growth--bystanders turning into key players. Curr Opin Genet Dev *19*, 67-73.

6. Folkman, J. (1985). Tumor angiogenesis. Adv Cancer Res *43*, 175-203.

7. Hilberg, F., Roth, G.J., Krssak, M., Kautschitsch, S., Sommergruber, W., Tontsch-Grunt, U., Garin-Chesa, P., Bader, G., Zoephel, A., Quant, J., et al. (2008). BIBF 1120: triple

angiokinase inhibitor with sustained receptor blockade and good antitumor efficacy. Cancer Res *68*, 4774-4782.

8. Kim, K.J., Li, B., Winer, J., Armanini, M., Gillett, N., Phillips, H.S., and Ferrara, N. (1993). Inhibition of vascular endothelial growth factor-induced angiogenesis suppresses tumour growth in vivo. Nature *362*, 841-844.

9. Amatschek, S., Kriehuber, E., Bauer, W., Reininger, B., Meraner, P., Wolpl, A., Schweifer, N., Haslinger, C., Stingl, G., and Maurer, D. (2007). Blood and lymphatic endothelial cell-specific differentiation programs are stringently controlled by the tissue environment. Blood *109*, 4777-4785.

10. Ruoslahti, E. (2002). Specialization of tumour vasculature. Nat Rev Cancer *2*, 83-90.

11. Kunz-Schughart, L.A., and Knuechel, R. (2002). Tumor-associated fibroblasts (part I): Active stromal participants in tumor development and progression? Histol Histopathol *17*, 599-621.

12. Bhowmick, N.A., Neilson, E.G., and Moses, H.L. (2004). Stromal fibroblasts in cancer initiation and progression. Nature *432*, 332-337.

13. Nakamura, T., Matsumoto, K., Kiritoshi, A., and Tano, Y. (1997). Induction of hepatocyte growth factor in fibroblasts by tumor-derived factors affects invasive growth of tumor cells: in vitro analysis of tumor-stromal interactions. Cancer Res *57*, 3305-3313.

14. Olumi, A.F., Grossfeld, G.D., Hayward, S.W., Carroll, P.R., Tlsty, T.D., and Cunha, G.R. (1999). Carcinoma-associated fibroblasts direct tumor progression of initiated human prostatic epithelium. Cancer Res *59*, 5002-5011.

15. Orimo, A., Gupta, P.B., Sgroi, D.C., Arenzana-Seisdedos, F., Delaunay, T., Naeem, R., Carey, V.J., Richardson, A.L., and Weinberg, R.A. (2005). Stromal fibroblasts present in invasive human breast carcinomas promote tumor growth and angiogenesis through elevated SDF-1/CXCL12 secretion. Cell 121, 335-348.

16. Garin-Chesa, P., Old, L.J., and Rettig, W.J. (1990). Cell surface glycoprotein of reactive stromal fibroblasts as a potential antibody target in human epithelial cancers. Proc Natl Acad Sci U S A *87*, 7235-7239.

17. Desmouliere, A., Guyot, C., and Gabbiani, G. (2004). The stroma reaction myofibroblast: a key player in the control of tumor cell behavior. Int J Dev Biol *48*, 509-517.

18. Ostman, A., and Heldin, C.H. (2007). PDGF receptors as targets in tumor treatment. Adv Cancer Res *97*, 247-274.

19. Egeblad, M., Littlepage, L.E., and Werb, Z. (2005). The fibroblastic coconspirator in cancer progression. Cold Spring Harb Symp Quant Biol *70*, 383-388.

20. Orimo, A., and Weinberg, R.A. (2007). Heterogeneity of stromal fibroblasts in tumors. Cancer Biol Ther *6*, 618-619.

21. Christian, S., Ahorn, H., Koehler, A., Eisenhaber, F., Rodi, H.P., Garin-Chesa, P., Park, J.E., Rettig, W.J., and Lenter, M.C. (2001). Molecular cloning and characterization of endosialin, a C-type lectin-like cell surface receptor of tumor endothelium. J Biol Chem *276*, 7408-7414.

22. Rettig, W.J., Garin-Chesa, P., Healey, J.H., Su, S.L., Jaffe, E.A., and Old, L.J. (1992). Identification of endosialin, a cell surface glycoprotein of vascular endothelial cells in human cancer. Proc Natl Acad Sci U S A *89*, 10832-10836.

23. St Croix, B., Rago, C., Velculescu, V., Traverso, G., Romans, K.E., Montgomery, E., Lal, A., Riggins, G.J., Lengauer, C., Vogelstein, B., et al. (2000). Genes expressed in human tumor endothelium. Science *289*, 1197-1202.

24. MacFadyen, J.R., Haworth, O., Roberston, D., Hardie, D., Webster, M.T., Morris, H.R., Panico, M., Sutton-Smith, M., Dell, A., van der Geer, P., et al. (2005). Endosialin (TEM1, CD248) is a marker of stromal fibroblasts and is not selectively expressed on tumour endothelium. FEBS Lett *579*, 2569-2575.

25. Brady, J., Neal, J., Sadakar, N., and Gasque, P. (2004). Human endosialin (tumor endothelial marker 1) is abundantly expressed in highly malignant and invasive brain tumors. J Neuropathol Exp Neurol *63*, 1274-1283.

26. Dolznig, H., Schweifer, N., Puri, C., Kraut, N., Rettig, W.J., Kerjaschki, D., and Garin-Chesa, P. (2005). Characterization of cancer stroma markers: in silico analysis of an mRNA expression database for fibroblast activation protein and endosialin. Cancer Immun *5*, 10.

27. Rupp, C., Dolznig, H., Puri, C., Sommergruber, W., Kerjaschki, D., Rettig, W.J., and Garin-Chesa, P. (2006). Mouse endosialin, a C-type lectin-like cell surface receptor: expression during embryonic development and induction in experimental cancer neoangiogenesis. Cancer Immun *6*, 10.

28. Nanda, A., Karim, B., Peng, Z., Liu, G., Qiu, W., Gan, C., Vogelstein, B., St Croix, B., Kinzler, K.W., and Huso, D.L. (2006). Tumor endothelial marker 1 (Tem1) functions in the growth and progression of abdominal tumors. Proc Natl Acad Sci U S A *103*, 3351-3356.

29. Tomkowicz, B., Rybinski, K., Foley, B., Ebel, W., Kline, B., Routhier, E., Sass, P., Nicolaides, N.C., Grasso, L., and Zhou, Y. (2007). Interaction of endosialin/TEM1 with extracellular matrix proteins mediates cell adhesion and migration. Proc Natl Acad Sci U S A *104*, 17965-17970.

30. Niedermeyer, J., Scanlan, M.J., Garin-Chesa, P., Daiber, C., Fiebig, H.H., Old, L.J., Rettig, W.J., and Schnapp, A. (1997). Mouse fibroblast activation protein: molecular cloning, alternative splicing and expression in the reactive stroma of epithelial cancers. Int J Cancer *71*, 383-389.

31. Niedermeyer, J., Garin-Chesa, P., Kriz, M., Hilberg, F., Mueller, E., Bamberger, U., Rettig, W.J., and Schnapp, A. (2001). Expression of the fibroblast activation protein during mouse embryo development. Int J Dev Biol *45*, 445-447.

32. Huber, M.A., Kraut, N., Park, J.E., Schubert, R.D., Rettig, W.J., Peter, R.U., and Garin-Chesa, P. (2003). Fibroblast activation protein: differential expression and serine protease activity in reactive stromal fibroblasts of melanocytic skin tumors. J Invest Dermatol *120*, 182-188.

33. Scanlan, M.J., Raj, B.K., Calvo, B., Garin-Chesa, P., Sanz-Moncasi, M.P., Healey, J.H., Old, L.J., and Rettig, W.J. (1994). Molecular cloning of fibroblast activation protein alpha, a member of the serine protease family selectively expressed in stromal fibroblasts of epithelial cancers. Proc Natl Acad Sci U S A *91*, 5657-5661.

34. Park, J.E., Lenter, M.C., Zimmermann, R.N., Garin-Chesa, P., Old, L.J., and Rettig, W.J. (1999). Fibroblast activation protein, a dual specificity serine protease expressed in reactive human tumor stromal fibroblasts. J Biol Chem *274*, 36505-36512.

35. Niedermeyer, J., Enenkel, B., Park, J.E., Lenter, M., Rettig, W.J., Damm, K., and Schnapp, A. (1998). Mouse fibroblast-activation protein--conserved Fap gene organization and biochemical function as a serine protease. Eur J Biochem *254*, 650-654.

36. Ostermann, E., Garin-Chesa, P., Heider, K.H., Kalat, M., Lamche, H., Puri, C., Kerjaschki, D., Rettig, W.J., and Adolf, G.R. (2008). Effective immunoconjugate therapy in cancer models targeting a serine protease of tumor fibroblasts. Clin Cancer Res *14*, 4584-4592.

37. Santos, A.M., Jung, J., Aziz, N., Kissil, J.L., and Pure, E. (2009). Targeting fibroblast activation protein inhibits tumor stromagenesis and growth in mice. J Clin Invest *119*, 3613-3625.

38. Alizadeh, A.A., Eisen, M.B., Davis, R.E., Ma, C., Lossos, I.S., Rosenwald, A., Boldrick, J.C., Sabet, H., Tran, T., Yu, X., et al. (2000). Distinct types of diffuse large B-cell lymphoma identified by gene expression profiling. Nature *403*, 503-511.

39. van 't Veer, L.J., Dai, H., van de Vijver, M.J., He, Y.D., Hart, A.A., Mao, M., Peterse, H.L., van der Kooy, K., Marton, M.J., Witteveen, A.T., et al. (2002). Gene expression profiling predicts clinical outcome of breast cancer. Nature *415*, 530-536.

40. Ramaswamy, S., Ross, K.N., Lander, E.S., and Golub, T.R. (2003). A molecular signature of metastasis in primary solid tumors. Nat Genet *33*, 49-54.

41. Amatschek, S., Koenig, U., Auer, H., Steinlein, P., Pacher, M., Gruenfelder, A., Dekan, G., Vogl, S., Kubista, E., Heider, K.H., et al. (2004). Tissue-wide expression profiling using cDNA subtraction and microarrays to identify tumor-specific genes. Cancer Res *64*, 844-856.

42. Casey, T., Bond, J., Tighe, S., Hunter, T., Lintault, L., Patel, O., Eneman, J., Crocker, A., White, J., Tessitore, J., et al. (2009). Molecular signatures suggest a major role for stromal cells in development of invasive breast cancer. Breast Cancer Res Treat *114*, 47-62.

43. Simone, N.L., Bonner, R.F., Gillespie, J.W., Emmert-Buck, M.R., and Liotta, L.A. (1998). Laser-capture microdissection: opening the microscopic frontier to molecular analysis. Trends Genet *14*, 272-276.

44. Fend, F., Emmert-Buck, M.R., Chuaqui, R., Cole, K., Lee, J., Liotta, L.A., and Raffeld, M. (1999). Immuno-LCM: laser capture microdissection of immunostained frozen sections for mRNA analysis. Am J Pathol *154*, 61-66.

45. Rupp, C., Dolznig, H., Puri, C., Schweifer, N., Sommergruber, W., Kraut, N., Rettig, W.J., Kerjaschki, D., and Garin-Chesa, P. (2006). Laser capture microdissection of epithelial cancers guided by antibodies against fibroblast activation protein and endosialin. Diagn Mol Pathol *15*, 35-42.

46. Pennica, D., Swanson, T.A., Welsh, J.W., Roy, M.A., Lawrence, D.A., Lee, J., Brush, J., Taneyhill, L.A., Deuel, B., Lew, M., et al. (1998). WISP genes are members of the connective tissue growth factor family that are up-regulated in wnt-1-transformed cells and aberrantly expressed in human colon tumors. Proc Natl Acad Sci U S A *95*, 14717-14722.

47. Xu, L., Corcoran, R.B., Welsh, J.W., Pennica, D., and Levine, A.J. (2000). WISP-1 is a Wnt-1- and beta-catenin-responsive oncogene. Genes Dev *14*, 585-595.

48. Desnoyers, L., Arnott, D., and Pennica, D. (2001). WISP-1 binds to decorin and biglycan. J Biol Chem *276*, 47599-47607.

49. Pilarsky, C., Ammerpohl, O., Sipos, B., Dahl, E., Hartmann, A., Wellmann, A., Braunschweig, T., Lohr, M., Jesnowski, R., Friess, H., et al. (2008). Activation of Wnt signaling in stroma from pancreatic cancer identified by gene expression profiling. J Cell Mol Med *12*, 2823-2835.

50. Subramanian, A., Tamayo, P., Mootha, V.K., Mukherjee, S., Ebert, B.L., Gillette, M.A., Paulovich, A., Pomeroy, S.L., Golub, T.R., Lander, E.S., et al. (2005). Gene set enrichment analysis: a knowledge-based approach for interpreting genome-wide expression profiles. Proc Natl Acad Sci U S A *102*, 15545-15550.

51. Levental, K.R., Yu, H., Kass, L., Lakins, J.N., Egeblad, M., Erler, J.T., Fong, S.F., Csiszar, K., Giaccia, A., Weninger, W., et al. (2009). Matrix crosslinking forces tumor progression by enhancing integrin signaling. Cell *139*, 891-906.

52. Kagan, H.M., and Li, W. (2003). Lysyl oxidase: properties, specificity, and biological roles inside and outside of the cell. J Cell Biochem *88*, 660-672.

53. Erler, J.T., Bennewith, K.L., Cox, T.R., Lang, G., Bird, D., Koong, A., Le, Q.T., and Giaccia, A.J. (2009). Hypoxia-induced lysyl oxidase is a critical mediator of bone marrow cell recruitment to form the premetastatic niche. Cancer Cell *15*, 35-44.

54. Postovit, L.M., Abbott, D.E., Payne, S.L., Wheaton, W.W., Margaryan, N.V., Sullivan, R., Jansen, M.K., Csiszar, K., Hendrix, M.J., and Kirschmann, D.A. (2008). Hypoxia/reoxygenation: a dynamic regulator of lysyl oxidase-facilitated breast cancer migration. J Cell Biochem *103*, 1369-1378.

55. Tan, P.L., Farmiloe, S., Yeoman, S., and Watson, J.D. (1990). Expression of the interleukin 6 gene in rheumatoid synovial fibroblasts. J Rheumatol *17*, 1608-1612.

56. Pilewski, J.M., Liu, L., Henry, A.C., Knauer, A.V., and Feghali-Bostwick, C.A. (2005). Insulin-like growth factor binding proteins 3 and 5 are overexpressed in idiopathic pulmonary fibrosis and contribute to extracellular matrix deposition. Am J Pathol *166*, 399-407.

57. Radisky, D.C., Kenny, P.A., and Bissell, M.J. (2007). Fibrosis and cancer: do myofibroblasts come also from epithelial cells via EMT? J Cell Biochem *101*, 830-839.

58. Pen, A., Moreno, M.J., Durocher, Y., Deb-Rinker, P., and Stanimirovic, D.B. (2008). Glioblastoma-secreted factors induce IGFBP7 and angiogenesis by modulating Smad-2-dependent TGF-beta signaling. Oncogene *27*, 6834-6844.

59. Hwa, V., Oh, Y., and Rosenfeld, R.G. (1999). The insulin-like growth factor-binding protein (IGFBP) superfamily. Endocr Rev *20*, 761-787.

60. Firth, S.M., and Baxter, R.C. (2002). Cellular actions of the insulin-like growth factor binding proteins. Endocr Rev *23*, 824-854.

61. Akaogi, K., Okabe, Y., Funahashi, K., Yoshitake, Y., Nishikawa, K., Yasumitsu, H., Umeda, M., and Miyazaki, K. (1994). Cell adhesion activity of a 30-kDa major secreted protein from human bladder carcinoma cells. Biochem Biophys Res Commun *198*, 1046-1053.

62. Kato, M.V., Sato, H., Tsukada, T., Ikawa, Y., Aizawa, S., and Nagayoshi, M. (1996). A follistatin-like gene, mac25, may act as a growth suppressor of osteosarcoma cells. Oncogene *12*, 1361-1364.

63. Burger, A.M., Leyland-Jones, B., Banerjee, K., Spyropoulos, D.D., and Seth, A.K. (2005). Essential roles of IGFBP-3 and IGFBP-rP1 in breast cancer. Eur J Cancer *41*, 1515-1527.

64. Ahmed, S., Jin, X., Yagi, M., Yasuda, C., Sato, Y., Higashi, S., Lin, C.Y., Dickson, R.B., and Miyazaki, K. (2006). Identification of membrane-bound serine proteinase matriptase as processing enzyme of insulin-like growth factor binding protein-related protein-1 (IGFBP-rP1/angiomodulin/mac25). FEBS J *273*, 615-627.

65. van Beijnum, J.R., Dings, R.P., van der Linden, E., Zwaans, B.M., Ramaekers, F.C., Mayo, K.H., and Griffioen, A.W. (2006). Gene expression of tumor angiogenesis dissected: specific targeting of colon cancer angiogenic vasculature. Blood *108*, 2339-2348.

66. Ruan, W., Xu, E., Xu, F., Ma, Y., Deng, H., Huang, Q., Lv, B., Hu, H., Lin, J., Cui, J., et al. (2007). IGFBP7 plays a potential tumor suppressor role in colorectal carcinogenesis. Cancer Biol Ther *6*, 354-359.

67. Komatsu, S., Okazaki, Y., Tateno, M., Kawai, J., Konno, H., Kusakabe, M., Yoshiki, A., Muramatsu, M., Held, W.A., and Hayashizaki, Y. (2000). Methylation and downregulated expression of mac25/insulin-like growth factor binding protein-7 is associated with liver tumorigenesis in SV40T/t antigen transgenic mice, screened by restriction landmark genomic scanning for methylation (RLGS-M). Biochem Biophys Res Commun *267*, 109-117.

68. Vizioli, M.G., Sensi, M., Miranda, C., Cleris, L., Formelli, F., Anania, M.C., Pierotti, M.A., and Greco, A. IGFBP7: an oncosuppressor gene in thyroid carcinogenesis. Oncogene.

69. Sato, Y., Chen, Z., and Miyazaki, K. (2007). Strong suppression of tumor growth by insulin-like growth factor-binding protein-related protein 1/tumor-derived cell adhesion factor/mac25. Cancer Sci *98*, 1055-1063.

70. Onder, T.T., Gupta, P.B., Mani, S.A., Yang, J., Lander, E.S., and Weinberg, R.A. (2008). Loss of E-cadherin promotes metastasis via multiple downstream transcriptional pathways. Cancer Res *68*, 3645-3654.

71. Kunz-Schughart, L.A., Freyer, J.P., Hofstaedter, F., and Ebner, R. (2004). The use of 3-D cultures for high-throughput screening: the multicellular spheroid model. J Biomol Screen *9*, 273-285.

72. Schmeichel, K.L., and Bissell, M.J. (2003). Modeling tissue-specific signaling and organ function in three dimensions. J Cell Sci *116*, 2377-2388.

73. Okawa, T., Michaylira, C.Z., Kalabis, J., Stairs, D.B., Nakagawa, H., Andl, C.D., Johnstone, C.N., Klein-Szanto, A.J., El-Deiry, W.S., Cukierman, E., et al. (2007). The functional interplay between EGFR overexpression, hTERT activation, and p53 mutation in esophageal epithelial cells with activation of stromal fibroblasts induces tumor development, invasion, and differentiation. Genes Dev *21*, 2788-2803.

74. Sadlonova, A., Novak, Z., Johnson, M.R., Bowe, D.B., Gault, S.R., Page, G.P., Thottassery, J.V., Welch, D.R., and Frost, A.R. (2005). Breast fibroblasts modulate epithelial cell proliferation in three-dimensional in vitro co-culture. Breast Cancer Res *7*, R46-59.

75. Gaggioli, C., Hooper, S., Hidalgo-Carcedo, C., Grosse, R., Marshall, J.F., Harrington, K., and Sahai, E. (2007). Fibroblast-led collective invasion of carcinoma cells with differing roles for RhoGTPases in leading and following cells. Nat Cell Biol *9*, 1392-1400.

76. Froeling, F.E., Mirza, T.A., Feakins, R.M., Seedhar, A., Elia, G., Hart, I.R., and Kocher, H.M. (2009). Organotypic culture model of pancreatic cancer demonstrates that stromal cells modulate E-cadherin, beta-catenin, and Ezrin expression in tumor cells. Am J Pathol *175*, 636-648.

77. Chang, H.Y., Sneddon, J.B., Alizadeh, A.A., Sood, R., West, R.B., Montgomery, K., Chi, J.T., van de Rijn, M., Botstein, D., and Brown, P.O. (2004). Gene expression signature of fibroblast serum response predicts human cancer progression: similarities between tumors and wounds. PLoS Biol *2*, E7.

78. Chi, J.T., Wang, Z., Nuyten, D.S., Rodriguez, E.H., Schaner, M.E., Salim, A., Wang, Y., Kristensen, G.B., Helland, A., Borresen-Dale, A.L., et al. (2006). Gene expression programs in response to hypoxia: cell type specificity and prognostic significance in human cancers. PLoS Med *3*, e47.

79. Sato, N., Maehara, N., and Goggins, M. (2004). Gene expression profiling of tumor-stromal interactions between pancreatic cancer cells and stromal fibroblasts. Cancer Res *64*, 6950-6956.

80. Gallagher, P.G., Bao, Y., Prorock, A., Zigrino, P., Nischt, R., Politi, V., Mauch, C., Dragulev, B., and Fox, J.W. (2005). Gene expression profiling reveals cross-talk between melanoma and fibroblasts: implications for host-tumor interactions in metastasis. Cancer Res *65*, 4134-4146.

Cancer associated fibroblasts as therapeutic targets

Christian Rupp*, Helmut Dolznig*[1], Christian Haslinger[#],
Norbert Schweifer[#] and Pilar Garin-Chesa*[#]

* Institute of Pathology, Medical University of Vienna, Waehringer Guertel 18-20, A-1090 Vienna, Austria

[#]Boehringer Ingelheim RCV GmbH & Co KG, Vienna, Austria, Dr. Boehringer-Gasse 5-11, A-1130 Vienna, Austria

[1] present address: Institute of Medical Genetics, Centre of Pathobiology and Genetics, Medical University of Vienna, Waehringer Strasse 10, A-1090 Vienna, Austria

Abstract

The tumor stroma plays an important role in tumorigenesis. During cancer progression the tumor stroma undergoes changes in architecture, gene expression, secretion of soluble factors and extracellular matrix deposition that are essential for the malignant epithelial cells to manifest the invasive and metastatic phenotype of malignant tumors. Altered gene expression in these non-transformed stromal cells has provided potential targets for therapy. Assessing the therapeutic utility of this new class of drugs requires the use of *in vitro* and *in vivo* tumor models that recapitulate the complex molecular and structural interactions between the malignant cells and the surrounding stroma. Appropriate *in vivo* models are also needed that are suitable to determine the efficacy and tolerability of the drugs. Considerable advances have been made in this respect and a number of drugs targeting signaling pathways of activated tumor fibroblasts are in clinical development.

Keywords: Cancer, targeted therapy, tumor stroma, activated tumor fibroblasts

Introduction

The tumor stroma is an essential, intrinsic part of epithelial cancers and plays a primary role during carcinogenesis. Extensive clinical evidence and a variety of experimental mouse models have demonstrated the active role of the tumor stroma in promoting tumor growth. The advances in our understanding of the molecular basis for cancer initiation and progression provide the basis for the design of novel targeted agents that selectively address deregulated pathways in malignant cells. Drugs that target the stromal component of tumors may represent a further important approach to the overall control of cancer.
The discovery and development of molecularly targeted drugs requires translational research, which include the identification of new molecular targets, target validation and the development of appropriate models to test the new drugs with regard to their mechanism of action, safety and efficacy before translating these findings into the clinic.
Here we will address the challenges for drug development of new therapeutic agents directed towards the tumor stroma, in particular those targeting the cancer associated fibroblasts (CAFs), the limitations in the available experimental models and the complexity of the model systems in which the new targets can be studied in detail.

Histological and molecular heterogeneity of human cancers

Carcinomas which comprise the majority of human cancers are composed of malignant epithelial cells as well as mesenchyme-derived stromal cells, such as fibroblasts, myofibroblasts, endothelial cells, pericytes, smooth muscle and hematopoietic cells embedded in a matrix of extracellular proteins (ECM). Different histological subtypes of carcinomas exist and the extent and composition of the stroma differs among tumors. Certain tumor types such as those occurring in the pancreas, breast, and colon (**Fig. 1**) are characterized by the presence of a prominent stromal reaction (desmoplasia). The fibroblasts in those tumors express markers of activated fibroblasts such as fibroblast activation protein alpha (FAPα) [1] and alpha-smooth muscle actin (α-SMA) [2] that differ from their expression in resting fibroblasts of the adjacent normal tissues (**Fig. 1A**), indicating the phenotypic differences between normal and tumor fibroblasts. Different subsets of CAFs have been observed to occur in different tumor types [3,4] suggesting that the activation programs of CAFs in cancer may be linked to the tissue of origin and might indicate functional differences of CAFs in tumor invasion and metastasis [5]. Several clinicopathologic studies have shown that the characteristics of the tumor stroma correlate with prognostic factors and patient survival [4,6,7].

Cancer associated fibroblasts (CAFs): Molecular characterization

Fibroblasts represent the major cellular component of the stroma of epithelial cancers. Several *in vitro* and *in vivo* studies have demonstrated that the growth, differentiation and invasive behaviour of malignant epithelial cells are influenced by the surrounding stroma [8-11]. Normal fibroblasts have been reported to prevent the progression of transformed epithelial cells [12], in contrast, the presence of activated tumor stromal fibroblasts was shown to enhance malignant epithelial transformation in several cancer models [13-15]. Cancer associated fibroblasts (CAFs) differ considerably from normal resting fibroblasts, and display distinct molecular signatures which can be linked to clinical outcome [16]. Recent studies have identified new functional roles for CAFs and the existence of different CAFs subsets in human cancers by gene expression analysis [17,18].

In vitro and *in vivo* models for tumor stroma interaction

Understanding the molecular mechanisms that control the heterotypic interactions between malignant cells and the surrounding stroma may help to develop new targeted therapies. However these studies have been hampered by the challenges in studying multi-cellular interactions in experimental models (**Fig. 2**).

The *in vitro* study of freshly dissociated cancer cells or established tumor cell lines and fibroblasts in two dimensional (2D) cultures has provided important insights into basic tumor cell biology and has enabled the identification of common genetic alterations in cancer cells that can be targeted therapeutically [19-22] . However, such *in vitro* approaches have proven somewhat limited in studying stromal targets. Only a limited number of stromal-derived cells are available in culture and phenotypic changes can be induced under culture conditions [15]. In addition, many physiological aspects of tumors such as cell-cell and cell-matrix interactions are lost under conventional 2D culture conditions.

Cells grown in three-dimensional (3D) scaffolds or as 3D multicellular spheroids recapitulate the architecture of tissues and tumors *in vivo* to a higher extent. They offer new opportunities to analyze the activation of differentiation programs and the pathways involved in cell migration and invasion when cells are grown in a heterotypic and physiologically relevant context [7,23]. Organotypic 3D co-culture models have been used to study the functional interplay between genetically altered epithelial cells and fibroblasts [24,25] and to study fibroblast-led invasion in models of skin, breast, pancreatic and brain cancers [26,27].

A novel experimental set-up has been developed (Dolznig H et al. manuscript in preparation) combining multi-cellular spheroids, 3D collagen gel cultures and co-cultures of human

epithelial cancer cells with normal human fibroblasts or CAFs in one assay (**Fig. 2**). Using this model system the feasibility to study the tumor - stroma interactions phenotypically and at the molecular level was demonstrated. Gene expression profiles from these 3D co-cultures have been obtained and ongoing studies are exploring the applicability of the model to study the role of these new stromal targets in tumor invasion using knock-in/knock-down experiments of selected genes in the tumor cells or in the fibroblast population.

Xenograft tumor models are commonly used to analyze new mechanisms of action and to validate the efficacy of novel drugs in preclinical studies. The majority of these *in vivo* assays are performed in immunodeficient mice following the inoculation of established tissue culture cell lines into ectopic sites. From a histopathological view these tumor models show a highly atypical morphology with very little stroma or histotypic features resembling the human cancer counterparts (**Fig. 1B**). A more authentic histological appearance is observed in carcinoma models derived by direct transplantation of surgical specimens, purified cell suspensions freshly obtained from surgical specimens or in orthotopically implanted tumors [28-31]. Nevertheless, most of the preclinical validation studies are carried out using the ectopic (mostly subcutaneous) *in vivo* models, that are relatively easy to set up and that can be generated in large numbers of similar-sized tumors for randomization as pre-requisite to assess the effects of drugs. However, in many cases, the results obtained from xenograft models do not translate well in subsequent clinical studies [31].

Genetically engineered mouse models (GEM) are promising alternatives [32,33]. These models, generated through the introduction of genetic mutations associated with specific human malignancies closely recapitulate the human disease at the pathophysiological and molecular level. To date, models have been developed for many common tumor types (e.g. lung, breast, prostate, colon and pancreatic cancer). Evidence for the usefulness of GEM has been demonstrated in preclinical studies evaluating targeted therapies in models of lung and breast cancer [9, 34-38]. These studies suggest that GEM can more accurately predict the therapeutic responses to those observed in the clinic.

Therapeutic opportunities

Different molecular targets have been shown to distinguish the cancer associated fibroblasts (CAFs) and different strategies to target these molecules are under evaluation Here we will focus on potential drug candidates with special attention to those in more advanced clinical development.

Fibroblast activation protein alpha

Fibroblast activation protein alpha (FAPα) is an integral cell surface protein selectively expressed by activated stromal fibroblasts of several types of human epithelial cancers. In normal tissues, FAPα expression is highly restricted to developing organs, healing wounds, and tissue remodeling. Epithelial tumor cells and most normal adult human tissues lack FAPα expression [1, 39-43]. FAPα is a serine protease capable of degrading type I collagen which places FAPα into the group of enzymes involved in tumor tissue remodeling [44-46]. FAPα activity can be detected in tumor samples and shows a good correlation with FAPα expression detected by immunohistochemistry [42,45]. Based on the selective expression of FAPα in the reactive stroma of many epithelial cancers, the lack of expression in normal adult tissues, and its protease activity, FAPα is an ideally suited stroma target to be exploited in the clinic.

Two different approaches have been used to target FAPα in tumors. The first was to employ FAPα -specific monoclonal antibodies. Initial studies with radiolabeled murine and humanized antibodies against human FAPα have shown highly specific tumor targeting properties [47,48], however no clinical efficacy could be demonstrated using the unlabeled humanized antibody in a study in metastatic colorectal cancer [49], probably due to the lack of effector-function properties of the naked antibody. More recently, a novel antibody-maytansinoid conjugate (FAP5-DM1), targeting a shared epitope of human, mouse and cynomolgus monkey fibroblast activation protein alpha, has been developed. Using this conjugate in stroma-rich histotypic cancer xenograft models we were able to induce long-lasting inhibition of tumor growth and complete regressions in models of lung, pancreas and head and neck cancers, with no evidence of toxicity [31].

The second approach has been to target the enzymatic activity of FAPα with small molecule inhibitors. Using the peptidase inhibitor PT-100 (talabostat) a reduction in tumor growth rate was shown in a variety of tumor models in mice [50,51]. This particular compound, however, inhibits multiple intracellular and extracellular dipeptidyl peptidases (e.g. FAPα, DPPIV,

DPP7), so that the anti-tumor effect could not be directly attributed to FAPα inhibition. More recently, using FAPα-null mice and a more selective inhibitor (PT-630), the endogenous role of FAPα in tumorigenesis and the control of tumor growth mediated by pharmacologic inhibition of FAPα enzymatic activity has been reported [38,52]. Deletion of FAPα resulted in a marked reduction of tumor growth in a *LSL-K-ras*^{G12D} genetic mouse model of lung cancer and in a syngeneic colon cancer model, suggesting a tumor promoting activity of endogenous FAPα. Treatment with PT-630 of tumor-bearing wild type animals resulted in a marked inhibition of tumor growth in both models, supporting further clinical studies.

Matrix metalloproteinases (MMPs)

Cancer associated fibroblasts are a major source of MMPs in tumors, including MMPs 1,2,3,9,11,13 and MT1-MMP [53,54]. Fibroblast derived MMPs have been extensively investigated in xenograft models, demonstrating the important role for these proteases in promoting tumor growth, metastasis, and angiogenesis [55]. Based on the results of the preclinical studies MMPs were seen as attractive anticancer targets and several inhibitors have been developed and tested in the clinic in a variety of cancer types [56]. These trials however had failed to demonstrate a survival benefit despite the promising activity shown in pre-clinical models [57]. Possible explanations include differences in the biology of the MMPs between mice and humans, lack of anti-immune response in the xenograft models used pre-clinically, dose-limiting toxicities at least in part due to off-target effects, a narrow therapeutic window for some of the inhibitors and perhaps the challenging fact that MMPs can have tumor-promoting as well as tumor-suppressor activities. Thus a better understanding of the functional complexity of this family of proteases and the use of second generation inhibitors with improved selectivity profile may provide better therapeutic outcomes [58].

Endosialin/TEM1

Endosialin is a highly sialylated, C-type lectin-like surface receptor structurally related to thrombomodulin and complement receptor C1qRp [59,60]. First identified with a monoclonal antibody, mAb FB5, endosialin was discovered independently through a SAGE screen (serial analysis of gene expression) of human cancer endothelial cells, leading to the alternative designation of tumor endothelial marker 1 (TEM1) [61]. Endosialin/TEM1 is expressed to varying degrees by tumor endothelial cells, pericytes and stromal fibroblasts [62-64]. Endosialin expression has not been detected in capillary endothelium in most normal tissues. The physiological role of endosialin is unknown. Endosialin/Tem1 knock-out mice are fertile and develop normally, however, when human HCT116 colon carcinoma cells were

implanted orthotopically onto the serosal surface of the large intestine of nude KO mice, both tumor take and growth rate were reduced [65]. Recent evidence suggests that endosialin/TEM1 might interact with extracellular matrix components, including collagen type I, IV and fibronectin in promoting cell adhesion and migration processes during tumor invasion and metastasis [66]. A humanized Endosialin/TEM1 blocking antibody (MORAb-004) is currently in clinical studies and might provide a therapeutic benefit in a broad range of tumors, based on its ability to target the endothelial cells as well as the peri-vascular stromal component of the tumors.

PDGF/PDGFR pathway

Platelet-derived growth factors (PDGFs) play important roles during embryonic development and wound healing [67] and expression of their tyrosine kinase receptors (PDGFRs) in the tumor stroma is a common feature of human cancers [68]. During tumorigenesis, PDGFR can drive tumor growth directly by autocrine stimulation of receptor-expressing tumor cells or in a paracrine manner by acting on the tumor stroma fibroblasts and pericytes [69]. The importance of the paracrine signaling network for the recruitment of cancer associated fibroblasts and pericytes has been shown in a number of studies [70,71]. Pericytes provide both survival signals and structural support to endothelial cells contributing to a mature, functional vasculature and thus to tumor growth [72].
Multiple tyrosine kinase inhibitors with anti-PDGFR activity, such as imatinib, sorafenib, and sunitinib, have been approved and are presently under further clinical development [73,74]. The most commonly used, imatinib, is a bcr-abl inhibitor with additional PDGFR and c-kit kinase inhibitory activity [75]. In experimental cancer models, imatinib has been shown to inhibit PDGFR activity on fibroblasts and pericytes and to significantly decrease the stromal reaction which was accompanied by a reduction in tumor cell proliferation and pericyte coverage of tumor vessels [69,76]. Furthermore, inhibition of PDGFRs increases the uptake and therefore the antitumor effect of conventional chemotherapeutics like paclitaxel by lowering tumor interstitial pressure [77]. Other multi-kinase inhibitors, such as BIBF1120, a triple angiokinase inhibitor of the VEGFR, PDGFR and FGFR families, has been shown to decrease the pericyte coverage of tumor blood vessels in experimental cancer models [78] which together with the reduction in tumor microvessel density contributed to the pronounced anti-tumor effects of the inhibitor. BIBF1120 is in clinical development for several tumor indications.

Collectively, these results indicate that inhibition of PDGF receptor signaling might provide a complementary approach to conventional treatments. To date, it is still unknown to what extent selective blockage of stromal PDGF signaling contributes to the observed anti-tumor effects of these multi-kinase inhibitors.

Transforming growth factor β (TGF-β) pathway

Transforming growth factor β (TFG-β) is recognized for its dual and opposing functions, a tumor-suppressor activity in the pre-malignant state and a tumor promoter activity during malignant progression [79, 80]. This dual role has made the design and development of drugs targeting this signaling pathway in cancer particularly complex. In tumors, activation of TGF-β is linked to the activity of several oncogenic pathways linked to the induction of epithelial mesenchymal transition (EMT) that enhances tumor cell invasion [81]. TGF-β can have an additional role in tumor growth that is mediated through its activity on the tumor stroma, facilitating tumor tissue remodeling and neoangiogenesis. Studies with fibroblast specific TGF-β type II receptor knock-out models provided evidence for the tumor suppressor role of TGF-β in fibroblasts, by blocking the production of tumor cell growth-promoting paracrine factors such as HGF (hepatocyte growth factor) [9,82]. On the other hand, it was demonstrated that TGF-β stimulates myofibroblast differentiation and that blocking of TGF-β signaling in stromal fibroblast leads to a significant reduction of tumor-growth in a co-transplantation xenograft model [83], suggesting that pro- or anti-tumoral effects of TGF-β signaling may very much depend on individual tumor models. Considering the direct effect of TGF-β on tumor cells and its indirect effect on the tumor stroma, TGF-β signaling appeared as an attractive therapeutic concept. Several approaches to inhibit the TGF-β pathway have been investigated in preclinical models and clinical studies. Neutralizing antibodies that inhibit the ligand-receptor interaction, antisense oligonucleotides and small molecule inhibitors of the TGF-β receptor kinase complex have been developed and are at different stages of clinical development [84,85]. It is expected that this class of agents will be active in a broad range of tumors but due to the complex roles of this growth factor receptor family in tumorigenesis a careful selection of patients will be required to address their therapeutic benefits in patients

Hedgehog pathway

The Hedgehog (Hh) family of proteins have been shown to control cell growth, survival and fate during embryonic development and when mutated or misregulated to contribute to tumorigenesis. Aberrant activation of the Hh pathway by mutations are causally

associated with basal cell carcinoma of the skin, medulloblastoma and rhabdomyosarcoma [86] . Furthermore, components of the Hh pathway have been described to play a role in the growth of a variety of epithelial cancer types, including small cell lung cancer, pancreatic and prostate cancer even in the absence of mutations [87-89]. Recent studies in experimental cancer models support a model in which Hh acts in a paracrine manner on stromal cells. Hh increases tumor growth by stimulating the expression of extracellular matrix proteins and factors like IGF or Wnt in the stroma and thereby promoting stromal desmoplasia [90]. The most commonly used Hh antagonists are the plant alkaloid cyclopamine and its derivatives [91]. The anti-tumor effect of the semisynthetic cyclopamine-derivative IPI-926 was investigated in a mouse model of pancreatic ductal adenocarcinoma refractory to gemcitabine (a drug commonly used in the clinic). Mice treated with IPI-926 alone or in combination with gemcitabine were depleted of desmoplastic stroma reaction in the tumors and displayed increased intratumoral vascular density. These changes correlated with a more effective delivery of the co-administrated gemcitabine, resulting in enhanced efficacy of the drug [92]. This study has identified a potential novel mechanism for anti-stroma therapy.

Identification of novel therapeutic targets by gene expression profiling

The recent technological advances for high-throughput DNA and RNA detection have shown that specific germline and somatic mutations, loss of heterozygosity, and DNA amplifications occur during cancer progression. Oncogenome signatures of human tumors have been shown to correlate with metastatic behaviour and clinical outcome in different cancer types [93-95]. However, the specific contribution of malignant epithelial cells and stromal cells to these genetic signatures is in most cases unclear, since most of the studies have used bulk tumor samples. Our approach to establish the molecular differences between CAFs and normal resting fibroblasts has been to generate gene expression signatures from microdissected cancer and corresponding normal tissues. We focussed on colorectal cancer and developed a protocol for laser capture microdissection guided by antibodies against FAP to separate epithelial cells from activated stromal fibroblasts [96]. We performed whole genome Affymetrix GeneChip® analysis and obtained transcriptional signatures from tumor cells and activated tumor stroma that were compared with the expression profiles from microdissected normal colonic epithelium and normal fibroblasts, obtained from the same patients (**Fig. 3**, Rupp et al manuscript in preparation). Bioinformatic analysis comparing the tumor stroma vs. the normal stroma signatures identified a number of selectively up-regulated genes. Well characterized tumor stroma markers such as FAPα, MMP-2, PDGFR-β and

FGFR1 among others appeared specifically up-regulated in the stroma compartment (**Fig. 3**) and served as a validation parameter for our screen. To further analyze the functional significance of these gene signatures in the context of tumorigenesis we performed a similar genetic screen in our above described 3D co-culture model of tumor cell spheroids and fibroblasts (normal and cancer-derived) grown in collagen gels. We established transcriptional profiles from the different cellular components grown in collagen gels in mono-cultures and compared the gene expression responses induced upon co-cultivation (Dolznig et al. manuscript in preparation). We observed a remarkable concordance between the gene sets obtained in our *ex vivo* study (colorectal cancer study from human samples) and this *in vitro* co-culture system. Examples of commonly regulated genes included COL11A1 and MMP3 (**Fig. 3**), well characterized markers of activated fibroblasts. Gene-Set Enrichment Analysis (GSEA) [97] using the gene-set collections from the Molecular Signature Database (Broad Institute) [98] and Pathway analysis (Ingenuity®) revealed datasets and gene-networks that were significantly enriched in both screens. Gene-sets involved in extracellular matrix deposition, angiogenesis, wound healing and EMT were significantly up-regulated in both studies.

Interestingly, many of the genes identified in our study have been reported in studies performed in vitro including the "wound response signature" of fibroblasts in response to serum stimulation [99], a hypoxia-associated response [100] as well as the signatures obtained from co-cultures of cancer cells and fibroblasts cell lines of different origins [101,102]. Using independent datasets from human cancers, it was shown that the "wound-response signature" was strongly predictive of metastasis and progression in breast, lung and gastric cancers and was an independent predictor of outcome in a follow-up study in breast cancer [99].

Other *in vivo* signatures have been described [103] comparing the expression patterns of good versus poor outcome in fibroblastic tumors. A subsequent comparison of these signatures with a breast cancer data set suggested that distinct patterns of stroma reaction defined two groups of breast cancers with significant differences in overall survival,indicating that the stromal response varies significantly in different subtypes of carcinomas and may be clinically relevant. Expression signatures from different tumor compartments have also been established using serial analysis of gene expression on antibody-sorted stromal components in breast cancers [104] or laser capture microdissection in breast cancer and basal cell carcinoma of the skin [105,106]. Using a set of genes expressed by the microdissected tumor stroma, a stroma-derived prognostic predictor signature (SDPP) was developed and shown to separate primary breast cancers into three distinct groups associated with different clinical outcomes

[16]. In another study, a stromal signature was shown to predict the response of estrogen-receptor negative breast tumors to chemotherapy [107]. The authors used a novel bioinformatics method that decomposes gene expression signals from a mixture of tumor and stromal cells into multiple independent signatures. They obtained a 50-gene stromal signature including FAPα, MMP2, MMP14, PDGFR-β which predicted resistance to chemotherapy. Taken together, these studies demonstrated that tumors expressed a variety of functionally different genes in their tumor stroma, representing different activation stages or different subtypes of CAFs that may be relevant for the invasiveness or clinical behavior of the tumors. The gene expression signatures derived from this type of analysis appear to have clinical significance in different cancer types and have provided new genetic markers in the tumor stroma that may serve as targets for novel therapeutic approaches.

Conclusions

The rapid progress of research in molecular cancer biology has contributed to a better understanding of the role of the tumor stroma during tumor growth and metastasis formation and has led to the identification of selected tumor stroma markers that serve as targets for novel therapies. A number of monoclonal antibodies, small-molecule inhibitors and anti-sense approaches have been developed and investigated in pre-clinical models, some of these molecules have entered clinical development. Future approaches to stroma-targeted therapy will have to be based on further refinement of our understanding of the molecular mechanisms that control the tumor-stroma interaction, improved preclinical models that adequately reproduce the complexity of the tumor tissue, and a biomarker-based selection of patients most likely to benefit from the novel therapies

References

1. Garin-Chesa, P., Old, L.J., and Rettig, W.J. (1990). Cell surface glycoprotein of reactive stromal fibroblasts as a potential antibody target in human epithelial cancers. Proc Natl Acad Sci U S A 87, 7235-7239.
2. Desmouliere, A., Guyot, C., and Gabbiani, G. (2004). The stroma reaction myofibroblast: a key player in the control of tumor cell behavior. Int J Dev Biol 48, 509-517.
3. Huber, M.A., Kraut, N., Schweifer, N., Dolznig, H., Peter, R.U., Schubert, R.D., Scharffetter-Kochanek, K., Pehamberger, H., and Garin-Chesa, P. (2006). Expression of stromal cell markers in distinct compartments of human skin cancers. J Cutan Pathol 33, 145-155.
4. Koperek, O., Scheuba, C., Puri, C., Birner, P., Haslinger, C., Rettig, W., Niederle, B., Kaserer, K., and Garin Chesa, P. (2007). Molecular characterization of the desmoplastic tumor stroma in medullary thyroid carcinoma. Int J Oncol 31, 59-67.
5. Sugimoto, H., Mundel, T.M., Kieran, M.W., and Kalluri, R. (2006). Identification of fibroblast heterogeneity in the tumor microenvironment. Cancer Biol Ther 5, 1640-1646.
6. Hasebe, T., Sasaki, S., Imoto, S., and Ochiai, A. (2001). Highly proliferative fibroblasts forming fibrotic focus govern metastasis of invasive ductal carcinoma of the breast. Mod Pathol 14, 325-337.
7. Kunz-Schughart, L.A., and Knuechel, R. (2002). Tumor-associated fibroblasts (part I): Active stromal participants in tumor development and progression? Histol Histopathol 17, 599-621.
8. Tlsty, T.D., and Hein, P.W. (2001). Know thy neighbor: stromal cells can contribute oncogenic signals. Curr Opin Genet Dev 11, 54-59.
9. Bhowmick, N.A., Chytil, A., Plieth, D., Gorska, A.E., Dumont, N., Shappell, S., Washington, M.K., Neilson, E.G., and Moses, H.L. (2004). TGF-beta signaling in fibroblasts modulates the oncogenic potential of adjacent epithelia. Science 303, 848-851.
10. Joyce, J.A. (2005). Therapeutic targeting of the tumor microenvironment. Cancer Cell 7, 513-520.
11. Mueller, M.M., and Fusenig, N.E. (2004). Friends or foes - bipolar effects of the tumour stroma in cancer. Nat Rev Cancer 4, 839-849.
12. Hayashi, N., and Cunha, G.R. (1991). Mesenchyme-induced changes in the neoplastic characteristics of the Dunning prostatic adenocarcinoma. Cancer Res 51, 4924-4930.

13. Nakamura, T., Matsumoto, K., Kiritoshi, A., and Tano, Y. (1997). Induction of hepatocyte growth factor in fibroblasts by tumor-derived factors affects invasive growth of tumor cells: in vitro analysis of tumor-stromal interactions. Cancer Res 57, 3305-3313.
14. Olumi, A.F., Grossfeld, G.D., Hayward, S.W., Carroll, P.R., Tlsty, T.D., and Cunha, G.R. (1999). Carcinoma-associated fibroblasts direct tumor progression of initiated human prostatic epithelium. Cancer Res 59, 5002-5011.
15. Orimo, A., Gupta, P.B., Sgroi, D.C., Arenzana-Seisdedos, F., Delaunay, T., Naeem, R., Carey, V.J., Richardson, A.L., and Weinberg, R.A. (2005). Stromal fibroblasts present in invasive human breast carcinomas promote tumor growth and angiogenesis through elevated SDF-1/CXCL12 secretion. Cell 121, 335-348.
16. Finak, G., Bertos, N., Pepin, F., Sadekova, S., Souleimanova, M., Zhao, H., Chen, H., Omeroglu, G., Meterissian, S., Omeroglu, A., et al. (2008). Stromal gene expression predicts clinical outcome in breast cancer. Nat Med 14, 518-527.
17. Chang, H.Y., Chi, J.T., Dudoit, S., Bondre, C., van de Rijn, M., Botstein, D., and Brown, P.O. (2002). Diversity, topographic differentiation, and positional memory in human fibroblasts. Proc Natl Acad Sci U S A 99, 12877-12882.
18. Iacobuzio-Donahue, C.A., Argani, P., Hempen, P.M., Jones, J., and Kern, S.E. (2002). The desmoplastic response to infiltrating breast carcinoma: gene expression at the site of primary invasion and implications for comparisons between tumor types. Cancer Res 62, 5351-5357.
19. Cornil, I., Theodorescu, D., Man, S., Herlyn, M., Jambrosic, J., and Kerbel, R.S. (1991). Fibroblast cell interactions with human melanoma cells affect tumor cell growth as a function of tumor progression. Proc Natl Acad Sci U S A 88, 6028-6032.
20. Elenbaas, B., Spirio, L., Koerner, F., Fleming, M.D., Zimonjic, D.B., Donaher, J.L., Popescu, N.C., Hahn, W.C., and Weinberg, R.A. (2001). Human breast cancer cells generated by oncogenic transformation of primary mammary epithelial cells. Genes Dev 15, 50-65.
21. Yashiro, M., Ikeda, K., Tendo, M., Ishikawa, T., and Hirakawa, K. (2005). Effect of organ-specific fibroblasts on proliferation and differentiation of breast cancer cells. Breast Cancer Res Treat 90, 307-313.
22. Jones, S., Zhang, X., Parsons, D.W., Lin, J.C., Leary, R.J., Angenendt, P., Mankoo, P., Carter, H., Kamiyama, H., Jimeno, A., et al. (2008). Core signaling pathways in human pancreatic cancers revealed by global genomic analyses. Science 321, 1801-1806.

23. Schmeichel, K.L., and Bissell, M.J. (2003). Modeling tissue-specific signaling and organ function in three dimensions. J Cell Sci 116, 2377-2388.
24. Okawa, T., Michaylira, C.Z., Kalabis, J., Stairs, D.B., Nakagawa, H., Andl, C.D., Johnstone, C.N., Klein-Szanto, A.J., El-Deiry, W.S., Cukierman, E., et al. (2007). The functional interplay between EGFR overexpression, hTERT activation, and p53 mutation in esophageal epithelial cells with activation of stromal fibroblasts induces tumor development, invasion, and differentiation. Genes Dev 21, 2788-2803.
25. Sadlonova, A., Novak, Z., Johnson, M.R., Bowe, D.B., Gault, S.R., Page, G.P., Thottassery, J.V., Welch, D.R., and Frost, A.R. (2005). Breast fibroblasts modulate epithelial cell proliferation in three-dimensional in vitro co-culture. Breast Cancer Res 7, R46-59.
26. Gaggioli, C., Hooper, S., Hidalgo-Carcedo, C., Grosse, R., Marshall, J.F., Harrington, K., and Sahai, E. (2007). Fibroblast-led collective invasion of carcinoma cells with differing roles for RhoGTPases in leading and following cells. Nat Cell Biol 9, 1392-1400.
27. Froeling, F.E., Mirza, T.A., Feakins, R.M., Seedhar, A., Elia, G., Hart, I.R., and Kocher, H.M. (2009). Organotypic culture model of pancreatic cancer demonstrates that stromal cells modulate E-cadherin, beta-catenin, and Ezrin expression in tumor cells. Am J Pathol 175, 636-648.
28. Rubio-Viqueira, B., Jimeno, A., Cusatis, G., Zhang, X., Iacobuzio-Donahue, C., Karikari, C., Shi, C., Danenberg, K., Danenberg, P.V., Kuramochi, H., et al. (2006). An in vivo platform for translational drug development in pancreatic cancer. Clin Cancer Res 12, 4652-4661.
29. Shu, Q., Wong, K.K., Su, J.M., Adesina, A.M., Yu, L.T., Tsang, Y.T., Antalffy, B.C., Baxter, P., Perlaky, L., Yang, J., et al. (2008). Direct orthotopic transplantation of fresh surgical specimen preserves CD133+ tumor cells in clinically relevant mouse models of medulloblastoma and glioma. Stem Cells 26, 1414-1424.
30. O'Brien, C.A., Pollett, A., Gallinger, S., and Dick, J.E. (2007). A human colon cancer cell capable of initiating tumour growth in immunodeficient mice. Nature 445, 106-110.
31. Ostermann, E., Garin-Chesa, P., Heider, K.H., Kalat, M., Lamche, H., Puri, C., Kerjaschki, D., Rettig, W.J., and Adolf, G.R. (2008). Effective immunoconjugate therapy in cancer models targeting a serine protease of tumor fibroblasts. Clin Cancer Res 14, 4584-4592.

32. Frese, K.K., and Tuveson, D.A. (2007). Maximizing mouse cancer models. Nat Rev Cancer 7, 645-658.
33. Gopinathan, A., and Tuveson, D.A. (2008). The use of GEM models for experimental cancer therapeutics. Dis Model Mech 1, 83-86.
34. Politi, K., Zakowski, M.F., Fan, P.D., Schonfeld, E.A., Pao, W., and Varmus, H.E. (2006). Lung adenocarcinomas induced in mice by mutant EGF receptors found in human lung cancers respond to a tyrosine kinase inhibitor or to down-regulation of the receptors. Genes Dev 20, 1496-1510.
35. Beppu, H., Mwizerwa, O.N., Beppu, Y., Dattwyler, M.P., Lauwers, G.Y., Bloch, K.D., and Goldstein, A.M. (2008). Stromal inactivation of BMPRII leads to colorectal epithelial overgrowth and polyp formation. Oncogene 27, 1063-1070.
36. Rottenberg, S., and Jonkers, J. (2008). Modeling therapy resistance in genetically engineered mouse cancer models. Drug Resist Updat 11, 51-60.
37. Perera, S.A., Li, D., Shimamura, T., Raso, M.G., Ji, H., Chen, L., Borgman, C.L., Zaghlul, S., Brandstetter, K.A., Kubo, S., et al. (2009). HER2YVMA drives rapid development of adenosquamous lung tumors in mice that are sensitive to BIBW2992 and rapamycin combination therapy. Proc Natl Acad Sci U S A 106, 474-479.
38. Santos, A.M., Jung, J., Aziz, N., Kissil, J.L., and Pure, E. (2009). Targeting fibroblast activation protein inhibits tumor stromagenesis and growth in mice. J Clin Invest 119, 3613-3625.
39. Rettig, W.J., Garin-Chesa, P., Healey, J.H., Su, S.L., Ozer, H.L., Schwab, M., Albino, A.P., and Old, L.J. (1993). Regulation and heteromeric structure of the fibroblast activation protein in normal and transformed cells of mesenchymal and neuroectodermal origin. Cancer Res 53, 3327-3335.
40. Niedermeyer, J., Scanlan, M.J., Garin-Chesa, P., Daiber, C., Fiebig, H.H., Old, L.J., Rettig, W.J., and Schnapp, A. (1997). Mouse fibroblast activation protein: molecular cloning, alternative splicing and expression in the reactive stroma of epithelial cancers. Int J Cancer 71, 383-389.
41. Niedermeyer, J., Garin-Chesa, P., Kriz, M., Hilberg, F., Mueller, E., Bamberger, U., Rettig, W.J., and Schnapp, A. (2001). Expression of the fibroblast activation protein during mouse embryo development. Int J Dev Biol 45, 445-447.
42. Huber, M.A., Kraut, N., Park, J.E., Schubert, R.D., Rettig, W.J., Peter, R.U., and Garin-Chesa, P. (2003). Fibroblast activation protein: differential expression and serine

protease activity in reactive stromal fibroblasts of melanocytic skin tumors. J Invest Dermatol 120, 182-188.
43. Dolznig, H., Schweifer, N., Puri, C., Kraut, N., Rettig, W.J., Kerjaschki, D., and Garin-Chesa, P. (2005). Characterization of cancer stroma markers: in silico analysis of an mRNA expression database for fibroblast activation protein and endosialin. Cancer Immun 5, 10.
44. Scanlan, M.J., Raj, B.K., Calvo, B., Garin-Chesa, P., Sanz-Moncasi, M.P., Healey, J.H., Old, L.J., and Rettig, W.J. (1994). Molecular cloning of fibroblast activation protein alpha, a member of the serine protease family selectively expressed in stromal fibroblasts of epithelial cancers. Proc Natl Acad Sci U S A 91, 5657-5661.
45. Park, J.E., Lenter, M.C., Zimmermann, R.N., Garin-Chesa, P., Old, L.J., and Rettig, W.J. (1999). Fibroblast activation protein, a dual specificity serine protease expressed in reactive human tumor stromal fibroblasts. J Biol Chem 274, 36505-36512.
46. Niedermeyer, J., Enenkel, B., Park, J.E., Lenter, M., Rettig, W.J., Damm, K., and Schnapp, A. (1998). Mouse fibroblast-activation protein--conserved Fap gene organization and biochemical function as a serine protease. Eur J Biochem 254, 650-654.
47. Welt, S., Divgi, C.R., Scott, A.M., Garin-Chesa, P., Finn, R.D., Graham, M., Carswell, E.A., Cohen, A., Larson, S.M., Old, L.J., et al. (1994). Antibody targeting in metastatic colon cancer: a phase I study of monoclonal antibody F19 against a cell-surface protein of reactive tumor stromal fibroblasts. J Clin Oncol 12, 1193-1203.
48. Scott, A.M., Wiseman, G., Welt, S., Adjei, A., Lee, F.T., Hopkins, W., Divgi, C.R., Hanson, L.H., Mitchell, P., Gansen, D.N., et al. (2003). A Phase I dose-escalation study of sibrotuzumab in patients with advanced or metastatic fibroblast activation protein-positive cancer. Clin Cancer Res 9, 1639-1647.
49. Hofheinz, R.D., al-Batran, S.E., Hartmann, F., Hartung, G., Jager, D., Renner, C., Tanswell, P., Kunz, U., Amelsberg, A., Kuthan, H., et al. (2003). Stromal antigen targeting by a humanised monoclonal antibody: an early phase II trial of sibrotuzumab in patients with metastatic colorectal cancer. Onkologie 26, 44-48.
50. Cheng, J.D., Valianou, M., Canutescu, A.A., Jaffe, E.K., Lee, H.O., Wang, H., Lai, J.H., Bachovchin, W.W., and Weiner, L.M. (2005). Abrogation of fibroblast activation protein enzymatic activity attenuates tumor growth. Mol Cancer Ther 4, 351-360.
51. Adams, S., Miller, G.T., Jesson, M.I., Watanabe, T., Jones, B., and Wallner, B.P. (2004). PT-100, a small molecule dipeptidyl peptidase inhibitor, has potent antitumor

effects and augments antibody-mediated cytotoxicity via a novel immune mechanism. Cancer Res 64, 5471-5480.
52. Pure, E. (2009). The road to integrative cancer therapies: emergence of a tumor-associated fibroblast protease as a potential therapeutic target in cancer. Expert Opin Ther Targets 13, 967-973.
53. Bisson, C., Blacher, S., Polette, M., Blanc, J.F., Kebers, F., Desreux, J., Tetu, B., Rosenbaum, J., Foidart, J.M., Birembaut, P., et al. (2003). Restricted expression of membrane type 1-matrix metalloproteinase by myofibroblasts adjacent to human breast cancer cells. Int J Cancer 105, 7-13.
54. Sternlicht, M.D., Lochter, A., Sympson, C.J., Huey, B., Rougier, J.P., Gray, J.W., Pinkel, D., Bissell, M.J., and Werb, Z. (1999). The stromal proteinase MMP3/stromelysin-1 promotes mammary carcinogenesis. Cell 98, 137-146.
55. Egeblad, M., and Werb, Z. (2002). New functions for the matrix metalloproteinases in cancer progression. Nat Rev Cancer 2, 161-174.
56. Coussens, L.M., Fingleton, B., and Matrisian, L.M. (2002). Matrix metalloproteinase inhibitors and cancer: trials and tribulations. Science 295, 2387-2392.
57. King, J., Zhao, J., Clingan, P., and Morris, D. (2003). Randomised double blind placebo control study of adjuvant treatment with the metalloproteinase inhibitor, Marimastat in patients with inoperable colorectal hepatic metastases: significant survival advantage in patients with musculoskeletal side-effects. Anticancer Res 23, 639-645.
58. Konstantinopoulos, P.A., Karamouzis, M.V., Papatsoris, A.G., and Papavassiliou, A.G. (2008). Matrix metalloproteinase inhibitors as anticancer agents. Int J Biochem Cell Biol 40, 1156-1168.
59. Rettig, W.J., Garin-Chesa, P., Healey, J.H., Su, S.L., Jaffe, E.A., and Old, L.J. (1992). Identification of endosialin, a cell surface glycoprotein of vascular endothelial cells in human cancer. Proc Natl Acad Sci U S A 89, 10832-10836.
60. Christian, S., Ahorn, H., Koehler, A., Eisenhaber, F., Rodi, H.P., Garin-Chesa, P., Park, J.E., Rettig, W.J., and Lenter, M.C. (2001). Molecular cloning and characterization of endosialin, a C-type lectin-like cell surface receptor of tumor endothelium. J Biol Chem 276, 7408-7414.
61. St Croix, B., Rago, C., Velculescu, V., Traverso, G., Romans, K.E., Montgomery, E., Lal, A., Riggins, G.J., Lengauer, C., Vogelstein, B., et al. (2000). Genes expressed in human tumor endothelium. Science 289, 1197-1202.

62. MacFadyen, J.R., Haworth, O., Roberston, D., Hardie, D., Webster, M.T., Morris, H.R., Panico, M., Sutton-Smith, M., Dell, A., van der Geer, P., et al. (2005). Endosialin (TEM1, CD248) is a marker of stromal fibroblasts and is not selectively expressed on tumour endothelium. FEBS Lett 579, 2569-2575.
63. Brady, J., Neal, J., Sadakar, N., and Gasque, P. (2004). Human endosialin (tumor endothelial marker 1) is abundantly expressed in highly malignant and invasive brain tumors. J Neuropathol Exp Neurol 63, 1274-1283.
64. Rupp, C., Dolznig, H., Puri, C., Sommergruber, W., Kerjaschki, D., Rettig, W.J., and Garin-Chesa, P. (2006). Mouse endosialin, a C-type lectin-like cell surface receptor: expression during embryonic development and induction in experimental cancer neoangiogenesis. Cancer Immun 6, 10.
65. Nanda, A., Karim, B., Peng, Z., Liu, G., Qiu, W., Gan, C., Vogelstein, B., St Croix, B., Kinzler, K.W., and Huso, D.L. (2006). Tumor endothelial marker 1 (Tem1) functions in the growth and progression of abdominal tumors. Proc Natl Acad Sci U S A 103, 3351-3356.
66. Tomkowicz, B., Rybinski, K., Foley, B., Ebel, W., Kline, B., Routhier, E., Sass, P., Nicolaides, N.C., Grasso, L., and Zhou, Y. (2007). Interaction of endosialin/TEM1 with extracellular matrix proteins mediates cell adhesion and migration. Proc Natl Acad Sci U S A 104, 17965-17970.
67. Betsholtz, C. (2004). Insight into the physiological functions of PDGF through genetic studies in mice. Cytokine Growth Factor Rev 15, 215-228.
68. Ostman, A., and Heldin, C.H. (2007). PDGF receptors as targets in tumor treatment. Adv Cancer Res 97, 247-274.
69. Pietras, K., Pahler, J., Bergers, G., and Hanahan, D. (2008). Functions of paracrine PDGF signaling in the proangiogenic tumor stroma revealed by pharmacological targeting. PLoS Med 5, e19.
70. Skobe, M., and Fusenig, N.E. (1998). Tumorigenic conversion of immortal human keratinocytes through stromal cell activation. Proc Natl Acad Sci U S A 95, 1050-1055.
71. Anderberg, C., Li, H., Fredriksson, L., Andrae, J., Betsholtz, C., Li, X., Eriksson, U., and Pietras, K. (2009). Paracrine signaling by platelet-derived growth factor-CC promotes tumor growth by recruitment of cancer-associated fibroblasts. Cancer Res 69, 369-378.
72. Carmeliet, P. (2003). Angiogenesis in health and disease. Nat Med 9, 653-660.
73. Levitzki, A. (2004). PDGF receptor kinase inhibitors for the treatment of PDGF driven diseases. Cytokine Growth Factor Rev 15, 229-235.

74. Steeghs, N., Nortier, J.W., and Gelderblom, H. (2007). Small molecule tyrosine kinase inhibitors in the treatment of solid tumors: an update of recent developments. Ann Surg Oncol 14, 942-953.
75. Carroll, M., Ohno-Jones, S., Tamura, S., Buchdunger, E., Zimmermann, J., Lydon, N.B., Gilliland, D.G., and Druker, B.J. (1997). CGP 57148, a tyrosine kinase inhibitor, inhibits the growth of cells expressing BCR-ABL, TEL-ABL, and TEL-PDGFR fusion proteins. Blood 90, 4947-4952.
76. Kitadai, Y., Sasaki, T., Kuwai, T., Nakamura, T., Bucana, C.D., and Fidler, I.J. (2006). Targeting the expression of platelet-derived growth factor receptor by reactive stroma inhibits growth and metastasis of human colon carcinoma. Am J Pathol 169, 2054-2065.
77. Pietras, K., Rubin, K., Sjoblom, T., Buchdunger, E., Sjoquist, M., Heldin, C.H., and Ostman, A. (2002). Inhibition of PDGF receptor signaling in tumor stroma enhances antitumor effect of chemotherapy. Cancer Res 62, 5476-5484.
78. Hilberg, F., Roth, G.J., Krssak, M., Kautschitsch, S., Sommergruber, W., Tontsch-Grunt, U., Garin-Chesa, P., Bader, G., Zoephel, A., Quant, J., et al. (2008). BIBF 1120: triple angiokinase inhibitor with sustained receptor blockade and good antitumor efficacy. Cancer Res 68, 4774-4782.
79. Bierie, B., and Moses, H.L. (2006). Tumour microenvironment: TGFbeta: the molecular Jekyll and Hyde of cancer. Nat Rev Cancer 6, 506-520.
80. Massague, J. (2008). TGFbeta in Cancer. Cell 134, 215-230.
81. Oft, M., Peli, J., Rudaz, C., Schwarz, H., Beug, H., and Reichmann, E. (1996). TGF-beta1 and Ha-Ras collaborate in modulating the phenotypic plasticity and invasiveness of epithelial tumor cells. Genes Dev 10, 2462-2477.
82. Cheng, N., Chytil, A., Shyr, Y., Joly, A., and Moses, H.L. (2007). Enhanced hepatocyte growth factor signaling by type II transforming growth factor-beta receptor knockout fibroblasts promotes mammary tumorigenesis. Cancer Res 67, 4869-4877.
83. Verona, E.V., Elkahloun, A.G., Yang, J., Bandyopadhyay, A., Yeh, I.T., and Sun, L.Z. (2007). Transforming growth factor-beta signaling in prostate stromal cells supports prostate carcinoma growth by up-regulating stromal genes related to tissue remodeling. Cancer Res 67, 5737-5746.
84. Lahn, M., Kloeker, S., and Berry, B.S. (2005). TGF-beta inhibitors for the treatment of cancer. Expert Opin Investig Drugs 14, 629-643.
85. Jones, E., Pu, H., and Kyprianou, N. (2009). Targeting TGF-beta in prostate cancer: therapeutic possibilities during tumor progression. Expert Opin Ther Targets 13, 227-234.

86. Varjosalo, M., and Taipale, J. (2008). Hedgehog: functions and mechanisms. Genes Dev 22, 2454-2472.
87. Watkins, D.N., Berman, D.M., Burkholder, S.G., Wang, B., Beachy, P.A., and Baylin, S.B. (2003). Hedgehog signaling within airway epithelial progenitors and in small-cell lung cancer. Nature 422, 313-317.
88. Thayer, S.P., di Magliano, M.P., Heiser, P.W., Nielsen, C.M., Roberts, D.J., Lauwers, G.Y., Qi, Y.P., Gysin, S., Fernandez-del Castillo, C., Yajnik, V., et al. (2003). Hedgehog is an early and late mediator of pancreatic cancer tumorigenesis. Nature 425, 851-856.
89. Karhadkar, S.S., Bova, G.S., Abdallah, N., Dhara, S., Gardner, D., Maitra, A., Isaacs, J.T., Berman, D.M., and Beachy, P.A. (2004). Hedgehog signaling in prostate regeneration, neoplasia and metastasis. Nature 431, 707-712.
90. Yauch, R.L., Gould, S.E., Scales, S.J., Tang, T., Tian, H., Ahn, C.P., Marshall, D., Fu, L., Januario, T., Kallop, D., et al. (2008). A paracrine requirement for hedgehog signaling in cancer. Nature 455, 406-410.
91. Taipale, J., Chen, J.K., Cooper, M.K., Wang, B., Mann, R.K., Milenkovic, L., Scott, M.P., and Beachy, P.A. (2000). Effects of oncogenic mutations in Smoothened and Patched can be reversed by cyclopamine. Nature 406, 1005-1009.
92. Olive, K.P., Jacobetz, M.A., Davidson, C.J., Gopinathan, A., McIntyre, D., Honess, D., Madhu, B., Goldgraben, M.A., Caldwell, M.E., Allard, D., et al. (2009). Inhibition of Hedgehog signaling enhances delivery of chemotherapy in a mouse model of pancreatic cancer. Science 324, 1457-1461.
93. Alizadeh, A.A., Eisen, M.B., Davis, R.E., Ma, C., Lossos, I.S., Rosenwald, A., Boldrick, J.C., Sabet, H., Tran, T., Yu, X., et al. (2000). Distinct types of diffuse large B-cell lymphoma identified by gene expression profiling. Nature 403, 503-511.
94. Perou, C.M., Sorlie, T., Eisen, M.B., van de Rijn, M., Jeffrey, S.S., Rees, C.A., Pollack, J.R., Ross, D.T., Johnsen, H., Akslen, L.A., et al. (2000). Molecular portraits of human breast tumours. Nature 406, 747-752.
95. Ramaswamy, S., Ross, K.N., Lander, E.S., and Golub, T.R. (2003). A molecular signature of metastasis in primary solid tumors. Nat Genet 33, 49-54.
96. Rupp, C., Dolznig, H., Puri, C., Schweifer, N., Sommergruber, W., Kraut, N., Rettig, W.J., Kerjaschki, D., and Garin-Chesa, P. (2006). Laser capture microdissection of epithelial cancers guided by antibodies against fibroblast activation protein and endosialin. Diagn Mol Pathol 15, 35-42.

97. Mootha, V.K., Lindgren, C.M., Eriksson, K.F., Subramanian, A., Sihag, S., Lehar, J., Puigserver, P., Carlsson, E., Ridderstrale, M., Laurila, E., et al. (2003). PGC-1alpha-responsive genes involved in oxidative phosphorylation are coordinately downregulated in human diabetes. Nat Genet 34, 267-273.
98. Subramanian, A., Tamayo, P., Mootha, V.K., Mukherjee, S., Ebert, B.L., Gillette, M.A., Paulovich, A., Pomeroy, S.L., Golub, T.R., Lander, E.S., et al. (2005). Gene set enrichment analysis: a knowledge-based approach for interpreting genome-wide expression profiles. Proc Natl Acad Sci U S A 102, 15545-15550.
99. Chang, H.Y., Sneddon, J.B., Alizadeh, A.A., Sood, R., West, R.B., Montgomery, K., Chi, J.T., van de Rijn, M., Botstein, D., and Brown, P.O. (2004). Gene expression signature of fibroblast serum response predicts human cancer progression: similarities between tumors and wounds. PLoS Biol 2, E7.
100. Chi, J.T., Wang, Z., Nuyten, D.S., Rodriguez, E.H., Schaner, M.E., Salim, A., Wang, Y., Kristensen, G.B., Helland, A., Borresen-Dale, A.L., et al. (2006). Gene expression programs in response to hypoxia: cell type specificity and prognostic significance in human cancers. PLoS Med 3, e47.
101. Sato, N., Maehara, N., and Goggins, M. (2004). Gene expression profiling of tumor-stromal interactions between pancreatic cancer cells and stromal fibroblasts. Cancer Res 64, 6950-6956.
102. Gallagher, P.G., Bao, Y., Prorock, A., Zigrino, P., Nischt, R., Politi, V., Mauch, C., Dragulev, B., and Fox, J.W. (2005). Gene expression profiling reveals cross-talk between melanoma and fibroblasts: implications for host-tumor interactions in metastasis. Cancer Res 65, 4134-4146.
103. West, R.B., Nuyten, D.S., Subramanian, S., Nielsen, T.O., Corless, C.L., Rubin, B.P., Montgomery, K., Zhu, S., Patel, R., Hernandez-Boussard, T., et al. (2005). Determination of stromal signatures in breast carcinoma. PLoS Biol 3, e187.
104. Allinen, M., Beroukhim, R., Cai, L., Brennan, C., Lahti-Domenici, J., Huang, H., Porter, D., Hu, M., Chin, L., Richardson, A., et al. (2004). Molecular characterization of the tumor microenvironment in breast cancer. Cancer Cell 6, 17-32.
105. Casey, T., Bond, J., Tighe, S., Hunter, T., Lintault, L., Patel, O., Eneman, J., Crocker, A., White, J., Tessitore, J., et al. (2009). Molecular signatures suggest a major role for stromal cells in development of invasive breast cancer. Breast Cancer Res Treat 114, 47-62.

106. Micke, P., Kappert, K., Ohshima, M., Sundquist, C., Scheidl, S., Lindahl, P., Heldin, C.H., Botling, J., Ponten, F., and Ostman, A. (2007). In situ identification of genes regulated specifically in fibroblasts of human basal cell carcinoma. J Invest Dermatol 127, 1516-1523.

107. Farmer, P., Bonnefoi, H., Anderle, P., Cameron, D., Wirapati, P., Becette, V., Andre, S., Piccart, M., Campone, M., Brain, E., et al. (2009). A stroma-related gene signature predicts resistance to neoadjuvant chemotherapy in breast cancer. Nat Med 15, 68-74.

Figure legends

Figure 1

A. *Cancer associated fibroblasts are the main cellular stromal component of carcinomas and display molecular heterogeneity.*
Carcinomas arising in the pancreas, breast and colon display prominent stroma reaction (desmoplasia) separating the clusters of tumor cells. The fibroblasts in those tumors express markers of activated fibroblasts such as fibroblast activation protein (FAPα) and alpha-smooth muscle actin (α-SMA). FAPα is selectively expressed in the tumour stroma and is absent in normal tissues (see normal colon vs. colon cancer). In contrast, expression of α-SMA can be seen in subsets of fibroblasts surrounding the crypts and in the muscularis mucosa of the normal colon as well as in activated tumor fibroblasts. FAPα and α-SMA expression (brown) visualized by the ABC immunoperoxidase method with hematoxylin counterstaining.
B. *Subcutaneous xenograft models in immunodeficient mice.*
Like in the majority of xenograft models, subcutaneous injection of Colo205 cells, a human colorectal cancer cell line, induces tumors with a highly atypical morphology, characterized by clusters of tumor cells, with very little tumor stroma, and absence of glandular differentiation (for comparison see the human colon cancer sample above). Certain human tumor cells such as FaDu cells, derived from a head and neck squamous cell carcinoma, are able to induce a more prominent stroma reaction, with FAPα positive activated stromal fibroblasts and histotypic features resembling the human counterpart. Therefore, a careful selection of the in vivo models is required to determine the efficacy of drugs targeting the activated tumor fibroblasts. Hemaoxylin-eosin and immunohistochemical staining for FAPα (brown; bottom panel).

Figure 2

Carcinomas are heterogeneous mixtures of malignant cells and stromal cells, such as fibroblasts, blood vessels and immune cells embedded in a matrix of extracellular proteins (ECM) and grow as three dimensional structures. An example for this heterogeneity is shown in a histologic picture from a human non-small cell lung cancer (left panel). Tumor cell clusters (blue) are separated by strands of activated fibroblasts which are PDGFR-β positive (brown) and blood vessels with CD31 positive endothelial cells (dark blue). In conventional cell culture models, cells are grown as homogeneous cultures on plastic surfaces. Under these

culture conditions many features of the in vivo growth, such as tissue architecture, cell-cell contact, heterotypic cellular interactions and signaling networks are lost (middle panel). Using 3D cultures in the presence of ECM components, the heterotypic interactions of tumor cells and stromal cells can be studied in detail. A phase contrast picture of this model shows a culture of tumor cells grown as a multicellular spheroid, co-cultured with fibroblast embedded in a collagen I gel, recapitulating the in vivo heterogeneity.

Figure 3

Identification of novel tumour stroma markers by expression profiling analysis.
A. Antibody-guided laser capture microdissection allows the separation of epithelial cells from the activated stromal compartment in colon cancer samples. Activated tumor stromal fibroblasts were visualized by immunohistochemical staining with an antibody to FAPα . In the figure, the borders between epithelial and stromal structures are indicated by red dotted lines. Normal fibroblasts were isolated from normal colonic tissue after hematoxylin staining and morphological examination. After RNA isolation, whole genome Affymetrix GeneChip analysis was performed. Bioinformatic evaluation identified novel tumor stroma targets by comparing the tumor stroma vs. the normal stroma signatures.
B. Well characterized tumor stroma markers such as FAPα , MMP2, PDGFRß and FGFR1 were significantly up-regulated in the tumor stroma compartment. The expression levels are indicated by whisker box plots, the bold centre-line indicates the median; the box represents the interquartile range (IQR). Whiskers extend to 1.5 times the IQR. TC, tumor cells; NS, normal stroma; TS, tumor stroma.
C. Comparison of the transcriptional profiles obtained in our ex vivo screen in colorectal cancer samples with those obtained in an in vitro screen with a colon cancer cell line (LS174T) cultured in the presence colon-derived human CAFs in a 3D co-culture assay. Gene-Set Enrichment Analysis (GSEA) revealed gene sets involved in extracellular matrix deposition, angiogenesis and wound healing significantly upregulated in both studies.Two representative examples, Collagen IX a1 (COL11A1) and matrix metalloprotease 3 (MMP3) are shown. TC, tumor cells; NS, normal stroma; TS, tumor stroma; blue whisker box blots indicate the expression levels after 3.5 days of LS174T/CAF co-cultivation (TC/CoCult); yellow box blots show the levels of expression of individually cultured LS174T cells and CAFs mixed together after cultivation (TC/CAF Mix). Whisker box plot as in B.

Figures

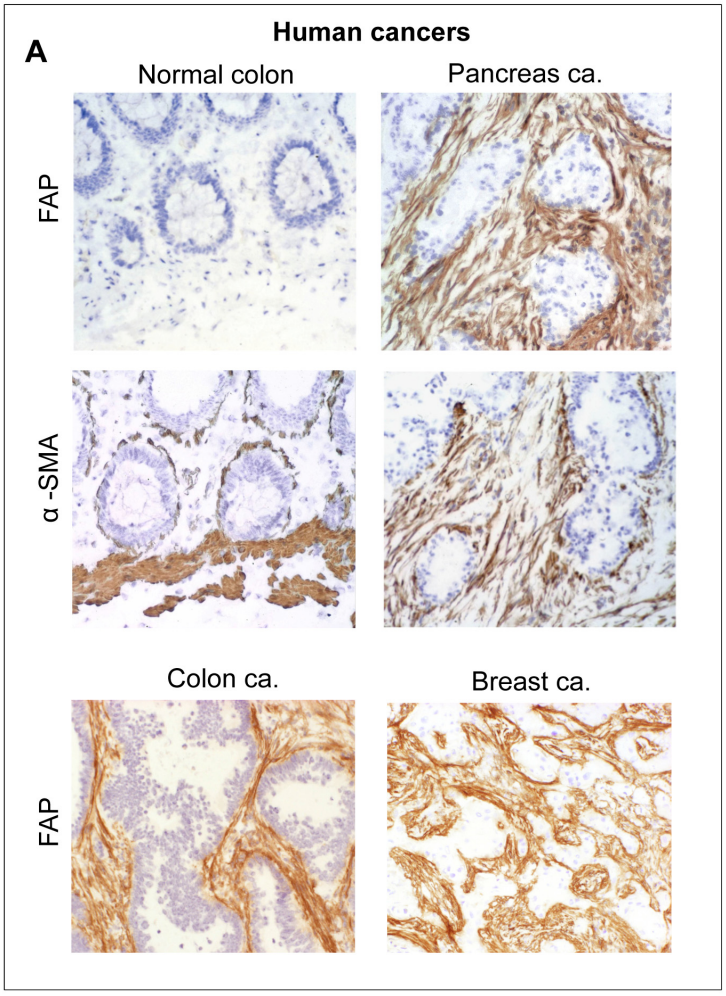

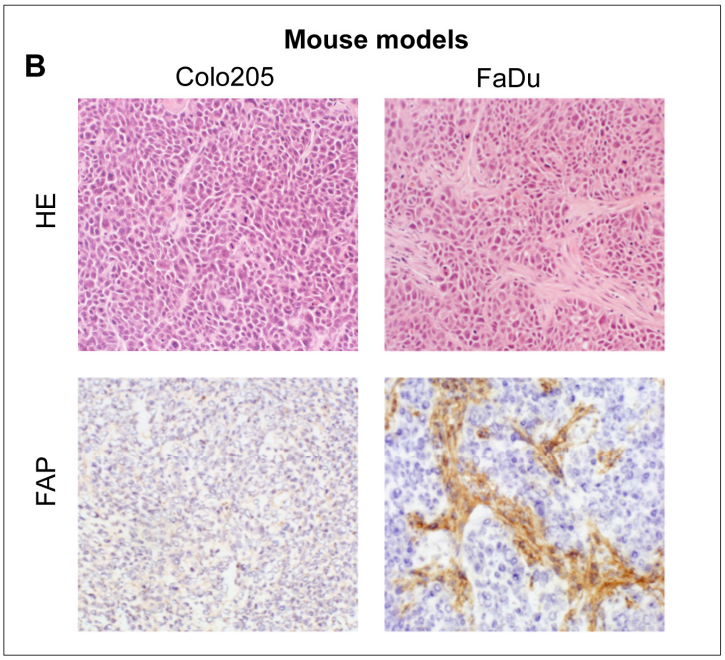

Figure 1

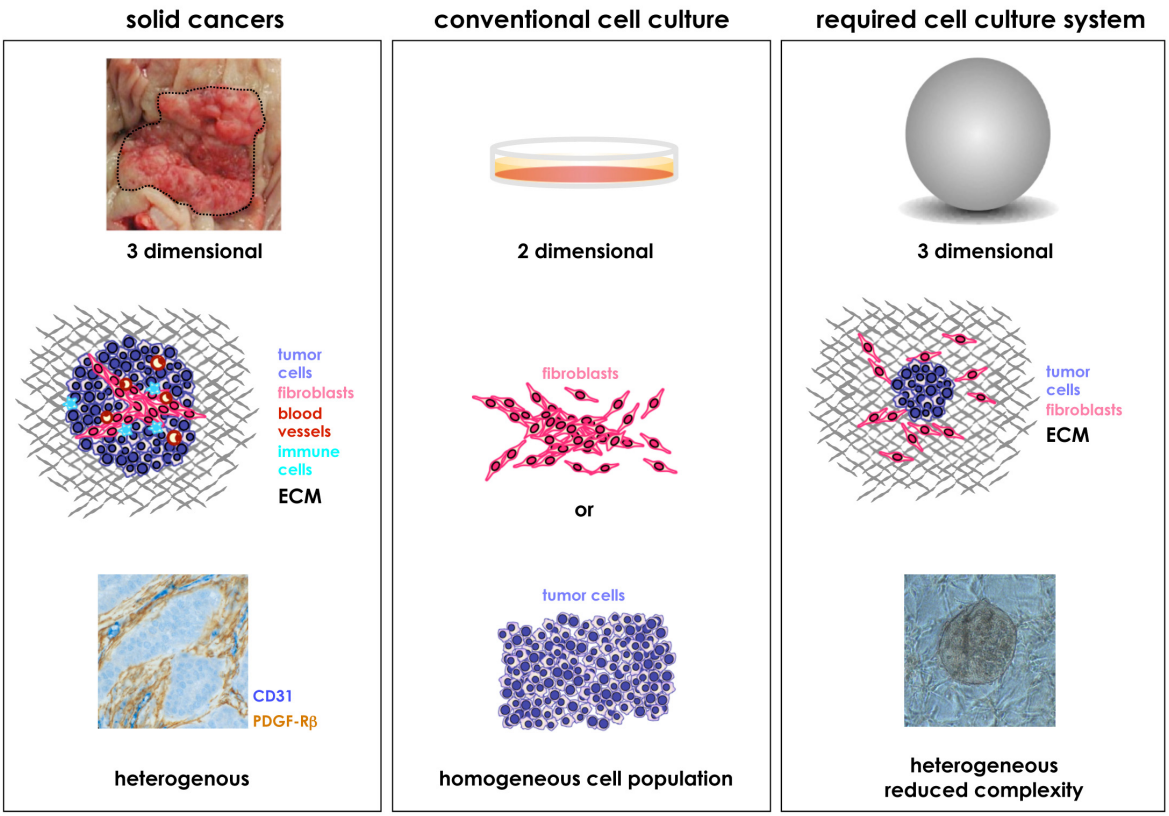
solid cancers
conventional cell culture
required cell culture system
3 dimensional
2 dimensional
3 dimensional
tumor cells
fibroblasts
blood vessels
immune cells
ECM
fibroblasts
or
tumor cells
tumor cells
fibroblasts
ECM
CD31
PDGF-Rβ
heterogenous
homogeneous cell population
heterogeneous reduced complexity

Figure 2

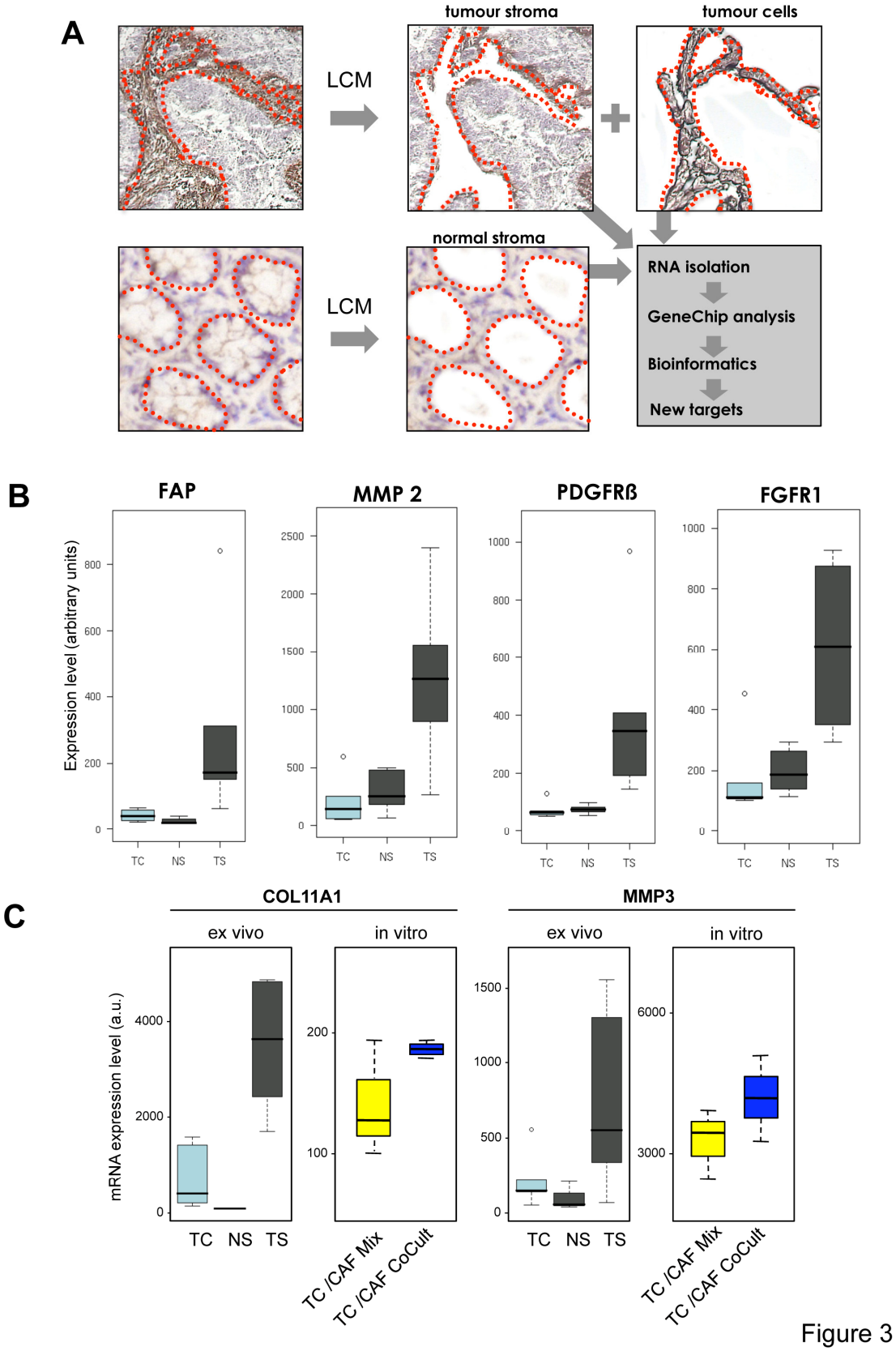
A
tumour stroma
tumour cells
LCM
normal stroma
LCM
RNA isolation
GeneChip analysis
Bioinformatics
New targets
B
FAP
MMP 2
PDGFRß
FGFR1
Expression level (arbitrary units)
TC
NS
TS
C
COL11A1
MMP3
ex vivo
in vitro
mRNA expression level (a.u.)
TC /CAF Mix
TC /CAF CoCult

Figure 3

Cancer Immunity, Vol. 6, p. 10 (31 July 2006)
Submitted: 25 April 2006. Accepted: 2 June 2006.
Communicated by: LJ Old

CANCER IMMUNITY
Article

Mouse endosialin, a C-type lectin-like cell surface receptor: Expression during embryonic development and induction in experimental cancer neoangiogenesis

Christian Rupp[1], Helmut Dolznig[1], Christina Puri[1], Wolfgang Sommergruber[2], Dontscho Kerjaschki[1], Wolfgang J. Rettig[2], and Pilar Garin-Chesa[1,2]

[1]Institute of Clinical Pathology, Medical University of Vienna, Waehringer Guertel 18-20, 1090 Vienna, Austria
[2]Boehringer Ingelheim Austria GmbH, Dr. Boehringer Gasse 5-10, 1120 Vienna, Austria

Keywords: mice, cultured tumor cells, xenograft, endosialin, immunohistochemistry, RT-PCR

Endosialin is a C-type lectin-like cell surface receptor of unknown function, with a distinctive pattern of endothelial expression in newly formed blood vessels in human cancers. The murine orthologue of endosialin has been identified, opening up the analysis of developmental regulation in the embryo and in aberrant tissue remodeling, notably cancer angiogenesis. To advance these studies we have generated an antibody to the extracellular domain of mouse endosialin and mapped protein expression from embryonic day E10.0 to the adult stage, complemented by mRNA quantification and co-typing for standard endothelial markers. Four main findings emerged. First, endosialin protein is restricted to vascular endothelium and fibroblast-like cells in developing organs, and largely disappears in the adult. Second, endothelial expression varies markedly between organs regarding spatial and temporal patterns. For instance, in the E10.0 embryo, endosialin is prominent in the endothelium of the dorsal aorta and, from E11.0 to E14.5, in vessels sprouting from the dorsal aorta, in perineural vascular plexuses, and in brain capillaries. Third, circumscribed mesenchymal expression in fibroblast-like cells was evident throughout development, most pronounced adjacent to certain budding epithelia, as exemplified by the lung and kidney glomeruli, but unrelated to the endothelial expression. The endosialin protein persists in the stromal fibroblasts of the adult uterus. Finally, in subcutaneous cancer xenograft models endosialin re-appears in the host-derived tumor stroma, both in neo-angiogenic vascular endothelium and in activated stromal fibroblasts. In future studies, the search for intrinsic or extrinsic signals contributing to endosialin induction in cancer stroma will be of interest.

Introduction

Human endosialin is a highly sialylated, C-type lectin-like cell surface receptor structurally related to thrombomodulin and complement receptor C1qRp (1, 2). First identified with a monoclonal antibody, mAb FB5 (1), endosialin was discovered independently through large-scale expression profiling of human cancer endothelial cells with the SAGE (serial analysis of gene expression) method (3), leading to the alternative designation of tumor endothelial marker 1 (TEM1). Both lines of investigation suggested that human TEM1/endosialin RNA and protein expression distinguish tumor endothelium from the endothelium of most normal adult tissues. The initial immunohistochemical studies with mAb FB5 pointed to a marked heterogeneity of antigen expression within a given tumor nodule and among similar cancer types derived from different patients (1), a finding extended by subsequent studies (4), while others using different anti-human endosialin antibodies described antigen expression in vascular pericytes in a small number of human breast cancer samples (5), and in tumor endothelium and pericytes in invasive brain tumors (6). Why some vascular endothelial cells show induction of endosialin *in vivo* has remained an open question, and commonly used *in vitro* systems, such as human umbilical vein endothelial cell cultures, fail to express endosialin under standard growth conditions or following stimulation with known endothelial activators (1, 5, 7).

The molecular cloning of the mouse orthologue of endosialin (mEs), with 77 percent overall sequence homology and comparable domain structure, has been described (7, 8). Mouse endosialin comprises a 92-kDa cell surface glycoprotein with highly sialylated, O-linked oligosaccharide side chains similar to the human protein. While non-quantitative RT-PCR studies suggested the presence of endosialin RNA in most tissues of the adult and embryonic mouse (7), a competing approach with *in situ* hybridization found endosialin mRNA specifically localized to tumor endothelium in experimentally-induced mouse cancers, in subsets of blood vessels in E15.5 mouse embryos (8), but not in most adult mouse tissues.

The present study was designed to generate an antibody against mouse endosialin and to clarify the pattern of protein expression in fetal and adult mouse tissues, as well as blood vessels of experimental cancer models in the mouse. The emphasis was placed on a systematic tissue analysis, complemented by mRNA quantification and co-typing with standard endothelial markers for selected tissues.

Results

Generation of a polyclonal antibody to mouse endosialin

A series of polyclonal rabbit antibodies (Ab) was raised against unique peptide epitopes of the extracellular domain of mouse endosialin, and the best candidate, Ab 171, was selected for

Cancer Immunity, Vol. 6, p. 10 (31 July 2006)

Figure 1

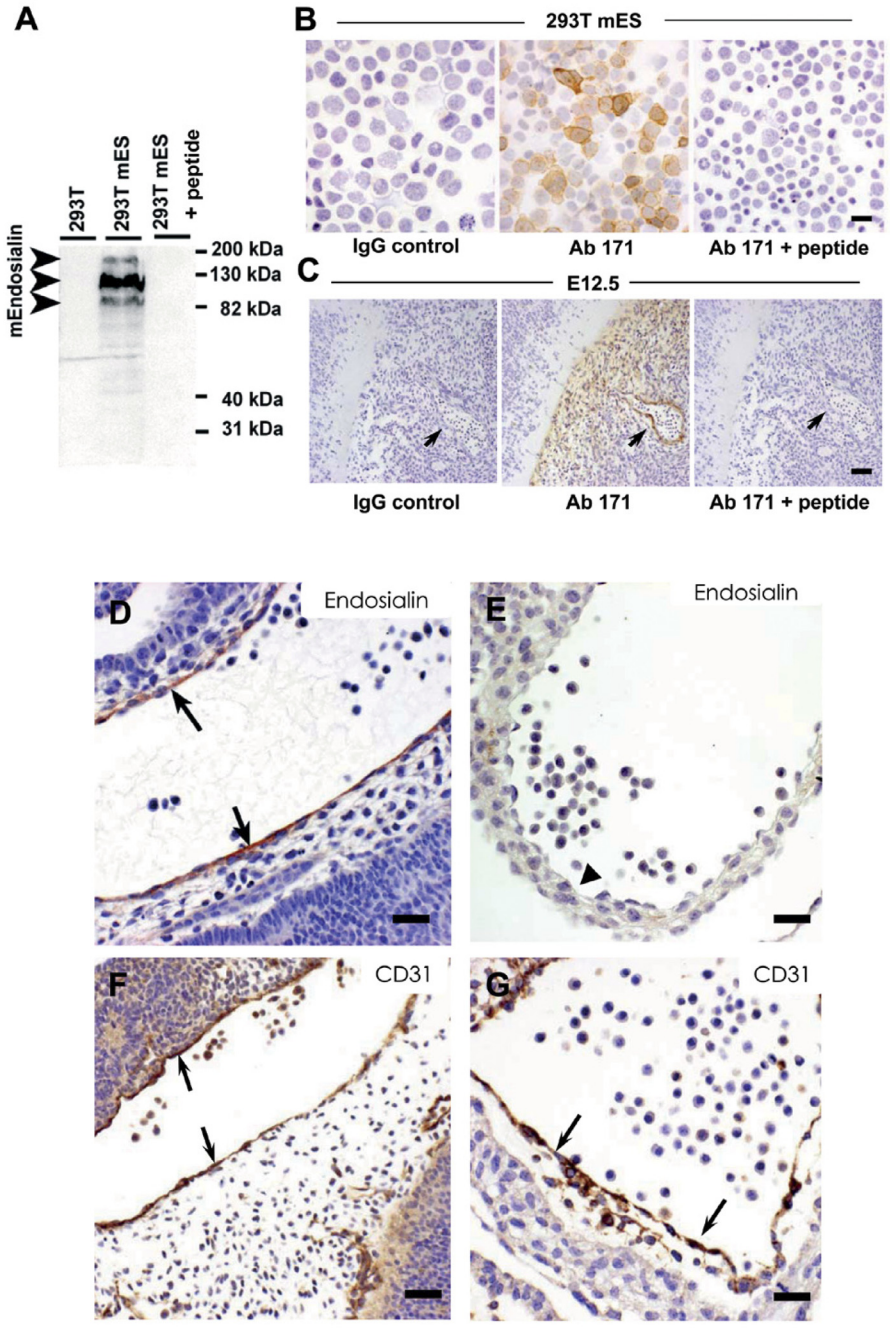

Generation of a polyclonal antibody to mouse endosialin. Antibody 171 specifically recognizes mouse endosialin in cell extracts (A) and in tissue sections (B, C). (A) Immunoblot analysis of cell extracts prepared from mEs-transfected 293T cells shows three bands, corresponding to the known 90-kD, 110-kDa and 160-kDa protein species. These bands are not seen in extracts prepared from non-transfected 293T cells, and they are abolished by preincubation with the immunizing peptide 171 (293T mEs + peptide). The positions of molecular size markers are indicated on the right. (B) Immunocytochemistry of mEs-transfected 293T cells (293T mEs) shows cell membrane staining in a subset of cells, which is not seen with a negative control IgG or following incubation with Ab 171 pre-incubated with the immunizing peptide. Cells were stained by the ABC immunoperoxidase method with hematoxylin counterstaining. (C) Immunohistochemical staining of paraffin-embedded sections from an E12.5 mouse embryo. Using Ab 171, endosialin is detected in endothelial cells of a blood vessel (arrow) and in scattered mesenchymal cells in the perineural space; no staining is seen with a negative control IgG or with Ab 171 pre-incubated with the immunizing peptide. Staining of selected cardiovascular structures in a E10.5 mouse embryo with Ab 171 to endosialin (D, E) and pan-endothelial marker CD31 (F, G) revealed strong expression of endosialin and CD31 along the endothelial lining of the dorsal aorta (arrows in D and F). The endothelial cells of the endocardium are endosialin-negative (E) in contrast to the strong staining seen with the anti-CD31 antibody (G, arrows). The ABC staining method was used, with hematoxylin counterstaining. Scale bars: 25 μm.

Figure 2

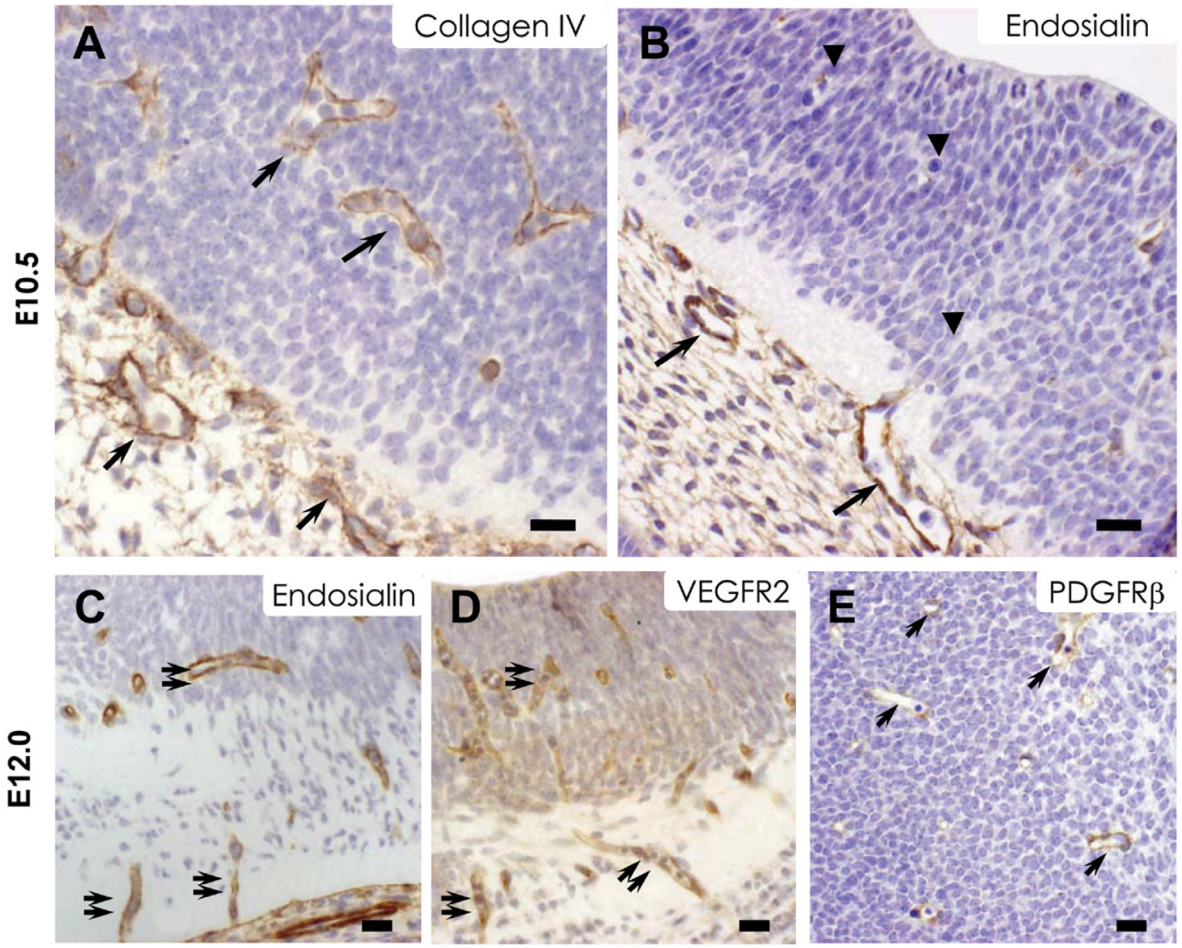

Endosialin expression by developing brain capillaries in E10.5 and E12.0 mouse embryos. Sections of forebrain from an E10.5 (A, B) mouse embryo were stained with anti-collagen type IV (A) or Ab 171 (B). Collagen type IV maps to blood vessels of the perineural plexus and angiogenic sprouts in the brain parenchyma (arrows in A). Most endosialin-positive vessels at this stage are localized to the perineural plexus (arrows in B), while most vessels in the brain lack endosialin (arrowheads in B). At E12.5 endosialin (C) localizes to small and medium-sized blood vessels, including those (double arrows) inside the brain, and the number and pattern of endosialin-positive vessels is similar to those expressing VEGFR-2 (D, double arrows). By contrast, PDGFR-β (E) is seen in subsets of vessels with a distinct, discontinuous pattern (arrows in E). Scale bars: 25 μm.

affinity-purification and detailed profiling. Ab 171 recognizes the predicted, differentially glycosylated forms of mouse endosialin (Figure 1, panel A) in immunoblot experiments, notably the 90-kDa, 110-kDa and 160-kDa protein species, using extracts of mEs-transfected 293T cells, but not in non-transfected 293T control cells. Pre-absorption of Ab 171 with the cognate peptide abolished this reactivity. Specific binding to cell surface-expressed mouse endosialin was detected by immunocytochemistry (Figure 1, panel B), using cytospin preparations of intact mEs-transfected 293T cells, as compared to non-transfected 293T cells. Importantly, we found that Ab 171 is suitable for immunohistochemical detection of endosialin in paraffin-embedded mouse tissue sections, again showing specific blocking with cognate peptides (Figure 1, panel C), as this allows higher resolution mapping of the endosialin protein localization.

Immunohistochemical analysis of embryonic mouse tissues

The analysis of endosialin protein expression in the mouse embryo covered stages E10.0 to E17.5. At embryonic stage E10.0, endosialin expression was exclusively seen in the endothelial cells of the dorsal aorta (Figure 1, panel D). The endothelial cells covering the cavity of the heart did not show any immunoreactivity with Ab 171 (Figure 1, panel E), in contrast to the general endothelial marker PECAM-1/CD31, which was present in the endothelium of the dorsal aorta (Figure 1, panel F) as well as in endocardium (Figure 1, panel G). Co-typing with antibodies to platelet-derived growth factor receptor-β (PDGFR-β) and α-smooth muscle actin (αSMA) identified the presence of pericytes expressing both markers, surrounding the endothelium of the dorsal aorta at this stage (not shown).

During stages E10.5 and E12.0, a prominent perineural vascular plexus develops in the head region (Figure 2, panels A and B)

Cancer Immunity, Vol. 6, p. 10 (31 July 2006)

which is endosialin positive (Figure 2, panel B). Angiogenic sprouts from this perineural plexus invade the proliferating neuroectoderm by embryonic day E11.0-E12.0. These newly formed vessels are elongated, give rise to many branches that anastomose with adjacent sprouts to form a plexus of immature capillaries in the developing brain. The extent of the perineural vascular plexus and its angiogenic sprouts were visualized by staining with an Ab directed to the basement membrane component collagen type IV, as illustrated in Figure 2, panel A. At E10.5, the majority of the vessels of the perineural plexus and those in close proximity to the outer layer of the brain showed strong endosialin expression (Figure 2, panel B, arrows), whereas only a small subset of vessels was endosialin-positive deeper in the brain parenchyma (Figure 2, panel B, arrowheads).

In the E12.0 embryo, the vascular system has developed considerably in the entire embryo and in particular in the brain. Numerous vessels sprouting from the perineural plexus into the brain can be observed at this stage (Figure 2, panels C-E). A comparison of the endosialin expression pattern (Figure 2, panel C) with the endothelial marker VEGFR-2 (Figure 2, panel D) revealed that all vessels in the perineural space, as well as those inside the brain, are positive for both markers. In contrast, αSMA was only observed in the larger vessels of the perineural space, and not in the small vessels inside the brain (not shown). The lack of αSMA in these vessels does not indicate that they are immature, since an Ab to PDGFR-β showed the expected pericyte labeling (Figure 2, panel E) in subsets of capillaries at this developmental stage. These findings are in agreement with previous reports indicating the lack of αSMA staining on most capillary-sized vessels in the mouse brain (9), and the presence of solitary PDFGR-β-positive pericytes in proximity to capillaries in mouse embryos by *in situ* hybridization (10).

Double-labeling studies on brain sections from E12.5 embryos (Figure 3) revealed that the endothelial cells lining the vessels co-expressed endosialin and VEGFR-2, whereas PDGFR-β was expressed by perivascular pericytes that did not show endosialin expression. For endosialin, we noted a predominantly abluminal distribution on the endothelial cells, compared with the preferentially apical localization of VEGFR-2 on the endothelial cells (Figure 3, panel A). Furthermore, we found as a consistent feature that PDGFR-β expressing, endosialin-negative pericytes (marked by arrowheads in Figure 3, panel B) come into close contact with the endosialin-positive, PDGFR-β negative endothelial cells, yet are spatially separated as revealed by the merged immunofluorescence images (Figure 3, panel B; right panel). Finally, in more mature vessels of the perineural plexus, endosialin-positive endothelial cells were found to be embedded in the basal membrane, as identified by labeling of collagen type IV (Figure 3, panel C).

By mid-gestation (E13.5 - E14.5), endosialin was detected in clusters of mesenchymal cells in the head region and surrounding the developing structures of the genitourinary system as shown in Figure 4, panel A. Furthermore, expression was observed in organs such as lung and salivary gland, where endosialin-positive, fibroblast-like cells were seen at the epithelial-mesenchymal interface, as shown for lung development in Figure 4, panel B. In some of the buds, a gradient of staining intensity was seen with strong expression by fibroblasts at the tip of the bud, and weaker expression at the stem. The epithelial cells lining the lung buds, as well as the blood vessels in the interstitial tissues, were endosialin-negative (Figure 4, panel B). Prominent endosialin expression at epithelial-mesenchymal interfaces was also observed in areas of epithelial folding, for instance during the formation of the optic cup (Figure 4, panel C), in the oropharynx, and surrounding the hair follicles (not shown).

By late-gestation (E17-17.5), clusters of endosialin-positive mesenchymal cells are seen in the folding mucosa of the gastric cavity (Figure 4, panel D). These cells are located in the lamina propria, underneath the gastric epithelium. Endosialin-expressing mesenchymal cells were also observed in the dermis, notably around hair follicles, and as dense bands of mesenchymal cells separating skeletal muscle fibers (Figure 4, panel D). In addition, endosialin staining was detected in subsets of cells in immature glomeruli (Figure 4, panel E), putatively identified as mesangial cells, a specialized type of pericyte in the kidney. No endosialin was detected at this stage in the lung (Figure 4, panel F), in contrast to αSMA, which was present in the smooth muscle layer of blood vessels and in myoepithelial cells surrounding the bronchi (Figure 4, panel G).

Immunohistochemical analysis of endosialin in newborn mouse tissues

Expression of endosialin in brain capillaries (Figure 5, panel D) of newborn mice coincides with the peak of angiogenesis in the early postnatal period (11). In addition, small clusters of endosialin-positive cells are seen in the renal glomeruli at this stage (Figure 5, panel E). By comparison, co-typing for CD31 showed a broader expression of this general endothelial marker in peritubular vessels and glomerular capillaries (Figure 5, panel F). Most other newborn organ systems tested lacked any endosialin expression, as illustrated for the liver, small intestine, and heart in Figure 5, panels A-C.

Immunohistochemical analysis of adult mouse tissues

In the adult mouse, endosialin was undetectable in all of the blood vessels of the organs and tissues examined, including cerebellum, cerebral cortex, liver and lung (Figure 5, panels G-L). In the kidney, the putative mesangial cells of the glomeruli remained endosialin-positive (Figure 5, panel K), but the proportion of labeled cells appeared to decrease compared to earlier developmental stages, and some labeled cells mapped to the juxtaglomerular apparatus. In female mice, strong endosialin staining was observed in the mesenchyme of the uterus (Figure 5, panel L).

Real-time RT-PCR for quantification of global endosialin mRNA patterns

Endosialin mRNA levels determined by quantitative, real-time RT-PCR corroborated the results of our immunohistochemical analysis. As shown in Figure 6, endosialin mRNA expression increases during development in whole embryos covering stages E11.5 to E14.5, with a drop in levels for most newborn and adult tissues, except the newborn kidney and adult uterus.

Immunohistochemical analysis of neoangiogenic endothelium in cancer models

Subcutaneously growing xenografts of human epithelial cancers in mice were analyzed for the expression of endosialin in the host-derived tumor stroma. In total, 15 different xenograft models were analyzed, including colorectal (Colo205, HCT116, HT29, LoVo and DLD1), breast (MCF7, MDA-MB231, MDA-MB468), lung (Calu6, NCI-H520, NCI-H157), prostate (DU145, PC3), pancreatic (AsPc1), and ovarian (SKOV3) carcinomas. In all cancer models, endosialin expression was observed in subsets of tumor-associated blood vessels, as shown in Figure 7, panels A and D. Co-typing with the standard endothelial marker, CD31 (Figure 7, panel B), suggested that endosialin can be assigned to

Figure 3

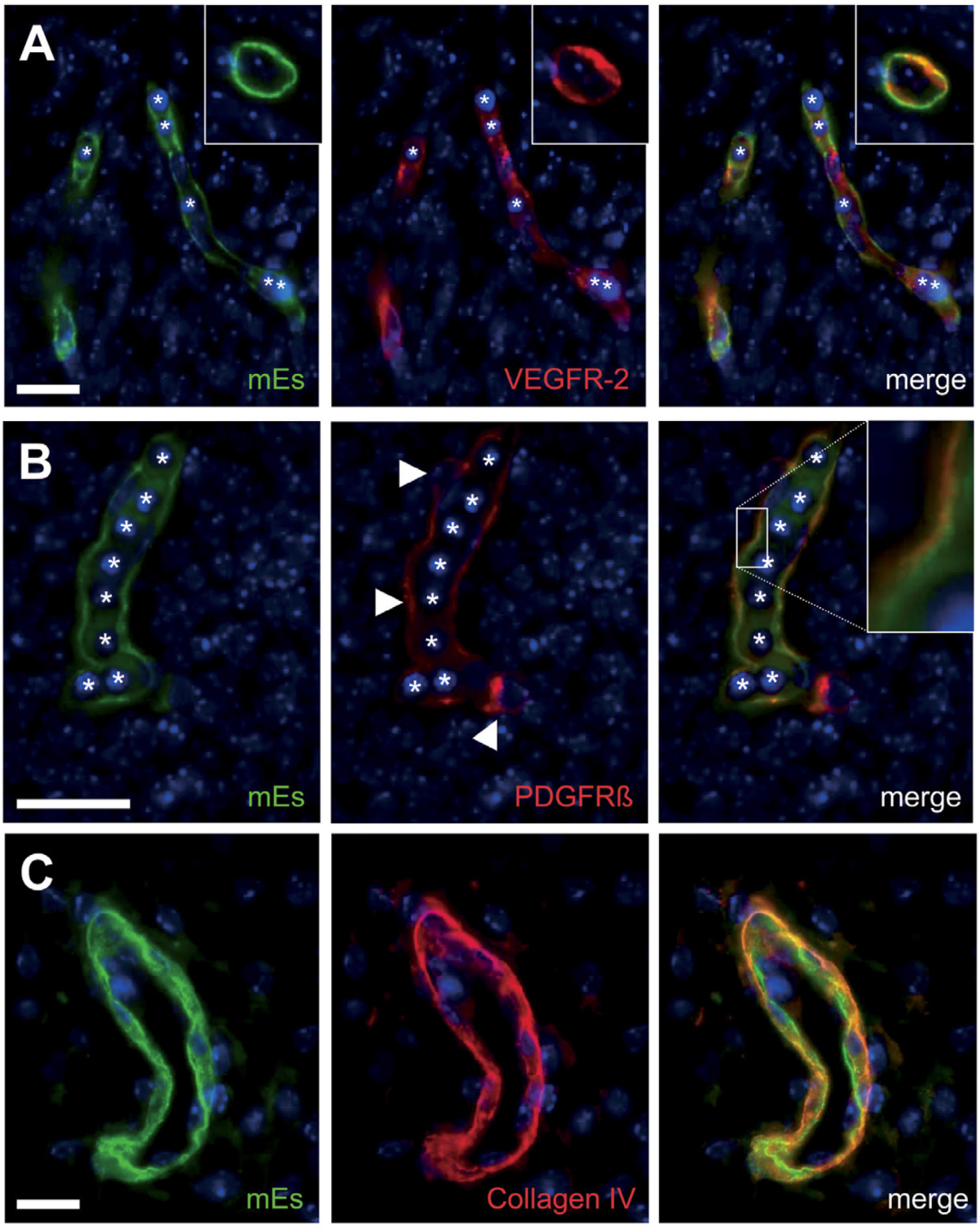

Endosialin expression in E12.5 mouse embryos. Brain sections from E12.5 embryos were double-labeled for endosialin and VEGFR-2 (A); endosialin and PDGFR-β (B) and endosialin and collagen type IV (C). Panel A illustrates the expression of endosialin (green) and VEGFR-2 (red) by the endothelial cells of brain capillaries in longitudinal and cross-sections (insert). Endothelial cells appeared to co-express both markers as seen in the merged images (yellow). Endosialin and PDGFR-β are expressed by distinct cell populations within the brain capillaries as indicated in panel B. Endosialin positive endothelial cells (green) are in close contact with PDGFR-β positive pericytes (red, arrowheads) from the adluminal side of the vessel wall, yet are spatially separated as revealed by the merged images (insert, right panel). In panel C, more mature vessels of the perineural plexus endothelial cells expressing endosialin (green) are embedded in the basal membrane, identified by labeling of collagen type IV (red). Cell nuclei were counterstained with DAPI (blue). Asterisks indicate the presence of nucleated erythrocytes within the vessels. Scale bars: 20 μm.

Cancer Immunity, Vol. 6, p. 10 (31 July 2006)

Figure 4

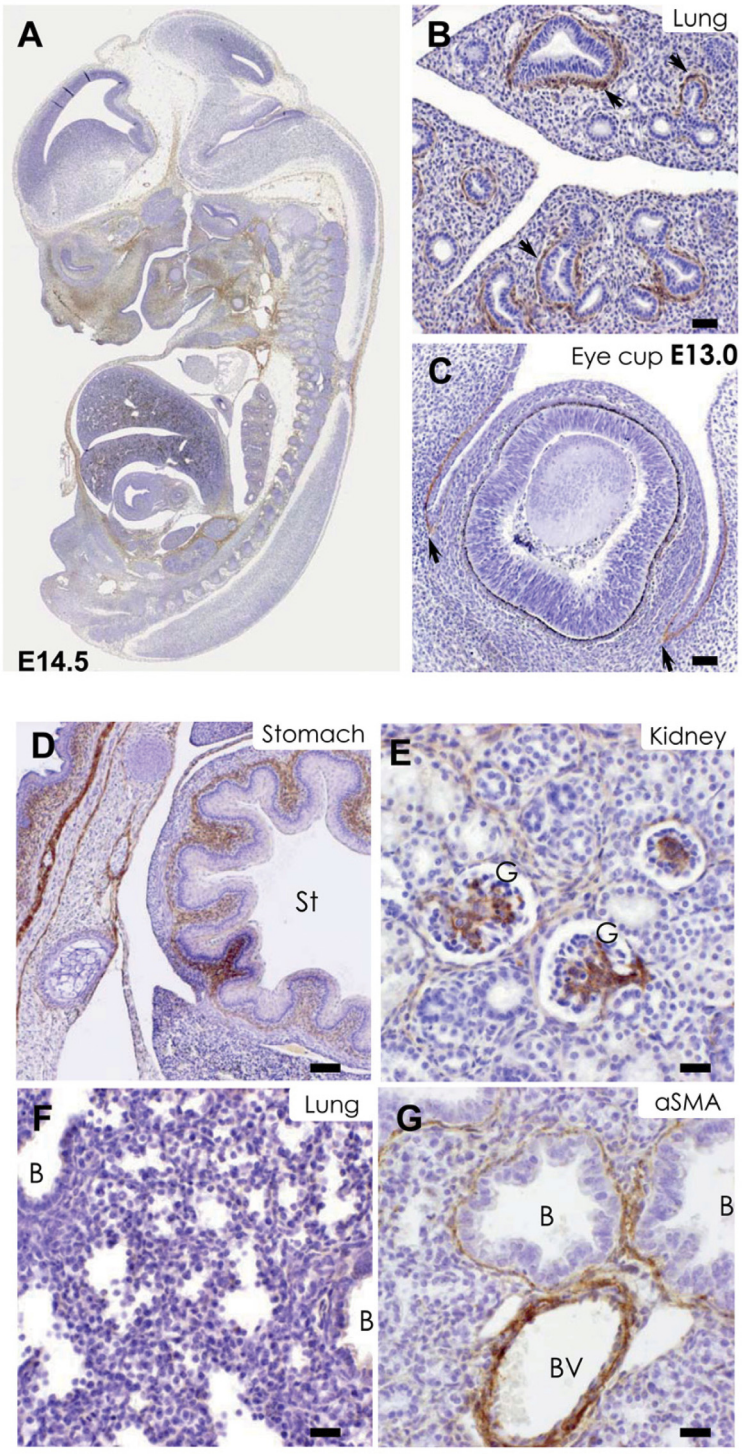

Endosialin expression patterns in stage E14.5 and E17.5 mouse tissues. Global pattern of endosialin expression in an E14.5 embryo (A), in the lung (B) and in the eye cup (C) at the same stage. In a parasagittal section (A), endosialin is seen in mesenchymal cells in the head and in the pelvic regions, in particular in organs of the genitourinary system. In the developing lung (B) and eye (C), endosialin is found at the epithelial-mesenchymal interface of developing lung buds and under the epidermal invagination of the skin during the development of the optic cup (arrows). In the stomach of a E17.5 embryo (D; gastric lumen marked St), endosialin is found in mesenchymal cells of the lamina propia; in the same panel (D) endosialin expression is also visible in the subcutaneous tissue of the skin, and in the perimysium of the intercostal muscles. In the kidney (E), endosialin maps chiefly to the immature glomeruli. In the lung (F, G), endosialin is not detectable (F), whereas αSMA (G) marks vascular smooth muscle (blood vessels marked BV) and myoepithelial cells around bronchial epithelium (marked B). Scale bars: 50 μm (B, C), 125 μm (D), 25 μm (E-G).

Figure 5

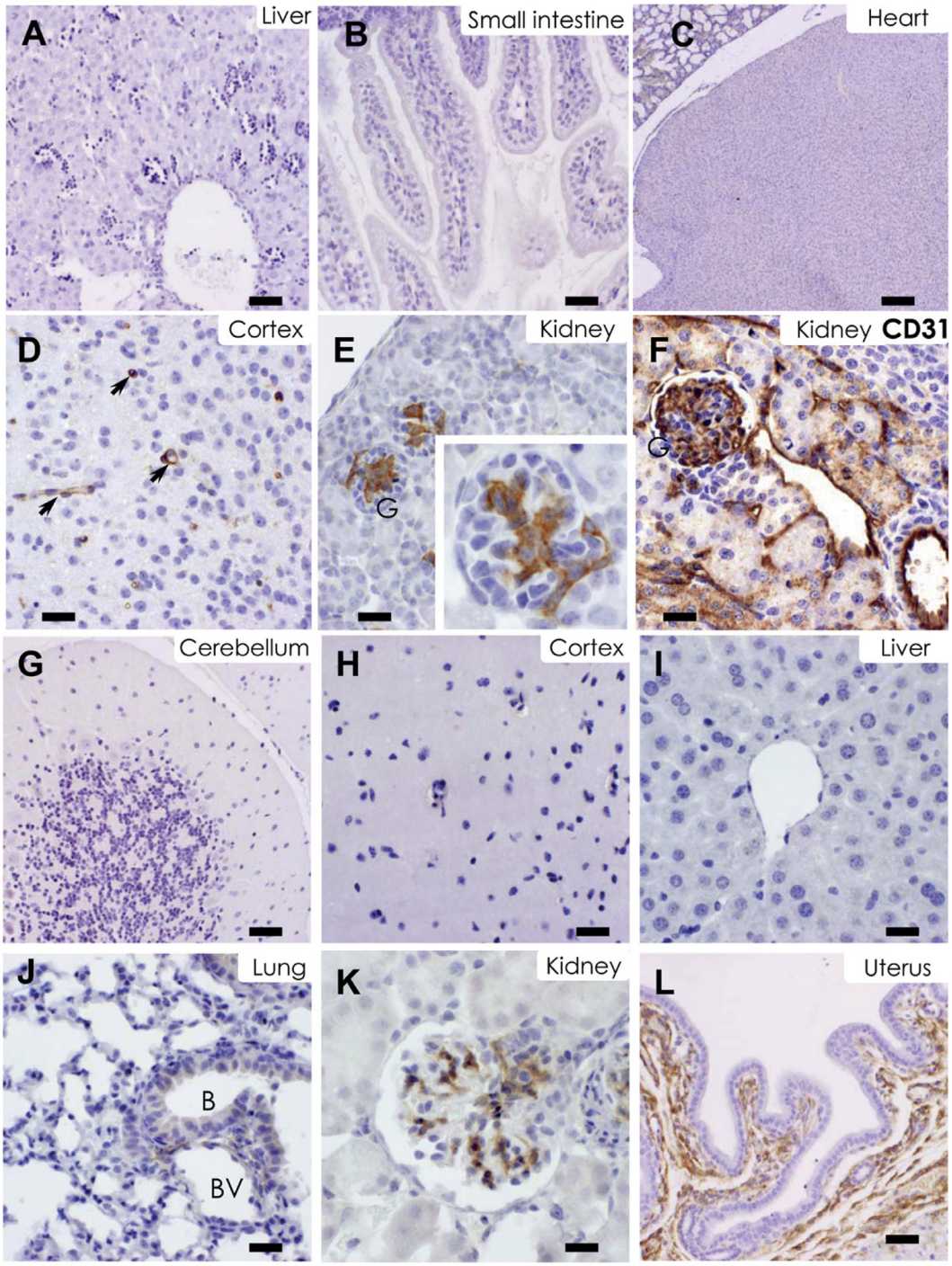

Endosialin expression in newborn (A-F) and adult (G-L) mouse tissues. Newborn liver (A), small intestine (B), and heart (C) lack endosialin immunostaining, whereas newborn brain capillaries are endosialin-positive (D), and newborn kidney glomeruli show endosialin expression in mesenchymal cells (E; insert with higher magnification). This pattern differed markedly from that seen with the pan-endothelial marker CD31 (F). Among the adult mouse tissues tested (G-L), the cerebellum (G), cerebral cortex (H), liver (I) and lung (J) lack detectable endosialin expression. In the adult kidney (K), endosialin maps to some glomeruli with a mesenchymal pattern, and in the uterus of pregnant mice (L), endosialin is expressed in fibroblastic stromal cells, but not in the lining epithelium or smooth muscle layer. Scale bars: 125 μm (C); 50 μm (A, B, G, J, L); or 25 μm (D-F, H, I, K).

Cancer Immunity, Vol. 6, p. 10 (31 July 2006)

Figure 6

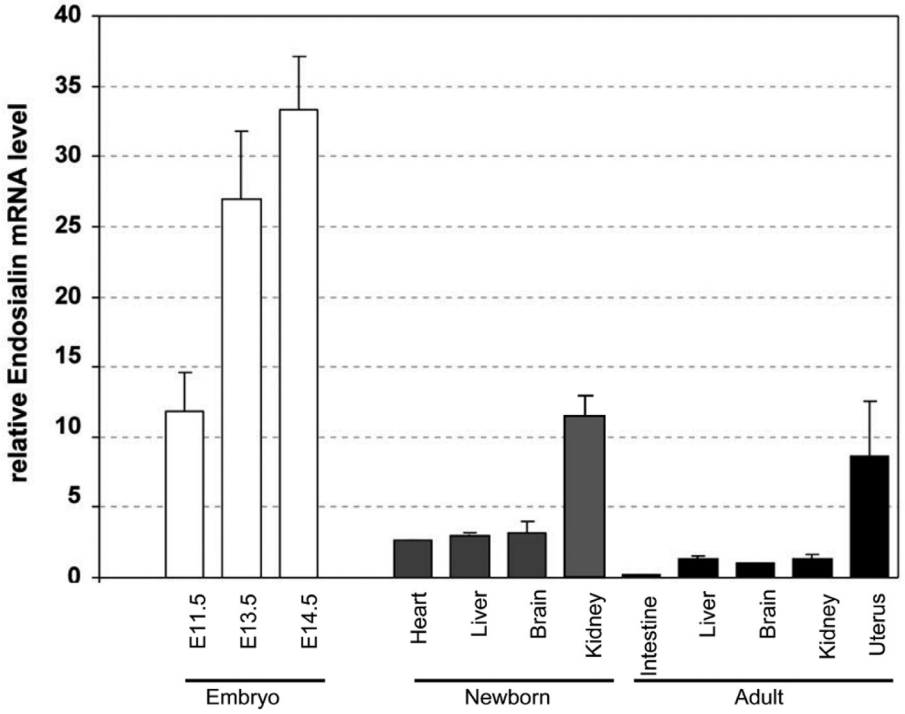

Mouse endosialin RNA expression. Quantitative real-time RT-PCR of total RNA extracted from whole mouse embryos at stages E11.5, E13.5 and E14.5, and distinct newborn and adult organs. The relative expression of endosialin is normalized to the amount of mGAPDH in the same cDNA sample, the standard deviation (indicated by the error bars) is calculated from a set of 3 independent experiments. Note that whole-embryo endosialin mRNA levels increase from E11.5 to E14.5, and are markedly lower, in the selected organs, in newborn and adult animal. The newborn kidney and adult pregnant uterus show higher mRNA levels, consistent with the immunohistochemical staining results.

neo-angiogenic capillary endothelial cells in these models, rather than to pericytes, as illustrated in Figure 7, panels A and B, for a colorectal cancer. In addition, scattered activated tumor stromal fibroblasts, located in close proximity to tumor cell clusters, also express endosialin (Figure 7, panel C). While similar patterns were observed in the various cancer models studied, the extent of endosialin induction in tumor angiogenesis appeared to vary widely, with no correlation to cancer type or histological growth patterns apparent from this survey.

Discussion

The study of endosialin or TEM1/Tem1 (1, 3), a putative C-type lectin-like cell surface receptor (2), as a marker of neo-angiogenesis and tumor stroma formation in human cancers and experimental mouse tumors (1, 3, 4, 6) is hampered by the lack of understanding concerning its molecular function, but has gained momentum with the recent description of a targeted disruption of *Tem1* in mice (12). Thus, Nanda *et al.* provide initial evidence that this protein is dispensable for normal development in *Tem1*$^{-/-}$ mice, for wound healing, and for subcutaneous tumor growth, but markedly modulates invasiveness and metastatic progression in an orthotopic, abdominal xenograft model of HCT116 colorectal cancer cells in immunodeficient mice.

There is currently no simple mechanistic model to accommodate these observations of Nanda *et al.* (12) regarding growth and progression of abdominal tumors in the *Tem1*$^{-/-}$ mice, and several levels of complexity have been identified and are of relevance for our present report on endosialin patterns in developing mouse organs and mouse cancer models.

First of all, as pointed out in the initial description of endosialin expression in human cancers, this molecule is expressed selectively in tumor endothelial cells but also, with a variable pattern, in activated tumor stromal fibroblasts (1), a cell type distinct from resting fibroblasts and previously shown to express the cell surface serine protease FAPα (4). We now show that this principle also holds for mouse endosialin, which can be found in tumor vascular endothelial cells and tumor stromal fibroblasts. Accordingly, it remains to be determined whether one or both of these cell types mediate the observed effects in the abdominal tumor model. Double-labeling for distinct stromal cell markers has allowed us to confirm our previous conclusion, based on human cancer studies, that endosialin is expressed by the endothelial cells proper and not by the pericytes that are found immediately juxtaposed to the endothelial cells. The fact that endosialin shows a predominantly abluminal localization in the endothelial cells, which differs from an apical endothelial marker such as VEGFR-2, has meant that the high resolution and tissue preservation possible in the formalin-fixed paraffin-embedded samples, the availability of our polyclonal antibody suited to study paraffin-embedded tissues, and the analysis of merged immunofluorescence patterns were all necessary to make this distinction.

Secondly, a distinctive feature of endosialin expression in human cancer tissues has been its heterogeneous presence on tumor endothelial cells, with marked differences between samples of a given histological type and also between different areas of a given cancer lesion (1, 13); this heterogeneity in expression in human cancers did not show any obvious correlation to clinico-pathological features. We now show that endosialin expression

Figure 7

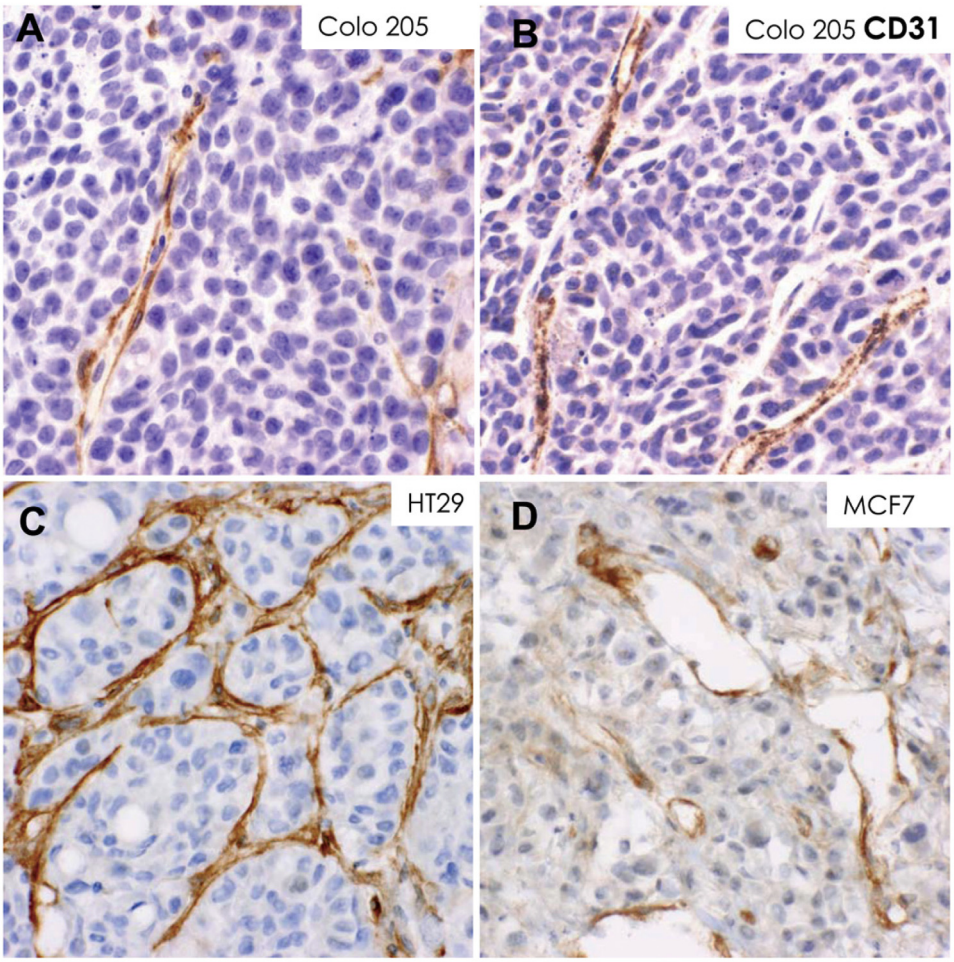

Endosialin induction during neo-angiogenesis in subcutaneous xenografts of human cancer cells in nu/nu mice. In the colon cancer model Colo 205 (A, B), endosialin is expressed by endothelial cells of the tumor capillaries (A), with a pattern very similar to the reference endothelial marker CD31 (B). In the colon cancer model HT29 (C), endosialin is also induced in the host-derived cancer stroma, but with a cellular pattern that extends to the tumor stromal fibroblasts. In the breast cancer model MCF7 (D), endosialin is seen in the endothelial cells of the cancer stroma. Scale bars: 25 µm.

in developing mouse tissues and, importantly, in a range of experimental cancer models in the mouse, recapitulates this level of complexity. For embryonic mouse tissues (no data available for the corresponding human tissues), this diversity includes differences among vascular structures in distinct regions, with endosialin expression in the endothelium of the dorsal aorta, intersomitic vessels, perineural plexus, and brain capillaries on the one hand, and its absence in many other developing organs and most of the adult organs tested on the other hand. At present, we cannot exclude completely that technical factors contribute to these results; for example, immunohistochemical methods may detect only high levels of endosialin, with lower levels being present more widely on vascular endothelium yet escaping detection. However, the presence of strongly labeled and unlabeled segments of the vasculature in close proximity in the same tissue section are more likely due to clear differences in expression than to subtle quantitative variations; if this is true, it will be of interest in future studies to determine the locally acting factors that control endosialin expression in a spatial and temporal manner. Since endosialin is not a constitutive endothelial cell surface marker, it comes as no surprise that one of the well-explored *in vitro* cell culture models of endothelial biology, namely human umbilical vein endothelial cells, fails to express endosialin, and shows no induction when stimulated with standard peptide growth and differentiation factors (1). The search for more appropriate cellular models, perhaps involving microvascular endothelial cells, should be rewarding.

Finally, by extending the tissue analysis of endosialin to the developing mouse, we have been able to substantiate the restricted expression pattern seen in normal human tissues (1, 4, 13) and to document the general disappearance of mouse endosialin during early postnatal development, with re-appearance in cancer tissues. In humans as well as in mice, the stromal fibroblasts of the uterus and specialized cells of the kidney glomeruli continue to express endosialin at the adult organ stage. The observation of normal development in *Tem1*$^{-/-}$ mice (12) does not necessarily mean that endosialin has no developmental function; instead, its role may be taken over by redundant physiological mechanisms in the gene knockout animals. By contrast, the critical steps in abdominal cancer progression identified by Nanda *et al.* (12)

Cancer Immunity, Vol. 6, p. 10 (31 July 2006)

may simply have fewer redundant molecular controls, thus leading to a phenotype that becomes apparent more readily under experimental conditions. Targeted disruptions of other endothelial markers, such as PECAM and CD34 in mice, have also failed to disrupt vasculogenesis on their own (14, 15, 16). Thus, a full understanding of endosialin function in normal development and cancer may not be possible without a clear understanding of its molecular function, overlapping functions carried out by other endothelial and tumor stromal markers, and the identification of the local factors that modulate the distinctive endosialin tissue patterns.

Abbreviations

mEs, mouse endosialin; αSMA, α-smooth muscle actin; TEM1, tumor endothelial marker 1 (endosialin)

Acknowledgements

We thank Anke Baum, Christine Hartmann and Herbert Lamche for valuable contributions.

References

1. Rettig WJ, Garin-Chesa P, Healey JH, Su SL, Jaffe EA, Old LJ. Identification of endosialin, a cell surface glycoprotein of vascular endothelial cells in human cancer. *Proc Natl Acad Sci U S A* 1992; **89**: 10832-6. (PMID: 1438285)

2. Christian S, Ahorn H, Koehler A, Eisenhaber F, Rodi HP, Garin-Chesa P, Park JE, Rettig WJ, Lenter MC. Molecular cloning and characterization of endosialin, a C-type lectin-like cell surface receptor of tumor endothelium. *J Biol Chem* 2001; **276**: 7408-14. (PMID: 11084048)

3. St Croix B, Rago C, Velculescu V, Traverso G, Romans KE, Montgomery E, Lal A, Riggins GJ, Lengauer C, Vogelstein B, Kinzler KW. Genes expressed in human tumor endothelium. *Science* 2000; **289**: 1197-202. (PMID: 10947988)

4. Dolznig H, Schweifer N, Puri C, Kraut N, Rettig WJ, Kerjaschki D, Garin-Chesa P. Characterization of cancer stroma markers: in silico analysis of an mRNA expression database for fibroblast activation protein and endosialin. *Cancer Immun* 2005; **5**: 10. (PMID: 16076089)

5. MacFadyen JR, Haworth O, Roberston D, Hardie D, Webster MT, Morris HR, Panico M, Sutton-Smith M, Dell A, van der Geer P, Wienke D, Buckley CD, Isacke CM. Endosialin (TEM1, CD248) is a marker of stromal fibroblasts and is not selectively expressed on tumour endothelium. *FEBS Lett* 2005; **579**: 2569-75. (PMID: 15862292)

6. Brady J, Neal J, Sadakar N, Gasque P. Human endosialin (tumor endothelial marker 1) is abundantly expressed in highly malignant and invasive brain tumors. *J Neuropathol Exp Neurol* 2004; **63**: 1274-83. (PMID: 15624764)

7. Opavsky R, Haviernik P, Jurkovicova D, Garin MT, Copeland NG, Gilbert DJ, Jenkins NA, Bies J, Garfield S, Pastorekova S, Oue A, Wolff L. Molecular characterization of the mouse Tem1/endosialin gene regulated by cell density in vitro and expressed in normal tissues in vivo. *J Biol Chem* 2001; **276**: 38795-807. (PMID: 11489895)

8. Carson-Walter EB, Watkins DN, Nanda A, Vogelstein B, Kinzler KW, St Croix B. Cell surface tumor endothelial markers are conserved in mice and humans. *Cancer Res* 2001; **61**: 6649-55. (PMID: 11559528)

9. Hellstrom M, Kalen M, Lindahl P, Abramsson A, Betsholtz C. Role of PDGF-B and PDGFR-beta in recruitment of vascular smooth muscle cells and pericytes during embryonic blood vessel formation in the mouse. *Development* 1999; **126**: 3047-55. (PMID: 10375497)

10. Lindahl P, Johansson BR, Leveen P, Betsholtz C. Pericyte loss and microaneurysm formation in PDGF-B-deficient mice. *Science* 1997; **277**: 242-5. (PMID: 9211853)

11. Robertson PL, Du Bois M, Bowman PD, Goldstein GW. Angiogenesis in developing rat brain: an in vivo and in vitro study. *Brain Res* 1985; **355**: 219-23. (PMID: 4084777)

12. Nanda A, Karim B, Peng Z, Liu G, Qiu W, Gan C, Vogelstein B, St Croix B, Kinzler KW, Huso DL. Tumor endothelial marker 1 (Tem1) functions in the growth and progression of abdominal tumors. *Proc Natl Acad Sci U S A* 2006; **103**: 3351-6. (PMID: 16492758)

13. Rupp C, Dolznig H, Puri C, Schweifer N, Sommergruber W, Kraut N, Rettig WJ, Kerjaschki D, Garin-Chesa P. Laser capture microdissection of epithelial cancers guided by antibodies against fibroblast activation protein and endosialin. *Diagn Mol Pathol* 2006; **15**: 35-42. (PMID: 16531767)

14. Duncan GS, Andrew DP, Takimoto H, Kaufman SA, Yoshida H, Spellberg J, Luis de la Pompa J, Elia A, Wakeham A, Karan-Tamir B, Muller WA, Senaldi G, Zukowski MM, Mak TW. Genetic evidence for functional redundancy of Platelet/Endothelial cell adhesion molecule-1 (PECAM-1): CD31-deficient mice reveal PECAM-1-dependent and PECAM-1-independent functions. *J Immunol* 1999; **162**: 3022-30. (PMID: 10072554)

15. Cheng J, Baumhueter S, Cacalano G, Carver-Moore K, Thibodeaux H, Thomas R, Broxmeyer HE, Cooper S, Hague N, Moore M, Lasky LA. Hematopoietic defects in mice lacking the sialomucin CD34. *Blood* 1996; **87**: 479-90. (PMID: 8555469)

16. Suzuki A, Andrew DP, Gonzalo JA, Fukumoto M, Spellberg J, Hashiyama M, Takimoto H, Gerwin N, Webb I, Molineux G, Amakawa R, Tada Y, Wakeham A, Brown J, McNiece I, Ley K, Butcher EC, Suda T, Gutierrez-Ramos JC, Mak TW. CD34-deficient mice have reduced eosinophil accumulation after allergen exposure and show a novel crossreactive 90-kD protein. *Blood* 1996; **87**: 3550-62. (PMID: 8611677)

Materials and methods

Animals and cell lines

Animal experiments were conducted in accordance with all applicable institutional guidelines. Mice of C57/Bl6, 129/Bl6 and OF1/SPF background were obtained from the Institute of Biomedical Research (Medical University of Vienna). Pregnant animals were sacrificed on day 10, 10.5, 11, 11.5, 12.5, 13.5, 14, 14.5 and 17.5 after the vaginal plug was determined, and embryos were fixed in 4% buffered formalin at 4°C overnight, either *in toto* (E10.0 to E12.5) or after sagittal sectioning, and embedded in paraffin. The following newborn and adult organs

were analyzed: cerebrum, cerebellum, lung, heart, liver, stomach, small and large intestine, pancreas, spleen, kidney, adrenal gland, uterus, and placenta.

Human colorectal carcinoma (Colo205, HCT116, HT29, LoVo, DLD1), breast carcinoma (MCF7, MDA-MB231, MDA-MB468), lung carcinoma (Calu-6, NCI-H520, NCI-H157), prostate carcinoma (DU145, PC3), pancreatic carcinoma (AsPc1) and ovarian carcinoma (SKOV3) cell lines were obtained from the ATCC.

For xenograft studies, 1 to 10 x 10^6 cancer cells were inoculated subcutaneously into the flanks of NMRI *nu/nu* mice and allowed to form tumors of about 1 cm^3. Animals were sacrificed under narcosis, and the tumors were removed, fixed in 4% buffered formalin, and embedded in paraffin.

Antibody generation and purification

For Ab generation ten different peptides from the extracellular domain of mouse endosialin were selected using the DNA Star Protean Sequence Analysis Software (version 4.03). Rabbits were immunized with these peptides using standard immunization protocols. Ab specificity was determined by Western blot and immunocytochemistry, followed by peptide blocking experiments on mouse endosialin-transfected HEK 293T cells and on mouse embryos. The selected Ab 171 was affinity-purified using the SulfoLink™ Kit (Pierce, Rockland, IL) with the cognate peptide, HLDPGDTTSKAHQHP.

Immunohistochemistry

The avidin-biotin complex (ABC) immunoperoxidase procedure was used as previously described (1). Briefly, 5 µm-thick sections were cut and mounted on poly-(L-lysine)-coated slides. After deparaffinization and epitope retrieval in 10 mM citrate buffer, the sections were blocked with 10% serum from the host of the secondary antibody and incubated with the primary antibody (Ab 171) at a 1:1000 dilution in PBS/2% BSA for 1 hour at room temperature or the other primary antibodies indicated below. Biotinylated secondary antibodies were added at a 1:100 dilution, followed by Vectastain ABC solution 1:100 (Vector Labs, Burlingame, CA). For the mouse monoclonal antibody to αSMA, the M.O.M. Kit (Vector Labs) was used. Staining with anti-CD31 (BD Pharmingen, Palo Alto, CA) at a 1:500 dilution required amplification with the Dako GenPoint Kit (Dako, Carpinteria, CA) after proteinase K treatment. Finally, slides were incubated in DAB solution (0.06% 3,3'-diaminobenzidine in PBS, 0.003% H_2O_2) for 2-5 min, dehydrated, and counterstained with hematoxylin. The other primary antibodies used were as follows: anti-VEGFR-2 (Upstate, Lake Placid, NY) at a 1:1000 dilution; anti-PDGFR-β (R&D Systems, Minneapolis, MN) at a 1:100 dilution; anti-collagen type IV (Chemicon, Temecula, CA) at a 1:500 dilution and anti-α smooth muscle actin (Dako, Carpinteria, CA) at a 1:100 dilution. Epitope heat retrieval in 10 mM citrate buffer was carried out for all these antibodies.

Co-localization studies for endothelial and pericyte markers were performed by double immunofluorescence methods. The following antibodies were used: Ab 171 at a 1:200 dilution, anti-VEGFR-2 (Abcam, ab10972, Cambridge, UK) at a 1:15 dilution, anti-PDGFR-β (R&D Systems, Minneapolis, MN) at a 1:50 dilution and anti-collagen type IV (Chemicon, Temecula, CA) at a 1:500 dilution. Epitope heat retrieval was carried out for all of these antibodies as described above. Primary antibodies were incubated for 1 hour at room temperature. Detection was performed with the following secondary antibodies: Alexa 594 donkey anti-goat; Alexa 594 goat anti-rabbit and Alexa 488 goat anti-rabbit (Molecular Probes, Eugene, OR).

Real-time PCR

Tissue samples were homogenized and total RNA was subsequently prepared with TRI reagent (MRC, Cincinnati, OH). Traces of genomic DNA were digested with Turbo-DNA *free* (Ambion, Austin, TX). First strand cDNA was synthesized with an input of 1 µg total RNA using oligo $d(T)_{16}$ primers and Transcriptor Reverse Transcriptase (Roche, Basel, Switzerland). TaqMan probes and primers for mEs and mGAPDH were obtained from Applied Biosystems, Foster City, CA as inventoried assays. TaqMan PCR was done with an ABI PRISM 7000 Sequence Detection System (Applied Biosystems) according to the manufacturer's instructions. The relative expression of endosialin mRNA was normalized to the amount of mGAPDH in the same cDNA by using the comparative C_T method described by the manufacturer.

Contact

Address correspondence to:

Dr. Pilar Garin-Chesa
Institute of Clinical Pathology
Medical University of Vienna
Waehringer Guertel 18-20
1090 Vienna
Austria
Tel.: +43 1 40400-4980
Fax: +43 1 40400-5179
E-mail: pilar.garin-chesa@meduniwien.ac.at

ORIGINAL ARTICLE

Laser Capture Microdissection of Epithelial Cancers Guided by Antibodies Against Fibroblast Activation Protein and Endosialin

Christian Rupp, MSc, Helmut Dolznig, PhD,* Christina Puri,* Norbert Schweifer, PhD,† Wolfgang Sommergruber, PhD,† Norbert Kraut, PhD,† Wolfgang J. Rettig, MD, PhD,† Dontscho Kerjaschki, MD,* and Pilar Garin-Chesa, MD, PhD*†*

Abstract: Transcriptional profiling of cancer biopsies is used extensively to identify expression signatures for specific cancer types, diagnostic and prognostic subgroups, and novel molecular targets for therapy. To broaden these applications, several challenges remain. For example, the integrity of RNA extracted even from small tissue samples has to be insured and monitored. Moreover, total tumor RNA may hide the marked histologic heterogeneity of human cancers. A principle approach to this heterogeneity has been provided by laser capture microdissection performed on antibody-stained tissue sections (immuno-LCM; iLCM). In this study, we have established a procedure to assess the quality of RNA obtained from tissue sections, coupled with immunostaining using antibodies to different tumor stromal markers, and subsequent iLCM to selectively capture the cancer stroma compartments. The procedure was applied to 53 frozen specimens of human epithelial cancers. Sections were stained for histopathological evaluation, and RNA was isolated from adjacent serial sections. RNA quality was assessed by the Agilent-Bioanalyzer (Agilent, Palo Alto, CA) and by multiplex RT-PCR. Two thirds of the specimens were found to yield good to excellent RNA quality. For microdissection of the tumor stroma with reactive fibroblasts and tumor blood vessels, a rapid incubation protocol with antibodies against fibroblast activation protein (FAP) and against endosialin was developed to ensure RNA integrity for subsequent iLCM. Using these procedures, RNA from distinct tumor compartments can be isolated, analyzed, amplified, and used for transcription profiling.

Key Words: immuno-laser capture microdissection, cancer stroma markers, FAP alpha, endosialin

(*Diagn Mol Pathol* 2006;15:35–42)

From the *Institute of Clinical Pathology, Medical University of Vienna, Vienna, Austria; and †Boehringer Ingelheim Austria GmbH, Vienna, Austria.

Supported in part by the GEN-AU program of the Austrian Ministry of Education, Science and Arts.

Reprints: Pilar Garin-Chesa, Institute of Clinical Pathology, Medical University of Vienna, Währinger Gürtel 18-20 1090, Vienna, Austria (e-mail: pilar.garin-chesa@meduniwien.ac.at).

Large-scale analysis of mRNA expression, determining transcript levels of thousands of genes in a single experiment with isolated cancer cells or cancer tissues, is providing a more comprehensive view of the molecular events occurring during carcinogenesis and tumor progression than has been possible in the past with single-gene studies.[1] The approach generates large sets of data for bioinformatic analysis, driven both by pattern recognition for expression signatures that distinguish normal tissues from their malignant counterparts,[2,3] separating out mRNA profiles of infiltrating lymphocytes against a background of normal tissue and cancer RNA profiles,[4] and intriguingly distinguishing cancer subtypes based on their transcriptional profiles that do not coincide with established clinicopathologic entities.[5,6]

However, there will clearly be limitations to using global transcription profiles in the refined analysis of complex cancer tissues, comprising malignant cells, by themselves highly heterogeneous in molecular phenotype, but also residual normal parenchyma and cancer stroma with tumor blood vessels, reactive tumor fibroblasts that may contribute to prominent desmoplastic reactions, and variable inflammatory infiltrates. To date, most large-scale gene expression studies in human cancer have been based on RNA extracted from nonseparated biopsies or surgical specimens, thus mixing the various cell types in any readout and attempts to deconvolute the results by in silico data mining. However, given the current interest of cancer biologists in the contribution of tumor stromal cells for growth regulation, invasion, and metastasis,[7,8] attempts to refine the experimental approach have gained importance.

As an attractive entry point for such targeted analyses, the method of laser capture microdissection (LCM)[9] may hold considerable promise.[10,11] However, because the challenge is also to distinguish normal, resting stromal cells from reactive stromal changes in cancer tissues, LCM guided only by general tissue stains, for instance haematoxylin/eosin (H&E), may not suffice. Thus, it has been an important development that LCM can be performed subsequent to immunohistochemical staining (immuno-LCM; iLCM), provided that rapid antibody-labeling procedures can be used that safeguard RNA integrity in the tissue sections.[12–14]

Building on this experience, we have developed an immunohistochemical staining procedure for 2 putative cancer stromal antigens, fibroblast activation protein (FAPα) recognized by monoclonal antibody F19,[15] and endosialin detected by monoclonal antibody FB5[16] to precede and guide iLCM in surgical specimens of human epithelial cancers.

Moreover, we noted that in earlier iLCM studies, due to technical limitations at the time in visualizing minute RNA amounts, the integrity of sample RNA in microdissected tissues had been assessed only by RT-PCR for one or a few marker genes, rather than a broader representation of the transcriptome. Therefore, we exploited in this study the recently introduced, highly sensitive Agilent RNA6000 Pico LabChip system (Agilent, Palo Alto, CA) to include more powerful quality parameters into the analysis, such as total RNA distribution, the 28S-to-18S rRNA ratio, and assessment of degradation products of the ribosomal RNAs, coupled with comparative multiplex RT-PCR analysis.

MATERIALS AND METHODS

Tissues

A total of 53 epithelial cancer specimens were collected at the Department of Pathology, Medical University of Vienna, in accordance with the guidelines of the institutional ethics committee. The samples were obtained within 30 minutes after surgical resection, embedded in OCT compound (Miles, Kankakee, IL), snap-frozen in isopentane, precooled in liquid nitrogen, and stored at −80°C until further use. Serial 5-μm frozen sections were cut using RNAse-free blades, mounted on StarFrost RNAse–free slides (Fisher Scientific, Pittsburgh, PA), and stained with H&E or antibodies for iLCM as described below.

Immunohistochemistry

Immunohistochemical staining was performed on 1 slide at a time, to optimize speed of handling. Thus, frozen sections were taken from −80°C storage, immediately fixed in cold acetone (4°C) for 2 minutes, rinsed for 3 to 5 seconds in phosphate-buffered saline (PBS), and incubated with the primary antibody (purified IgG; 5–10 μg/mL) for 2 minutes. This and subsequent steps were carried out at room temperature. The primary antibodies used were F19,[15] FB5,[16] and H572 (Bender MedSystems, Vienna, Austria) directed against the vascular endothelial marker EndoGlyx-1.[17] Subsequently, the slide was incubated for 1 minute with secondary antibody (Biotinylated Universal Antibody, Vector Labs, Burlingame, CA), followed by incubation with Vectastain ABC solution (Vector Elite Kit, Vector Labs) for 1 minute. Both secondary antibody and ABC solution were diluted 1:5 in PBS containing 400 U/mL RNAs in (Promega, Madison, WI), and sections were rinsed in PBS between these steps. The signal was developed in DAB solution (0.06% 3, 3′-diaminobenzidine in PBS, 0.003% H_2O_2) for 2 minutes. Sections were counterstained with hematoxylin for 30 seconds and dehydrated twice in 96% EtOH (15 seconds each) and xylene (15 seconds followed by 5 minutes). The critical sample time in aqueous solutions at room temperature was thus reduced to 6 to 7 minutes.

Isolation of Total RNA

To evaluate the quality of the RNA in the snap-frozen starting material, total RNA was extracted from 5-μm unstained frozen sections by direct lysis of cells on the slides with 100 μL extraction buffer XB. The Arcturus Pico Pure RNA Isolation Kit (Arcturus Engineering Inc, Mountain View, CA) and the Qiagen RNeasy kit (Qiagen, Hilden, Germany) were used following the manufacturers' instructions. Both kits are based on tissue lysis in the presence of guanidine isothiocyanate and β-mercaptoethanol, with subsequent selective adsorption of RNA onto a silica membrane to yield sufficient amounts of high-quality RNA. A 15-minute DNAse I incubation was carried out directly on the silica membranes in both protocols to remove traces of genomic DNA. The same protocol was used for the microdissected tissue samples after iLCM (see below).

Agilent RNA6000 Pico LabChip Assay

To assess the quality of the total RNA extracted from 5-μm sections and from microdissected tissues, the Agilent RNA6000 Pico Assay was used following the manufacturer's instructions. This system is based on a combination of microfluidics, capillary electrophoresis, and laser-induced fluorescence to detect total RNA, providing exceptional sensitivity of RNA detection, with 200 pg total RNA readily and reproducibly detected. The RNA 6000 ladder (Ambion, Austin, TX) was used as a size standard (fragment sizes: 6 kb, 4 kb, 2 kb, 1 kb, 0.5 kb, and 0.2 kb) and as quantitative reference. To avoid overloading of the Pico Chip, total RNA extracted directly from 5-μm sections was diluted 1:10 in RNA Storage Buffer (Ambion) prior to loading of the chip, whereas total RNA isolated from microdissected cells was used undiluted. Routinely, 1 μL of RNA solution was measured. RNA quality was evaluated with the manufacturer's software to display electropherograms with fluorescence intensity over time, showing the 18S and 28S rRNA peaks, or as a virtual image of stained RNA, size fractionated on a denaturing gel.

Multiplex One-Step RT-PCR

A multiplex RT-PCR, essentially as described,[18] was used as a second method to assess the quality of the total RNA and to validate the data obtained with the Agilent Pico Assay. Fragments of the following genes were amplified: the B-cell receptor (BC-R, 377 bps), β_2-microglobulin (B2M, 287 bps), the Abelson proto-oncogene (ABL, 193 bps), and porphobilinogen deaminase (PBGD, 128 bps). As a modification, we included a 1-step protocol (Titan One-Tube RT-PCR kit; Roche Applied Science, Basel, Switzerland) following the instruction of the manufacturer with a total number of 35 amplification cycles. Appropriate negative controls

were performed in each run. The PCR products were separated on a 1% to 2% agarose gel stained with ethidium bromide and visualized with a UV transilluminator.

Antibody-Guided Laser Capture Microdissection

The iLCM procedure was performed on the PixCell IIe system (Arcturus Engineering Inc). Immunostained, dehydrated tissue sections were overlaid with a thermoplastic membrane mounted on optically transparent caps (Arcturus Engineering Inc), and cells were captured by focal melting of the membrane through laser activation with an infrared laser. The 15-µm laser spot size was used for the microdissection of tumor cells (6,000–10,000 shots). A smaller spot size (7.5 µm) was required to microdissect the mAb F19-stained tumor stromal fibroblasts or mAb FB5 and mAb H572-stained tumor endothelial cells, and 20,000 to 40,000 shots were necessary for sufficient RNA with these samples. Reaction tubes with 50 µL lysis buffer were closed with the caps, incubated upside down on a shaking platform (42°C for 30 minutes; occasional vortexing for 30 seconds), and lysates were collected by centrifugation (14,000 g, 5 minutes). Aliquots of 1 µL lysate were used to determine RNA quality on the RNA6000 Pico LabChip, and the remaining solutions were snap frozen in liquid nitrogen and stored at −80°C until further use.

TABLE 1. Quality of Total RNA Directly Isolated from Different Cancer Samples

		RNA Quality			
Specimen	n	Excellent	Good	Moderate	Poor
Colorectal cancer	38	14	11	9	4
Gastric cancer	4		3	1	1
Lung cancer	3		1	2	
Thyroid cancer	2	2			
Pancreatic cancer	2		1		1
Others*	4	3		1	
	53	19	16	13	5

Total RNAs were isolated from 53 different tumor specimens by direct lysis of 5 µm cryosections and analyzed using the Agilent RNA6000 Pico LabChip kit. The integrity of the RNA was ranked according to our quality control system (see Results) into excellent, good, moderate and poor.

*Others: tumor types represented only once in our analysis, including a renal cell carcinoma, an esophageal carcinoma, a hepatocellular carcinoma and a seminoma.

RESULTS

Quality Control of RNA in Frozen Tissue Sections

The 53 human cancer specimens procured for this study (Table 1) were snap frozen within 30 minutes after surgical resection, and 5-µm frozen sections were

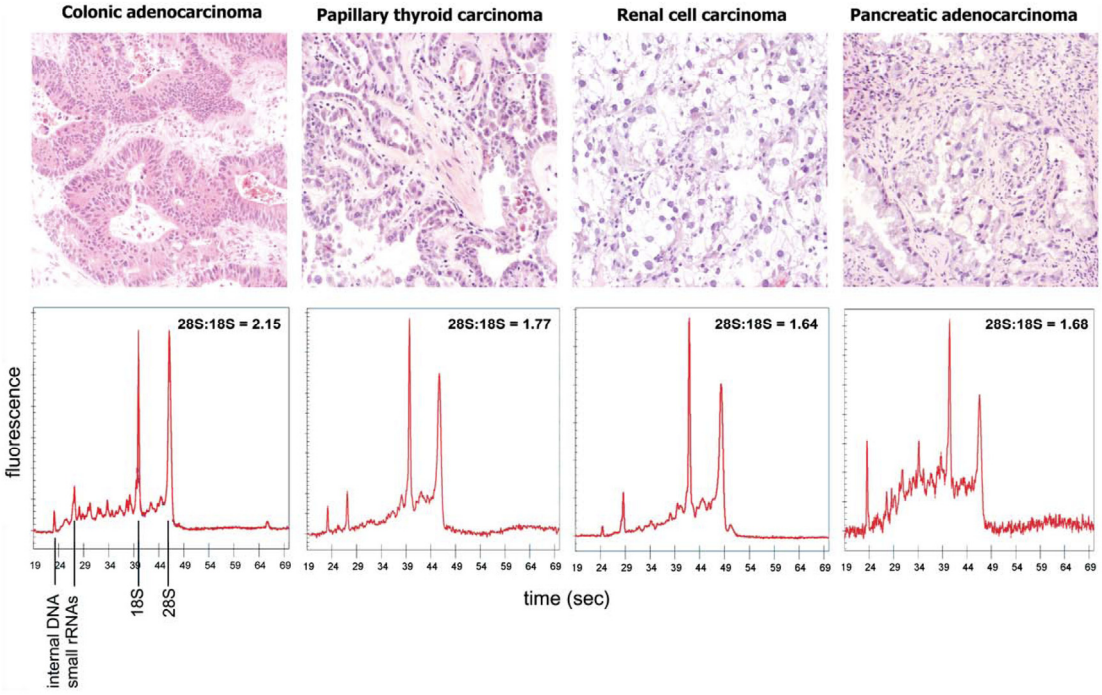

FIGURE 1. Assessment of the RNA quality of tumor samples using the LabChip RNA6000 Pico kit. H&E-stained frozen sections from different tumor samples are shown at the top. The corresponding Agilent 2100 Bioanalyzer RNA profiles from adjacent tissue sections are depicted below. The 2 main peaks represent the 18S and 28S rRNA species. The internal DNA standard included in the sample buffer (0.2 kb) and small rRNA peaks consisting of 5S, 5.8S rRNAs, and tRNAs are indicated.

analyzed for all cases to assess tissue preservation by histopathological evaluation after H&E staining. All cancer samples were of acceptable quality by morphologic criteria, without signs of extensive necrosis or tissue degradation, as illustrated in Figure 1 (top panel) for representative examples.

As a second quality control step, we assessed the integrity of RNA in the starting tissue samples. For this purpose, 5-μm frozen sections, mounted on RNAse-free slides, were directly lysed with 100 μL RNA extraction buffer. The RNA quality was examined with the RNA 6000 Pico LabChip Kit on the Agilent 2100 Bioanalyzer. We ranked the total RNA as excellent when the ratio between 28S and 18S rRNA peaks was above 1.75 and a low baseline was seen; good RNA quality was defined by an 28S-to-18S ratio between 1.5 and 1.75 with a low baseline; moderate RNA quality with an rRNA ratio below 1.5; and poor RNA quality if the bioanalyzer failed to calculate an interpretable rRNA ratio and obvious RNA degradation products were seen. Only tissues with excellent or good RNA quality ranking were selected for further analysis, and Figure 1 (bottom panel) shows representative examples.

As shown in Table 1, more than two thirds of the cancer specimens included in this study (35 of 53) showed an RNA quality ranking of excellent or good. Even some tumors derived from organs such as the pancreas, known to contain high levels of RNAse activity, displayed low levels of RNA degradation, as evidenced by a moderately elevated baseline to the left of the 18S rRNA peak (Fig. 1, lower right-hand panel). This observation, although not systematically explored in a larger series of pancreatic cancers, serves as an indication that the tissue procurement and freezing procedures employed in this study yield acceptable results across a range of diverse cancer types.

To corroborate the results obtained with the Agilent Bioanalyzer, we compared these findings with the results of a 1-step multiplex RT-PCR in 14 independent experiments. As illustrated in Figure 2 for a papillary thyroid carcinoma (top panels) and a colonic adenocarcinoma (bottom panels), we were able to demonstrate the expected BC-R, B2M, ABL, and porphobilinogen deaminase (PBGD) products, whereas confirming the observation of others[18] that the B2M product is not invariably detected, presumably due to primer competition in the multiplex setting.

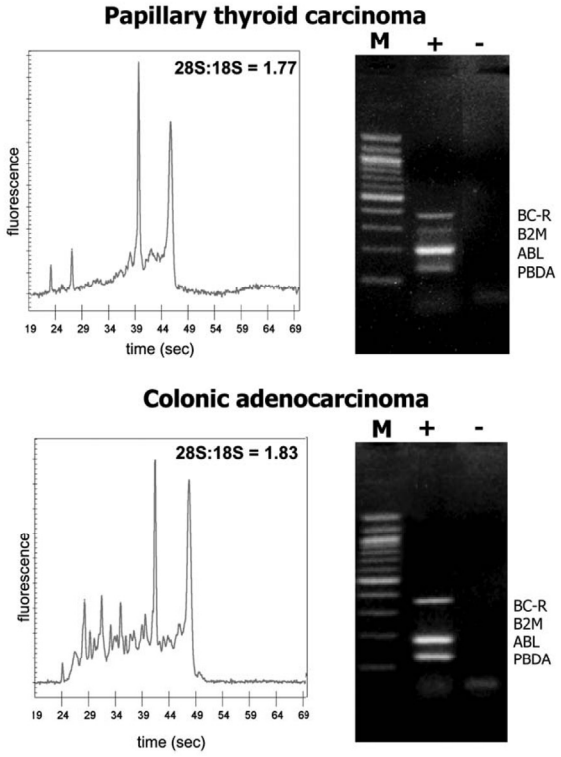

FIGURE 2. Comparison of Agilent electropherograms and multiplex RT-PCR data. Total RNA from a papillary thyroid carcinoma and a colon adenocarcinoma was analyzed on an Agilent Bioanalyzer (left panels) and an aliquot of the RNA was subjected to a 1-step reverse transcription multiplex PCR reaction. Fragments specific for the B-cell receptor (BC-R, 377 bps), β2-microglobulin (B2M, 287 bps), c-abl proto-oncogene (ABL, 193 bps), and porphobilinogen deaminase (PBGD, 128 bps) were amplified simultaneously, separated on a 1% agarose gel, and visualized with ethidium bromide staining under UV light (right, +). Notably, no signals were observed after amplification of the negative RT control without addition of RNA template (−). To estimate the length of the PCR fragments a DNA mass ladder was loaded and shown in the left lane (M).

Morphology-Guided LCM

Based on the positive outcome of the RNA quality assessment in our cancer collection, we next tried to separate malignant epithelial cancer cell and cancer stromal cell compartments from the same frozen sections by LCM. Specifically, we performed LCM on H&E-stained, dehydrated tissue sections of 7 different samples of colonic adenocarcinoma. As shown in Figure 3, we found RNA of excellent quality in lysates of the pre-LCM frozen sections (left panel; 28S-to-18S peak ratio 2.35). By comparison, the LCM-selected cancer cell compartment was found by RNA Pico Assay to rank as excellent RNA quality also (Fig. 3, middle panel; 28S-to-18S peak ratio 2.24) and the microdissected cancer stroma compartment showed a good ranking for RNA quality (Fig. 3, right panel; 28S-to-18S ratio 1.75), even if the RNA amount in this sample was close to the detection limit of the RNA6000 Pico LabChip.

Antibody-Guided LCM

To fully exploit the potential of iLCM procedures in the context of cancer stromal markers and to move beyond the capabilities of the simpler, morphology-guided LCM (see above), we optimized the immuno-chemical staining procedures for the anti-FAPα mAb F19

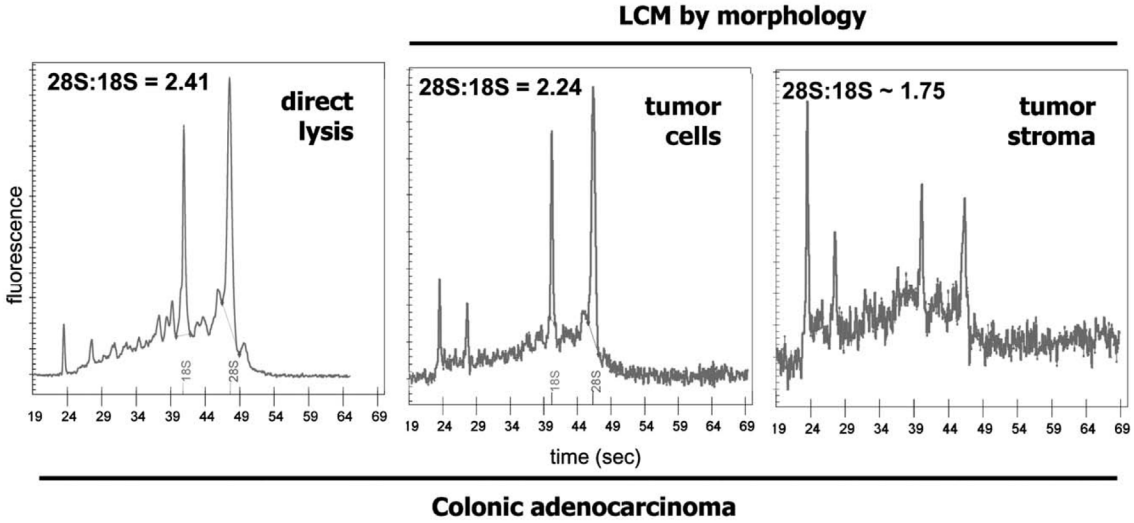

FIGURE 3. LCM of H&E-stained frozen sections of a colonic adenocarcinoma. A high-quality colon adenocarcinoma sample was selected on the basis of direct lysis of a 5-μm cryosection and subsequent RNA analysis using the Agilent RNA6000 Pico LabChip kit. An adjacent section was rapidly stained with H&E and subjected to laser microdissection of tumor cells (tumor cells) and stromal cells (tumor stroma) on an Arcturus PixCell II. Total RNA was prepared from the captured cells and subjected to RNA analysis on an Agilent RNA6000 Pico LabChip.

and the antiendosialin mAb FB5 to reduce the critical time period in which the tissue sections are kept at room temperature in aqueous solutions to 6 or 7 minutes, well below the 10-minute limit for safeguarding RNA integrity which we established in preliminary experiments. As shown in Figure 4A, for a colonic adenocarcinoma, this rapid immunostaining protocol yields excellent signal strength for all 3 antigenic systems tested, namely FAPα, endosialin, and EndoGlyx-1. RNA extraction subsequent to this rapid immunostaining procedure, either by direct lysis without LCM (Fig. 4B, top graph) or following lysis of a mAb F19-guided iLCM sample (Fig. 4B, bottom graph) showed comparable, high-quality RNA, with similar 18S-to-28S peak ratios and only moderate increase in the baseline.

In a further experiment, we tested whether activated tumor stromal fibroblasts, as detected by mAb F19, as well as tumor vascular endothelial cells, detected by mAb FB5, can be microdissected from complex human cancer samples by iLCM (3 colon carcinomas and 1 thyroid carcinoma). As shown in Figure 5 (panel A), for a colonic adenocarcinoma different from previous samples shown, the anti-FAPα mAb F19 and antiendosialin mAb FB5 identify distinct subsets of cancer stromal cells in this specimen (top panels labeled "before"). The middle panels (labeled "after") and bottom panels (labeled "cap") indicate that after iLCM guided by the respective antibodies, the captured cell compartments are highly enriched for the desired stromal cell types expressing FAPα or endosialin, respectively ("cap" panels), whereas being largely deleted from the middle panels. In line with the prior quality control studies, Figure 5B shows that the iLCM-selected tumor stromal fibroblasts (track labeled "stroma") and the tumor endothelial cell-enriched fractions (track labeled "vessels") show high-quality RNA by multiplex RT-PCR comparable to the unselected cancer sample (track labeled "tumor").

DISCUSSION

Large-scale mRNA expression profiling is used extensively to characterize biopsy and surgical specimens of human cancers and to identify molecular genetic changes linked to carcinogenesis, disease progression, prognostic markers, and novel targets for cancer therapy. There may be some use in expression profiles compiled for cultured human cancer cell lines, but the major interest is focused on global expression profiles for cancer tissues, comprising malignant cells as well as the supporting cancer stroma. However, there is considerable interest to find experimental approaches capable of separating out various cell types within a given cancer lesion for individual analysis, such as neoangiogenic blood vessels, reactive tumor fibroblasts, or tumor-infiltrating lymphocytes and inflammatory cells.

In the present study, we extend earlier findings for LCM[9,12–14,19–25] and show, with carefully controlled tissue handling and newly available RNA quality control assays, such as the Agilent RNA6000 Pico LabChip, that LCM approaches can yield high-quality RNA samples that may form the basis for future, genome-wide electronic Northern databases.

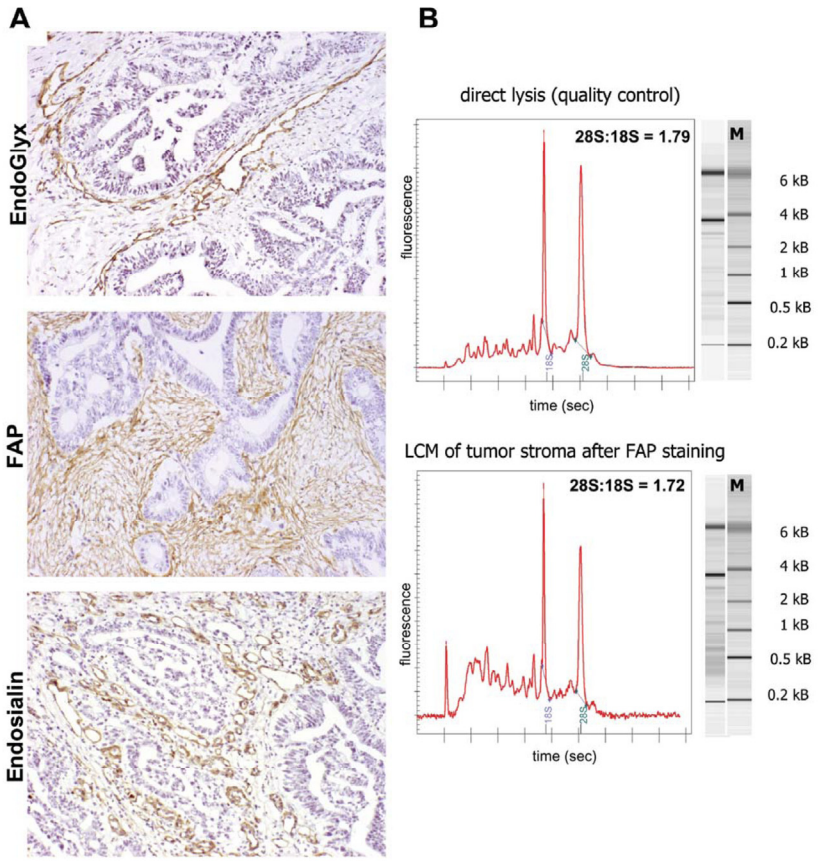

FIGURE 4. Immunohistochemical detection of endoGlyx-1, FAPα, and endosialin after staining with the optimized protocol and total RNA profiles from captured cells. A, Cryosections of a colon adenocarcinoma were stained with either mAbs H572, F19, and FB5 using the short optimized IHC protocol. The signal intensities were comparable to standard IHC procedures and clearly showed strong and specific signals in the tumor blood vessels (top and bottom panels) and activated tumor stromal fibroblasts (middle panel). Original magnification: 10 ×. B, The RNA quality of the tissue samples shown in A was very good as shown by direct lysis of a 5-μm adjacent section to the FAPα-stained specimen (direct lysis). RNA was also isolated from microdissected tumor stromal fibroblasts after staining with mAb F19 and analyzed on the Agilent Bioanalyzer (LCM of tumor stroma after FAPα staining). The pictures right to the Agilent profiles represent virtual images of stained RNA size fractionated on a denaturing gel. M, RNA ladder with the molecular masses of the bands indicated to the right.

Furthermore, we show that 3 antigenic systems represented in human cancer stromal cells can be used to isolate iLCM samples of high-quality RNA that may be used in cancer stroma-related gene expression databases. Of the 3 antigenic systems studied, FAPα is most closely linked to the reactive tumor stroma of various epithelial cancers,[15,26,27] including those with prominent desmoplastic components. The second antigenic system, endosialin,[16] is also known as tumor endothelial marker TEM1[28,29] and linked to tumor neoangiogenesis. The third antigenic system, EndoGlyx-1,[17,30] identifies a vascular endothelial marker consistently expressed in normal and malignant tissues.

Taken together, the encouraging quality of iLCM procedures demonstrated in this study, if properly controlled during sample procurement and RNA extraction, in combination with the ability to select very specifically distinct cancer stromal cell subsets with mAbs such as F19, FB5, or H572 if supported by further gene expression analysis may open up a line of investigation into cancer biology that is not available for single-gene studies or global cancer expression databases alone.[31–33] On a more general level, we propose that quality control steps similar to the ones employed in this study should be incorporated into future iLCM investigations. This will not only be a prerequisite for high-quality results, it may also help establish a standard for databases that can be searched and cross-referenced in virtual gene expression studies for any number of marker genes.

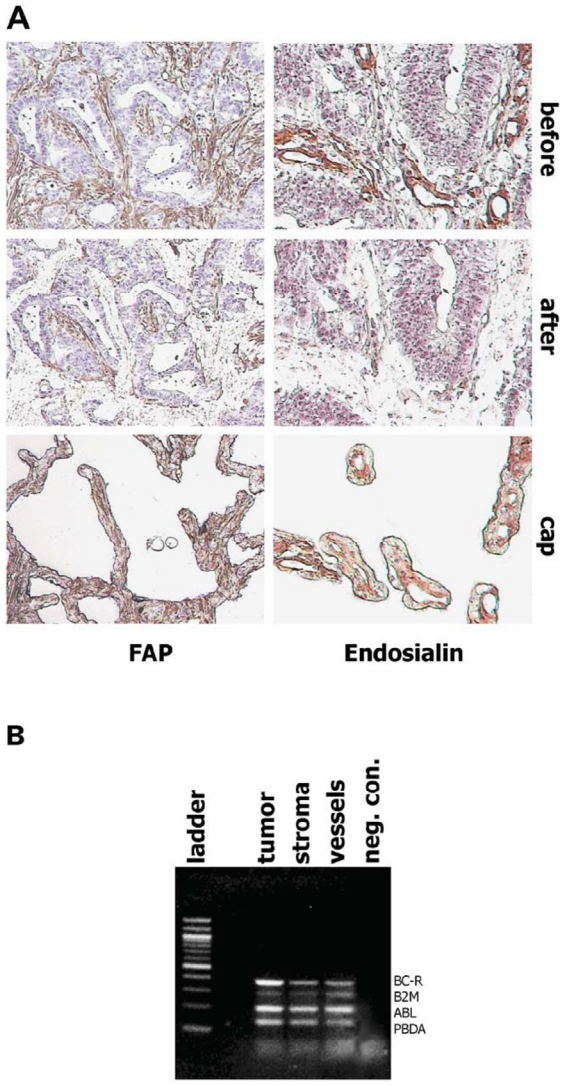

FIGURE 5. Immuno-LCM and multiplex RT-PCR RNA quality control of activated tumor stroma and tumor blood vessels from a colonic adenocarcinoma. A, The top panel depicts FAPα-positive activated stromal fibroblasts (left) and tumor endothelial blood vessels positive for endosialin (right) before capture. After capture and removal of the cap, the remaining tissue can be inspected and the transfer efficiency of the captured cells can be evaluated (see white space appearing between the tumor cells, middle panel). Efficient transfer and purity of the captured sections can also be checked on the removed cap placed on a fresh RNAse free slide (bottom panel). Original magnification: 10 ×. B, The quality of the total RNA isolated from the captured cells shown in A was analyzed by multiplex RT-PCR. Captured hematoxylin-stained tumor cells (tumor) as well as FAP-expressing activated tumor stromal fibroblasts (stroma) and endosialin-positive tumor endothelial cells (''vessels'') showed the expected 4 bands in multiplex RT-PCR indicative of good RNA quality.

REFERENCES

1. Ramaswamy S, Golub TR. DNA microarrays in clinical oncology. *J Clin Oncol*. 2002;20:1932–1941.
2. Perou CM, Sorlie T, Eisen MB, et al. Molecular portraits of human breast tumours. *Nature*. 2000;406:747–752.
3. Thykjaer T, Workman C, Kruhoffer M, et al. Identification of gene expression patterns in superficial and invasive human bladder cancer. *Cancer Res*. 2001;61:2492–2499.
4. Amatschek S, Koenig U, Auer H, et al. Tissue-wide expression profiling using cDNA subtraction and microarrays to identify tumor-specific genes. *Cancer Res*. 2004;64:844–856.
5. Alizadeh AA, Eisen MB, Davis RE, et al. Distinct types of diffuse large B-cell lymphoma identified by gene expression profiling. *Nature*. 2000;403:503–511.
6. Bittner M, Meltzer P, Chen Y, et al. Molecular classification of cutaneous malignant melanoma by gene expression profiling. *Nature*. 2000;406:536–540.
7. De Wever O, Mareel M. Role of tissue stroma in cancer cell invasion. *J Pathol*. 2003;200:429–447.
8. Liotta LA, Kohn EC. The microenvironment of the tumour-host interface. *Nature*. 2001;411:375–379.
9. Becker I, Becker KF, Rohrl MH, et al. Single-cell mutation analysis of tumors from stained histologic slides. *Lab Invest*. 1996;75:801–807.
10. Fend F, Kremer M, Quintanilla-Martinez L. Laser capture microdissection: methodical aspects and applications with emphasis on immuno-laser capture microdissection. *Pathobiology*. 2000; 68:209–214.
11. Simone NL, Bonner RF, Gillespie JW, et al. Laser-capture microdissection: opening the microscopic frontier to molecular analysis. *Trends Genet*. 1998;14:272–276.
12. Fend F, Emmert-Buck MR, Chuaqui R, et al. Immuno-LCM: laser capture microdissection of immunostained frozen sections for mRNA analysis. *Am J Pathol*. 1999;154:61–66.
13. Murakami H, Liotta L, Star RA. IF-LCM: laser capture microdissection of immunofluorescently defined cells for mRNA analysis rapid communication. *Kidney Int*. 2000;58:1346–1353.
14. Lindeman N, Waltregny D, Signoretti S, et al. Gene transcript quantitation by real-time RT-PCR in cells selected by immuno-histochemistry-laser capture microdissection. *Diagn Mol Pathol*. 2002;11:187–192.
15. Rettig WJ, Garin-Chesa P, Beresford HR, et al. Cell-surface glycoproteins of human sarcomas: differential expression in normal and malignant tissues and cultured cells. *Proc Natl Acad Sci USA*. 1988;85:3110–3114.
16. Rettig WJ, Garin-Chesa P, Healey JH, et al. Identification of endosialin, a cell surface glycoprotein of vascular endothelial cells in human cancer. *Proc Natl Acad Sci USA*. 1992;89: 10832–10836.
17. Sanz-Moncasi MP, Garin-Chesa P, Stockert E, et al. Identification of a high molecular weight endothelial cell surface glycoprotein, endoGlyx-1, in normal and tumor blood vessels. *Lab Invest*. 1994;71:366–373.
18. Watzinger F, Lion T. Multiplex PCR for quality control of template RNA/cDNA in RT-PCR assays. *Leukemia*. 1998;12:1984–1986.
19. Bohm M, Wieland I, Schutze K, et al. Microbeam MOMeNT: non-contact laser microdissection of membrane-mounted native tissue. *Am J Pathol*. 1997;151:63–67.
20. Bonner RF, Emmert-Buck M, Cole K, et al. Laser capture microdissection: molecular analysis of tissue. *Science*. 1997; 278:1481–1483.
21. Dean-Clower E, Vortmeyer AO, Bonner RF, et al. Microdissection-based genetic discovery and analysis applied to cancer progression. *Cancer J Sci Am*. 1997;3:259–265.
22. Schutze K, Lahr G. Identification of expressed genes by laser-mediated manipulation of single cells. *Nat Biotechnol*. 1998; 16:737–742.
23. Suarez-Quian CA, Goldstein SR, Pohida T, et al. Laser capture microdissection of single cells from complex tissues. *Biotechniques*. 1999;26:328–335.
24. Gjerdrum LM, Abrahamsen HN, Villegas B, et al. The influence of immunohistochemistry on mRNA recovery from microdissected

frozen and formalin-fixed, paraffin-embedded sections. *Diagn Mol Pathol*. 2004;13:224–233.
25. Tangrea MA, Chuaqui RF, Gillespie JW, et al. Expression microdissection: operator-independent retrieval of cells for molecular profiling. *Diagn Mol Pathol*. 2004;13:207–212.
26. Garin-Chesa P, Old LJ, Rettig WJ. Cell surface glycoprotein of reactive stromal fibroblasts as a potential antibody target in human epithelial cancers. *Proc Natl Acad Sci USA*. 1990;87: 7235–7239.
27. Park JE, Lenter MC, Zimmermann RN, et al. Fibroblast activation protein, a dual specificity serine protease expressed in reactive human tumor stromal fibroblasts. *J Biol Chem*. 1999;274: 36505–36512.
28. St Croix B, Rago C, Velculescu V, et al. Genes expressed in human tumor endothelium. *Science*. 2000;289:1197–1202.
29. Christian S, Ahorn H, Koehler A, et al. Molecular cloning and characterization of endosialin, a C-type lectin-like cell surface receptor of tumor endothelium. *J Biol Chem*. 2001;276:7408–7414.
30. Christian S, Ahorn H, Novatchkova M, et al. Molecular cloning and characterization of EndoGlyx-1, an EMILIN-like multisubunit glycoprotein of vascular endothelium. *J Biol Chem*. 2001;276: 48588–48595.
31. van't Veer LJ, Dai H, van de Vijver MJ, et al. Gene expression profiling predicts clinical outcome of breast cancer. *Nature*. 2002;415:530–536.
32. Sugiura T, Nagano Y, Inoue T, et al. A novel mitochondrial C1-tetrahydrofolate synthetase is upregulated in human colon adenocarcinoma. *Biochem Biophys Res Commun*. 2004;315:204–211.
33. Iacobuzio-Donahue CA, Maitra A, Shen-Ong GL, et al. Discovery of novel tumor markers of pancreatic cancer using global gene expression technology. *Am J Pathol*. 2002;160:1239–1249.

IGFBP7, a novel tumor stroma marker with dual roles in epithelial- and mesenchymal-type tumor cells

Christian Rupp*, Helmut Dolznig*[1] Christian Haslinger[#],
Norbert Schweifer[#], Matthias Artaker[2] and Pilar Garin-Chesa*[#]

*Institute of Pathology, Medical University of Vienna, Waehringer Guertel 18-20, A-1090 Vienna, Austria

[#]Boehringer Ingelheim RCV GmbH & Co KG, Vienna, Austria, Dr. Boehringer-Gasse 5-11, A-1130 Vienna, Austria

[2]Max F. Perutz Laboratories, Department of Medical Biochemistry, Medical University of Vienna, Austria

[1] present address: Institute of Medical Genetics, Centre of Pathobiology and Genetics, Medical University of Vienna, Waehringer Strasse 10, A-1090 Vienna, Austria

Abstract

The activated tumor stroma participates in many processes that control tumorigenesis, including tumor cell growth, invasion and metastasis. Cancer associated fibroblasts (CAFs) represent the major cellular component of the stroma and are the main source for connective tissue components of the extracellular matrix (ECM) and various classes of proteolytic enzymes. The signaling pathways involved in the interactions between tumor and stromal cells and the molecular characteristics that distinguish normal "resting" fibroblasts from cancer associated or "activated" fibroblasts remain poorly defined. Recent studies emphasized the prognostic and therapeutic significance of CAF-related molecular signatures and the identification of novel stromal targets.

We have used immuno-laser capture microdissection and whole genome Affymetrix GeneChip® analysis to obtain transcriptional signatures from the activated tumor stroma of colon carcinomas that were compared with the expression profiles from normal resting fibroblasts. Several members of the Wnt-signaling pathway and gene sets related to hypoxia, epithelial-to-mesenchymal transition (EMT) and TGFβ pathway activation were induced in CAFs. The putative TGFβ target IGFBP7 was identified as a tumor stroma marker of epithelial cancers and as a tumor antigen in mesenchyme-derived sarcomas. IGFPB7 was shown to promote anchorage-independent growth in malignant mesenchymal cells and malignant epithelial cells with an EMT-phenotype, whereas a tumor suppressor function was observed in tumor epithelial cells.

Introduction

Carcinomas consist of complex mixtures of neoplastic epithelial cells and non-neoplastic cell, collectively referred to as "tumor stroma". The tumor stroma, which in some carcinomas makes up more than 80% of the tumor mass, is composed of blood and lymphatic endothelial cells, infiltrating immune cells, pericytes and specialized fibroblasts, termed cancer associated fibroblasts (CAFs), embedded in a network of extracellular matrix (ECM). During the past years, it has become increasingly evident that far from being a mere bystander, the tumor stroma participates in many of the processes that control tumorigenesis (1-3). Cancer associated fibroblasts, which are the main source for extracellular matrix degrading enzymes, including cysteine-, serine-, and matrix metalloproteinases where shown to act as key players in remodeling the tumor microenviroment and to be essential for the local spread of tumor cells into the adjacent normal tissues and the formation of distant metastasis (4)(5). However, the molecular characteristics that distinguish a normal "resting" fibroblast from a cancer associated or "activated" fibroblast remain poorly defined. Presently, CAFs are defined by morphological characteristics and by the expression of specific sets of markers including fibroblast activation protein alpha (FAPα) (6), alpha-smooth-muscle actin (α-SMA) (7), fibroblast-specific protein 1 (FSP1/S100A4) (8) or PDGFRβ (9).This molecular heterogeneity has been linked to the diverse origin of CAFs, which have been reported to be derived from resident local fibroblasts, from bone-marrow derived progenitor cells or from transformed epithelial cells which have undergone an epithelial-to-mesenchymal transition (EMT) during tumorigenesis (10)(11). An increasing number of translational studies have recently emphasized the prognostic significance of different CAF-related molecular signatures (12)(13) and clinical studies targeting CAFs in human cancers have been proposed (14-16). We have used immuno-laser capture microdissection (iLCM) (17) and whole genome Affymetrix GeneChip® analysis to obtain transcriptional signatures from the tumor cells and the activated tumor stroma that were compared with the expression profiles from normal colonic epithelium and normal fibroblasts, derived from the same patients. Induced genes included several members of the Wnt-signaling pathway or collagen cross-linking enzymes such as lsyl oxidases. Moreover, increased expression of gene sets related to hypoxia, epithelial-to-mesenchymal transition (EMT) and TGFβ pathway activation were found in CAFs *vs.* their normal counterparts. We have identified a putative TGFβ target gene (18), IGFBP7, as a tumor stroma marker of epithelial cancers that can act as a tumor antigen in mesenchyme-derived tumors such as fibrosarcomas. We could further show, that IGFBP7 promotes anchorage-independent growth in malignant mesenchyme-derived cells and

malignant epithelial cells with an EMT phenotype, whereas a tumor suppressor function was observed on malignant epithelial cells.

Materials and Methods

Tissues & immuno-laser capture microdissection (iLCM)

Human tumor samples from patients with colorectal cancer were obtained from the Department of Pathology, Medical University of Vienna; the samples were collected in accordance with the guidelines of the institutional ethics committee. Matched pairs of tumor and normal colonic mucosa were snap frozen within 30 min after surgical resection. Five µm sections were stained with H&E to assess tissue preservation and for histopathological evaluation. The samples were analyzed for their expression of fibroblast activation protein alpha (FAPα) followed by laser capture on a PixCell IIe System (Arcturus Engineering Inc., Mountain View, CA) as previously described (17).

RNA processing & global gene expression profiling

Total RNA was extracted from the captured cells with the Arcturus Pico Pure RNA Isolation Kit (Arcturus Engineering Inc., Mountain View, CA) and amplified and labeled with the MassageAmp™ II-Biotin *Enhanced* Kit (Ambion, Austin, TX). Fragmented aRNA (15 µg) was used for hybridization of the Human Genome U133 Plus 2.0 GeneChip© arrays (Affymetrix, Santa Clara, CA). The arrays were hybridized and scanned using standard Affymetrix protocols. Microarray data were normalized using the Robust Multi-Array Analysis as implemented in Bioconductor (19)(20). All analyses were performed with $\log_2$-transformed data. Hypothesis tests were performed using a modified *t* statistics with an empirical Bayes approach as implemented in Bioconductor LIMMA package (21). P-values were adjusted by the FDR method of Benjamini and Hochberg (22). For our gene set enrichment analysis we used two gene set collections from the Molecular Signature Database provided by the Broad Institute, namely the curated gene sets (C2) and the Gene Ontology (GO) gene sets (C5) (23). The core genes of statistically significant genes were used to calculate PCA plots.

Immunohistochemistry/immunofluorescence

For IGFBP7 stainings on paraffin sections the avidin-biotin complex (ABC) immunoperoxidase method was used as previously described (6). Epitope retrieval was carried out in poteinase K solution (20 µg/ml in TE Buffer; pH 8.0).The primary goat anti-IGFBP7 antibody was obtained from R&D Systems, Minneapolis, MA, Cat. # AF 1334 and used at 0.5µg/ml. Co-localization studies were done on acetone/methanol fixed frozen sections or chamber slides by double immunofluorescence methods. The following antibodies were used: monoclonal antibody F19 1:50 (6), monoclonal antibody H572 1:20 (24), rabbit anti-podoplanin 1:1000 (25), goat anti-NG2 (R&D Systems) 1:100, monoclonal antibody V9 mouse anti-vimentin (Invitrogen, Carlsbad, CA) 1:1000, rabbit anti-β-Catenin 1:1000 (ab6302 Abcam,Cambridge, UK) Detection was performed with the following secondary antibodies: Alexa Fluor© 594 donkey anti-goat; Alexa Fluor© 594 goat anti-rabbit and Alexa Fluor© 488 goat anti-rabbit from Molecular Probes (Invitrogen).

Generation of stable IGFBP7/E-Cadherin knock-downs

For shRNA mediated IGFBP7 knock-down we obtained five constructs (TRC0000077943 to TRC0000077947 in pLK0.1) developed by the the RNAi consortium (TRC) from Open Biosystems (Thermo Fisher Scientific, Waltham, MA). The constructs were packaged into lentiviral particles using a 2nd generation packaging system (Invitrogen) and used to infect the following cell lines HT1080, Caki-1 or SW480 (ATCC numbers: CCL-121, HTB-46, CCL-228). 2 x 10^4 cells were seeded into a 24-well plate and incubated with full medium containing 5µl of the virus concentrates and 8µg/ml hexadimethrine bromide (Sigma, St. Louis, MO). To stably knock-down E-Cadherin in DLD-1 cells (CCL-221), we obtained SMARTvector 2.0 lentiviral particles from Dharmacon (Thermo Fisher Scientific) and used them according to the manufacturers´ instructions. For all constructs and cell lines, selection was carried out with puromycin (Invitrogen) at 1µg/ml final concentration. All work was done according to local biosafety regulations.

IGFBP7 overexpression

IGFBP7 Lentifect ™ lentiviral particles were obtained from GeneCopoeia, Rockville, MD to overexpress the protein in DLD-1 cells. The infection and selection process was carried out as described in the previous section.

Realtime PCR

Total RNA was extracted using the Qiagen RNeasy® Mini Kit (Qiagen Hilden, Germany) following the manufacturers´ instructions. First strand cDNA was synthesized with an input of 2µg total RNA using the Applied Biosystems´ High-Capacity cDNA Reverse Transcription Kit (Applied Biosystems, Carlsbad, CA). TaqMan probes and primers for IGFBP7 and GAPDH were obtained from Applied Biosystems. TaqMan PCR was done with an ABI PRISM 7000 Sequence Detection System (Applied Biosystems) according to the manufacturer's instructions. The relative expression of IGFBP7 mRNA was normalized to the amount of GAPDH in the same cDNA using the comparative C_T method described by the manufacturer.

Immunoblotting

Conditioned media obtained from Caki-1, HT1080, SW480, LS174T (CL-188), HT-29 (HTB-38) and DLD-1 cells was concentrated with a centricon centrifugal filter device (Millipore, Billerica, MA) and used for IGFBP7 detection by immunoblotting. For all antigens, SDS gel electrophoresis was carried out on precast 4-12% gels (Biorad, Hercules, CA) under reducing conditions. The blotted membranes were blocked with 20% FCS in TBS-T for 1 hour at RT. Incubation with the appropriate primary antibody (anti-IGFBP7 0.1µg/ml; V9 mouse anti-vimentin 1:10.000; Abcam, HECD-1 mouse anti-E-Cadherin 1:1000; Bethyl Laboratories, Montgomery, TX rabbit anti-matriptase 1:1000; Trevigen, Gaithersburg, MD rabbit anti-GAPDH 1:25.000) in blocking buffer (20% FCS in TBS-T) was carried out at 4°C overnight. The corresponding secondary HRP-conjugated antibodies (JacksonImmunolabs, West Grove, PA) were applied at 1:2500 in blocking buffer for one hour at RT. Immunoreactive signals were detected with the ECLplus system (GE Healthcare, Chalfont St. Giles, UK) and the Lumi Imager (Roche, Basel, Switzerland).

Assessment of cell proliferation by *in-vitro* EdU labelling

For proliferation analysis, HT1080 cells were grown to 50% confluence and then pulsed for 30, 120 and 240 min. with 10µM EdU (5-ethynyl-2'-deoxyuridine, Invitrogen, Carlsbad, CA). Cells were then harvested and processed according to the manufacturers´ instructions (Click-iT® EdU Alexa Fluor® 647 Flow Cytometry Assay Kit, Invitrogen). Flow cytometric data acquisition was performed on a FACSCalibur (BD Biosciences, San Jose, CA) and collected data were analyzed using FlowJo software 8.8.4 (Tree Star, Ashland, OR).

Soft agar colony formation assay

Anchorage-independent cell growth was analyzed using the colony formation assay in soft agar culture. Single cells were suspended in standard medium containing 0.4% (w/v) low-melting agarose (Invitrogen) and platted at a cell density of 3×10^4 cells/dish on solidified 1.2% agar-containing medium in six well plates. After 14 days of incubation, the cell colonies were fixed in acetone/methanol and stained with 0.005% crystal violet. The stained cell colonies were photographed and counted with ImageJ.

Xenografts

HT1080 cells were harvested and suspended in PBS/1% BSA. 100 µl of the cell suspension containing 10^8 cells was injected into the flanks of SCID mice (Charles River, Wilmington, MA). Tumor sizes were measured every two days after the tumors became visible.

Results

Cancer-associated fibroblasts (CAFs) show increased expression levels of genes related to hypoxia, epithelial-to-mesenchymal transition (EMT) and TGFβ pathway activation.

For our iLCM screen we analyzed a set of colon cancer samples together with their normal counterparts and captured the tumor cells, the tumor stroma as well as the normal stroma from these specimens (Supplementary figure 1). RNA extracted from the captured cells was processed for whole genome Affymetrix GeneChip® hybridization. After normalization and bioinformatic analysis, the three compartments (tumor cells, tumor stroma and normal stroma) could be clearly separated by unsupervised hierachical cluster analysis (Fig. 1A) and principal component analysis (data not shown). 1299 genes were differently expressed between the tumor stroma and the normal stroma, with 627 of these genes significantly up-regulated in the tumor stroma (false discovery rate $p<0.01$). Among the genes up-regulated in the tumor stroma *vs*. normal stroma were well established tumor stroma markers such as PDGFRβ, FGFR1, MMP2 or FAPα, the marker used to capture the activated fibroblasts from the tissue samples (Fig. 1B). Interestingly, induced genes included several members of the Wnt-signaling pathway such as secreted frizzled-related protein 2 (SFRP2), WNT2, WNT5a or Wnt-1 induced protein 1 (WISP-1). The up-regulation of WISP-1 and its putative binding partner biglycan (BGN) on the RNA and protein levels were confirmed in validation assays performed in independent colorectal cancer samples (Fig. 1B).
For the further identification of tumor stroma specific genes sets we used the gene set enrichment analysis (GSEA) with two gene set collections derived from the Molecular Signature Database (Broad Institute); c2, the curated-gene sets, and c5 the gene ontology (GO)-gene sets (23). Among the GO datasets most significantly enriched (fdr $q<0.25$) were gene sets involved in response to wounding, extracellular matrix deposition, inflammatory response, cell migration, cytokine activity, cell-matrix adhesion, and vascular development (Fig. 1A, right). In addition, we identified 192 significantly enriched curated gene sets, including gene sets related to hypoxia, epithelial-to-mesenchymal transition (EMT), IL-6 and TGFβ pathway activation (Table 1).
Enriched hypoxia related gene sets contained angiogenic growth factors such as VEGFC or angiopoetin-like 4 (ANGPTL4). Other genes in that category encoded collagens (COL1A2, COL4A1, COL5A1, COL9A1 and COL18A1) and their modifying enzymes (lysyl oxidase LOX, lysyl oxidase-like 2 LOXL2), suggesting that the collagen biosynthesis in the stromal

compartment undergoes multiple hypoxia-induced changes. Interesting examples for enriched genes related to IL-6 treatment comprised several pro-inflammatory cytokines such as CXCL3 or IL-6 itself. IL-6 is induced in large quantities during the transition from inflammatory response to early wound healing and is especially up-regulated by fibroblasts involved in fibrosis, associated with diseases such as rheumatoid arthritis (26). Gene sets involved in EMT included the mesenchymal marker N-Cadherin (CDH2), several tumor promoting matrix metalloproteinases such as MMP2 and MMP12 as well as extracellular matrix proteins implicated in invasion and metastasis such as tenascin C (TNC), laminin B1 (LAMB1) or secreted protein acidic and rich in cysteine (SPARC). Many of the EMT related genes were also found among TGFβ induced gene sets, together with genes encoding fibrillar collagens (COL1A1, COL1A2, COL3A1 and COL5A2*)* and members of the insulin-like growth factor binding proteins family, such as IGFBP3 and IGFBP5. Another putative TGFβ target (18), IGFBP7, has appeared as one of the most significantly induced tumor stroma markers in our screen (tumor stroma *vs*.normal stroma, p< 2,14E-05) (Fig.2A).

IGFBP7 is a tumor stroma marker of activated fibroblasts and endothelial cells in epithelial cancers.

Immunohistochemical studies in tissue samples from colorectal cancer showed selective expression of IGFBP7 in tumor-associated vessels and in subsets of activated fibroblasts in the tumor stroma. Stainings performed in a variety of epithelial cancers revealed that IGFBP7 is frequently induced in the stromal compartment of solid tumors including samples of colon, NSCLC, pancreatic, ovarian and breast carcinomas (Fig. 2B). In none of the cases analyzed IGFBP7 was observed in the tumor cells. In contrast, IGFBP7 was expressed in the tumor cells as well as in the tumor stroma of soft tissue sarcomas, particularly in the tumor associated vasculature (Fig. 2B). This pattern of expression closely resembles that of two other tumor-stroma markers FAPα and Endosialin previously identified by our group. In double-labeling studies IGFBP7 co-localized with EndoGlyx, a marker for blood vascular endothelial cells (24) and the pericyte marker NG2 (27), indicating that IGFBP7 is a marker of endothelial cells and the surrounding mural cells. To further characterize and to ascertain whether IGFBP7 is a marker of blood (BECs) or lymphatic endothelial cells (LECs), we have tested primary BECs and LECs isolated from human dermal microvascular endothelial cells (HDMECs) for IGFBP7 expression. IGFBP7 was present both in BECs and LECs as demonstrated by its co-expression with CD31 and Prox1 (Fig.3A). As expected from the studies with tumor tissues freshly isolated colon cancer associated fibroblasts (CAFs) in short

term culture were shown to express IGFBP7 and vimentin, a marker of mesenchymal differentiation (Fig. 3A).

IGFBP7 is expressed by malignant mesenchyme-derived cells and malignant epithelial cells with a mesenchymal phenotype and promotes anchorage-independent growth in these cells.

IGFBP7 expression was observed in malignant mesenchymal cells in soft tissue sarcomas by immunohistochemistry (Fig. 2B) and was further confirmed by Western blotting analysis on a panel of selected cell lines including the fibrosarcoma cell line HT1080 (Fig. 3B). Moreover, high expression of IGFBP7 was observed in cancer cell lines, which have undergone EMT such as Caki-1 and SW480 cells. Colon cancer cell lines, which maintained the epithelial phenotype such as LS174T, HT29, DLD-1 lacked IGFBP7 expression (Fig. 3B). Expression of E-Cadherin and vimentin was used to characterize the phenotype of the cell lines included in the study (Fig. 3B). To establish the potential role of IGFBP7 in malignant mesenchyme-derived cells and epithelial tumor cells after EMT, IGFBP7 shRNA mediated knock-down experiments were carried out. In HT1080 cells, shRNA mediated knock-down of IGFBP7 resulted in >90% reduction on the protein level (Fig. 3C). The IGFBP7 knock-down had no effect on cell proliferation in 2D-cultures as demonstrated by an EdU incorporation assay (Supplementary figure 2). In a further next step, we analyzed the anchorage independent growth of the IGFBP7 knock-down and control cells by comparing their ability to grow and form colonies in soft agar culture. Intriguingly, the number of colonies growing anchorage independently after two weeks in soft-agar culture was significantly reduced after IGFBP7 depletion in HT1080, Caki-1 and SW480 cells (Fig. 3D and data not shown). The ability of mammalian cells to proliferate anchorage independently often correlates with their ability to form tumors *in vivo*. In line with this, we have shown a delayed tumor take of the IGFBP7 knock-down cells compared to the control cells at day 14 after implantation in a xenograft experiment with HT1080 cells grown subcutaneously in SCID mice (Supplementary figure 3).

Proteolytically cleaved IGFBP7 reduces the anchorage-independent growth ability of epithelial tumor cells.

To examine how IGFBP7 affects the anchorage-independent growth abilities of epithelial tumor cells, we overexpressed the protein in DLD-1 cells. These cells were shown to express E-Cadherin and to lack endogenous IGFBP7 expression (Fig. 3B). We compared the abilities of mock and IGFBP7 transfected DLD-1 cells to form colonies in soft agar culture. As demonstrated in Fig. 4A, DLD-1/IGFBP7 cells formed far fewer colonies than DLD-1/mock cells. Conditioned medium derived from the overexpressing cells showed two IGFBP7 bands representing a native 33 kDa form and a 26 kDa form, which previously has been reported to result from proteolytic cleavage by the type II transmembrane serine protease matriptase (MT-SP1) (28). Matriptase is present in several differentially processed intra- and extracellular forms and, as demonstrated by Western blotting, is expressed at high levels in the epithelial-type DLD-1 and HT-29 cells (Fig. 4B).

IGFBP7 expression is induced in DLD-1 cells following E-Cadherin knock-down.

Our results indicate that IGFBP7 secreted by activated tumor fibroblasts and tumor endothelial cells might function as a tumor suppressor on epithelial tumor cells during the early stages of tumorigenesis and as a promoter of tumor growth when the tumor cells have acquired a mesenchymal phenotype as a result of EMT. To further substantiate this hypothesis, we examined whether the loss of E-Cadherin, which was previously shown to induce EMT (29), leads to an induction of IGFBP7 expression. Therefore we knocked-down E-Cadherin in DLD-1 cells via stable shRNA expression. High knockdown efficiency was verified by Western blotting. Phenotypically, the E-Cadherin knock-down cells displayed a more mesenchymal phenotype in comparison to the control cells. In addition, we could demonstrate a redistribution of β-Catenin protein from the cytoplasma membrane to the nucleus, indicating β-Catenin activation in the cells lacking E-Cadherin. Most importantly the induction of the mesenchymal phenotype correlated with a significant induction of IGFBP7 expression (Fig. 5 and Supplementary figure 3).

Discussion

We have analyzed the molecular differences between CAFs and normal resting fibroblasts described by generating gene expression signatures from microdissected colon cancer and corresponding normal tissues. Among well-characterized tumor stroma markers, that served as validation parameter for our screen, several members of the Wnt-signaling pathway such as WISP-1, WNT2 or WNT5a appeared up-regulated in the stromal compartment. WISP-1 (Wnt-1 induced secreted protein 1) has recently been demonstrated to be induced in the tumor stroma in a paracrine fashion by Wnt-1 released by the tumor cells (30)(31) and to bind biglycan on the fibroblast surface (32). WNT5a, a gene involved in the non-canonical Wnt signaling, was induced in fibroblasts during co-cultivation with a pancreatic carcinoma cell line, suggesting that it could contribute to the strong desmoplastic reaction commonly found in this type of tumor (33). Thus, cancer associated fibroblasts could be regarded as primary candidates for locally modulating Wnt/β-Catenin signaling, which may result in heterogeneous patterns of β-Catenin intracellular localization observed within colorectal tumors (34).

Tumor stroma specific gene sets related to hypoxia contained several collagens and their modifying enzymes, such as lysyl oxidase (LOX) and lysyl oxidase-like 2 (LOXL2). Lysyl oxidase is a copper-dependent amine oxidase that initiates the process of covalent intra- and intermolecular cross-linking of collagens (35). Collagen cross-linking by lysyl oxidase has recently been identified as a critical regulator of desmoplasia implying that the nature and level of ECM cross-links could impact cancer risk and alter tumor behavior (36). Interestingly, LOXL2 has also been observed in a “wound response signature” of fibroblasts in response to serum stimulation. Using independent datasets from human cancers, it has been shown that this “wound-response signature” was strongly predictive of metastasis and progression in breast, lung and gastric cancers and was an independent predictor of outcome in a follow-up study in breast cancer (12).

In the TGFβ induced gene sets several members of the insulin-like growth factor binding proteins family, including IGFBP3, -5 and -7 were present. IGFBP3 up-regulation in the tumor stroma of prostate cancers has recently been demonstrated by global gene expression profiling following LCM (37) and a role as mediator for tumor - stroma interactions has been suggested in this type of tumors (38). Both IGFBP3 and -5 have been implicated in matrix deposition during fibrosis (39) which contributes to the early stages of malignant

transformation. Moreover, IGFBP3 has been recently shown to increase drug tolerance of tumor cells by promoting IGF-1R signaling (40).

IGFBP7 belongs to a group of low-affinity IGF binders, which have been implicated in diverse biological roles independent of their ability to bind IGF. Numerous studies demonstrated their direct association with a variety of extracellular and cell surface molecules with effects on cell proliferation and adhesion (41)(42). IGFBP7 knock-out mice showed significant changes in ovaries, muscle tissues and liver even though the mice were viable (43). Secreted IGFBP7 protein is a cell adhesive glycoprotein, which is regulated by proteolytic cleavage into a two-chain form by a membrane-bound serine protease matriptase (MT1-SP1) (28). Because IGFBP7 is expressed in blood vessels of various human cancer tissues including colon cancer, it is also referred to as "angiomodulin" (44)(45). Previously, it has been demonstrated that IGFBP7 serves as a selective biomarker for tumor-associated vessels in glioblastoma, that it is pro-angiogenic and induced by Smad-2 dependent TGFβ signaling (18). Apart from its expression in tumor vessels, variable IGFBP7 expression patterns have been reported in different tumor types and expression in tumor cells has been shown to be modulated by DNA methylation, retinoic acid and TGFβ (46)(47)(41). IGFBP7 might function as a secreted tumor suppressor (48)(46) and in this context, it has been shown that overexpression of IGFBP7 in a colon tumor cell line leads to a significant increase of cell adhesion to several substrates mediated by cell-bound IGFBP7 via syndecan-1 and to a reduction of anchorage independent growth (49).

We have demonstrated that IGFBP7 is a tumor stroma marker for several epithelial cancers expressed in activated fibroblasts and tumor vessels. We provide first evidence that IGFBP7 is both expressed in lymphatic as well as blood endothelium in human carcinomas. Furthermore we demonstrate for the first time that IGFBP7 is selectively expressed in malignant mesenchyme-derived tumor cells. In these mesenchyme derived cells and epithelial tumor cells, which have acquired a mesenchymal phenotype by undergoing EMT, IGFBP7 promotes anchorage-independent growth. Moreover, we could show that IGFBP7 reduces anchorage-independent growth when overexpressed in tumor cells with an epithelial phenotype (DLD-1) and that in those cells IGFBP7 is cleaved to its to chain form. The proteolytic processing of IGFBP7 by the type II transmembrane serine protease matriptase was previously shown to greatly reduce its insulin/IGF-dependent growth promoting activity and to enhance its syndecan-1-mediated cell adhesion activity (50). Matriptase is a type II transmembrane serine protease and in striking contrast to FAPα it is a strictly epithelial protease, which does not appear to be expressed in tumors of mesenchymal origin, suggesting

a specific function in epithelial carcinogenesis (51). Thus, IGFBP7 secreted by activated fibroblasts or endothelial cells might be cleaved by matriptase on the surface of epithelial cells and then act as a tumor suppressor by reducing the anchorage-independent growth ability of these cells, whereas uncleaved IGFBP7 could enhance the growth of mesenchymal cells or cells undergone EMT through its insulin/IGF promoting activity. IGFBP7 may therefore act as tumor suppressor during early stage tumorigenesis and as a promoter of tumorigenesis, when tumor cells have acquired a mesenchymal phenotype by undergoing EMT. Supporting this model, we could demonstrate that IGFBP7 expression is induced in DLD-1 E-Cadherin knock-down cells. These results are corroborated by previous results which demonstrated the induction of IGFBP7 following E-Cadherin knock-down in a breast cancer model sytem (29). In that study it was further shown that neither the overexpression of a dominant negative form of E-Cadherin nor an E-Cadherin /β-Catenin double knock-down led to an increase of IGFBP7 expression, implying that this induction depends on the adoption of a mesenchymal cell state via the β-Catenin pathway.

In conclusion, we could demonstrate the feasibility of our iLCM for the identification of tumor stroma targets such as IGFBP7. To further pursue the characterization of these newly identified targets, we have recently developed a novel 3D *in vitro* co-culture system (Dolznig H et al. manuscript in preparation). In combination, these approaches may provide new genetic markers in the tumor stroma, which may serve as novel targets for anti-cancer therapy.

Acknowledgements

This work was supported by Boehringer Ingelheim Austria. We are grateful to Christina Puri, Daniela Milovanovic and Harini Nivarthi for help with imunohistochemistry, cell culture and the xenograft experiments and Oliver Bergner for critically reading the manuscript and helpful discussions.

References

1. Bhowmick NA, Chytil A, Plieth D, et al. TGF-beta signaling in fibroblasts modulates the oncogenic potential of adjacent epithelia. Science 2004; 303: 848-51.

2. Orimo A, Gupta PB, Sgroi DC, et al. Stromal fibroblasts present in invasive human breast carcinomas promote tumor growth and angiogenesis through elevated SDF-1/CXCL12 secretion. Cell 2005; 121: 335-48.

3. Mueller MM, Fusenig NE. Friends or foes - bipolar effects of the tumour stroma in cancer. Nat Rev Cancer 2004; 4: 839-49.

4. Kunz-Schughart LA, Knuechel R. Tumor-associated fibroblasts (part I): Active stromal participants in tumor development and progression? Histol Histopathol 2002; 17: 599-621.

5. Joyce JA, Pollard JW. Microenvironmental regulation of metastasis. Nat Rev Cancer 2009; 9: 239-52.

6. Garin-Chesa P, Old LJ, Rettig WJ. Cell surface glycoprotein of reactive stromal fibroblasts as a potential antibody target in human epithelial cancers. Proc Natl Acad Sci U S A 1990; 87: 7235-9.

7. Desmouliere A, Guyot C, Gabbiani G. The stroma reaction myofibroblast: a key player in the control of tumor cell behavior. Int J Dev Biol 2004; 48: 509-17.

8. Grum-Schwensen B, Klingelhofer J, Berg CH, et al. Suppression of tumor development and metastasis formation in mice lacking the S100A4(mts1) gene. Cancer Res 2005; 65: 3772-80.

9. Ostman A, Heldin CH. PDGF receptors as targets in tumor treatment. Adv Cancer Res 2007; 97: 247-74.

10. Orimo A, Weinberg RA. Heterogeneity of stromal fibroblasts in tumors. Cancer Biol Ther 2007; 6: 618-9.

11. Mani SA, Guo W, Liao MJ, et al. The epithelial-mesenchymal transition generates cells with properties of stem cells. Cell 2008; 133: 704-15.

12. Chang HY, Sneddon JB, Alizadeh AA, et al. Gene expression signature of fibroblast serum response predicts human cancer progression: similarities between tumors and wounds. PLoS Biol 2004; 2: E7.

13. Finak G, Bertos N, Pepin F, et al. Stromal gene expression predicts clinical outcome in breast cancer. Nat Med 2008; 14: 518-27.

14. Ostermann E, Garin-Chesa P, Heider KH, et al. Effective immunoconjugate therapy in cancer models targeting a serine protease of tumor fibroblasts. Clin Cancer Res 2008; 14: 4584-92.

15. Santos AM, Jung J, Aziz N, Kissil JL, Pure E. Targeting fibroblast activation protein inhibits tumor stromagenesis and growth in mice. J Clin Invest 2009; 119: 3613-25.

16. Pure E. The road to integrative cancer therapies: emergence of a tumor-associated fibroblast protease as a potential therapeutic target in cancer. Expert Opin Ther Targets 2009; 13: 967-73.

17. Rupp C, Dolznig H, Puri C, et al. Laser capture microdissection of epithelial cancers guided by antibodies against fibroblast activation protein and endosialin. Diagn Mol Pathol 2006; 15: 35-42.
18. Pen A, Moreno MJ, Durocher Y, Deb-Rinker P, Stanimirovic DB. Glioblastoma-secreted factors induce IGFBP7 and angiogenesis by modulating Smad-2-dependent TGF-beta signaling. Oncogene 2008; 27: 6834-44.
19. Irizarry RA, Bolstad BM, Collin F, Cope LM, Hobbs B, Speed TP. Summaries of Affymetrix GeneChip probe level data. Nucleic Acids Res 2003; 31: e15.
20. Gentleman RC, Carey VJ, Bates DM, et al. Bioconductor: open software development for computational biology and bioinformatics. Genome Biol 2004; 5: R80.
21. Smyth GK. Linear models and empirical bayes methods for assessing differential expression in microarray experiments. Stat Appl Genet Mol Biol 2004; 3: Article3.
22. Benjamini Y, Drai D, Elmer G, Kafkafi N, Golani I. Controlling the false discovery rate in behavior genetics research. Behav Brain Res 2001; 125: 279-84.
23. Subramanian A, Tamayo P, Mootha VK, et al. Gene set enrichment analysis: a knowledge-based approach for interpreting genome-wide expression profiles. Proc Natl Acad Sci U S A 2005; 102: 15545-50.
24. Christian S, Ahorn H, Novatchkova M, et al. Molecular cloning and characterization of EndoGlyx-1, an EMILIN-like multisubunit glycoprotein of vascular endothelium. J Biol Chem 2001; 276: 48588-95.
25. Breiteneder-Geleff S, Soleiman A, Kowalski H, et al. Angiosarcomas express mixed endothelial phenotypes of blood and lymphatic capillaries: podoplanin as a specific marker for lymphatic endothelium. Am J Pathol 1999; 154: 385-94.
26. Tan PL, Farmiloe S, Yeoman S, Watson JD. Expression of the interleukin 6 gene in rheumatoid synovial fibroblasts. J Rheumatol 1990; 17: 1608-12.
27. Ozerdem U, Grako KA, Dahlin-Huppe K, Monosov E, Stallcup WB. NG2 proteoglycan is expressed exclusively by mural cells during vascular morphogenesis. Dev Dyn 2001; 222: 218-27.
28. Ahmed S, Jin X, Yagi M, et al. Identification of membrane-bound serine proteinase matriptase as processing enzyme of insulin-like growth factor binding protein-related protein-1 (IGFBP-rP1/angiomodulin/mac25). FEBS J 2006; 273: 615-27.
29. Onder TT, Gupta PB, Mani SA, Yang J, Lander ES, Weinberg RA. Loss of E-cadherin promotes metastasis via multiple downstream transcriptional pathways. Cancer Res 2008; 68: 3645-54.

30. Pennica D, Swanson TA, Welsh JW, et al. WISP genes are members of the connective tissue growth factor family that are up-regulated in wnt-1-transformed cells and aberrantly expressed in human colon tumors. Proc Natl Acad Sci U S A 1998; 95: 14717-22.
31. Xu L, Corcoran RB, Welsh JW, Pennica D, Levine AJ. WISP-1 is a Wnt-1- and beta-catenin-responsive oncogene. Genes Dev 2000; 14: 585-95.
32. Desnoyers L, Arnott D, Pennica D. WISP-1 binds to decorin and biglycan. J Biol Chem 2001; 276: 47599-607.
33. Pilarsky C, Ammerpohl O, Sipos B, et al. Activation of Wnt signalling in stroma from pancreatic cancer identified by gene expression profiling. J Cell Mol Med 2008; 12: 2823-35.
34. Brabletz T, Jung A, Reu S, et al. Variable beta-catenin expression in colorectal cancers indicates tumor progression driven by the tumor environment. Proc Natl Acad Sci U S A 2001; 98: 10356-61.
35. Kagan HM, Li W. Lysyl oxidase: properties, specificity, and biological roles inside and outside of the cell. J Cell Biochem 2003; 88: 660-72.
36. Levental KR, Yu H, Kass L, et al. Matrix crosslinking forces tumor progression by enhancing integrin signaling. Cell 2009; 139: 891-906.
37. Gregg JL, Brown KE, Mintz EM, Piontkivska H, Fraizer GC. Analysis of gene expression in prostate cancer epithelial and interstitial stromal cells using laser capture microdissection. BMC Cancer; 10: 165.
38. Massoner P, Haag P, Seifarth C, et al. Insulin-like growth factor binding protein-3 (IGFBP-3) in the prostate and in prostate cancer: local production, distribution and secretion pattern indicate a role in stromal-epithelial interaction. Prostate 2008; 68: 1165-78.
39. Pilewski JM, Liu L, Henry AC, Knauer AV, Feghali-Bostwick CA. Insulin-like growth factor binding proteins 3 and 5 are overexpressed in idiopathic pulmonary fibrosis and contribute to extracellular matrix deposition. Am J Pathol 2005; 166: 399-407.
40. Sharma SV, Lee DY, Li B, et al. A chromatin-mediated reversible drug-tolerant state in cancer cell subpopulations. Cell; 141: 69-80.
41. Hwa V, Oh Y, Rosenfeld RG. The insulin-like growth factor-binding protein (IGFBP) superfamily. Endocr Rev 1999; 20: 761-87.
42. Firth SM, Baxter RC. Cellular actions of the insulin-like growth factor binding proteins. Endocr Rev 2002; 23: 824-54.
43. Burger AM, Leyland-Jones B, Banerjee K, Spyropoulos DD, Seth AK. Essential roles of IGFBP-3 and IGFBP-rP1 in breast cancer. Eur J Cancer 2005; 41: 1515-27.

44. Akaogi K, Okabe Y, Funahashi K, et al. Cell adhesion activity of a 30-kDa major secreted protein from human bladder carcinoma cells. Biochem Biophys Res Commun 1994; 198: 1046-53.
45. van Beijnum JR, Dings RP, van der Linden E, et al. Gene expression of tumor angiogenesis dissected: specific targeting of colon cancer angiogenic vasculature. Blood 2006; 108: 2339-48.
46. Ruan W, Xu E, Xu F, et al. IGFBP7 plays a potential tumor suppressor role in colorectal carcinogenesis. Cancer Biol Ther 2007; 6: 354-9.
47. Komatsu S, Okazaki Y, Tateno M, et al. Methylation and downregulated expression of mac25/insulin-like growth factor binding protein-7 is associated with liver tumorigenesis in SV40T/t antigen transgenic mice, screened by restriction landmark genomic scanning for methylation (RLGS-M). Biochem Biophys Res Commun 2000; 267: 109-17.
48. Vizioli MG, Sensi M, Miranda C, et al. IGFBP7: an oncosuppressor gene in thyroid carcinogenesis. Oncogene.
49. Sato Y, Chen Z, Miyazaki K. Strong suppression of tumor growth by insulin-like growth factor-binding protein-related protein 1/tumor-derived cell adhesion factor/mac25. Cancer Sci 2007; 98: 1055-63.
50. Ahmed S, Yamamoto K, Sato Y, et al. Proteolytic processing of IGFBP-related protein-1 (TAF/angiomodulin/mac25) modulates its biological activity. Biochem Biophys Res Commun 2003; 310: 612-8.
51. List K, Bugge TH, Szabo R. Matriptase: potent proteolysis on the cell surface. Mol Med 2006; 12: 1-7.

Figure legends

Figure 1.

Genes and gene-sets induced in the tumor stroma. (**A**) Unsupervised hierarchical cluster analysis of tumor cell, tumor stroma and normal stroma samples. 1299 genes were differentially expressed between the tumor stroma and the normal stroma. Heat map colors represent mean-centered fold change expression in log-space. (**A,** right) Gene-Set Enrichment Analysis (GSEA) revealed gene sets involved in response to wounding, extracellular matrix deposition, inflammatory response and cell migration significantly induced in the tumor stroma. The numbers of enchriched genes in each category are represented in a pie chart. (**B**) Well characterized tumor stroma markers such as FAPα , biglycan or Wisp-1 were found to be significantly induced in the tumor stroma compartment *vs.* the normal stroma. The expression levels are indicated by whisker box plots, the bold centre-line indicates the median; the box represents the interquartile range (IQR). Whiskers extend to 1.5 times the IQR. TC, tumor cells; NS, normal stroma; TS, tumor stroma. Immunohistochemical stainings demonstrate the induction of these genes at the protein level (inserts).

Figure 2.

Induction of IGFBP7 in the tumor stroma. (**A**) The whisker box plot shows the induction of IGFBP7 in the tumor stroma (TC, tumor cells; NS, normal stroma; TS, tumor stroma). (**B)** As demonstrated by immunohistochemical staining on representative examples of colon and lung carcinomas, IGFBP7 is expressed in cancer associated fibroblasts and tumor vessels in those epithelial cancer samples. In soft tissue sarcomas, such as MFH (malignant fibrous histiocytoma), IGFBP7 is expressed by the malignant mesenchyme-derived cells. Paraffin sections were stained with the avidin-biotin immunoperoxidase (ABC) method and counterstained with haematoxylin (blue)

Figure 3.

IGFBP7 is a tumor stroma marker in epithelial cancers and a marker for malignant mesenchyme-derived tumor cells **.** (**A**) Double-labeling studies with EndoGlyx and NG2 (green) on a colon adenocarcinoma section, demonstrating that IGFBP7 (red) is expressed by the tumor endothelial cells and the surrounding mural cells. *In vitro,* blood and lymphatic

human dermal microvascular endothelial cells (HDMECs) and freshly isolated colon cancer associated fibroblasts (CAFs) are shown to be positive for IGFBP7. CD31, Prox1 and vimentin were used as established markers to characterize the individual cell types. (**B**) As demonstrated by Western blotting, IGFBP7 is expressed by malignant-mesenchyme derived cells (HT1080) and epithelial cells with a mesenchymal phenotype (Caki-1, SW480), whereas tumor cells with an epithelial phenotype (LS174T, HT29,DLD-1, Colo205) are IGFBP7 negative. E-Cadherin and vimentin were used as markers to determine the phenotype of the cell lines. GAPDH was used as a loading control. Soluble IGFBP7 was detected in the supernatant (SN), vimentin, E-Cadherin and GAPDH in the corresponding cell lysates. (**C**) In HT1080 cells, shRNA mediated knock-down resulted in a significant IGFBP7 protein reduction in the supernatant. (**D**) As illustrated with a colony formation assay in soft agar, IGFBP7 knock-down results in a significant reduction of anchorage independent growth of HT1080 and Caki-1 cells. Colonies were stained with crystal violet and counted with ImageJ, the graphs represent the average results of three independent experiments.

Figure 4.

Proteolytically cleaved IGFBP7 reduces the anchorage-independent growth ability of epithelial tumor cells. (**A**) Soft agar colony formation assays shows a significant reduction of anchorage-independent growth of DLD-1 cells overexpressing cleaved IGFBP7, when compared to the mock transfectants. Colonies were stained with crystal violet and counted with ImageJ, the graphs repesent the average results of three independent experiments. (**B**) Conditioned medium from IGFBP7 overexpressing DLD-1 cells contained two IGFBP7 bands, representing a native 33 kDa form and a 26 kDa form, which potentially results from proteolytic cleavage by matriptase (MT1-SP1). As indicated by Western blotting, type II transmembrane serine protease matriptase is a strictly epithelial protease, expressed by DLD-1 cells at high levels. Soluble IGFBP7 was detected in the supernatant (SN) and GAPDH was used as a loading control and detected in the cell lysates.

Figure 5.

IGFBP7 expression is induced in DLD-1 cells following E-Cadherin knock-down. shRNA mediated E-Cadherin knock-down in DLD-1 cells results in significant protein reduction determined by Western blotting and a translocation of β-Catenin into the nucleus as shown by immunofluorescence. In comparison to the control cells, E-Cadherin knock-down cells show a

significant induction of IGFBP7 expression. The expression level of IGFBP7 was determined by realtime PCR relative to GAPDH.

Supplementary figure legends

Figure 1.

Work flow for identification of novel tumour stroma markers by expression profiling analysis. The antibody-guided laser capture microdissection allowed the separation of epithelial cells from the activated stromal compartment in colon cancer samples. Activated tumor stromal fibroblasts were visualized by immunohistochemical staining with an antibody to FAPα . In the figure, the borders between epithelial and stromal structures are indicated by red dotted lines. Normal fibroblasts were isolated from normal colonic tissue after hematoxylin staining and morphological examination. After RNA isolation and amplification whole genome Affymetrix GeneChip® analysis was performed followed by bioinformatic evaluation to identify novel tumor stroma targets. Numbers and arrows indicate the numbers of genes and their change in transcript levels; red: up, green: down.

Figure 2.

Cell proliferation assays by Fluorescence Activated Cell Sorting (FACS). Cell proliferation assays were done with EdU (5-ethynyl-2´-deoxyuridine) incorporation and the DNA content was determined on the basis of fluorescence intensity for Propidium Iodide (PI). Plots display fluorescence intensity for EdU incorporation (Y-axis) and DNA content (X-axis) with colors representing increasingly higher number of cells with a given fluorescence intensity (orange, highest cell number; blue lowest cell number). After pulsing with EdU for 30 min, the fraction of EdU^{high} HT1080 control and shRNA IGFBP7 cells was determined (41,4 *vs*.40,9%).

Figure 3.

Xenograft growth curves. Xenografts were established by injection of 1.10^7 HT1080 control and shRNA IGFBP7 cells in both flanks of SCID mice (n=3) and tumor growth was measured over a 14-day period. As indicated by the respective single and median tumor volumes, a delayed tumor take of the IGFBP7 knock-down cells was observed in comparison to the control cells.

Figure 4.

In vitro phenotype resulting from E-Cadherin knock-down. In contrast to the control cells, which grew in monolayer culture as epithelial clusters, shRNA E-Cadherin knock-downs lost cell-cell contacts and displayed a more elongated, fibroblastic morphology.

Gene set name	Brief description (Pubmed ID)	Size	FDR q-value
TGFBETA_ALL_UP	Upregulated by TGF-beta treatment of skin fibroblasts, at any timepoint (11279127)	40	0.000
EMT_UP	Up-regulated during the TGFbeta-induced epithelial-to-mesenchymal transition (EMT) of Ras-transformed mouse mammary epithelial (EpH4) cells (14562044)	25	0.001
IL6_FIBRO_UP	Upregulated following IL-6 treatment in normal skin fibroblasts (15095275)	21	0.003
MANALO_HYPOXIA_UP	Genes upregulated in human pulmonary endothelial cells under hypoxic conditions or after exposure to AdCA5, an adenovirus carrying constitutively active hypoxia-inducible factor 1 (HIF-1alpha). (15374877)	27	0.029

Table 1

List of the most significantly enriched pathways sorted by the Normalized Enrichment Score (NES) using the c2 curated gene sets of genes upregulated in the tumor stroma. Size indicates the number of genes in the gene set. FDR q-val indicates the false discovery rate.

Figures

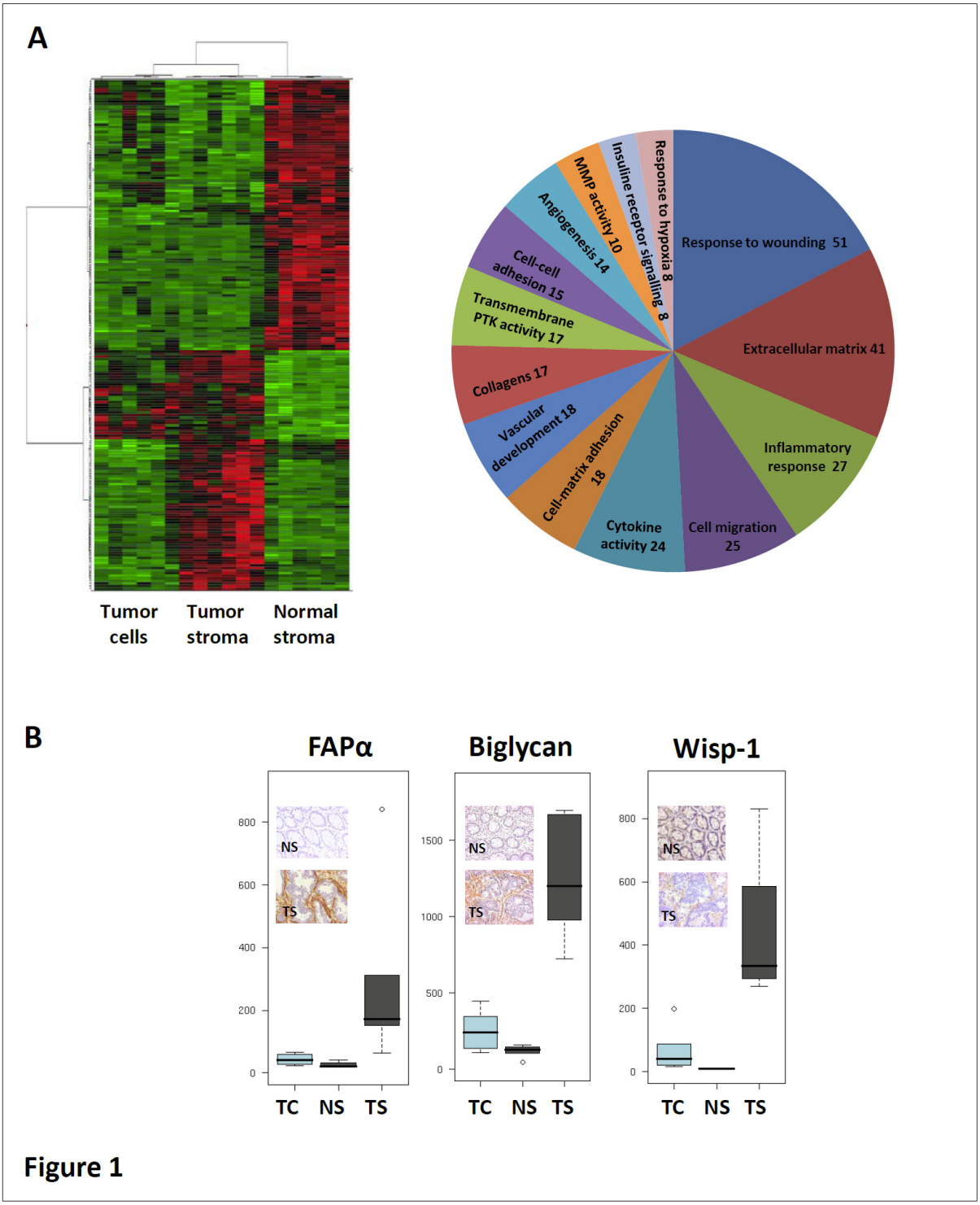

Figure 1

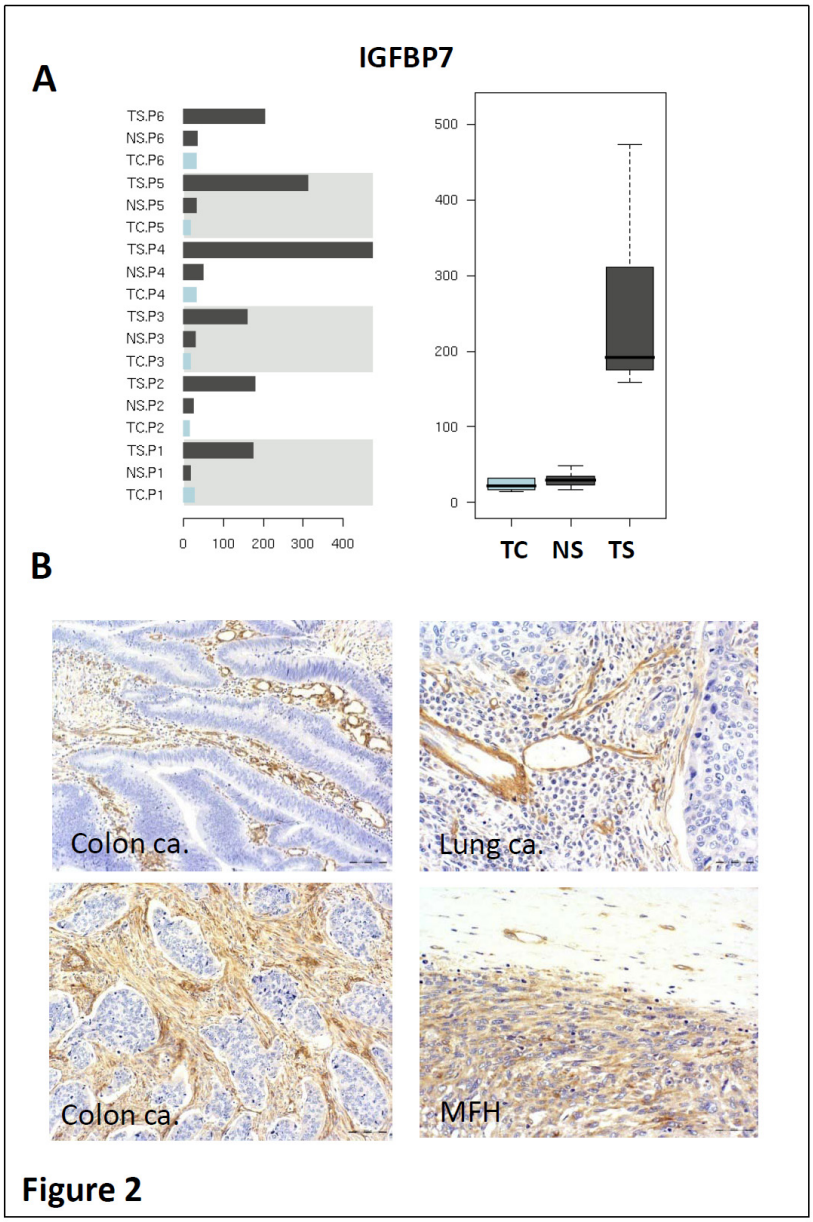
A
IGFBP7
TS.P6
NS.P6
TC.P6
TS.P5
NS.P5
TC.P5
TS.P4
NS.P4
TC.P4
TS.P3
NS.P3
TC.P3
TS.P2
NS.P2
TC.P2
TS.P1
NS.P1
TC.P1
0 100 200 300 400
500
400
300
200
100
0
TC NS TS
B
Colon ca.
Lung ca.
Colon ca.
MFH

Figure 2

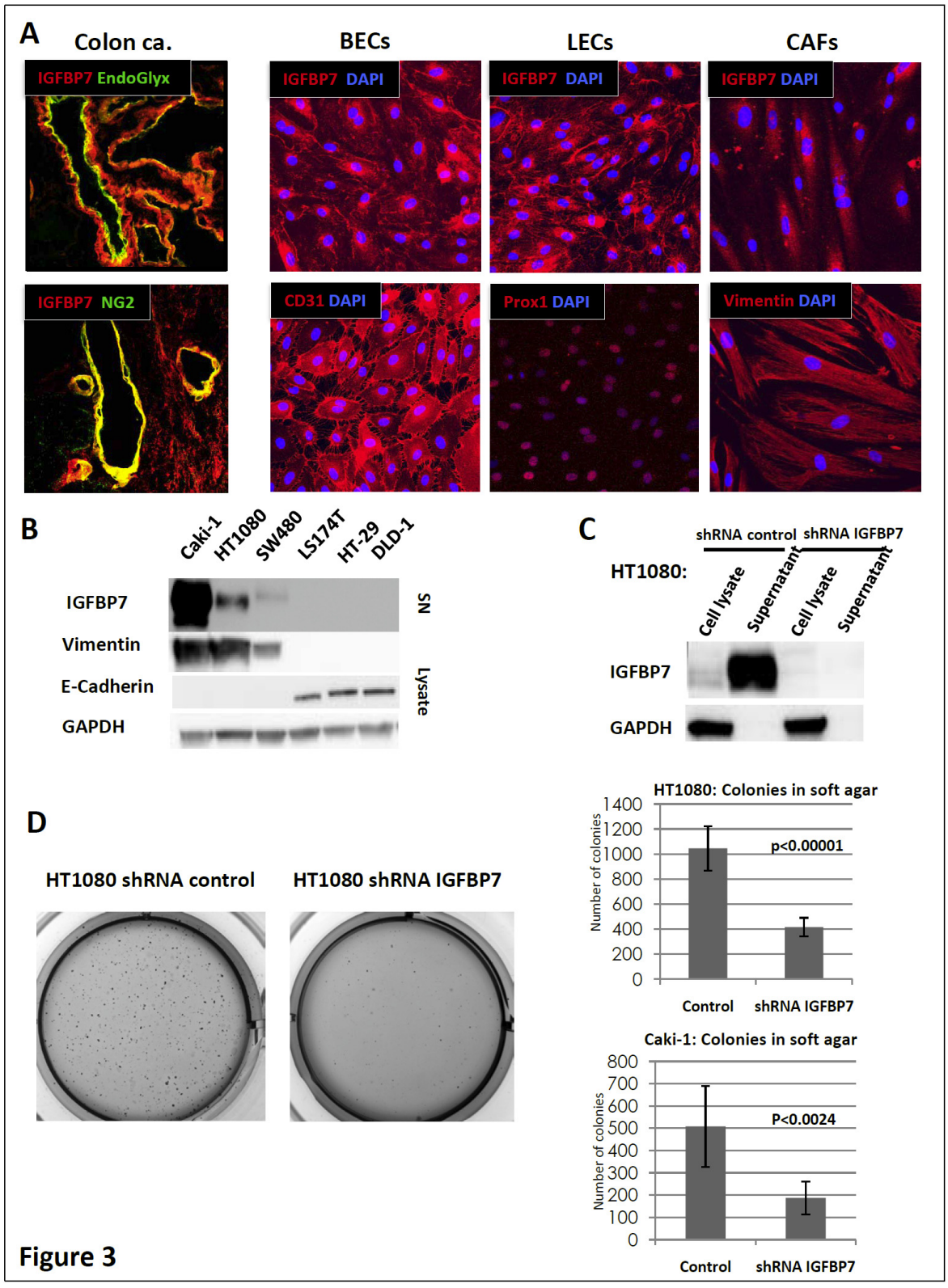
A
Colon ca.
BECs
LECs
CAFs
IGFBP7 EndoGlyx
IGFBP7 DAPI
IGFBP7 DAPI
IGFBP7 DAPI
IGFBP7 NG2
CD31 DAPI
Prox1 DAPI
Vimentin DAPI
B
Caki-1
HT1080
SW480
LS174T
HT-29
DLD-1
IGFBP7
Vimentin
E-Cadherin
GAPDH
SN
Lysate
C
shRNA control
shRNA IGFBP7
HT1080:
Cell lysate
Supernatant
Cell lysate
Supernatant
IGFBP7
GAPDH
D
HT1080 shRNA control
HT1080 shRNA IGFBP7
HT1080: Colonies in soft agar
Number of colonies
1400
1200
1000
800
600
400
200
0
p<0.00001
Control
shRNA IGFBP7
Caki-1: Colonies in soft agar
Number of colonies
800
700
600
500
400
300
200
100
0
P<0.0024
Control
shRNA IGFBP7

Figure 3

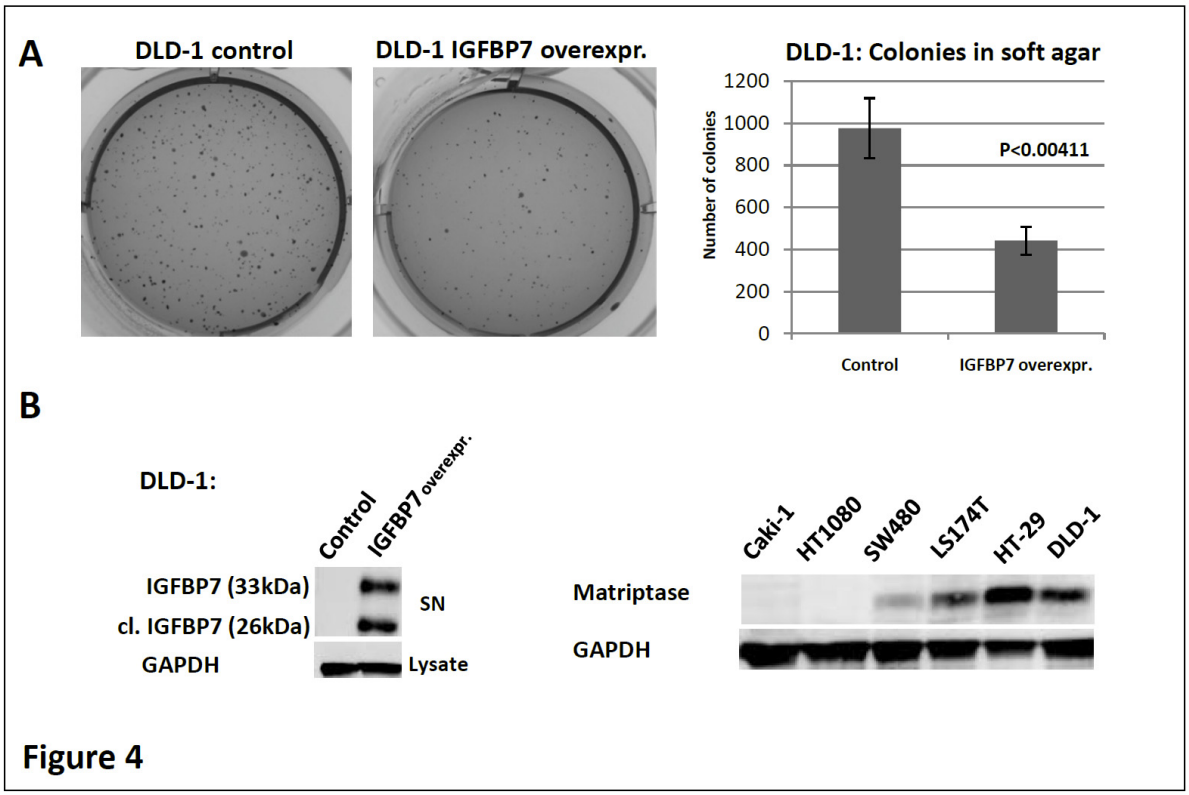

Figure 4

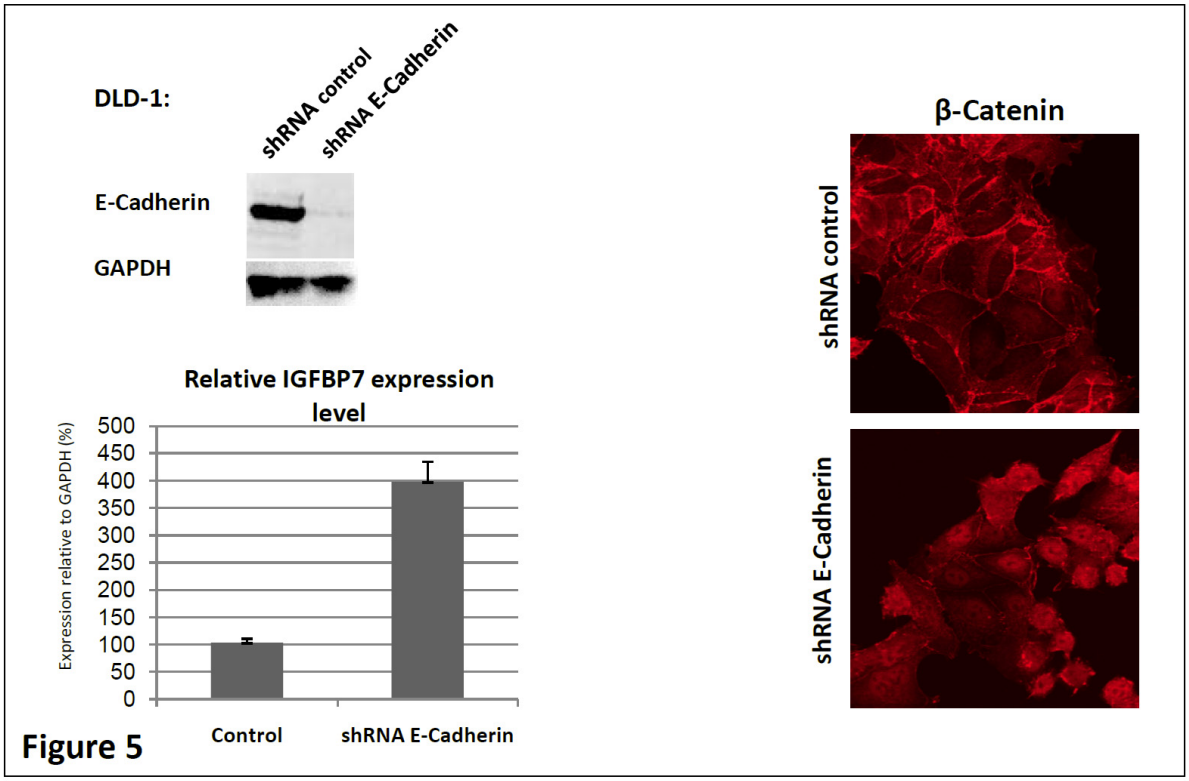

Figure 5

Supplementary figures

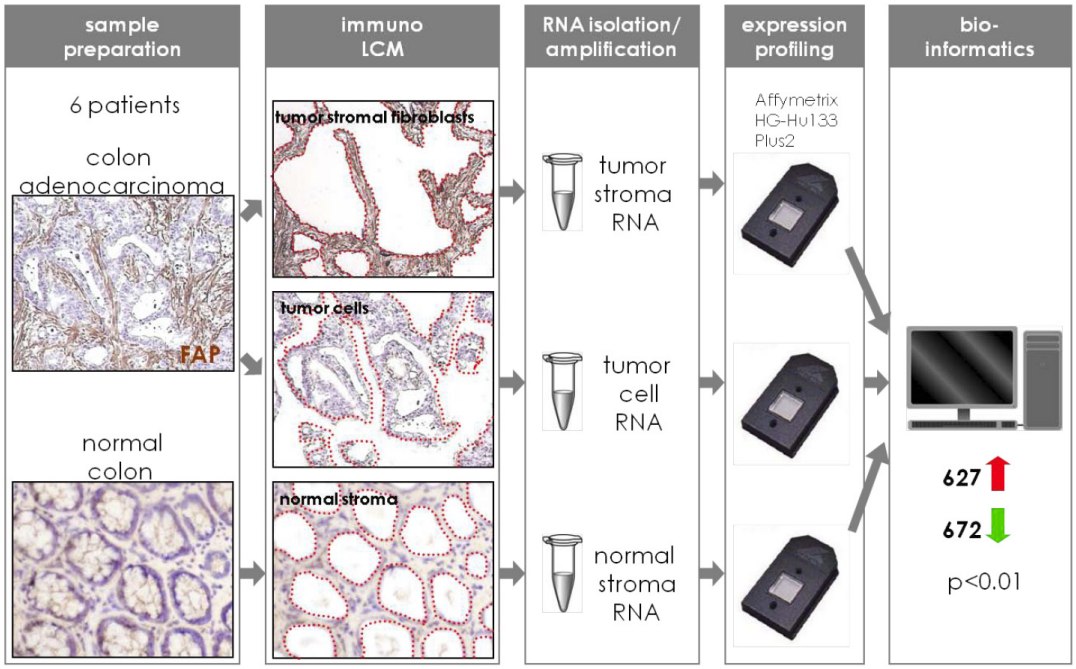

Supplementary figure 1

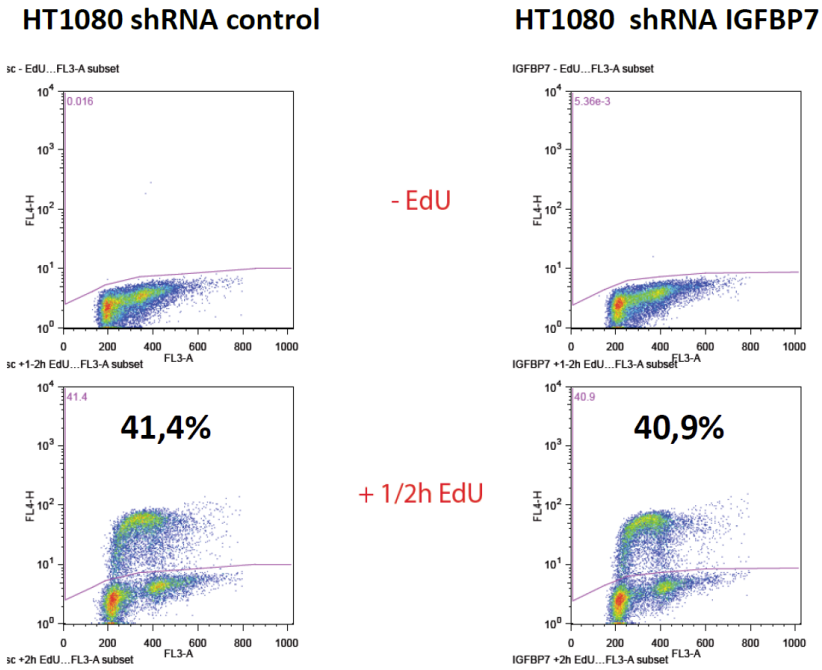

Supplementary figure 2

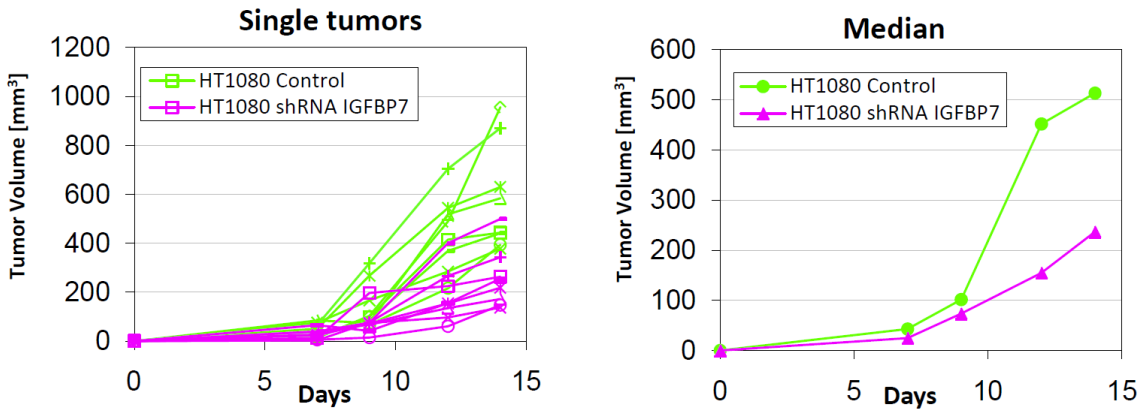

Supplementary figure 3

DLD-1 shRNA control

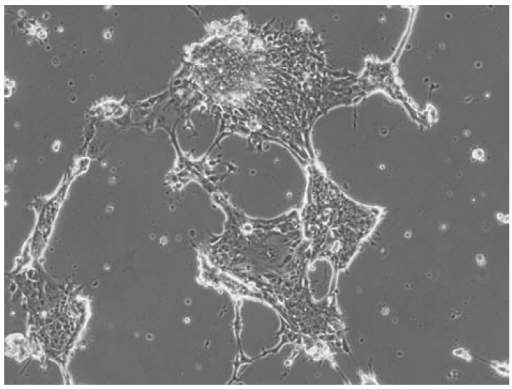

DLD-1 shRNA E-Cadherin

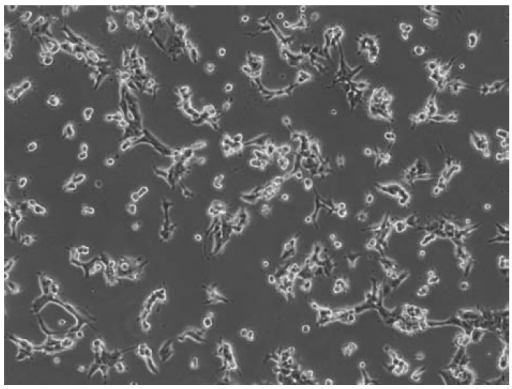

Supplementary figure 4

Modeling adenocarcinomas in vitro*:*

a novel 3D co-culture system induces cancer relevant pathways upon tumor cell and stromal fibroblast interaction

Helmut Dolznig*[1], Christian Rupp*, Christina Puri*[#], Christian Haslinger[#], Norbert Schweifer[#], Elisabeth Wieser*, Dontscho Kerjaschki* and Pilar Garin-Chesa*[#]

* Institute of Pathology, Medical University of Vienna, Waehringer Guertel 18-20, A-1090 Vienna, Austria

[#]Boehringer Ingelheim RCV GmbH & Co KG, Vienna, Austria, Dr. Boehringer_Gasse 5-11, A-1121 Vienna, Austria

[1] Institute of Medical Genetics, Medical University of Vienna, Waehringer Strasse 10, A-1090 Vienna, Austria

Abstract

Activated tumor stroma participates in tumor cell growth, invasion and metastasis. Normal fibroblasts and cancer-associated fibroblasts (CAFs) have been shown to display distinct gene expression signatures. This molecular heterogeneity may influence the way tumor cells migrate, proliferate and survive during tumor progression. To test this hypothesis and to better understand the molecular mechanisms that control these interactions we have established a three-dimensional (3D) human cell culture system that recapitulates the tumor heterogeneity observed *in vivo*.

Human tumor cells were grown as multicellular spheroids and subsequently co-cultured with normal fibroblasts or CAFs in collagen-I gels. This *in vitro* model system closely mirrors the architecture of human epithelial cancers and allows the characterization of the tumor cell-stroma interactions phenotypically and at the molecular level.

Using GeneChip analysis, antibody arrays and ELISA assays, we demonstrate that stromal fibroblasts induced different highly relevant cancer expression profiles. Genes involved in invasion, ECM remodeling, inflammation and angiogenesis were differentially regulated in our 3D carcinoma model.

The modular setup, reproducibility and the robustness of the model make it a powerful tool to identify target molecules involved in signaling pathways that mediate paracrine interactions in the tumor microenvironment and to validate the influence of these molecular targets during tumor growth and invasion in the supporting stroma.

Introduction

Carcinomas comprise about 90% of all human cancers, including lung-, colon-, breast- and prostate carcinomas, which together cause about 50% of all cancer deaths [1]. They consistently develop as highly complex structures composed of genetically altered tumor cells, together with fibroblasts, endothelial cells, pericytes and inflammatory cells embedded in a matrix of extracellular proteins (ECM). The tumor stroma influences the development of malignant tumors [2-4], for example the recruitment of blood vessels is ultimately required for tumor growth [3, 5]. Fibroblasts comprise the major cellular component of the stroma of carcinomas. These cancer associated fibroblasts (CAF) have been shown to stimulate tumor progression of initiated non-tumorigenic prostate epithelial cells [6], and to promote the growth of breast and colon cancer in animal models [7,8]. Recently it was demonstrated that the interaction of colon cancer cells with stromal cells activates the beta-catenin pathway in the cancer cells and led to an increase in colon cancer stem cells [9]. Therefore, understanding the molecular mechanisms involved in the paracrine interactions between the tumor and the surrounding stroma will help to identify new molecules that may serve as potential drug targets.

The culture of cells on two dimensional (2D) surfaces has provided groundbreaking insights into basic cell biology and tumorigenesis [10,11,12]. However, most physiological parameters of organs or tumors such as tissue architecture, cell to cell- and cell to matrix interaction, mechanical properties and biochemical networks are lost under these simplified conditions. Cells grown in three-dimensional (3D) scaffolds or as 3D aggregates (multicellular spheroids) much better recapitulate the *in vivo* situation of tissues [13-15] or tumors [16-21]. These 3D culture systems were rarely used to address the mechanisms of interaction between human tumor-and stromal cells embedded in ECM [22-24].

We have combined well-established 3D cellular assays (multicellular spheroids, 3D collagen gel cultures, co-cultures) into one experimental setup, which we call the "*in vitro* carcinoma assay". We show that this model system is physiologically relevant and allows live imaging, histological examination, biochemical assays and functional experiments to be performed in parallel. In addition, expression-profiling analysis identified genes differentially regulated upon tumor stroma interaction, which are relevant for carcinogenesis. Finally, we demonstrate that the assay format is suitable for *in vitro* drug testing.

Results

Multicellular tumor spheroid – fibroblast co-culture experiments in a 3D collagen gel matrix

Seventeen human tumor cell lines were tested for their ability to grow as multicellular spheroids. Eleven cell lines formed spheroids, whereas six cell lines only formed loose cell aggregates under any of the experimental conditions tested. Spheroids from different cell lines behaved differently when placed into collagen gels. Some remained as compact spheres and did not show signs of invasion; others displayed moderate invasion, and other cell types such as SK-OV-3 showed extensive invasive structures characterized by multicellular astral outgrowth into the collagen gels (Figure 1A, Supplementary Table 1 and Supplementary Figure 1).

The colon cancer cell line LS174T, defined as non-invasive in our assay, was selected for further studies. LS174T spheroids were prepared, harvested and mixed with freshly trypsinized fibroblasts (Supplementary Material and Supplementary Figure 1). The mixture was centrifuged and the pellet resuspended in collagen I solution and poured into silicone moulds (Figure 1B). This gave rise to flat collagen gel-cylinders, which were mechanically stabilized by submerging nylon mesh rings before polymerization (Figure 1B, bottom). The gel-cylinders harbored either 96 tumor cell spheroids surrounded by $2x10^5$ normal fibroblasts or CAFs. In addition tumor cell spheroids without fibroblasts or fibroblasts alone were prepared in a similar way. The fibroblasts used were normal embryonic colon fibroblasts (CCD18-Co, designated NCF), hTERT immortalized skin fibroblasts (BJ-1, designated SF) and primary fibroblast cultures isolated from human colon carcinoma specimen (cancer associated fibroblasts, CAF1, CAF2, Supplementary Figure 2).

The ring-shaped nylon meshes facilitated the microscopic analysis by phase-contrast of living cells (Figures 1C, 2A, 8A+C) and by fluorescence-microscopy of labeled cells (Figures 5, Supplementary Figures 4, 5). When tumor spheroids and fibroblasts were cultured without the supporting nylon mesh, the free floating collagen gel cylinders shrunk and appeared as dense, refractive structures within 2-3 days due to the contractile forces of the fibroblasts in the gels as described [25], which hindered microscopic evaluation (Figure 1C). In contrast, embedded nylon meshes resisted the contracting force of the fibroblasts and completely abolished shrinking (Figure 1C). The morphology of the co-cultures could thus be monitored easily by live-microscopy.

Phenotypic characterization and morphology of the tumor cell clusters

In the presence of fibroblasts, LS174T tumor spheroids (Figure 2A) displayed well organized glandular structures after 24-48 hrs co-culture as revealed by transmission light microscopy and after H&E staining. The epithelial cells expressed the luminal tight junction protein ZO-1, predominantly membrane associated beta-catenin and secreted mucin into the glandular structures (Figure 2B). Electron microscopy revealed the characteristic intestinal cell microvillus seam at the luminal side on LS174T cells when grown alone or in the LS174T-NCF co-cultures. Differences in the electron density of the mucus were observed when comparing LS174T spheroids cultured alone versus the co-cultures, probably indicating a different composition of the mucin (Figure 2C). Differences were also noted in the cell-cell interactions, with well established desmosomes, adherens-junctions and tight-junctions observed in the LS174T cells co-cultured with fibroblasts, which were less developed in LS174T cells grown alone (Figure 2D).

Fibroblast-tumor cell interaction

Fibroblasts, when added to the cultures, formed a well-organized network around the tumor cell spheroids within 2-3 days (Figure 3A, left), regardless of the source of fibroblasts. The fibroblasts expressed PDGFRbeta and when in vicinity of the LS174T spheroid were closely attached to the tumor spheroid surface (Figure 3A). Electron microscopy revealed close cell-cell interactions between epithelial cells and fibroblasts in tumor spheroid/fibroblast co-cultures (Figure 3B). Fibroblasts in the collagen gels, like in tissues, displayed spindle shaped morphology (Figure 2A, Figure 3C), which did not change upon co-cultivation with tumor cell spheroids. They expressed vimentin, alpha-smooth muscle actin (in subsets) and fibroblast activation protein alpha (FAP), a tumor stromal fibroblast marker [26], closely resembling activated fibroblasts in tumor stroma *in vivo* (Figure 3C). In summary, the in vitro cultures closely mimic the cellular architecture of human colon carcinoma samples at the histological level (Figure 3C).

Co-cultivation experiments of other human cancer cells such as colon cancer (HCT116, HT-29) and mammary tumor cell spheroids (MCF7, BT474) with CAFs displayed similar phenotypes with respect to their *in vivo* counterparts (data not shown), demonstrating the general feasibility of the assay to study heterotypic interactions in epithelial cancers.

The in vitro system recapitulates major features of colon carcinomas in vivo

Tumor cells within the spheroids were highly proliferative as shown by staining for phosphorylated retinoblastoma protein (phospho-Rb)[27] similar to colon carcinomas in vivo [28]. In contrast, co-cultured fibroblasts were predominantly quiescent, displaying very rare Rb phosphorylation (Figure 4A). These immunofluorescence results were confirmed by Western Blot analysis. The co-culture did not significantly change the phospho-Rb status of the cells (Figure 4A, right). When tumor spheroids grew beyond > 450 micrometer diameter they showed a ring of proliferating cells surrounding apoptotic/necrotic central areas [29] (Supplementary Figure 4), mimicking *in vivo* observations [30].

Subsequently,we analysed the status of the HGF-Met axis, which is one of the best-characterized epithelial-stromal paracrine pathways. c-Met overexpression and paracrine activation by HGF, which is produced by stromal cells [31], has been implicated in colon cancer development, invasiveness and clinical outcome [32, 33]. Using receptor-tyrosine-kinase arrays we showed that c-Met was tyrosine phosphorylated in the LS174T tumor cells, when incubated with conditioned medium (CM) from LS174T spheroid/fibroblast co-cultures, however c-Met was not phosphorylated when incubated with CM from tumor spheroid- or fibroblast mono-cultures (Figure 4a). On the other hand, HGF was selectively produced by the fibroblasts as demonstrated by cytokine array analysis (Figure 4a). This indicated a selective proteolytic activation of the HGF precursor in the co-cultures which is in line with the reported expression of an HGF activator (HGFA) protease by colon cancer cells [34].

A recent report demonstrated that high Wnt pathway activity in colon adenocarcinoma cells was induced by the presence of stromal myofibroblasts both in vitro and in vivo. This paracrine stimulation of the Wnt pathway was accompanied by the induction of a cancer stem cell phenotype [9]. A similar behavior was observed in our model. First, we observed a heterogeneous activation of the Wnt pathway on the LS174T spheroids as revealed by the staining with beta-catenin, a marker protein for Wnt pathway activation. In LS174T spheroids the majority of the cells displayed membrane bound beta-catenin, with only few cells showing nuclear beta-catenin localization (Figure 4C). When LS174T cells were co-cultivated with colon-derived fibroblasts (NCF and CAFs) the percentage of nuclear beta-catenin positive cells increased more than fivefold (Figure 4C, bottom, right), indicative of Wnt pathway activation via the stromal fibroblasts. Thus, we demonstrate that the in vitro assay closely recapitulated physiological aspects and activation of essential pathways described *in vivo* in colon cancer.

Fibroblasts induced invasive spreading of LS174T cells

LS174T cells were transfected with DsRed and stable clones were selected (LS174TdsR). LS174TdsR cell spheroids were embedded in collagen gels in the presence or absence of fibroblasts, incubated and followed by light- and fluorescence microscopy. After about 4 days, the presence of fibroblasts in the cultures induced an invasive phenotype in the LS174T cells (Figure 5A). Collective and single cell invasion was observed by confocal imaging (Figure 5A, B) and time-lapse microscopy of fluorescently labeled tumor cells (Supplementary Figure 5). In contrast, LS174T cell spheroids in the absence of fibroblasts displayed a non-invasive phenotype in collagen gels even after 11 days in culture (Figure 5A, B).

Expression profiling

To further substantiate the suitability of the novel system for molecular analysis we determined changes in gene expression upon co-cultivation of tumor cells with stromal fibroblasts by GeneChip arrays. Ninety-six LS174T tumor cell spheroids and $2x10^5$ fibroblasts were cultured in collagen gels either separately or as co- cultures for 3.5 days (Supplementary Figure 6). We used SF, NCF and CAFs to reveal common and different responses induced by co-cultivation. Lysates from LS174T mono-cultures were mixed with fibroblast mono-culture lysates (designated as mono-culture mixed) thereby ensuring the same amount of tumor cells and fibroblasts present as in the co-culture experiments. All experiments were done in biological triplicates. We used a direct-lysis approach of the entire collagen gel cultures rather than isolating and sorting of cancer cells and fibroblasts to avoid changes in RNA expression during the isolation process (duration >1.5 hrs). RNA extracted from the mixed and the co-culture experiments was processed for whole genome Affymetrix GeneChip analysis (Supplementary Figure 6). After normalization and bioinformatics analysis (Supplementary Methods) we identified genes differentially regulated in co-cultures compared to cultures identical in the cellular composition but without physical contact during culture. In addition, co-cultivation of LS174T cells with fibroblasts of different origin allowed determining specific responses to the various fibroblast types. Principal component analysis (PCA) detected four clusters dependent on the fibroblasts present in the experimental setup, with the skin fibroblasts clustering apart from the colon fibroblast clouds (NCF, CAF1, CAF2). All co-culture clusters were shifted in the same direction close to the corresponding mix clusters (Figure 6A). 535 genes were differentially expressed in colon fibroblast co-cultures as compared to the mixed mono-cultures (fdr, $p<0.01$, $FC>1.5$; 396 up, 139 down).

176 genes were regulated in the co-cultures with CAFs (134 up and 42 down; FC>1.5, fdr, p<0.01; Supplementary Figure 7A). 180 genes were differently expressed between colon derived- and skin fibroblasts (fdr, p<0.01, 96 up in skin fibroblasts, 84 up in colon derived fibroblasts), when compared under the mono-culture mix conditions.

Pathway analysis

Gene-Set Enrichment Analysis (GSEA[35]) was used to identify predefined gene sets regulated upon co-cultivation. We used two gene set collections from the Molecular Signature Database (Broad Institute [36]), the c2 curated-gene sets, and the c5 GO-gene sets. Among the datasets most significantly enriched in the co-cultures were gene-sets involved in hypoxia, ras-signalling, inflammation, extracellular matrix deposition, angiogenesis, tissue development, wound healing and EMT (Table 1, Supplementary Table 1). The core genes of statistically significant gene-sets were used to calculate PCA plots. A clear-cut segregation of the individual co-culture and the mixed-mono-culture experiments was evident for all gene-sets tested. Examples for activation of ras-oncogenic signaling (Figure 6B) and cell-cell-signaling (Supplementary Figure 7B) are shown.
Pathway analysis (Ingenuity®) revealed similar gene-networks, e.g. linked to cancer, embryonic and tissue development, cell growth and proliferation, cell to cell signaling, immune response, being extensively regulated in tumor/stroma co-cultures (Table 1, Supplementary Table 2). A 35 gene network clustering around NF-kappa B displayed extensive regulation (Figure 6C). 11 genes were regulated by all fibroblast types, expression of 10 genes was changed by the presence of colon fibroblasts, whereas 8 genes were solely altered by CAFs. Expression profiles of selected genes are shown in Figure 7. CEACAM5 encoding the diagnostically relevant carcinoembryogenic antigen (CEA) was most potently induced by colon CAFs, with intermediate induction by normal colon fibroblasts, whereas skin fibroblasts had no effect (Figure 7A, left panel). Elevated CEA protein levels in tumor spheroids co-cultured with CAFs validated the RNA expression data (Figure 7A, right panel). The induction of CXCL8 (IL-8) on the mRNA level upon co-culture with colon-derived fibroblasts (Figure 7B, left) was verified by ELISA in the respective culture supernatants. CXCL8 levels were low in LS174T cultures and were raised by a factor of two to 5-7 ng/ml in the co-cultures with colon-derived fibroblasts. LS174T spheroid/skin fibroblast co-cultures did not show a synergistic upregulation in concordance with the RNA data (Figure 7B, right).

One of the most significantly regulated genes from the NF kappa B network was DMBT1 (deleted in malignant brain tumors 1). DMBT1 was selectively induced by LS174T/CAF co-

culture (Figure 7C, left). Loss of DMBT1 in astrocytomas and in squamous carcinomas is well established and indicates that DMBT1 might be a tumor suppressor. However, in gastrointestinal carcinomas DMBT1 expression is transiently upregulated during tumorigenesis and decreased only in very dedifferentiated cancers [37, 38] and has been shown to be induced upon proinflammatory stimuli via the NF kappa B pathway [39]. Using a large expression database (Affymetrix Exon Chip, BioExpress, GeneLogic) we could demonstrate that DMBT1 mRNA was present in normal colon and lung and absent or very weakly expressed in normal breast, prostate and thyroid gland. DMBT1 expression was significantly reduced in lung carcinomas, whereas colon cancer samples displayed increased DMBT1 levels. In perfect correlation with the literature (see above), DMBT1 levels decreased in metastatic colon cancers. Breast, prostate and thyroid cancers were almost negative for DMBT1 mRNA (Figure 7C, right). The obtained data were confirmed in a different set of database using Affymetrix Plus GeneChip based BioExpress databases (Supplementary Figure 8A). Prominent upregulation of DMBT1 was also observed in stomach-, pancreatic-, esophagus-, and colon mucinous carcinomas when compared to the levels of the respective normal tissue counterparts (Supplementary Figure 8B).

Monitoring tumor growth and apoptosis upon inactivation of the PI3K Pathway in the in vitro assay

First, we determined the growth rate of the tumor spheroids by calculating the size of individual spheroids at different time points (Figure 8A). The mean size of 8-10 spheroids was calculated. The rate in tumor spheroid volume increase was similar whether fibroblasts were present in the cultures or not (Figure 8B). In order to demonstrate the applicability of the system for drug testing we treated the LS174T/fibroblast co-cultures with the PI3K inhibitor LY294002. Tumor cell growth was measured daily as described. In the presence of LY294002 the size of the spheroids increased 1.5 times during the observation period, whereas the untreated controls displayed a fivefold increase (Figure 8C). Fibroblast morphology or cell number did not change upon LY294002 treatment, indicating no or minor effects on the stromal compartment. Staining of sections with activated-caspase-3 antibody revealed 25 % apoptosis in tumor cell spheroids upon PI3K inhibition, whereas control cultures displayed an average apoptotic rate of <10% (Figure 8D). Activation of caspase-3 in the fibroblasts was detectable in 4% of the untreated- and in 3% of the treated cultures, indicating that the low apoptosis rate in fibroblasts was not affected by the inhibitor (Figure 8D). The mitotic index of tumor cells was determined by phospho-Histone H3 staining and

found to be reduced more than threefold upon treatment with LY294002 as compared to controls (Figure 8E). Phospho-H3 positive fibroblasts were not detected, indicating absent or very low mitotic activity. Representative IHC-stainings for those markers are shown in Supplementary Figure 9.

Discussion

There is strong evidence that demonstrates the active role of the tumor stroma in tumorigenesis, however with only few exceptions the molecular mechanisms involved in the paracrine interactions between the tumor and the surrounding stroma remained poorly understood [40]. This was probably due to the limitations of available *in vitro*-models to reflect the heterogeneous (cellular and molecular) composition of human cancers and the cellular complexity of animal models.

Cellular heterogeneity and interaction in a 3D environment is not reproduced by standard tissue culture techniques on 2D surfaces. 3D in vitro models closely mimic features of the in vivo situation and provide unique possibilities to study the behavior of cancer [41]. Organotypic 3D co-culture models have been used to study the functional interplay between tumor cells and fibroblasts [18, 24, 42]. Our "*in vitro carcinoma assay*" aims to further close the gap between conventional *in vitro* assays and the *in vivo* situation, because it innovatively combines spheroid cultures with collagen gel assays and heterotypic cell interactions. In a reductionist approach the *in vivo* cellular complexity was reduced to two cell types: the tumor cells and stromal fibroblasts, in order to get clear information about the specific molecular interactions of these cells during their growth in vitro. Additionally, we introduce other important features of the *in vivo* growth, the three-dimensionality achieved by using spheroids 3D cultures and by embedding the cellular components into a collagen I rich ECM matrix. The system is modular and offers the possibility to compare results from single component cultures with the co-cultures, thus allowing molecular screens to identify pathways, which are not active in mono-cultures but induced upon co-cultivation. In addition, it is possible to exchange the modules in the co-cultivation experiments or to even extend the cellular components in the co-cultivation screens to three or four cellular components (e.g. to add tumor associated macrophages or endothelial cells).

In summary, we provide evidence that our model: i) Mimics the cellular architecture of human cancer tissues both histologically and phenotypically. ii) The invasive potential of colon cancer cells is induced in the co-culture system. LS174T cells displayed invasive behavior with features of collective cell migration as frequently seen in human carcinomas [43], when in contact with stromal fibroblasts (Figure 5). Fibroblast-led cancer cell invasion was recently shown to operate in invasive HNSQCC [24]. iii) Molecular profiling of mono and co-cultures can be used to characterize known and to identify novel pathways in tumor-stroma interaction. iv) The potential to study the role of drug targets was demonstrated. Additional

advantages for therapeutic studies can be envisioned. It has been shown that cancer cells grown as spheroids display multicellular resistance (MCR), which make them less susceptible to different therapies [44]. Cancer cells in patients often display the same MCR, therefore the impact of MCR can be closely investigated pre-clinically in this model. The effect of stromal cells on tumor cells upon chemo- and radiotherapy can be addressed. Recent reports demonstrated decreased sensitivity of tumor cells to therapy when co-cultured with activated stromal fibroblasts [45, 46] and finally the effects of novel agents targeting the tumor stroma can be investigated in detail.

The molecular analysis of the tumor-stroma interaction has revealed that the well-defined paracrine HGF/c-Met crosstalk and the activation of the Wnt pathway were recapitulated in our model. Comparison of the gene expression profiling in monocultures versus co-cultures revealed a number of pathways, which were selectively activated upon co-cultivation of tumor cells with CAFs. For example, the Ras signalling pathway or the NF-kappa B signaling pathway was altered upon co-cultivation with colon-derived fibroblasts (33 out of 36 genes regulated in the NF-kappa B network). The activation of NF-kappa B is associated with inflammation associated colon carcinoma and tumor progression [47]. We provide first evidence for NF-kappa B activation by interaction of tumor cells with stromal fibroblasts. The NF-kappa B target CXCL8 was specifically induced in co-cultures and may promote tumor growth, neutrophil activation, invasion and tumor angiogenesis as proposed [48-50]. Since only human cells are used in the system, concerns about species specificity of cytokines and growth factors and their respective receptors (as it is the case in xenograft mouse models) can be neglected. At the moment– due to the technical setup of the screening procedure - we were not able to distinguish in which compartment certain pathways are regulated. A protocol to separate fibroblasts from tumor cells in the assay is currently under development (Dolznig, data not shown). Another NF-kappa regulated gene, DMBT1, plays a not well-defined role in carcinogenesis. DMBT1 functions as a tumor suppressor in many squamous epithelial cancers and in brain tumors, the role of DMBT1 in gastrointestinal cancers is less clear [38, 39, 51]. DMBT1 was selectively induced by co-culture of cancer cells with CAFs and is upregulated in gastrointestinal cancers, whereas it seems to be non-relevant for prostate, breast and thyroid cancer development. The increase in DMBT1 expression in primary colon cancers and its downregulation in metastatic colon carcinomas points to an early role in tumorigenesis as already discussed in the literature. Taken together the involvement of many genes of the identified NF kappa B network in cancer makes this tumor-stroma interaction induced pathway highly relevant for colon cancer development.

Both, Ras signalling and NF-kappa B activity are essential for epithelial mesenchymal transition (EMT). The EMT specific gene set was specifically enriched in the co-cultivation experiments, suggesting that epithelial-fibroblast interaction in colon carcinomas induces EMT by parallel activation of the ras pathway and the inflammatory NF-kappa B response [52], which can easily be addressed in the system in the future.

Moreover, we could demonstrate that many gene sets (including ECM remodeling, EMT), which were regulated exclusively upon co-cultivation of LS174T tumor cells with CAFs, were also activated in an ex vivo screen, in which laser-capture-microdissected tumor stroma was compared to normal stroma from colon cancer patient samples ([53] and Rupp et al, manuscript in preparation). The complementarities of the two approaches emphasized the relevance of the 3D co-culture model to dissect and to identify specific pathways involved in tumorigenesis.

Novel molecular targets can be validated by genetically modifying the tumor cell compartment or the stromal cells in the system [54] and the functional relevance demonstrated in *in vivo* animal models. The possibility to compare the in vitro data with the data obtained from human material, linked to the fact that it is robust and highly versatile should allow the use of our model as an accurate tool for target identification/validation with the potential to reduce animal experiments during drug discovery.

Methods

Conventional methods on cell culture, immunohistochemistry, histochemistry, RNA isolation, real time PCR, Affymetrix GeneChip hybridisation and normalisation, GSEA, Western blotting, phospho-tyrosine kinase and cytokine arrays, and transmission electron microscopy are described in Supplementary Information.

Spheroid formation

Multicellular spheroids were generated essentially as published for endothelial cell spheroids [55]. In brief, tumor cells were grown on plastic, trypsinised, counted and resuspended in DMEM/5% serum containing 12mg/ml methylcellulose (Sigma, #0512). The cells were seeded into non-adhesive u-shaped 96-well-plates for suspension culture (Greiner, #650185) at a concentration of 150-200 cells per well. Compact multicellular spheroids were harvested after 2-3 days, washed and 96 tumor cell spheres each were transferred into 1.5 ml microcentrifuge tubes. Fibroblasts for co-culture experiments were cultivated on plastic in serum free fibroblast growth medium (FGM, Promocell). After trypsinisation, cells were counted; $2x10^5$ cells were transferred into 1.5 ml tubes and centrifuged at 250 g. In case of co-culture experiments the cells were centrifuged onto the previously prepared spheroid pellets. The entire supernatant was carefully removed and the cells / cell-spheroid pellets were kept on ice until further use.

Collagen gel culture

Gel casting devices were produced by cutting out 2 x 2 cm squares of a silicone foil (Gel dryer sealing gasket, Biorad, 1 mm thickness, #1651748) into which holes of 1.4 cm diameter were cut with a puncher. Nylon filters were prepared from the nylon mesh inserts of Medicon syringe filters (BD, 100 µm, #340612), of which a hole of 1 cm diameter was cut out in the centre. The silicone casting devices and the nylon meshes were autoclaved and placed onto the inside surface of lids of 10 cm cell culture dishes, where they firmly attached.

For the collagen gel preparation all steps were performed on ice. Collagen solutions were prepared by mixing 0,2 ml of 10x PBS, 0,8 ml of FGM/20% Methylcellulose, 1 ml of Collagen I (rat, BD, 3.48mg/ml, #354236) and neutralized with 23 µl of 1M NaOH. The solution was mixed carefully; air bubbles were removed by centrifugation at 300g for 2 min. 200 µl each of the collagen solution was transferred into the tubes containing the spheroid/cell pellets, which were gently resuspended. The spheroid/cell suspensions were transferred into

the casting devices; a nylon filter was added and submerged. After polymerisation of the collagen solution for 30 min at 37°C/5% CO_2 the silicone foil was removed, leaving collagen gel cylinders. The gels were transferred into 24 well plates containing 1 ml of FGM supplemented with 2.5% serum. The culture medium was replaced every second day and conditioned medium was kept, sterile-filtered and snap-frozen in liquid nitrogen. Celltracker Green CMFDA (Molecular Probes, Invitrogen, CatNr. C2925) was used for long term tracing of fibroblasts for live cell imaging as recommended by the supplier. The growth rate of the tumor spheroids was determined by calculating the mean volume of 8-10 spheroids, using the formula (length x width^2 x $\pi/6$) as used to determine the size of subcutaneous xenograft tumors in mice [56, 57].

The TissueQuest^{TM} software (TissueGnostics GmbH, Vienna) was used to quantify fluorescent photomicrographs. Cell detection is based on identification of nuclei by DAPI staining. Fluorescence intensity quantification was done independently in different channels. All photomicrographs were taken with the same settings (exposure time, signal amplification, objectives).

Acknowledgements

This work was supported by Boehringer Ingelheim RCV GmbH & Co KG and the Herzfelder Family Foundation (HD). We are grateful to Peter Steinlein and Pavel Pasierbek for help with confocal imaging, Markus Hengstschläger, Norbert Kraut and Günther Adolf for critically reading the manuscript and helpful discussions.

References

1. Jemal, A. et al. Cancer statistics, 2007. *CA Cancer J Clin* **57**, 43-66 (2007).
2. Bhowmick, N.A., Neilson, E.G. & Moses, H.L. Stromal fibroblasts in cancer initiation and progression. *Nature* **432**, 332-337 (2004).
3. Bissell, M.J. & Radisky, D. Putting tumours in context. *Nat Rev Cancer* **1**, 46-54 (2001).
4. Mueller, M.M. & Fusenig, N.E. Friends or foes - bipolar effects of the tumour stroma in cancer. *Nat Rev Cancer* **4**, 839-849 (2004).
5. Folkman, J. & Hanahan, D. Switch to the angiogenic phenotype during tumorigenesis. *Princess Takamatsu Symp* **22**, 339-347 (1991).
6. Olumi, A.F. et al. Carcinoma-associated fibroblasts direct tumor progression of initiated human prostatic epithelium. *Cancer Res* **59**, 5002-5011 (1999).
7. Orimo, A. & Weinberg, R.A. Stromal fibroblasts in cancer: a novel tumor-promoting cell type. *Cell Cycle* **5**, 1597-1601 (2006).

8. Yauch, R.L. et al. A paracrine requirement for hedgehog signalling in cancer. *Nature* **455**, 406-410 (2008).
9. Vermeulen, L. et al. Wnt activity defines colon cancer stem cells and is regulated by the microenvironment. *Nat Cell Biol* **12**, 468-476 (2010).
10. Bodnar, A.G. et al. Extension of life-span by introduction of telomerase into normal human cells. *Science* **279**, 349-352 (1998).
11. Hahn, W.C. et al. Creation of human tumour cells with defined genetic elements. *Nature* **400**, 464-468 (1999).
12. Iyer, V.R. et al. The transcriptional program in the response of human fibroblasts to serum. *Science* **283**, 83-87 (1999).
13. Bell, E., Ehrlich, H.P., Buttle, D.J. & Nakatsuji, T. Living tissue formed in vitro and accepted as skin-equivalent tissue of full thickness. *Science* **211**, 1052-1054 (1981).
14. Runswick, S.K., O'Hare, M.J., Jones, L., Streuli, C.H. & Garrod, D.R. Desmosomal adhesion regulates epithelial morphogenesis and cell positioning. *Nat Cell Biol* **3**, 823-830 (2001).
15. Gudjonsson, T. et al. Normal and tumor-derived myoepithelial cells differ in their ability to interact with luminal breast epithelial cells for polarity and basement membrane deposition. *J Cell Sci* **115**, 39-50 (2002).
16. Kunz-Schughart, L.A., Heyder, P., Schroeder, J. & Knuechel, R. A heterologous 3-D coculture model of breast tumor cells and fibroblasts to study tumor-associated fibroblast differentiation. *Exp Cell Res* **266**, 74-86 (2001).
17. Fischbach, C. et al. Engineering tumors with 3D scaffolds. *Nat Methods* **4**, 855-860 (2007).
18. Okawa, T. et al. The functional interplay between EGFR overexpression, hTERT activation, and p53 mutation in esophageal epithelial cells with activation of stromal fibroblasts induces tumor development, invasion, and differentiation. *Genes Dev* **21**, 2788-2803 (2007).
19. Takagi, A. et al. Three-dimensional cellular spheroid formation provides human prostate tumor cells with tissue-like features. *Anticancer Res* **27**, 45-53 (2007).
20. Wolf, K. et al. Multi-step pericellular proteolysis controls the transition from individual to collective cancer cell invasion. *Nat Cell Biol* **9**, 893-904 (2007).
21. Pickl, M. & Ries, C.H. Comparison of 3D and 2D tumor models reveals enhanced HER2 activation in 3D associated with an increased response to trastuzumab. *Oncogene* **28**, 461-468 (2009).
22. Kunz-Schughart, L.A. & Knuechel, R. Tumor-associated fibroblasts (part I): Active stromal participants in tumor development and progression? *Histol Histopathol* **17**, 599-621 (2002).
23. Schmeichel, K.L. & Bissell, M.J. Modeling tissue-specific signaling and organ function in three dimensions. *J Cell Sci* **116**, 2377-2388 (2003).
24. Gaggioli, C. et al. Fibroblast-led collective invasion of carcinoma cells with differing roles for RhoGTPases in leading and following cells. *Nat Cell Biol* **9**, 1392-1400 (2007).
25. Elsdale, T. & Bard, J. Collagen substrata for studies on cell behavior. *J Cell Biol* **54**, 626-637 (1972).
26. Rettig, W.J. et al. Regulation and heteromeric structure of the fibroblast activation protein in normal and transformed cells of mesenchymal and neuroectodermal origin. *Cancer Res* **53**, 3327-3335 (1993).
27. Knudsen, E.S. & Wang, J.Y. Dual mechanisms for the inhibition of E2F binding to RB by cyclin-dependent kinase-mediated RB phosphorylation. *Mol Cell Biol* **17**, 5771-5783 (1997).

28. Yamamoto, H. et al. Paradoxical increase in retinoblastoma protein in colorectal carcinomas may protect cells from apoptosis. *Clin Cancer Res* **5**, 1805-1815 (1999).
29. Sutherland, R.M. et al. Oxygenation and differentiation in multicellular spheroids of human colon carcinoma. *Cancer Res* **46**, 5320-5329 (1986).
30. Hlatky, L., Hahnfeldt, P. & Folkman, J. Clinical application of antiangiogenic therapy: microvessel density, what it does and doesn't tell us. *J Natl Cancer Inst* **94**, 883-893 (2002).
31. De Wever, O. et al. Tenascin-C and SF/HGF produced by myofibroblasts in vitro provide convergent pro-invasive signals to human colon cancer cells through RhoA and Rac. *Faseb J* **18**, 1016-1018 (2004).
32. Kammula, U.S. et al. Molecular co-expression of the c-Met oncogene and hepatocyte growth factor in primary colon cancer predicts tumor stage and clinical outcome. *Cancer Lett* **248**, 219-228 (2007).
33. Peschard, P. & Park, M. From Tpr-Met to Met, tumorigenesis and tubes. *Oncogene* **26**, 1276-1285 (2007).
34. Kataoka, H., Hamasuna, R., Itoh, H., Kitamura, N. & Koono, M. Activation of hepatocyte growth factor/scatter factor in colorectal carcinoma. *Cancer Res* **60**, 6148-6159 (2000).
35. Mootha, V.K. et al. PGC-1alpha-responsive genes involved in oxidative phosphorylation are coordinately downregulated in human diabetes. *Nat Genet* **34**, 267-273 (2003).
36. Subramanian, A. et al. Gene set enrichment analysis: a knowledge-based approach for interpreting genome-wide expression profiles. *Proc Natl Acad Sci U S A* **102**, 15545-15550 (2005).
37. Mollenhauer, J. et al. Deleted in Malignant Brain Tumors 1 is a versatile mucin-like molecule likely to play a differential role in digestive tract cancer. *Cancer Res* **61**, 8880-8886 (2001).
38. Conde, A.R. et al. DMBT1 is frequently downregulated in well-differentiated gastric carcinoma but more frequently upregulated across various gastric cancer types. *Int J Oncol* **30**, 1441-1446 (2007).
39. Rosenstiel, P. et al. Regulation of DMBT1 via NOD2 and TLR4 in intestinal epithelial cells modulates bacterial recognition and invasion. *J Immunol* **178**, 8203-8211 (2007).
40. Witz, I.P. Yin-yang activities and vicious cycles in the tumor microenvironment. *Cancer Res* **68**, 9-13 (2008).
41. Yamada, K.M. & Cukierman, E. Modeling tissue morphogenesis and cancer in 3D. *Cell* **130**, 601-610 (2007).
42. Froeling, F.E. et al. Organotypic culture model of pancreatic cancer demonstrates that stromal cells modulate E-cadherin, beta-catenin, and Ezrin expression in tumor cells. *Am J Pathol* **175**, 636-648 (2009).
43. Friedl, P. & Gilmour, D. Collective cell migration in morphogenesis, regeneration and cancer. *Nat Rev Mol Cell Biol* **10**, 445-457 (2009).
44. Desoize, B. & Jardillier, J. Multicellular resistance: a paradigm for clinical resistance? *Crit Rev Oncol Hematol* **36**, 193-207 (2000).
45. Muerkoster, S. et al. Tumor stroma interactions induce chemoresistance in pancreatic ductal carcinoma cells involving increased secretion and paracrine effects of nitric oxide and interleukin-1beta. *Cancer Res* **64**, 1331-1337 (2004).
46. Shekhar, M.P., Santner, S., Carolin, K.A. & Tait, L. Direct involvement of breast tumor fibroblasts in the modulation of tamoxifen sensitivity. *Am J Pathol* **170**, 1546-1560 (2007).
47. Karin, M. Nuclear factor-kappaB in cancer development and progression. *Nature* **441**, 431-436 (2006).

48. Matsuo, Y. et al. CXCL8/IL-8 and CXCL12/SDF-1alpha co-operatively promote invasiveness and angiogenesis in pancreatic cancer. *Int J Cancer* **124**, 853-861 (2009).
49. Martin, D., Galisteo, R. & Gutkind, J.S. CXCL8/IL8 stimulates vascular endothelial growth factor (VEGF) expression and the autocrine activation of VEGFR2 in endothelial cells by activating NFkappaB through the CBM (Carma3/Bcl10/Malt1) complex. *J Biol Chem* **284**, 6038-6042 (2009).
50. Huang, S. et al. Fully humanized neutralizing antibodies to interleukin-8 (ABX-IL8) inhibit angiogenesis, tumor growth, and metastasis of human melanoma. *Am J Pathol* **161**, 125-134 (2002).
51. Mollenhauer, J. et al. An integrative model on the role of DMBT1 in epithelial cancer. *Cancer Detect Prev* **26**, 266-274 (2002).
52. Huber, M.A. et al. NF-kappaB is essential for epithelial-mesenchymal transition and metastasis in a model of breast cancer progression. *J Clin Invest* **114**, 569-581 (2004).
53. Rupp, C. et al. Laser capture microdissection of epithelial cancers guided by antibodies against fibroblast activation protein and endosialin. *Diagn Mol Pathol* **15**, 35-42 (2006).
54. Rosner, M. et al. Efficient siRNA-mediated prolonged gene silencing in human amniotic fluid stem cells. *Nat Protoc* **5**, 1081-1095 (2010).
55. Korff, T. & Augustin, H.G. Integration of endothelial cells in multicellular spheroids prevents apoptosis and induces differentiation. *J Cell Biol* **143**, 1341-1352 (1998).
56. Tomayko, M.M. & Reynolds, C.P. Determination of subcutaneous tumor size in athymic (nude) mice. *Cancer Chemother Pharmacol* **24**, 148-154 (1989).
57. Euhus, D.M., Hudd, C., LaRegina, M.C. & Johnson, F.E. Tumor measurement in the nude mouse. *J Surg Oncol* **31**, 229-234 (1986).

Figure legends

Figure 1

Experimental setup. **(A)** Examples of cancer cell line spheroids embedded in collagen gels. HCT116 cells were non-invasive, whereas SK-OV-3 cells formed invasive structures within 24 hrs of cultivation. Caco-2 cells did not form spheroids. **(B)** Scheme of workflow. Spheroid formation was induced by seeding tumor cells in round-bottom shaped 96 well plates. After 2-3 days tumor spheroids were harvested and resuspended in collagen I solution in the presence or absence of $2x10^5$ normal colon fibroblasts. The suspension was transferred into a silicone casting mould and a ring-shaped nylon mesh was submerged. After collagen gel polymerisation, the mould was removed and the collagen gel was transferred into a 24 well plate and incubated with growth medium. **(C)** Contractile force created by fibroblasts shrunk collagen gels within three days. The embedded nylon mesh averted shrinking of the collagen gel. Dashed white circles highlight the outline of the gels (top). The contraction of the collagen gel hindered light microscopic morphological examination in non-supported gels at day two. Embedded tumor spheroids (TS, arrowheads) could hardly be distinguished from the

surrounding fibroblasts and ECM, whereas cells in nylon mesh reinforced collagen gels could be easily evaluated. The nylon mesh is visible as dark netlike structure (scale bar: 200 μm).

Figure 2

Microscopic evaluation of the tumor cell spheroids. **A** Co-culture of LS174T spheroids with colon fibroblasts (LS174T+NCF) in collagen gels induced morphological changes in the tumor cell aggregates as compared to tumor spheroids cultured under the same conditions alone (insert: LS174T). At 2 days of co-cultivation hollow structures were clearly visible within the tumor spheroid (arrowheads, size bar: 200 μm). **B** H&E staining of collagen gel sections revealed more frequent and bigger acinous structures (white areas inside the spheroids) in LS174T spheroids co-cultured with fibroblasts (LS174T+NCF). Glandular structures were filled with mucus as determined by PAS staining (magenta areas) and displayed full polarisation (ZO-1 staining in green, beta-catenin in red, blue: DAPI). **C** Transmission electron microscopy (EM) revealed that well-developed gland like structures with microvilli at their luminal side (L) were present in LS174T spheroids as well as in tumor spheroid/fibroblast co-cultures (LS174T + FB, top). Nuclei of tumor cells are labeled (N). Scale bars: 500 nm. **D** Junctional complexes containing desmosomes (D), tight junctions (T), and adherens junctions (A) were formed between LS174T tumor cells in the presence of fibroblasts (bottom), whereas LS174T spheroids alone displayed more rudimentary desmosomal structures (top). Interdigitations (I) and microvilli (MV) were present on LS174T cells under both conditions (scale bars: 200 nm).

Figure 3

Tumor cell spheroid-fibroblast interaction. **A** Confocal imaging of *in gel* immuno–fluorescence staining. The left panel shows a superimposed 28 micrometer z-stack (vimentin in red, E-cadherin in green). Middle panel: PDGFRbeta positive normal colon fibroblasts (green) make close contacts to LS174T spheroids. The border of the spheroid is outlined (white dashed line). Right panel: Single plane confocal image of vimentin positive fibroblasts (red), which surrounded E-cadherin positive tumor spheroids (green). Nuclei were stained with DAPI (blue), (scale bar: 50 μm). **B** Epithelial cells developed tight cell-cell contact with fibroblasts (F, encircled by dotted line) at the invasive structures (black arrowheads in insert, bottom) as revealed by EM. The inset is a higher magnification of the area indicated by the white lined rectangle. The orientation of the inset is indicated by a white triangle. Nuclei of tumor cells are labelled (N). Scale bars: 500 nm. **C** Fibroblast activation protein alpha (FAP)

stained the fibroblasts in the co-cultures (top) strikingly similar to activated fibroblasts in a human colon adenocarcinoma (bottom, scale bars: 200 μm). H&E stains of LS174T spheroids plus NCFs in collagen gels after three days of culture display close cell-cell interaction and tumor cell heterogeneity. In the presence of NCFs condensed and restructured collagen fibres were present and fibroblasts were nestled around tumor epithelial cell islands in similar density and morphology as compared to a representative human colon carcinoma specimen (scale bars: 50 μm).

Figure 4

Molecular pathway analysis. **A** Phosphorylated retinoblastoma protein (pRb, green), was predominantly found in tumor cell nuclei, whereas vimentin positive fibroblasts (red) were rarely positive for pRb. Nuclei were stained with DAPI (blue), (scale bars: 20 μm). Western blots of collagenase B released cells confirmed the pRb status from the immunofluorescence analysis (right). **B** LS174T cells were starved for six hours and subsequently treated either with conditioned media from LS174T spheroid collagen cultures (LS-CM), fibroblast collagen gel cultures (NCF-CM) or LS174T/fibroblast co-cultures (LS/NCF-CM) for 15 min. Further starvation (starved) and treatment with fresh culture medium (medium) served as controls. After lysing the cells phospho receptor tyrosine kinase (pTyr) arrays demonstrated c-Met phosphorylation in LS174T cells, when treated with conditioned medium from LS174T-fibroblast co-cultures (LS/NCF-CM). c-Met was phosphorylated neither upon tumor cells nor in fibroblasts, when individually cultured in collagen gels (left, top). Cytokine arrays (left, bottom) revealed the presence of HGF in both tumor cell/fibroblast co-cultures as well as in fibroblast mono-cultures. Quantitative evaluation of the phospho-c-Met and HGF levels by chemiluminiscent imaging are shown in the right panel. **C** Distribution of beta-catenin protein (red) in LS174T cells grown in spheroids for 5 days either alone (LS) or as LS174T-CAF co-cultures (LS+CAF). The percentage of nuclear beta-catenin positive cells was determined using quantitative image analysis (scattergrams). Cell nuclei were staine with DAPI (blue). The numbers of cells analyzed (n) are indicated.

Figure 5

Invasion into the ECM. **A** Spheroids were made from LS174T cells expressing dsRed and cultivated in collagen gels for 11 days in the absence (LS174T-dsR) or presence of cancer associated fibroblasts (LS174T-dsR+CAF1). Photomicrographs depict an overlay of dsRed fluorescence with phase contrast microscopy. In the presence of fibroblasts tumor cells

invaded into the collagen gel as single cells (white arrows) and cell clusters (black arrows), whereas without fibroblasts the tumor spheroids remained with a perfectly distinct border and showed no sign of invasion (scale bars: 100 μm). **B** Confocal imaging revealed collective invasion of LS174T (CK18 positive, red) into collagen gel areas with high fibroblast density (PDGFRß positive, green). Control cultures without fibroblasts did not invade (left panel). Nuclei were stained with DAPI (blue), (scale bars: 50 μm).

Figure 6

Profiling experiments and pathway analysis. **A** 96 tumor cell spheroids (of defined cell numbers) and $2x10^5$ fibroblasts were cultured for 3.5 days in collagen gels either as co-cultures or as individual cultures. The whole lysates from LS174T mono-cultures were mixed with fibroblast mono-culture lysates (mix), thereby ensuring the same amount of tumor and fibroblast components present as in the co-culture experiments. Skin fibroblasts (BJ-1, SF), normal embryonic colon fibroblasts (CCD18-Co, NCF) and colon cancer associated fibroblasts (12051CAF, 13388CAF; CAF1 and CAF2 respectively) were used. All experiments were done in biological triplicates. RNA extracted from the mixed as well as from the co-culture experiments was processed for Affymetrix GeneChip analysis (see also Supplementary Figure 11). A Sammon's blot is shown. **B** From GSEA the core genes of statistically significant gene-sets were used to calculate PCA plots. A clear-cut segregation of the co-culture and the mixed-mono-culture experiments can be made (dotted line). Activation of ras-oncogenic-signalling detected in the c2 curated gene sets is shown. **C** A 35 gene network clustering around NF-kappa B revealed by Pathway analysis (Ingenuity®). In this network regulation (up: red, down: green) by distinct fibroblast origins is indicated. Dashed blue circles indicate gene expression changed by the presence of colon fibroblasts; genes altered by CAFs are boxed by dashed orange squares. Genes regulated by the presence of any fibroblast type are not encircled.

Figure 7

Selected genes induced by the co-cultivation of LS175T cells with stromal fibroblasts. **A** Left: Whisker-box plots displaying the expression profile of CEACAM5 (yellow: mixed individual cultures, blue: co-cultures). Right: Confocal images and quantification of CEA immunofluorescence staining (green) of LS174T spheroids alone and LS174T spheroids co-cultured with 13388CAFs (CAF2). Nuclei are counterstained with DAPI (blue). Determination of the mean pixel intensity/spheroid revealed a twofold increase in CEA

protein expression upon co-culture. Error bars are S.D. from four different spheroids. **B** The expression profile of CXCL8 (IL-8, left) was validated by determining CXCL8 levels in conditioned medium of mono- and co-cultures (right). Error bars: S.D. of three measurements. **C** DMBT1 expression was selectively induced by the co-culture with CAFs (left). DMBT1 displayed a unique expression pattern in normal tissues versus major tumor types as determined by the GeneExpress database (GeneLogic). The bold centre-line indicates the median; the box represents the interquartile range (IQR). Whiskers extend to 1.5 times the IQR. Outliers are depicted as black circles.

Figure 8

Reduced tumor growth by inhibition of the PI3K pathway. **A** LS174T spheroids were cultured individually or together with fibroblasts in collagen gels and photographed daily. The top panel shows photomicrographs of a time-lapse experiment. **B** The increase in the mean volume of six spheroids is shown graphically (error bars: S.D.) and can be defined to be equal to tumor growth. **C** LS174T spheroids were cultured in fibroblast containing collagen gels for three days and subsequently treated with 5µM of the PI3K inhibitor LY294002 for another four days. Untreated control cultures are shown for comparison. The bars indicate the mean volume of eight individual spheroids followed for four days under each condition. Error bars are S.D. Treated versus untreated cultures at day 7 are depicted in micrographs above the diagram. **D** Sections of LY294002 treated and untreated cultures from (a) were stained with anti-cleaved-caspase 3. The percentage of positive tumor cells and fibroblasts were determined based on total cell number (present nuclei) and were graphically displayed (total number of nuclei: n=494 in control cultures, n=335 in LY294002 treated gels, error bars are S.D. of 10 microscopic fields). **E** Sections as in D were stained with anti phospho-Histone H3. The mitotic indices were determined by counting phospho-H3 positive tumor cells from different sections. (control, n=454, +LY, n=397).

NAME	SIZE	FDR q-val	DESCRIPTION	PUBLICATION
MENSE_HYPOXIA_UP	107	0,000	**Hypoxi**a-induced genes in Astrocytes and HeLa Cells	Mense et al., Physiol Genomics. 2006 May 16;25(3):435-49.
RAS_ONCOGENIC_SIGNATURE	265	0,000	Genes induced by **activated H-Ras oncogene** in HMEC cells	Bild et al., Nature. 2006 Jan 19;439(7074):353-7
CHEN_HOXA5_TARGETS_UP	229	0,000	Genes induced by **HOXA5** in Hs578T breast cancer cells	Chen et al., J Biol Chem. 2005 May 13;280(19):19373-80.
HINATA_NFKB_UP	106	0,000	Genes upregulated by **NF-kappa B** in keratinocytes and fibroblasts	Hinta et al., Oncogene. 2003 Apr 3;22(13):1955-64.
MANALO_HYPOXIA_UP	94	0,000	Genes upregulated in pulmonary endothelial cells under **hypoxia** or expressing constitutively active HIF-1alpha.	Manalo er al., Blood. 2005 Jan 15;105(2):659-69.
LEE_DENA_UP	59	0,000	Genes upregulated in **hepatoma** induced by diethylnitrosamine	Lee et al., Nat Genet. 2004 Dec;36(12):1306-11.
EMT_UP	61	0,000	Genes upregulated during the **TGFbeta-induced EMT** of Ras-transformed mouse mammary epithelial (EpH4) cells	Jechlinger et al., Oncogene. 2003 Oct 16;22(46):7155-69
CARIES_PULP_UP	205	0,000	Genes upregulated in **pulpal tissue from extracted carious teeth**, compared to healthy teeth tissues	McLachlan et al., Biochim Biophys Acta. 2005 Sep 25;1741(3):271-81.
HYPOXIA_REVIEW	81	0,000	Genes known to be induced by **hypoxia**	Harris, Nat Rev Cancer. 2002 Jan;2(1):38-47.
GERY_CEBP_TARGETS	111	0,000	Genes upregulated by inducible **C/EBPs** in NIH3T3 fibroblasts	Gery et al., Blood. 2005 Oct 15;106(8):2827-36
DORSEY_DOXYCYCLINE_UP	29	0,000	Genes upregulated by Dox inducible **Gab2 (Erk2/Elk1 pathway)** in K562 cells	Dorsey et al., Blood. 2002 Feb 15;99(4):1388-97.
HYPOXIA_FIBRO_UP	20	0,004	Genes upregulated by **hypoxia in normal fibroblasts** from young and old donors	Kim et al., Mech Ageing Dev. 2003 Aug-Sep;124(8-9):941-9.
LEE_CIP_UP	60	0,004	Genes upregulated in **hepatoma** induced by ciprofibrate	Lee et al., Nat Genet. 2004 Dec;36(12):1306-11.
IRS_KO_ADIP_UP	28	0,006	Genes up-regulated in **preadipocytes** with **defects in adipocyte differentiation** (Irs4 KO, Irs2 KO, Irs3 KO, Irs1 KO)	Tseng et al., Nat Cell Biol. 2005 Jun;7(6):601-11.

Table 1
List of the most significantly enriched pathways sorted by the Normalized Enrichment Score

(NES) using the c2 curated gene sets of genes upregulated in LS174T / colon fibroblast co-

cultures. Size indicates the number of genes in the gene set. FDR q-val indicates the false discovery rate.

Figures

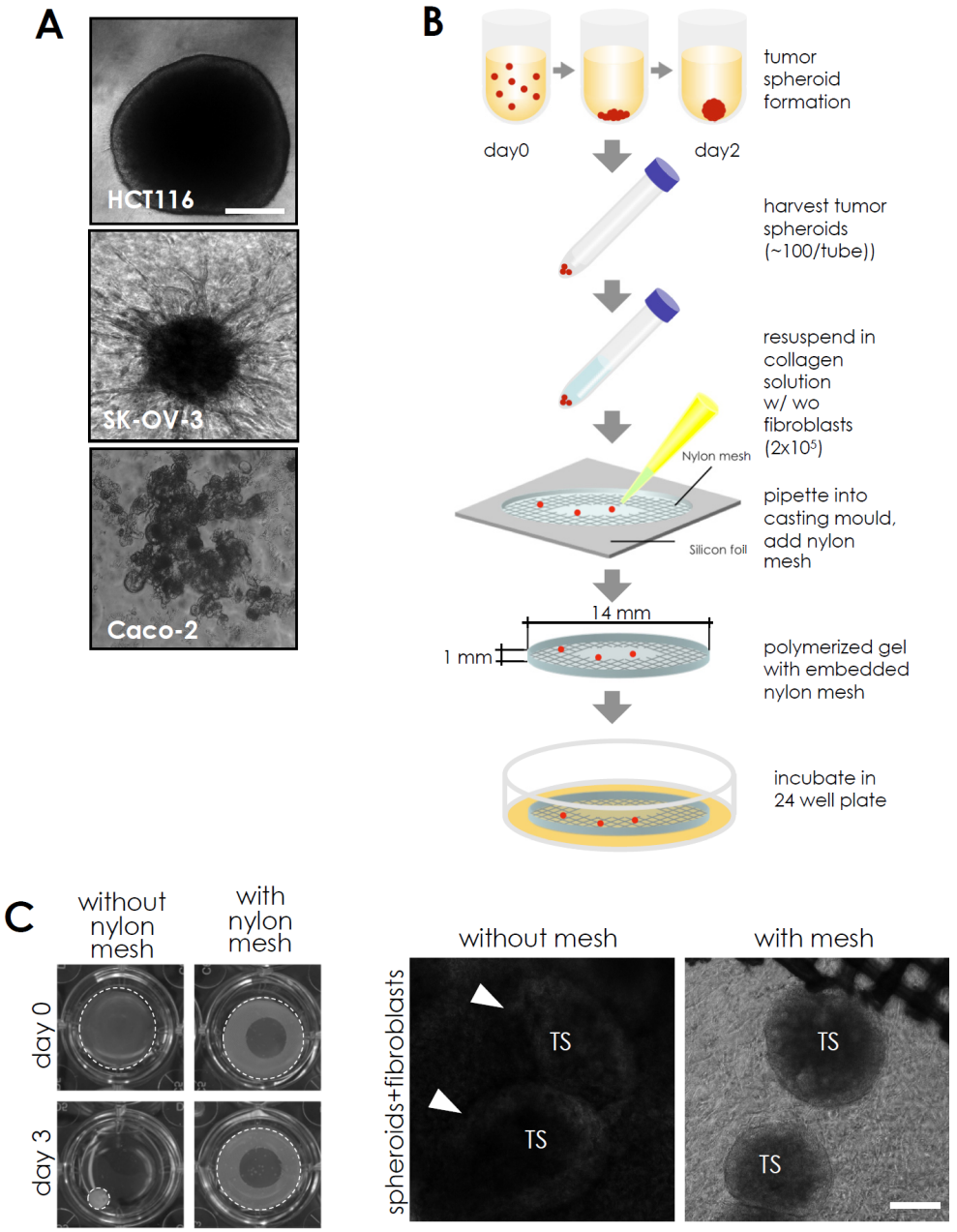

Figure 1

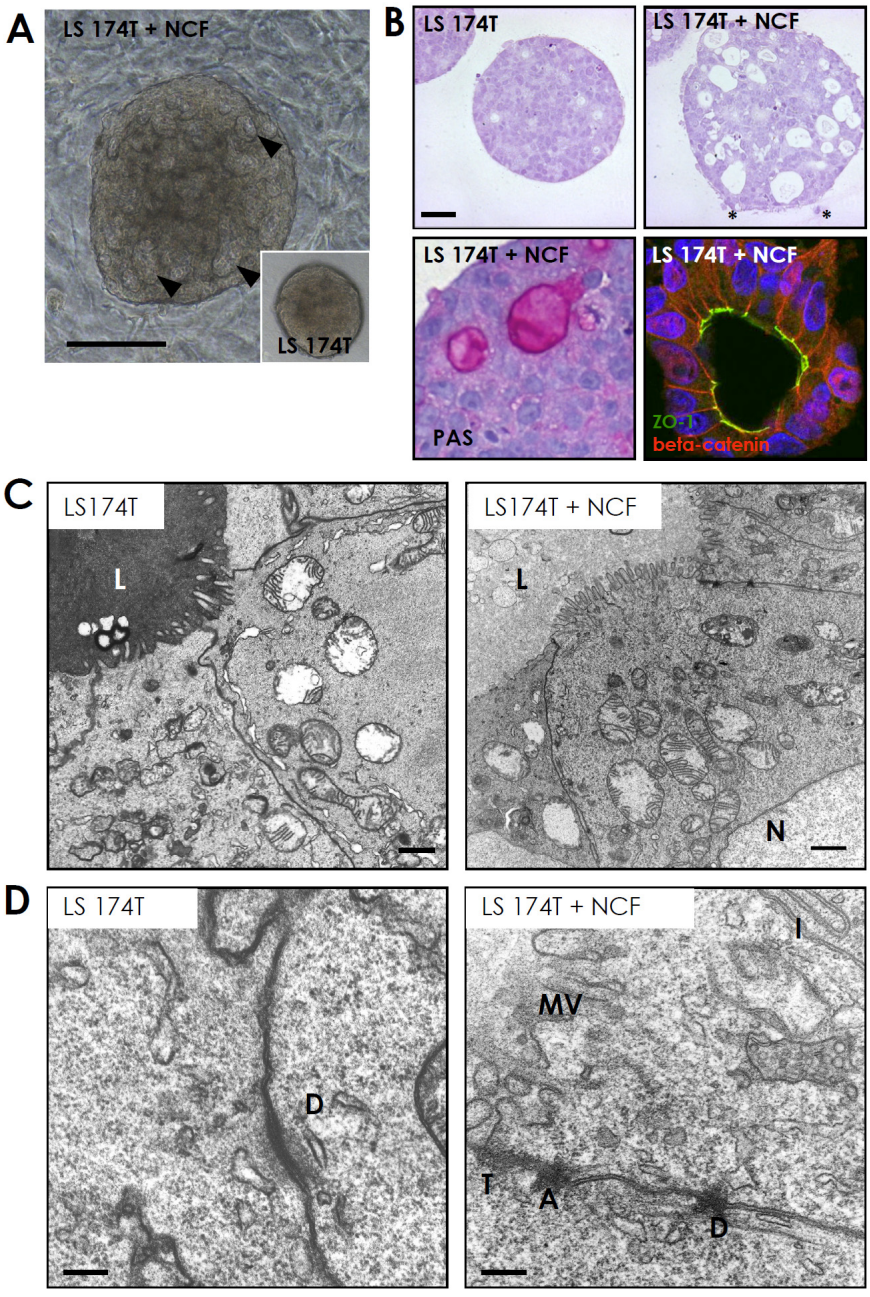
A
LS 174T + NCF
LS 174T
B
LS 174T
LS 174T + NCF
LS 174T + NCF
PAS
LS 174T + NCF
ZO-1
beta-catenin
C
LS174T
L
LS174T + NCF
L
N
D
LS 174T
D
LS 174T + NCF
I
MV
T
A
D

Figure 2

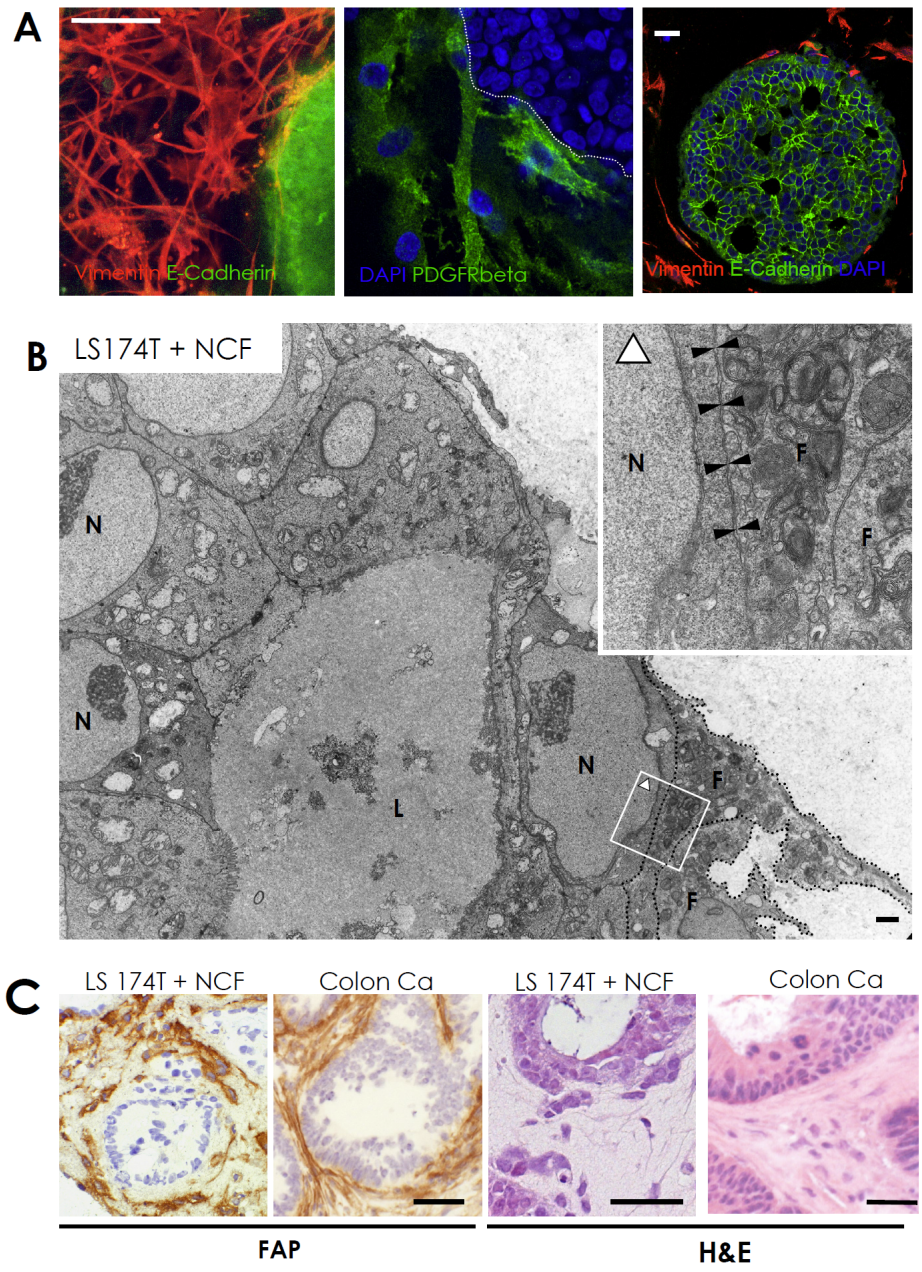
A
Vimentin E-Cadherin
DAPI PDGFRbeta
Vimentin E-Cadherin DAPI
B
LS174T + NCF
N
F
L
C
LS 174T + NCF
Colon Ca
LS 174T + NCF
Colon Ca
FAP
H&E

Figure 3

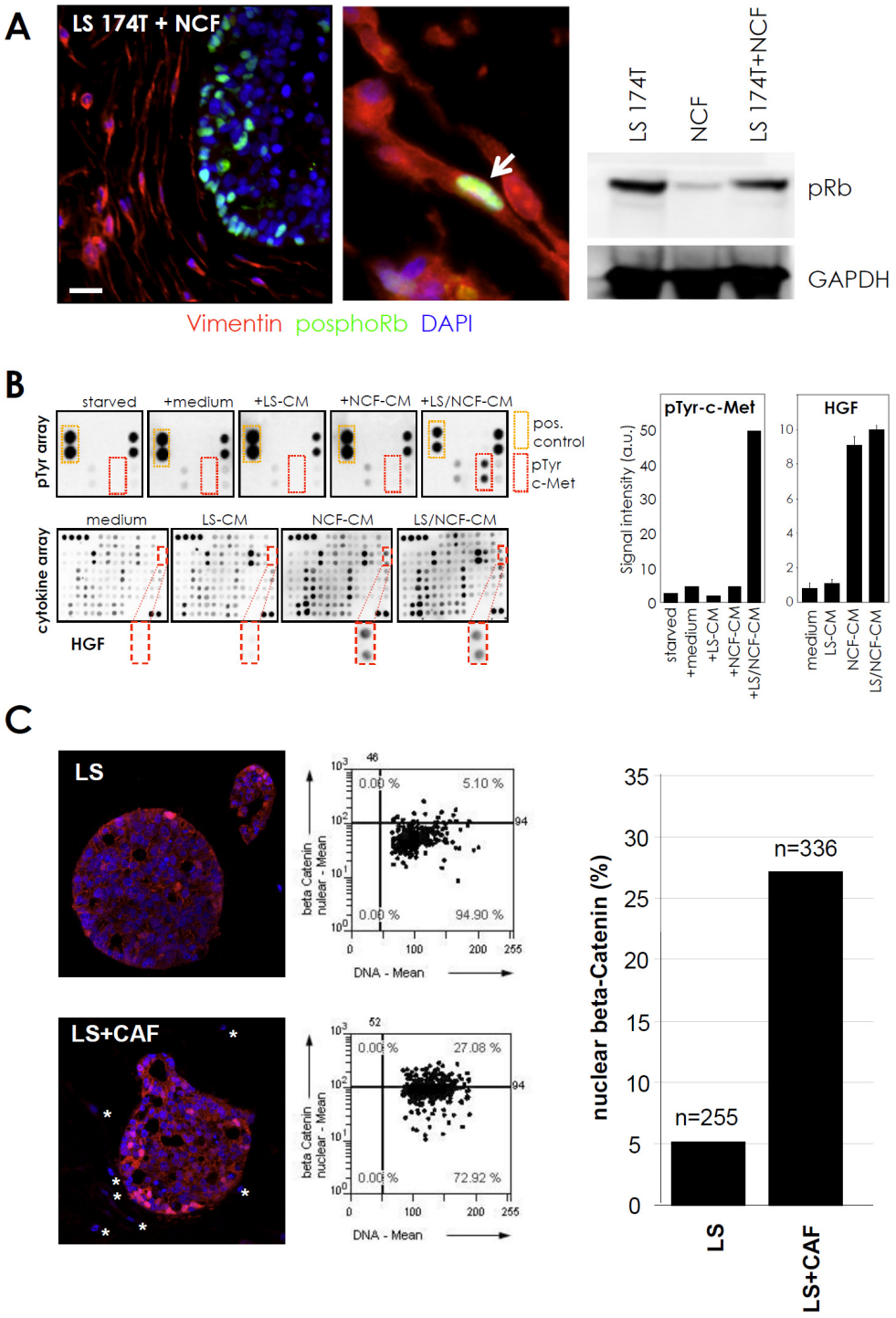
A
LS 174T + NCF
Vimentin posphoRb DAPI
LS 174T
NCF
LS 174T+NCF
pRb
GAPDH
B
starved
+medium
+LS-CM
+NCF-CM
+LS/NCF-CM
pos. control
pTyr c-Met
pTyr array
medium
LS-CM
NCF-CM
LS/NCF-CM
cytokine array
HGF
pTyr-c-Met
HGF
Signal intensity (a.u.)
C
LS
LS+CAF
beta Catenin nuclear - Mean
DNA - Mean
0.00 %
5.10 %
94.90 %
27.08 %
72.92 %
nuclear beta-Catenin (%)
n=255
n=336

Figure 4

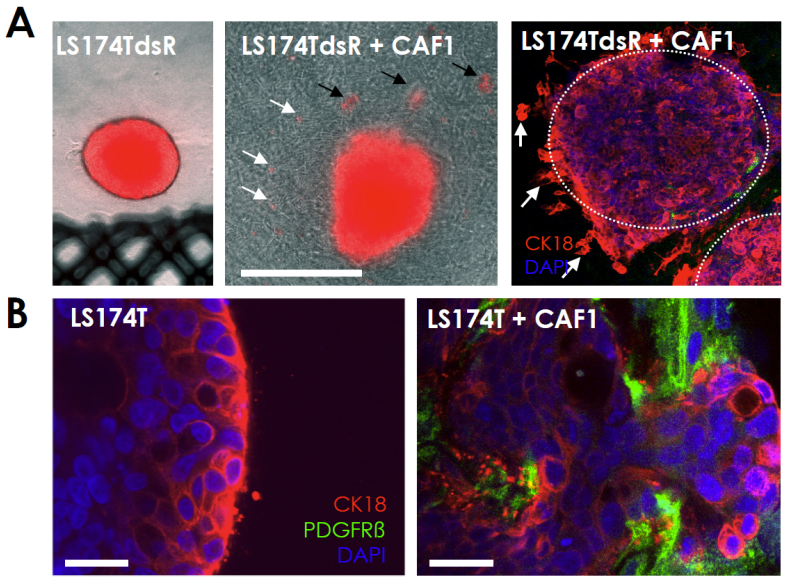
A
LS174TdsR
LS174TdsR + CAF1
LS174TdsR + CAF1
CK18
DAPI
B
LS174T
CK18
PDGFRß
DAPI
LS174T + CAF1

Figure 5

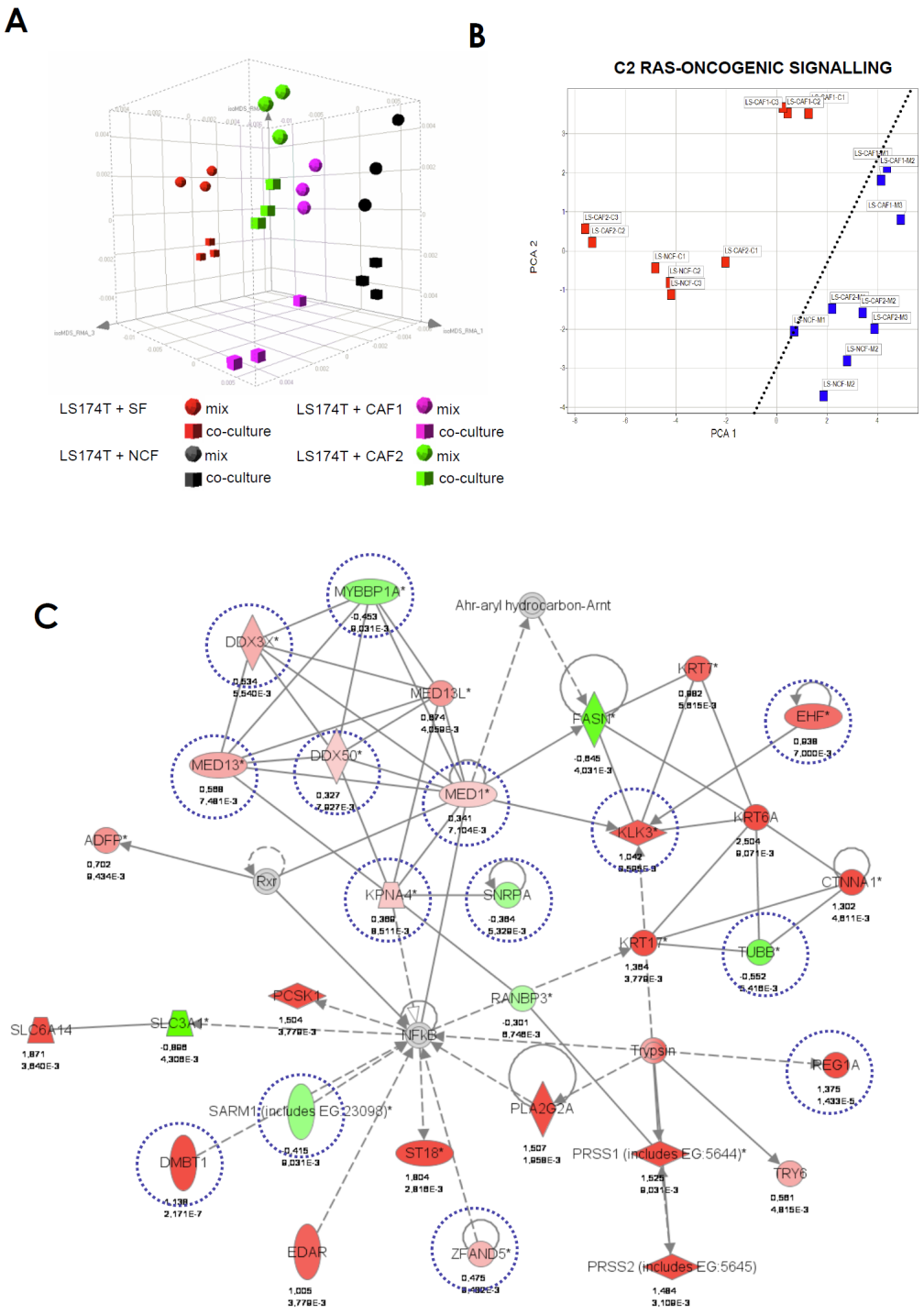
A
LS174T + SF
mix
co-culture
LS174T + CAF1
mix
co-culture
LS174T + NCF
mix
co-culture
LS174T + CAF2
mix
co-culture
B
C2 RAS-ONCOGENIC SIGNALLING
PCA 1
PCA 2
C
MYBBP1A*
Ahr-aryl hydrocarbon-Arnt
DDX3X*
MED13L*
KRT7*
FASN*
EHF*
MED13*
DDX50*
MED1*
KLK3*
KRT6A
ADFP*
Rxr
KPNA4*
SNRPA
CTNNA1*
KRT17*
TUBB*
PCSK1
RANBP3*
SLC6A14
SLC3A1*
NFkB
Trypsin
REG1A
SARM1 (includes EG:23098)*
PLA2G2A
DMBT1
ST18*
PRSS1 (includes EG:5644)*
TRY6
EDAR
ZFAND5*
PRSS2 (includes EG:5645)

Figure 6

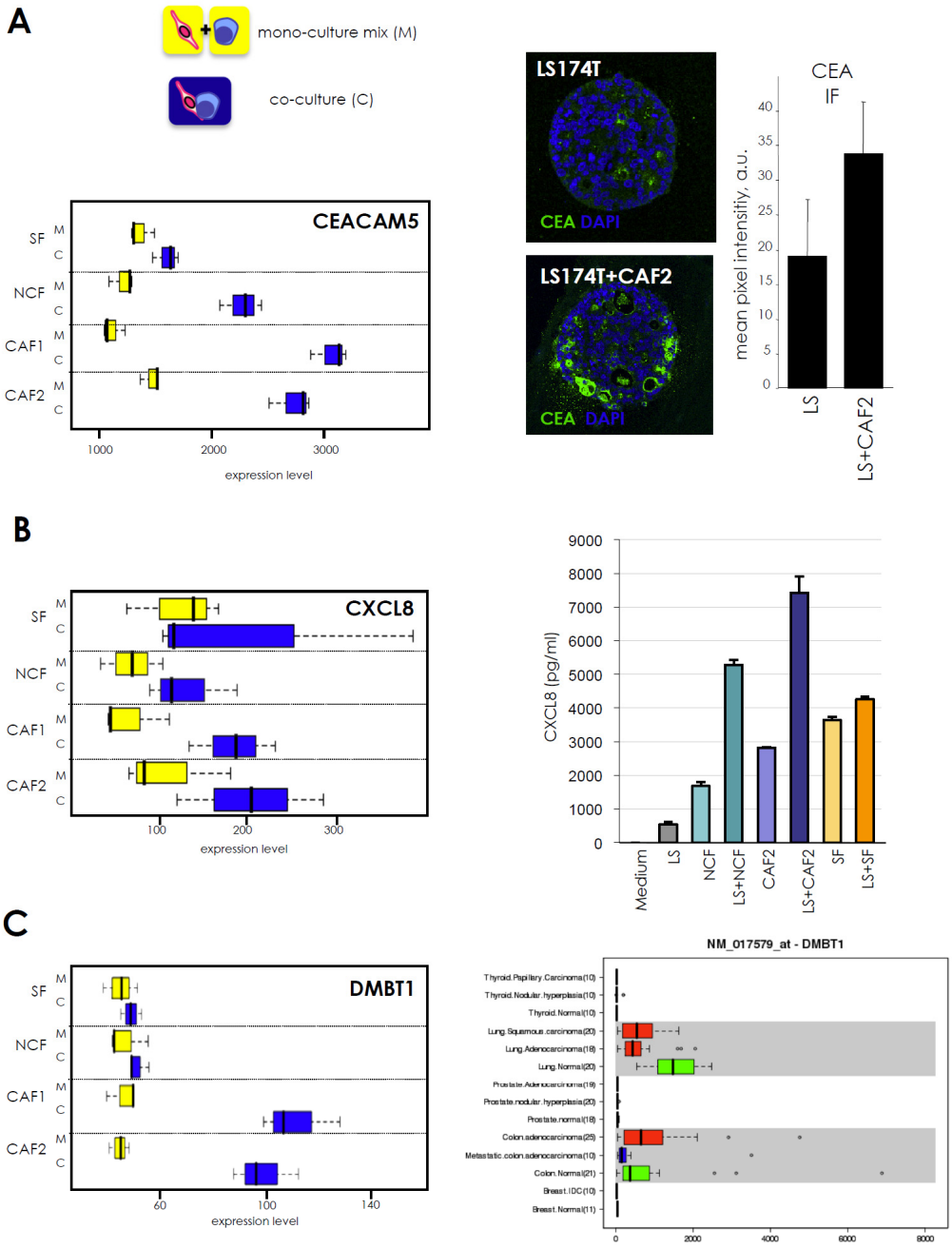
A
mono-culture mix (M)
co-culture (C)
CEACAM5
SF
NCF
CAF1
CAF2
M
C
1000
2000
3000
expression level
LS174T
CEA DAPI
LS174T+CAF2
CEA DAPI
CEA IF
mean pixel intensity, a.u.
40
35
30
25
20
15
10
5
0
LS
LS+CAF2
B
CXCL8
SF
NCF
CAF1
CAF2
100
200
300
expression level
CXCL8 (pg/ml)
9000
8000
7000
6000
5000
4000
3000
2000
1000
0
Medium
LS
NCF
LS+NCF
CAF2
LS+CAF2
SF
LS+SF
C
DMBT1
SF
NCF
CAF1
CAF2
60
100
140
expression level
NM_017579_at - DMBT1
Thyroid.Papillary.Carcinoma(10)
Thyroid.Nodular.hyperplasia(10)
Thyroid.Normal(10)
Lung.Squamous.carcinoma(20)
Lung.Adenocarcinoma(18)
Lung.Normal(20)
Prostate.Adenocarcinoma(19)
Prostate.nodular.hyperplasia(20)
Prostate.normal(18)
Colon.adenocarcinoma(25)
Metastatic.colon.adenocarcinoma(10)
Colon.Normal(21)
Breast.IDC(10)
Breast.Normal(11)
0
2000
4000
6000
8000

Figure 7

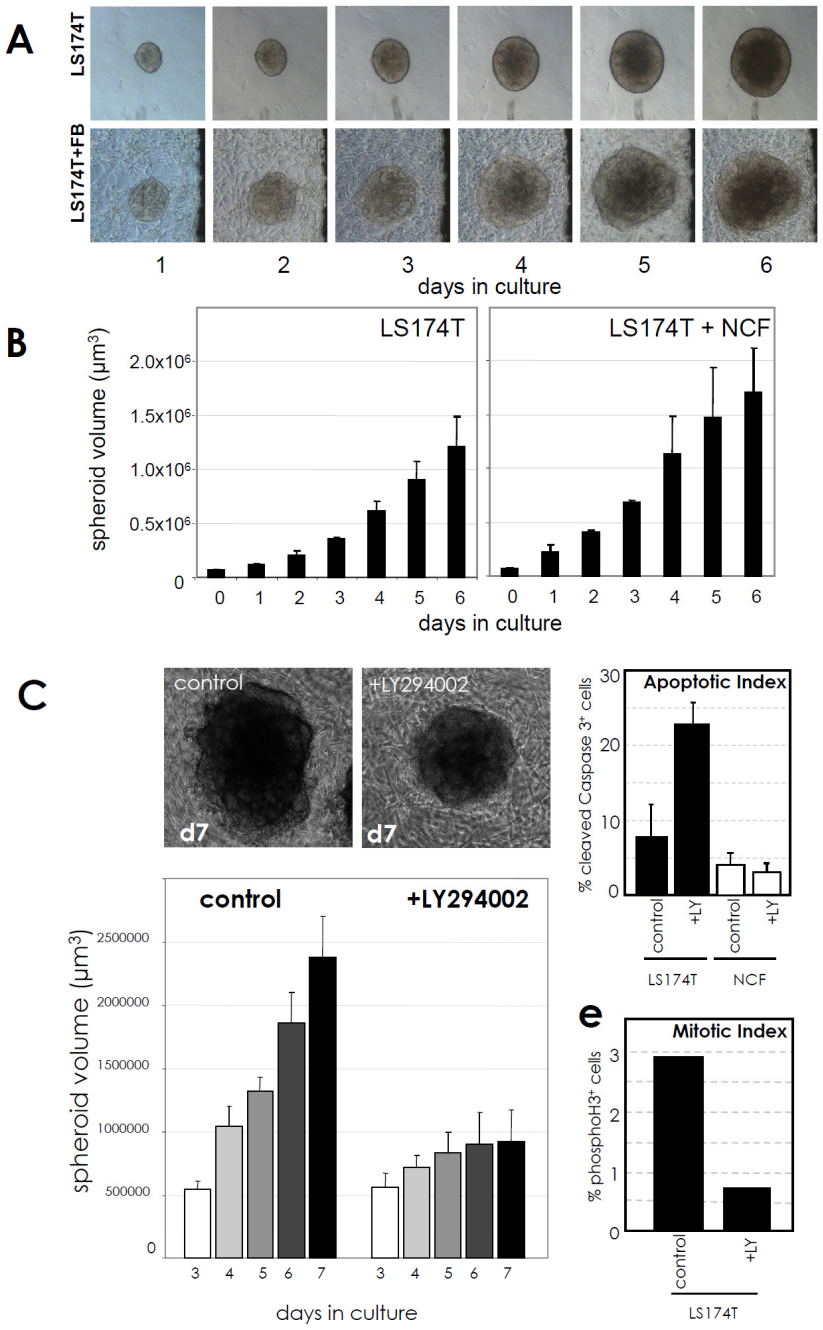
A
LS174T
LS174T+FB
1
2
3
4
5
6
days in culture
B
LS174T
LS174T + NCF
spheroid volume (µm³)
2.0x10⁶
1.5x10⁶
1.0x10⁶
0.5x10⁶
0
0 1 2 3 4 5 6
days in culture
C
control
+LY294002
d7
d7
control
+LY294002
spheroid volume (µm³)
2500000
2000000
1500000
1000000
500000
0
3 4 5 6 7 3 4 5 6 7
days in culture
Apoptotic Index
% cleaved Caspase 3⁺ cells
30
20
10
0
control
+LY
control
+LY
LS174T
NCF
e
Mitotic Index
% phosphoH3⁺ cells
3
2
1
0
control
+LY
LS174T

Figure 8

Supplementary figures

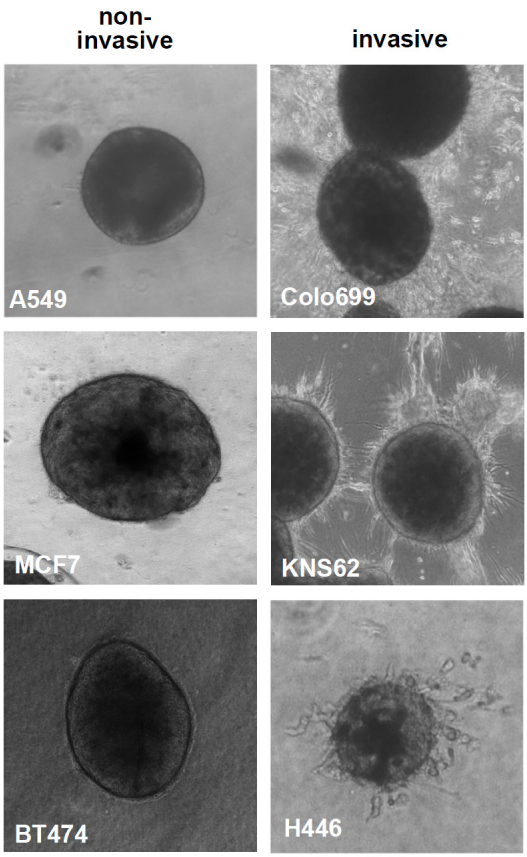

Supplementary Figure 1:
Collagen gel assays. Spheroids of different tumour cell lines were grown for 3-7 days in collagen I gels and photographed. Some cell lines showed strong invasive capacity (Colo699, KNS5, H446), whereas others remained compact with sharp boarders (A549, MCF7, BT474).

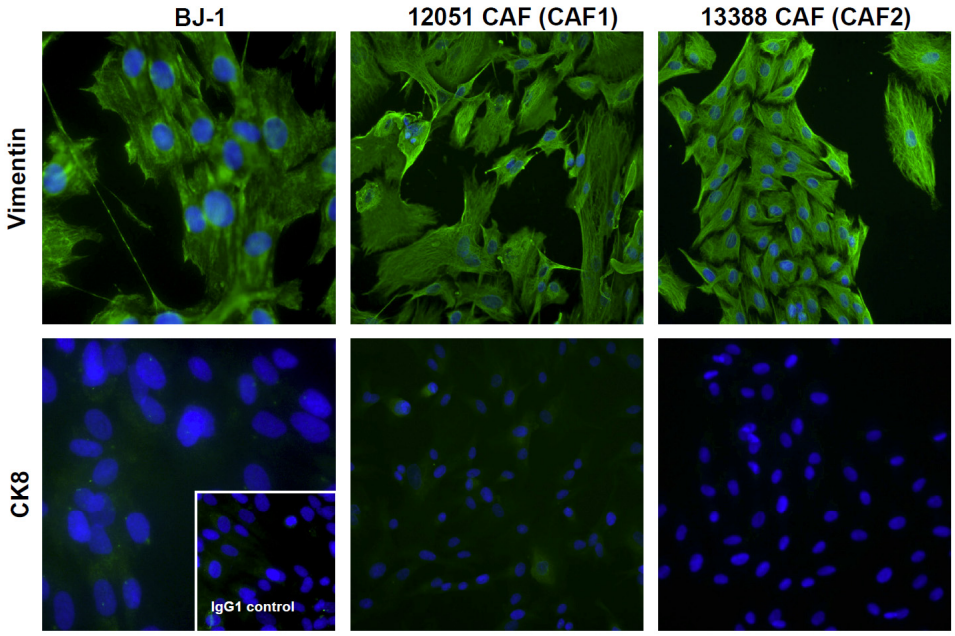

Supplementary Figure 2:
Phenotypic characterisation of freshly isolated cancer associated fibroblasts. CAFs from two different colon carcinoma specimens at low passage numbers (p2-p3) were analysed for the presence of the mesenchymal marker vimentin and the absence of the epithelial keratin 8 by immunofluorescence staining.

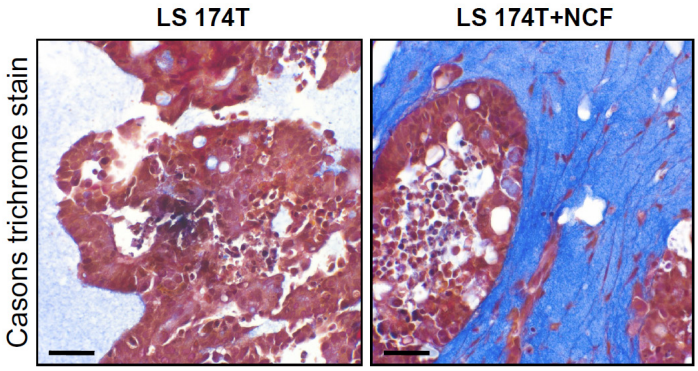

Supplementary Figure 3:
ECM remodelling as demonstrated by Cason's trichrome staining. Co-cultures of LS174T cells with fibroblasts (LS174T+FB) showed a remodelled and dense collagen matrix (dark blue collagen staining) as compared to tumour spheroid cultures alone (LS174T, pale blue collagen staining). Cellular structures are stained in brown (scale bars: 50 micrometer).

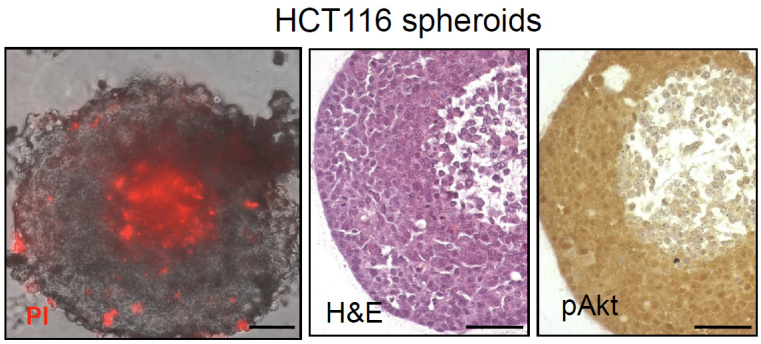

Supplementary Figure 4:
Cell death in the spheroid core. When HCT116 tumour cell spheroids reached a diameter of about 500 micrometer, cell death occurred in the centre of the 3D structures as indicated by the uptake of propidium iodide (PI, red) in living cultures (left). Morphological examination (H&E) revealed loss of cell-cell contacts in the centre of the spheroids accompanied by reduction of phospho-Akt in that central area. Scale bar: 100 micrometer.

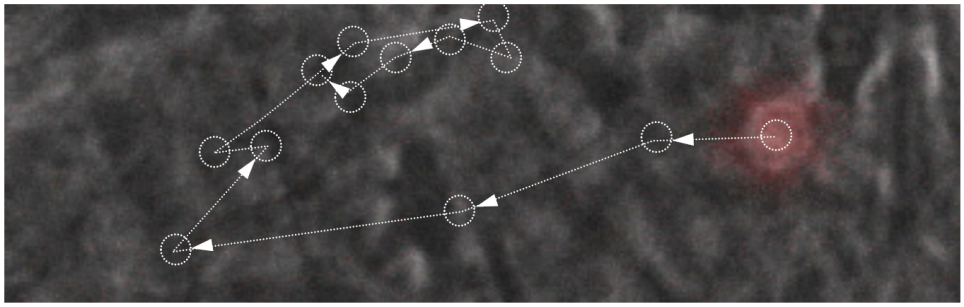

Supplementary Figure 5:
Tumour cell motility. dsRed labelled LS174T spheroids were co-cultured with colonic fibroblasts and followed by time lapse videomicroscopy for 11 hours. White arrows indicate the track of a single tumour cell (red), the position of the cell was determined every hour (circles).

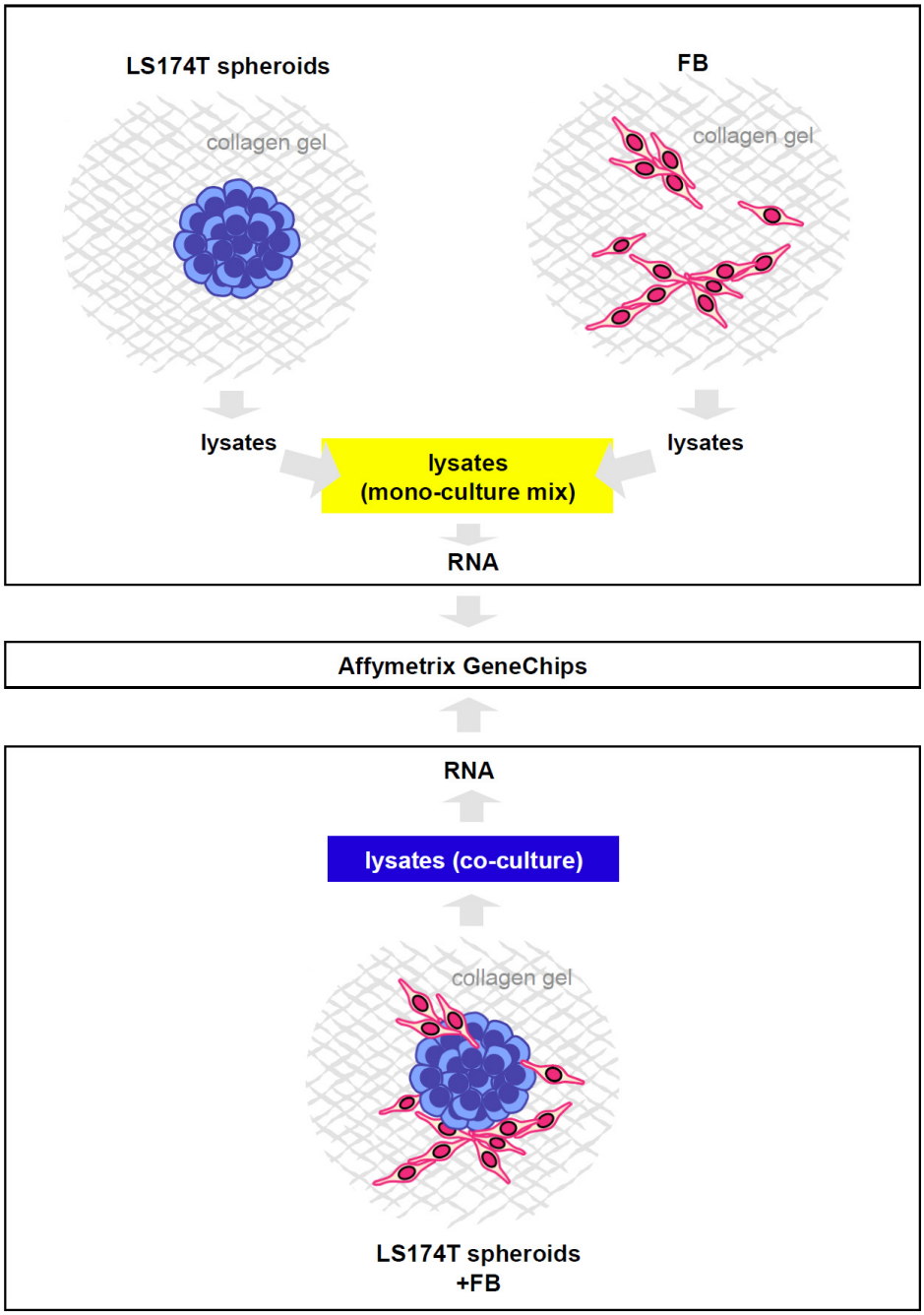

Supplementary Figure 6:
Illustration of the workflow to obtain a mixture of RNA from tumour cell spheroids (blue cell cluster) and fibroblast (elongated cells in magenta) mono-cultures as well as RNA from co-cultures. A defined number of tumour cell spheroids grown for 2 days (96 spheroids initially seeded with 150 LS174T cells) and exactly determined cell numbers of the different fibroblasts (2 x 10^5) were used. The whole lysates from LS 174T mono-cultures were mixed with fibroblast mono-culture lysates (lysates, mono-culture mix) thereby ensuring the same amount of tumour and fibroblast components present as in the co-culture experiments (lysates, co-culture). RNA extracted from the mono-culture mixed as well as from the co-culture experiments was processed for Affymetrix GeneChip analysis.

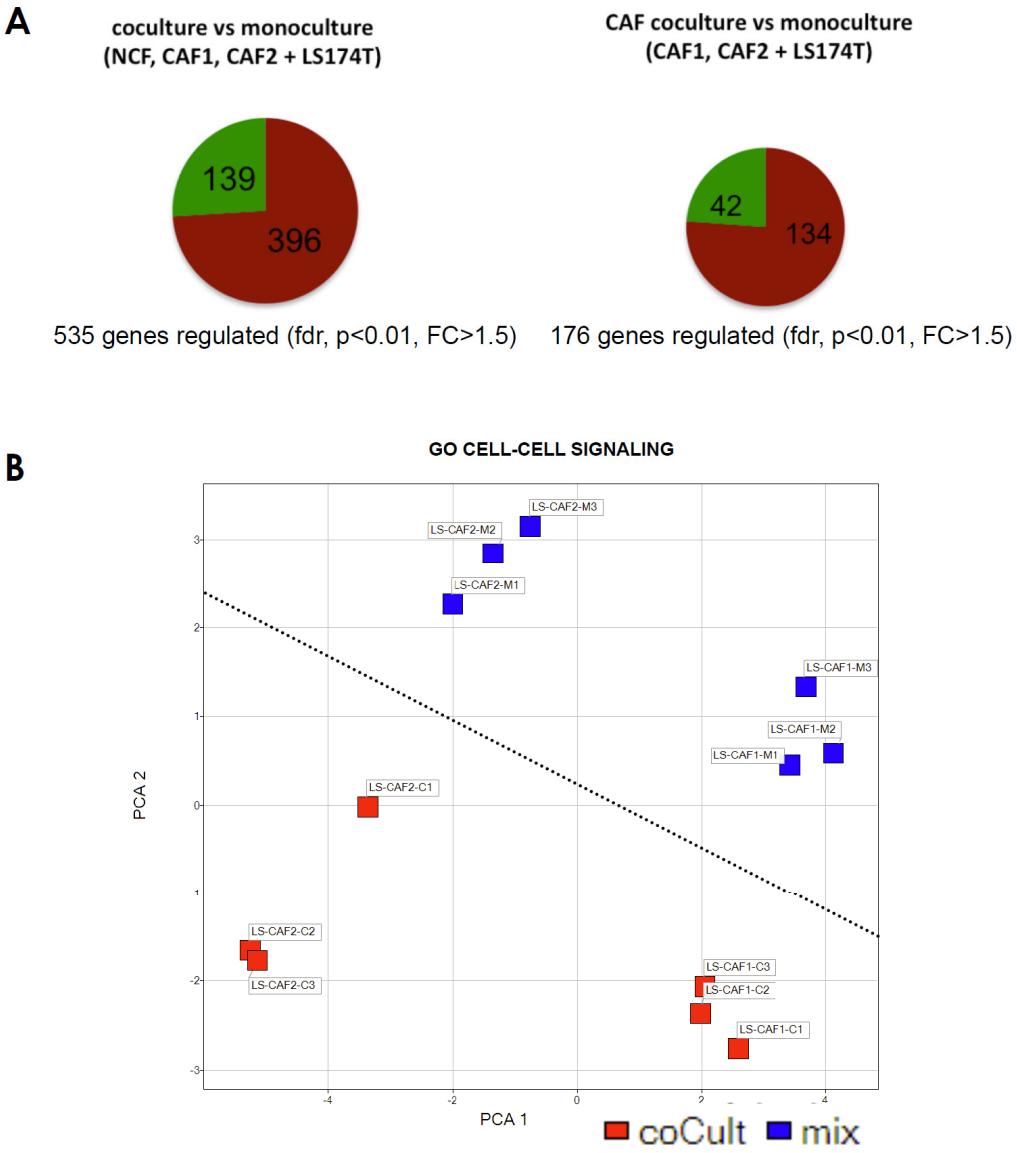

Supplementary Figure 7:
(**a**) Number of regulated genes in co-cultivation experiments as compared to mono-culture mix experiments. Genes with a fold change > 1.5 and adjusted FDR P-values of less than 0.01 were defined as significantly regulated. Left: co-cultivation of LS174T spheroids with colon fibroblasts (NF, CAF1, CAF2 + LS174T); numbers of upregulated genes are shown in red, downregulated genes are displayed in green. Right: number of genes specifically regulated by the co-culture of CAFs with tumour cells (CAF1, CAF2 + LS174T). Red: upregulated, green: downregulated. (**b**) Co-culture of LS174T spheroids with CAFs changed cell-cell-communication pathways. GSEA identified cell-cell signalling as defined by gene ontology (GO) terms. In this set PCA analysis separated the individual mixed mono-cultures (blue) from the corresponding co-cultures (red).

A

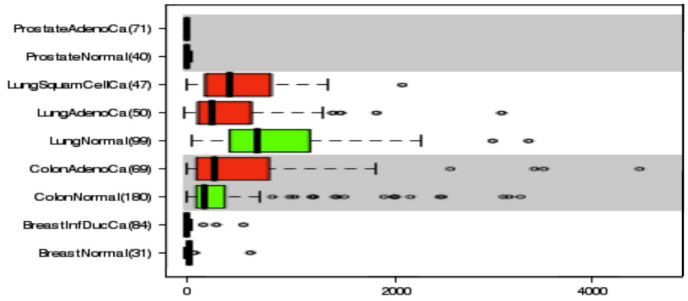

B

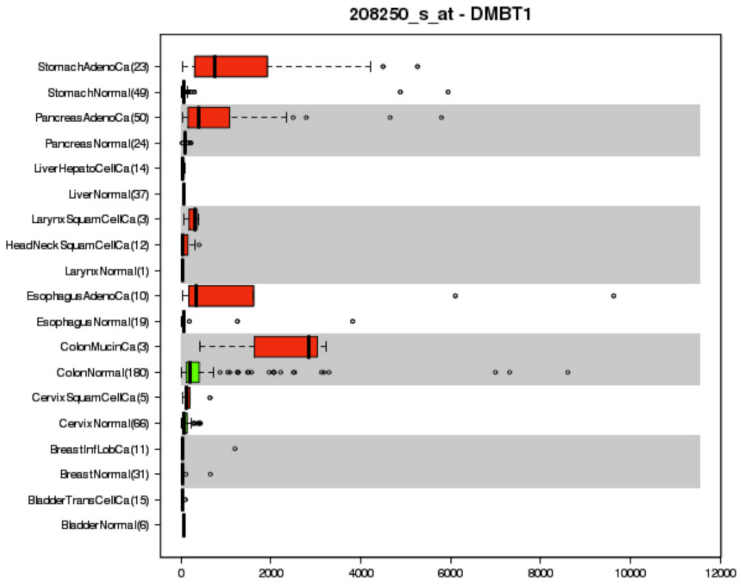

Supplementary Figure 8:
DMBT1 expression in major human tumours and their normal tissue counterpartsin large expression databases (BioExpress, GeneLogic, Affymetrix Human Genome U133 Plus 2.0 GeneChip based database). **A** DMBT1 mRNA wasexpressed in normal colon and increased in colon carcinomas, whereas normal lung was positive for DMBT1 and DMBT1 decreased in lung tumors. **B** DMBT1 RNA was significantly increased in mucinous colon carcinomas, esophagous carcinomas, stomach and pancreas carcinomas. Cancer samples, red; normal tissue samples, green. The bold centre-line indicates the median; the box represents the interquartile range (IQR). Whiskers extend to 1.5 times the IQR. Outliers are shown as small circles.

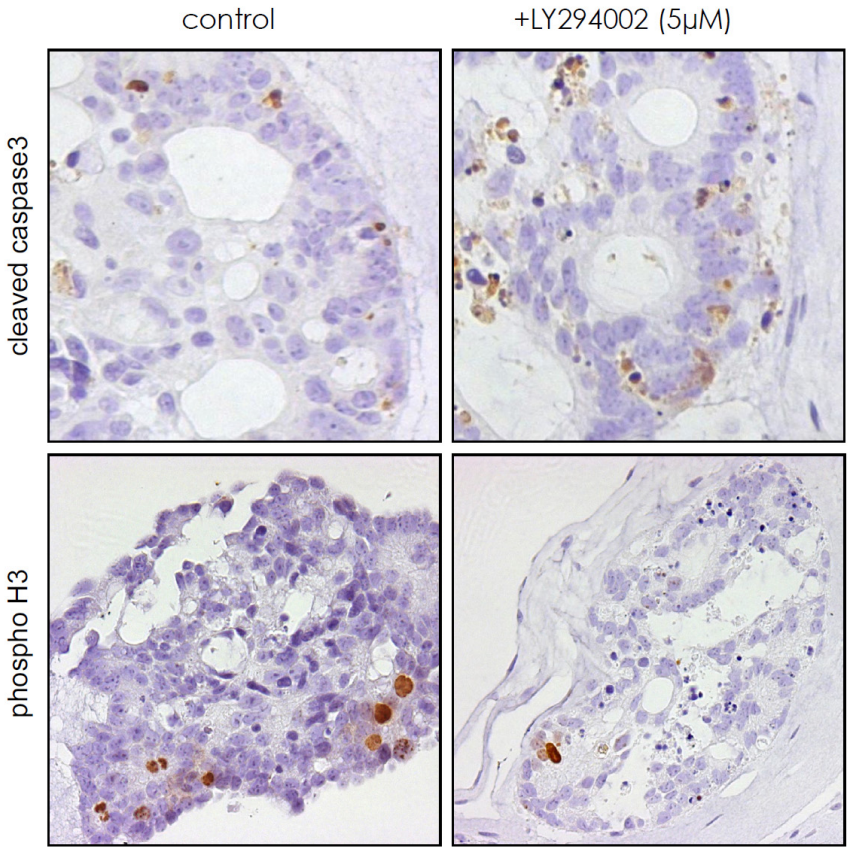

Supplementary Figure 9:
PI3K inhibitor (LY294002) treatment of LS174T colon fibroblast 3D co-cultures. Sections from DMSO-control and LY294002 treated co-cultures were stained for cleaved-caspase 3 (top) as a marker for apoptotic cells. The number of cleaved-caspase 3 positive tumour cells was increased as compared to the control. Fibroblast were not affected. Cell proliferation was assessed by the mitosis marker phospho-H3 (bottom). LY294002 treated cultured showed reduced numbers of phospho-H3 positive tumour cells as compared to the DMSO controls. Fibroblasts showed very low and therefore non-quantifiable phospho-H3 staining under both conditions.

Cell line	Tumour type	Spheroid formation	Phenotype in CG
H446	lung carcinoma	+	invasive
Colo699	NSCLC	+	invasive
KNS62	NSCLC	+	invasive
SK-OV-3	ovarian carcinoma	+	invasive
BT474	breast carcinoma	+	non-invasive
MCF7	breast carcinoma	+	non-invasive
HCT116	colorectal carcinoma	+	non-invasive
HT-29	colorectal carcinoma	+	non-invasive
LS174T	colorectal carcinoma	+	non-invasive
HN5	head/neck SQCC	+	non-invasive
A549	lung carcinoma	+	non-invasive
Caco-2	colorectal carcinoma	-	n.a.
Colo205	colorectal carcinoma	-	n.a.
SW620	colorectal carcinoma	-	n.a.
CaLu-6	lung carcinoma	-	n.a.
H69	SCLC	-	n.a.
H82	SCLC	-	n.a.

Supplementary Table 1:
Phenotype of tumour cell lines grown as spheroids and transferred into collagen gels (CG). Abbreviatons: NSCLC, non-small cell lung cancer; SCLC, small cell lung cancer, SQCC, squamous cell carcinoma, n.a. not applicable.

NAME	SIZE	FDR q-val	GO TERM	DESCRIPTION
EXTRACELLULAR_REGION, _MATRIX, _SPACE	321; 94; 425; 92; 234; 54	0,038; 0,026; 0,040; 0,034; 0,035, 0,055	GO:0044421; GO:0031012; GO:0005576; GO:0005578; GO:0005615; GO:0005615	A structure lying external to one or more cells, which provides structural support for cells or tissues; may be completely external to the cell (as in animals)
TISSUE_DEVELOPMENT	131	0,047	GO:0009888	The process whose specific outcome is the progression of a tissue over time, from its formation to the mature structure.
ECTODERM_DEVELOPMENT	76	0,031	GO:0007398	The process whose specific outcome is the progression of the ectoderm over time, from its formation to the mature structure. In animal embryos, the ectoderm is the outer germ layer of the embryo, formed during gastrulation.
GENERATION_OF_A_SIGNAL_INVOLVED_IN_CELL_CELL_SIGNALING	27	0,029	GO:0003001	The cellular process by which a physical entity or change in state, a signal, is created that originates in one cell and is used to transfer information to another cell. This process begins with the initial formation of the signal and ends with the mature form and placement of the signal.
ANGIOGENESIS	42	0,038	GO:0001525	lood vessel formation when new vessels emerge from the proliferation of pre-existing blood vessels
EPIDERMIS_DEVELOPMENT	68	0,037	GO:0008544	The process whose specific outcome is the progression of the epidermis over time, from its formation to the mature structure. The epidermis is the outer epithelial layer of a plant or animal, it may be a single layer that produces an extracellular material (e.g. the cuticle of arthropods) or a complex stratified squamous epithelium, as in the case of many vertebrate species.
VASCULATURE_DEVELOPMENT	49	0,049	GO:0001944	The process whose specific outcome is the progression of the vasculature over time, from its formation to the mature structure.
GTPASE_ACTIVITY	89	0,054	GO:0003924	Catalysis of the reaction: GTP + H2O = GDP + phosphate.
ANATOMICAL_STRUCTURE_FORMATION	50	0,059	GO:0048646	The process pertaining to the initial formation of an anatomical structure from unspecified parts. This process begins with the specific processes that contribute to the appearance of the discrete structure and ends when the structural rudiment is recognizable. An anatomical structure is any biological entity that occupies space and is distinguished from its surroundings. Anatomical structures can be macroscopic such as a carpel, or microscopic such as an acrosome.
RESPONSE_TO_WOUNDING	180	0,063	GO:000961	A change in state or activity of a cell or an organism (in terms of movement, secretion, enzyme production, gene expression, etc.) as a result of a stimulus indicating damage to the organism.
REGULATION_OF_RESPONSE_TO_STIMULUS	57; 295; 40	0,062; 0,059; 0,074	GO:0048583; GO:0009605; GO:0048584	Any process that modulates the frequency, rate or extent of a response to a stimulus. Response to stimulus is a change in state or activity of a cell or an organism (in terms of movement, secretion, enzyme production, gene expression, etc.) as a result of a stimulus.
CELL_CELL_SIGNALING	394	0,060	GO:0007267	Any process that mediates the transfer of information from one cell to another.
NEGATIVE_REGULATION_OF_CELL_PROLIFERATION	148	0,078	GO:0008285	Any process that stops, prevents or reduces the rate or extent of cell proliferation.
WOUND_HEALING	53	0,078	GO:0042060	The series of events that restore integrity to a damaged tissue, following an injury.
REGULATION_OF_CELL_GROWTH	43	0,076	GO:0001558	Any process that modulates the frequency, rate or extent of cell growth.
COLLAGEN	23	0,074	GO:0005581	Any of the various assemblies in which collagen chains form a left-handed triple helix; may assemble into higher order structures.
EXTRACELLULAR_STRUCTURE_ORGANIZATION_AND_BIOGENESIS	30	0,082	GO:0043062	A process that is carried out at the cellular level which results in the formation, arrangement of constituent parts, or disassembly of structures in the space external to the outermost structure of a cell. For cells without external protective or external encapsulating structures this refers to space outside of the plasma membrane, and also covers the host cell environment outside an intracellular parasite.
EPIDERMAL_GROWTH_FACTOR_RECEPTOR_SIGNALING_PATHWAY	19	0,088	GO:0007173	The series of molecular signals generated as a consequence of an epidermal growth factor receptor binding to one of its physiological ligands.
NEGATIVE_REGULATION_OF_GROWTH	37	0,100	GO:0045926	Any process that stops, prevents or reduces the rate or extent of growth, the increase in size or mass of all or part of an organism.
LYMPHOCYTE_DIFFERENTIATION	26	0,121	GO:0030098	The process whereby a relatively unspecialized precursor cell acquires specialized features of B cells, T cells, or natural killer cells

Supplementary Table 2:
GSEA of Genes upregulated in LS174T / CAF co-cultures (GO Terms). The 20 most significant gene sets are shown.

Curriculum vitae

Christian Rupp

Personal Details

Date of Birth:	06.09.1976
Place of Birth:	Vienna, Austria
Nationality:	Austrian
Adress:	Hervicusgasse 2/13 1120 Vienna
Tel.:	+43 664 7816650
Email:	christian.rupp@meduniwien.ac.at

Educational Background

1997-2004	University of Vienna Study of Microbiology & Genetics 29.11.2004 Final examination passed with distinction
1987-1995	Secondary school, Vienna Final examination passed with distinction
1983-1987	Elementary school, Vienna

Employment History

04/2005-now	Clinical Institute of Pathology, Medical University of Vienna PhD-Project with Boehringer-Ingelheim: “Characterization of novel tumor stroma markers.”
04/2003-11/2004	Clinical Institute of Pathology, Medical University of Vienna Diploma Thesis with Boehringer-Ingelheim: “Analysis of Endosialin expression during mouse development and tumorigenesis.”
2002-2003	Undergraduate work with Prof. Franz Klein, Institute of Botany, University of Vienna
1997-2004	Several summer jobs in the pharmaceutical industry (Baxter), social work with disabled people
1996-1997	GRUFT-Hostel for the Homeless, Alternative Civilian Service

Publications:

Original articles:

1: **Rupp C**, Dolznig H, Haslinger C, Schweifer N, Artaker M**,** Garin-Chesa P.
IGFBP7, a novel tumor stroma marker with dual roles in epithelial- and mesenchymal-type tumor cells
Manuscript prepared for submission to“Cancer Research”.

2:Dolznig H, **Rupp C**,Puri C,Haslinger C,Schweifer N, Wieser E, Kerjaschki D, Garin-Chesa P
Modeling adenocarcinomas *in vitro*: A novel 3D co-culture system induces cancer relevant pathways upon tumor stroma interaction
Manuscript prepared for submission to "American Journal of Pathology"

3: **Rupp C**, Dolznig H, Puri C, Sommergruber W, Kerjaschki D, Rettig WJ, Garin-Chesa P
Mouse endosialin, a C-type lectin-like cell surface receptor: expression during embryonic development and induction in experimental cancer neoangiogenesis.
Cancer Immun. 2006 Jul 31;6:10.

4: **Rupp C**, Dolznig H, Puri C, Schweifer N, Sommergruber W, Kraut N, Rettig WJ,Kerjaschki D, Garin-Chesa P
Laser capture microdissection of epithelial cancers guided by antibodies against fibroblast activation protein and endosialin.
Diagn Mol Pathol. 2006 Mar;15(1):35-42.

5: Zierhut C, Berlinger M, **Rupp C**, Shinohara A, Klein F
Mnd1 is required for meiotic interhomolog repair.
Curr Biol. 2004 May 4;14(9):752-62

6:Rabitsch KP, Tóth A, Gálová M, Schleiffer A, Schaffner G, Aigner E, **Rupp C**, Penkner AM, Moreno-Borchart AC, Primig M, Esposito RE, Klein F, Knop M, Nasmyth K.
A screen for genes required for meiosis and spore formation based on whole-genome expression.
Curr Biol. 2001 Jul 10;11(13):1001-9.

Review:

Rupp C, Dolznig H, Haslinger C, Schweifer N, Garin-Chesa P
Cancer associated fibroblasts as therapeutic targets
Accepted for publication in:
"Tumor associated fibroblasts and their matrix" published by Springer, edited by N. Fusenig & M. Mueller (DKFZ, Heidelberg)

Several poster presentations

Languages & Computer Skills

Languages: German (native); English (fluent); French (good knowledge); Italian (basics)

Computer skills: Microsoft Office; Graphic programs (Adobe Photoshop, Macromedia Freehand); Biological databases (EMBL, Swissprot, Medline…); Expression profiling (GeneLogic Bioexpress)